Investigating the role of Yes-associated protein (YAP) in neural crest development

Gesell, Anne

Award date:
2015

Awarding institution:
University of Bath

Investigating the role of Yes-associated protein (YAP) in neural crest development

Anne E Gesell

A thesis submitted for the degree of Doctor of Philosophy

University of Bath

Department of Biology & Biochemistry

October 2014

Signed:……..

Date:……

Acknowledgement

Most of all I like to thank my supervisor and mentor Professor Robert N. Kelsh for taking me on as his student, guiding me patiently throughout my PhD and for our valuable discussions. Without his help, commitment and enthusiasm for this topic, my PhD and this project would have taken a completely different turn. I hugely enjoyed the trust and scientific freedom I was given in his lab, through which I gained a lot of experience and which allowed me to develop into the person I am now. I knew that his door was and is always open for me and any other students when problems or questions came up, so again, thank you Robert.

I would also like to thank Dr Makoto Furutani-Seiki for his generous offer in letting me use the *hirame* mutant for my dissertation project and providing me the pCS2_*yap*(wt/S87) plasmids. Without this collaboration, none of the data in this thesis would have been possible. Thanks go to Marc Shedden for the maintenance of the fish facility and his care of my Medaka strains, Ursula Potter for preparing and imaging the TEM sections and my MSc student Isabel Bravo for generating some of the *sox9b*, *phox2b* and *mbp in situ* pictures.

I would also give my thanks to Professor D. Tosh and postgraduate adviser Dr J. Doughty for their help and support which proved invaluable within my PhD.

One of my biggest acknowledgements goes to Dr H. Hashimoto for kindly letting me use all of the Medaka neural crest *in situ* probes he established, which are: *Dct*, *gch*, *sox9b*, *elavl3/HuC*, *phox2b, mbp, foxd3*, *snail*, twist and *pax3*. After arriving in Robert´s lab it was through Dr Hashimoto's probes and Dr Tomoko Adachi-Sambe's help which kick-started this project. Thank you so much guys! Thank you Alberto, Laura and the other brilliant people in lab 0.76, who are not only colleagues, they became friends and I want to thank you for your moral support, technical advice and most of all the fun moments with you guys (which still make me giggle when I think about them ;-)). My thanks also go to Alec, who was kind enough to proof-read all my chapters.

I also want to take the opportunity to express my very great appreciation to Dr K. Kaji for his loving support, understanding, much needed motivation and scientific guidance as a close friend throughout most of my PhD time.

One of my special thanks go to my family, Vati, Mutti & brother Falk, who encourage me to go my own way in life, keeping my way free and for letting me know I will always have a home to come back to wherever I go and whatever I do. My thoughts also go to my beloved great-grandma Lissi, who I owe so many precious memories and who I´ll never forget in life.

Lastly but by no means the least, I would also like to thank the University of Bath for the studentship.

Abstract

The neural crest (NC) is a multipotent embryonic cell type derived from the ectoderm during neurulation giving rise to a variety of cell lineages such as neurons, glia and pigment cells. Most genes associated with the correct initiation, differentiation and migration of the neural crest have been found through reverse genetics. Similarities between neural crest development and some features of cancer progression are remarkable. For instance, it has been suggested that some cancer types recapitulate NC processes in an unregulated manner such as epithelial-mesenchymal transition or active cell migration throughout the body to form distant metastases. However, to date very little is known about initiators and drivers that direct neural crest cell migration to specific target sites.
The Medaka mutant *hirame* represents an interesting melanocyte specific migration defect on the yolk sac caused by a loss of functional Yes-associated protein (YAP). Medaka *hirame* mutants were initially studied for their profound changes in body morphology. Genomic mapping identified the causal mutation as a nonsense point mutation within the first WW domain in the Yes-associated protein 1 (YAP1), causing translation of a dysfunctional YAP protein. YAP is a downstream transcriptional co-activator of the recently discovered and evolutionarily conserved Hippo pathway. Alterations within Hippo signalling are linked to cell survival, proliferation and abnormal tissue overgrowth.
We demonstrate that *hirame* melanocyte precursors (melanoblasts) are initially present in normal abundance, but show an early migration defect with a lack of melanoblasts on the yolk sac, and corresponding accumulation in the lateral parts of the body. Subsequently, we observe an overall decline in differentiated melanocyte numbers during late stage embryogenesis. We designed an overexpression cassette linking enhanced GFP to either wild type or a mutated activated version of YAP and present evidence that it can efficiently rescue the melanocyte defect after injection of mRNA into one-cell stage embryos. Furthermore, analysis of the yolk sac anatomy via transmission electron microscopy indicates that a fraction of yolk membrane cells undergo apoptosis and we propose that this may contribute to the establishment of altered environmental cues leading to abnormal melanoblast migration onto the yolk sac. Injection of *yap* mRNA directly into the yolk sac however, failed to rescue melanoblast patterning.
To advance our study, we isolated and characterised a 3.6 kb Medaka *dopachrome tautomerase (Dct)* promoter fragment, and used it to drive expression of enhanced green fluorescent protein (eGFP) *in vivo*. We generated germline transgenics with this construct that showed lineage-specific expression of eGFP within early migrating melanoblasts, a phenotype that is maintained in differentiated melanocytes throughout embryogenesis. In addition, using this promoter we overexpressed our *egfp-yap* fusion cassette and established transgenic lines to assess the cell autonomy of YAP within

the melanocyte lineage. However, no fluorescent signal could be detected in the latter transgenics, necessitating future experimentation to properly characterise these lines.

Finally, we analysed a range of neural crest markers to examine the extent of the neural crest defects in *hirame* mutants. In addition to the melanocyte phenotype, we identified a dramatic reduction in xanthophore numbers, although early leucophore development appears unaffected. We also observed a decreased number of dorsal root ganglia in the peripheral nervous system as well as smaller and partly ectopic cranial neural crest ganglia populations within the epibranchial arches. The characterisation of a novel Medaka melanocyte specific promoter as well as additional novel NC markers will be widely applicable and useful to the wider Medaka research community as a tool for the study of neural crest related mechanisms during development.

Table of Contents

Table of Figures

Table of Graphs:

Table of Tables:

Abbreviations

% (w/v)	Percent weight per volume
(e)GFP	(enhanced) Green fluorescent protein
°C	Degrees Celcius
µ	micro
A, C, G, T	Adenine, cytosine, guanine, thyamine
AP	Alkaline phosphatase
bHLH	Basic helix-loop-helix
BMP	Bone Morphogenic Protein
bp, kb	Base pair(s)s, kilo base pair(s)
BrdU	5-bromo-2´-deoxyuridine
BSA	Bovine serum albumin
$CaCl_2$	Calcium Chloride
CCNC	Cranial Neural crest
cDNA	Deoxyribonucleic acid complementary to ribonucleic acid
CNS	Central nervous system
C-terminal	Amino-terminal
Dct	*Dopachrome tautomerase*
DIG	Digoxigenin
DNA	Deoxyribonucleic acid
dpf	Days post fertilisation
ECM	Extracellular matrix
EDTA	Ethylenediaminetetra-acetic acid
Elavl3	ELAV-like neuron-specific RNA binding protein 3
EMT	Epithelial-mesenchymal transition
ENS	Enteric nervous system
ENU	N-ethyl-N-nitrosourea
FGF	Fibroblast Growth factor
Fig.	Figure
G	Gram
gch	GTP-cyclohydrolase I
GTP	Guanosine triphosphate
H_2O_2	Hydrogen peroxide
HCl	Hydrochloric acid

HD	Hirschsprung's disease
Hir, hir	*Hirame*
HM	Hybridisation mix
hpf	Hours post fertilisation
hpi	Hours post injection
KCl	Potassium chloride
KOD	Thermococcus kodakaraensis
KOH	Potassium hydroxide
l, ml, µl, nl	Liter, millilitre, microliter, nanoliter
LB	Luria Broth
LiCl	Lithium Chloride
m	Milli
M, mM, µM	Moles per liter, millimoles per liter, micromoles per liter
MC	Melanocytes
mg, µg, ng, pg	Milligram(s), microgram(s), nanogram(s), pictogram(s)
$MgSO_4$	Magnesium sulphate
min	Minute
mitf	Microphthalmia related transcription factor
mbp	Basic myogenic protein 1
mRNA	Messenger ribonucleic acid
NaAc	Sodium acetate
NaCl	Sodium Chloride
NBT	Nitro blue tetrazolium chloride
NC	Neural crest
NCC	Neural crest cell
nt	Nucleotide
N-terminal	Amino-terminal
PBS	Phosphate buffered saline
PBST	Phosphate buffered saline supplemented with 0.1% Tween-20
PCR	Polymerase chain reaction
PFA	Paraformaldehyde
phox2b	Paired-like homeobox 2 protein
pLL	Posterior lateral line
PNS	Peripheral nervous system
RNA	Ribonucleic acid

RT	Room temperature
SDS	Sodium dodecyl sulphate
SNPs	Single nucleotide polymorphism
sox9	Sry -related high-mobility group (HMG) box protein 9
SSC	Saline sodium citrate
TAE	Tris-Acetate-EDTA
Taq	*Thermus aquaticus*
TCRNC	Trunk neural crest
TEM	Transmission Electron microscope
tetra-primer ARMS-PCR	Multiplex Tetra-Primer Amplification Refractory Mutation System PCR
TUNEL	Terminal transferase dUTP nick end labelling
tyr	Tyrosinase
U	Unit(s) of enzyme
UTR	Untranslated region
WISH	Whole-mount *in situ* hybridisation
WT,wt	wild type
YAP	Yes-associated protein
Z-fin	Zebrafish Information Network

1 Chapter: Introduction

1.1 Fish as a model organism

Zebrafish and Medaka fish provide excellent model organisms because of their high fecundity – single Zebrafish females lay up to 200 eggs per week and Medaka up to 30 eggs daily and their easy husbandry in large numbers. Embryogenesis can be examined ex-utero over a time frame of 5 days in Zebrafish and 9 days in Medaka (Kimmel et al. 1995; Kinoshita, Murata & Naruse *et al*. 2009) thus, allowing an advantage of Medaka is that embryos provide an extended time for testing in which general embryogenic development is slower. In addition Zebrafish and Medaka fish embryogenesis has been extensively described in detail (Kimmel et al. 1995; Iwamatsu 2004) making it a good model in which to carry out replicable experiments (Appendix 4,5). Zebrafish and Medaka are two related teleost species with 115–200M years of independent evolution, thus making divergent and conserved principles of development easy to observe by comparison between them (Furutani-Seiki & Wittbrodt 2004). Furthermore, whole genome sequences are available for both species.

Zebrafish (*Danio rerio*) is an established model organism originating as a small tropical freshwater fish from India. It has been increasingly popular as a genetic system since the 1980´s (Streisinger et al. 1981; Driever et al. 1994). Systematic genome-wide mutagenesis screens published in 1996 by teams working in Tübingen and Boston were instrumental in augmenting the importance of Zebrafish as a vertebrate model organism to study embryogenesis, regeneration and human diseases. This project commonly referred to Tübingen/Boston screen described around 1500 mutations in more than 400 new genes that caused abnormal embryonic and early larval phenotypes (Nüsslein-Volhard 2012). Later in 2001 the Sanger Institute started the genome sequencing project in Zebrafish from which it generated a high-quality sequence assembly to the human genome (Howe et al. 2013).

Medaka (*Oryzias latipes*), is a small Asian freshwater teleost usually confined to rice paddys or shallow brooks primarily in Japan. Medaka is the first vertebrate in which Mendelian inheritance was proven valid (Ishikawa 2000). Around 80 spontaneous natural colour mutants exist such as orange-red, albino or brown/grey wild-type (Tomita collection; Kelsh et al. 2004) and are maintained in a stock center for research (NRPB Medaka). There are two main advantages of Medaka in comparison to Zebrafish: firstly the small genome size of 800–1000 Mb being approximately half the size of the Zebrafish, and one-third that of the human genome (Lamatsch et al. 2000). Secondly, robust inbred strains are available which are as a results of their genetic consistency a useful tool for regards to mutagenesis screens and genetic mapping (Wittbrodt et al. 2002). In addition a large mutagenesis screen has been carried out identifying mutants with defects in organogenesis (Furutani-Seiki et al. 2004).

Those advantages make small laboratory teleosts an attractive model organism to work with, and a valuable source of obtaining experimental data, which can be related to human developmental

events. Many studies have used teleost models to explain fundamental basics of cell specification, organisation and migration (Nüsslein-Volhard 2012; Furutani-Seiki et al. 2004; Loosli et al. 2000). In addition, disease models help explain molecular drivers of oncogenic cell transformation and active metastases formation in human (Mione & Trede 2010). Our work focuses on the analysis of one Medaka fish model with striking implications for neural crest impairments during early embryogenesis.

1.2 Onset of Gastrulation and cell arrangements leading to neurulation

Although the basic events of gastrulation during early embryogenesis are similar in most species, cell organisation during late gastrula can differ between animals (Niehrs 2004). Here, I focus and explain briefly the anatomical processes leading up to, and subsequent during gastrulation found in teleosts such as Zebrafish (*Danio rerio*) or Medaka (*Oryzias latipes*), which will help to explain later interpretations of this thesis' experimental data.

After cleavage and late blastula stage, the blastoderm and yolk syncytium spreads in a thin layer over the yolk sac. This process termed "epiboly", is completed once the entire yolk cell is engulfed by the blastoderm layer (Carvalho, 2007). The blastoderm is a general term, which includes deep cells (endoderm, mesoderm, ectoderm) and the enveloping layer, and an outermost layer of extra-embryonic tissue. The cell arrangement within the blastoderm is as follows: mesoderm and endoderm together form the hypoblast between the yolk syncytial layer and the epiblast; the epiblast comprises cells forming the embryonic layer. Both hypoblast and epiblast are surrounded by the enveloping layer (Figure 1.1)(Carvalho & Heisenberg 2010). The three important germ layers which are present during this early process will later define and give rise to various tissues and organs. The endoderm develops organs of the digestive system and their epithelium such as the gut, liver and pancreasas as well as the lining of the respiratory system. The mesoderm forms somites, muscle, notochord, blood and vasculature endothelium, cartilage of the ribs and vertebrae, dermis and connective tissue. At last, the ectoderm comprises the neural crest, nerve tissue and forms the epidermis (Gilbert & Singer 2006). At the time of 60% epiboly, gastrulation begins in which the three germ layers undergo a dramatic change of re-organisation after which the fundamental body plan of the embryo is formed (Montero et al. 2005). Here the mesoderm and endoderm involute and internalise through the blastopore of the primitive streak, and move towards the animal pole, whilst the ectoderm remains outside. At that stage, the germ ring has formed and the embryonic organiser or "shield" is visible (Kimmel et al. 1990). The molecular drivers that control the onset of vertebrate

gastrulation include gradients of bone morphogenetic proteins (BMPs), Wnt/ β-catenin (Niehrs 2004), and Nodal/TGF-beta signals, such as Squint (ndr1/ sqt) and Cyclops (ndr2/cyc) (Rebagliati et al. 1998; Cells 1998; Erter et al. 1998). Other important signals are fibroblast growth factor (FGF) and retinoic acid (Böttcher & Niehrs 2005; Maden 2002). During mid-gastrulation, cells which do not internalise move towards the dorsal side of the embryo (convergence) and extend along the animal-vegetal pole (extension) resulting in the embryonic anterior-posterior midline defined by the developed notochord from aggregated mesoderm. Shortly after gastrulation, the ectoderm folds above the notochord into a neural plate and neurulation starts, in which neural crest cells are initiated.

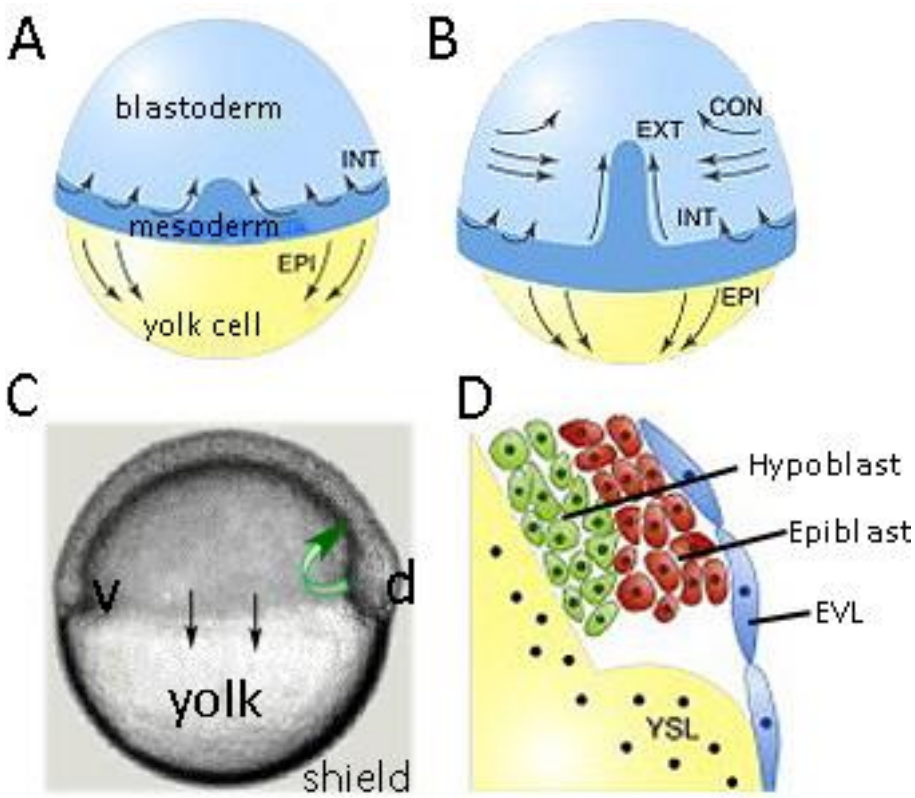

Figure 1.1: Schematic representation of cell movements during gastrulation

Anterior (animal pole) is to the top, vegetal pole is at the bottom (A-C). **A)** During epiboly (EPI) move towards the vegetal pole. At 60% epiboly hypoblast cells internalise (INT) at the margin and migrate towards the animal pole. **B)** At mid-gastrulation, cells converge (CON) towards the dorsal part, which subsequently extend (EXT) towards the animal-vegetal pole to form the anterior-posterior-midline and the embryo. Epiboly and internalisations continues until the blastoderm covers the entire yolk cell. **C)** Shield stage Zebrafish embryo (6 hpf) showing ventral (v, left) and dorsal (d, right) of the anterior-posterior midline. Green arrow indicates internalisation, black arrows symbolise epiboly movement. **D)** Cross section at the blastoderm margin shows the arrangements of yolk syncytial layer (YSL), hypoblast, epiblast and enveloping layer (EVL). Modified after (Carvalho & Heisenberg 2010).

1.3 Neurulation and Neural crest

It is during neurulation that the neural crest makes its first appears. Neural development begins with the formation of a neural plate, which subdivides into three distinct parts, the neuroectoderm, the non-neural ectoderm and the neural plate border. These three individual regions later give rise to the central nervous system, the epidermis and the neural crest cells.

There are two different types of neurulation, primary and secondary (Holmdahl 1932). Primary neurulation occurs in amphibians, mammals and birds within the region of the brain and anterior future trunk (Gammill & Bronner-Fraser 2003). Therein the neural plate folds inwards initially forming a neural groove from which the neural plate borders converge to form the neural tube (Figure 1.2A). Secondary neurulation in mammals occurs normally in the posterior tail region in which mesenchymal cells coalesce into a solid rod (the medullary cord) followed by the formation of the presumptive neuroepithelium. The neuroepithelium then develops a lumen to create the neural tube (Griffith et al. 1992). However in teleosts such as Zebrafish and Medaka, primary neurulation does not occur. Instead, the neural keel extends through the entire length of the embryo. Thereby the neural keel forms through an infolding of the neural plate at the midline, which changes into a neural neural rod in which a lumen is formed through cavitation. The lumen opens up as cells detach from each other along the midline to shape the neural tube (Figure 1.2B) (Miyayama & Fujimoto 1977; Papan & Campos-Ortega 1994; Lowery & Sive 2004). During both types of neurulation, neural crest cells arise from the dorsal midline of the neural tube, go through an epithelial-mesenchymal-transition (EMT) and migrate actively along the medial and dorsolateral pathway (Figure 1.2A) (Gammill & Bronner-Fraser 2003).

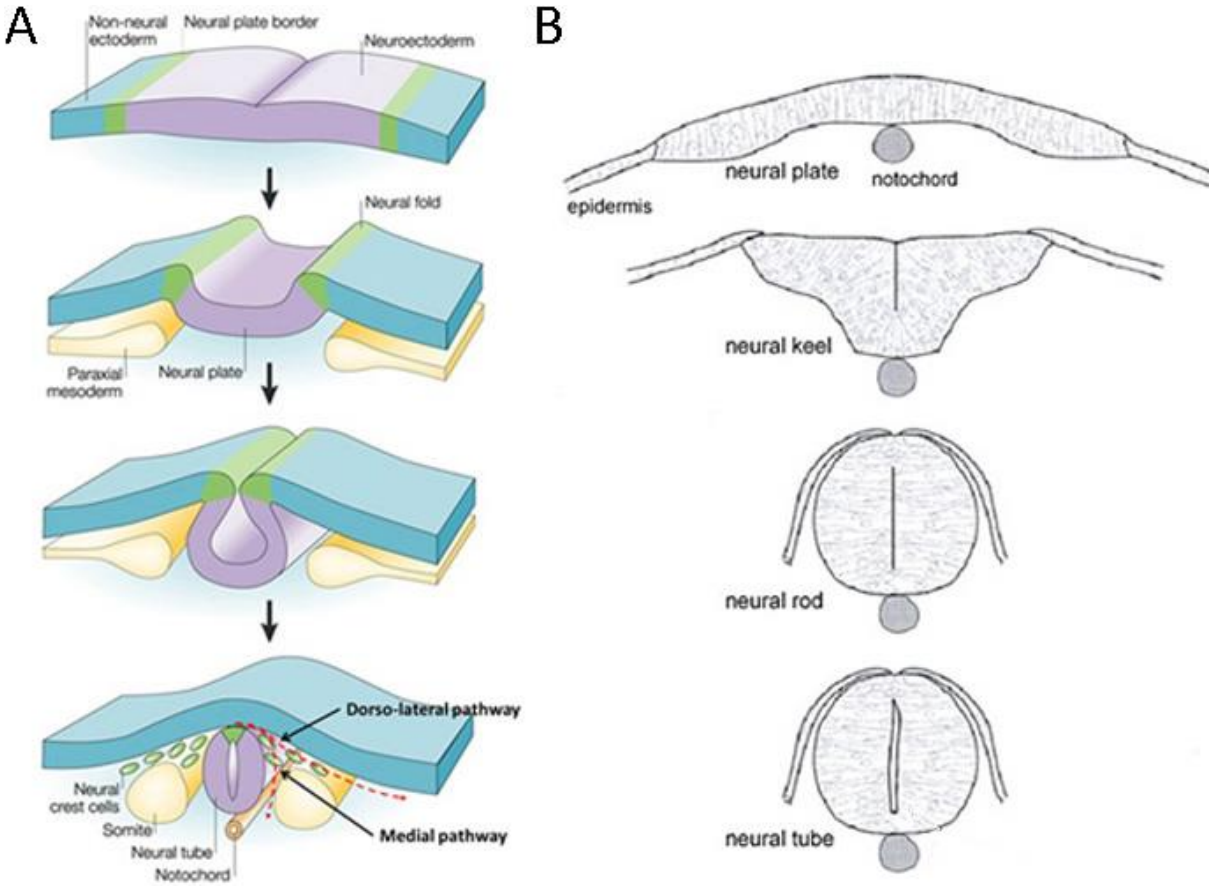

Figure 1.2: Primary and secondary neurulation and induction of the neural crest

Primary (A) and secondary (B) neurulation: A) In primary neurulation the convergence of the neural plate borders creates first a neural fold which then closes up to form the neural tube underlying the non-neural ectoderm above. This process occurs in mammals and birds. B) Secondary neurulation seen in teleosts involves the infolding of the neural plate to form a neural keel which then develops into a neural rod. After mesenchymal cell re-arrangement a lumen is initiated from which the neural tube develops. Neural crest cells arise from the dorsal part of the neural tube in both types of neurulation. After initiation neural crest cell progenitors commit to their derivatives and migrate along the dorsalateral and medial pathways to distant sites within the body (represented in A, red dashed lines). Adapted and modified after (Gammill & Bronner-Fraser 2003) (Papan & Campos-Ortega 1994).

1.4 Molecular initiation of neural crest, delamination and derivatives

The induction of the neural crest comprises three major pathways, bone morphogenetic (BMP), fibroblast growth factors (FGF) and the Wnt signalling pathway (LaBonne & Bronner-Fraser 1998). Intermediate levels of BMP within the paraxial mesoderm are established through BMP antagonists such as chordin, noggin and follistatin. This gradient is one of the events thought to mediate NC induction at the neural plate borders (Marchant et al. 1998). Fibroblast growth factors such as fgf2

combined with BMP anatgonists can induce NC markers (Mayor et al. 1997), whereas fgf8 secreted from the paraxial mesoderm is sufficient to cause neural crest induction (Monsoro-Burq et al. 2003). Furthermore Wnt signalling, especially the canonical β-catenin-dependent pathway from the adjacent non-neuronal ectoderm and underlying mesoderm has been shown to be essential for NC induction (García-Castro et al. 2002; Lewis et al. 2004). In addition studies in frog and chick demonstrated the involvement of Delta-Notch in the promotion and restriction of neural crest formation to the neural plate border (Endo et al. 2002). Together, BMP, FGF, Wnt and possibly Notch then activate transcription factors, the so called neural plate border specifiers Zic, Msx1/2, Pax3 and Pax7 within the neural plate border (Spengler & Bronner-Fraser 2008; Bae et al. 2014). Together they synergistically trigger expression of transcription factors described as neural crest specifiers including foxd3, id, slug/snail, twist, sox9 and sox10 to name a few (Donoghue et al. 2008). Together, these neural crest specifiers define neural crest progenitors, which then delaminate from the dorsal neural tube via epithelial-mesenchymal transition (EMT) and migrate onto specified pathways within the body: the medial and the dorsolateral pathway (highlighted in Figure 1.2A).

During and after cell migration, the neural crest differentiates into numerous cell types, grouped into the non-ectomesenchymal and ectomesenchymal lineages. Ectomesenchymal lineage derivatives include bone, connective tissue, cartilage and dentine. Non-ectomesenchymal derivatives comprise neurons, glia and diverse pigment cells (chromatophores) (Figure 1.3) (Donoghue et al. 2008). They also form and contribute to secretory cells and the outflow of the heart (Gammill & Bronner-Fraser, 2003). During migration neural crest cells are influenced and interact actively with surrounding extracellular matrix components for instance cadherins, integrins, matrix metalloproteases (ADAM-10) and chemoattractants such as semaphorin and ephrins, which help to regulate directed cell migration (Mayor & Theveneau, 2013; McKeown et al. 2013; Santiago & Erickson, 2002).

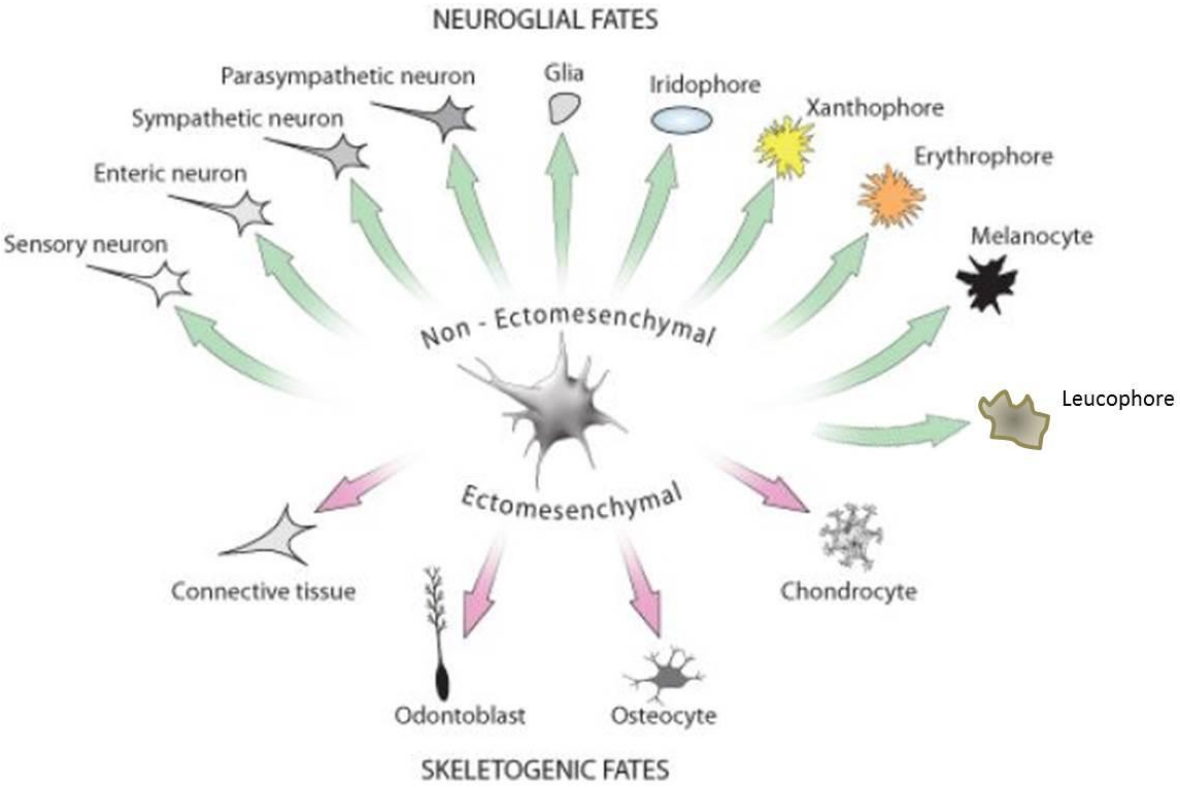

Figure 1.3: Cell derivatives derived from the neural crest

Neural crest derivatives form from an early neural crest progenitors into non-ectomesenchymal and ectomesenchymal lineages which then further split apart into specific cell fate derivatives. Modified after Donoghue et al. 2008.

1.5 Teleost pigment cell development

In birds and mammals the neural crest develops into only one pigment cell type, the melanocyte; black, brown or pale in colouration (Uong & Zon 2010). In contrast, pigmentation patterns in teleosts are made from up to five chromatophore cell types. Zebrafish have black melanocytes, orange xanthophores, silver-reflective iridophores (Kelsh 2004) and a few white leucophores in adult tail fins (RN Kelsh pers. comm.). Medaka fish however develop a higher number of leucophores already during embryogenesis. Another cell type, cyanophores, also found in some teleosts, develops a blue biochrome and is only present in some species such as mandarinfish (Kelsh et al. 2004). The migration of chromatophores takes place on the medial and dorsolateral pathway as mentioned above. The final pigment pattern in Zebrafish and Medaka embryos consists of three distinct melanocyte stripes: the dorsal, lateral, and ventral stripe (Appendix 1). The fourth melanophore stripe in Zebrafish is the Yolk Sac Stripe which is replaced by a cluster of melanocytes on the yolk sac in Medaka (Lamoreux et al. 2005). Xanthophores and iridophores are predominantly located dorsally with some cells scattered along the lateral and ventral stripe (Kelsh et al. 2000b). In contrast, in

Medaka a minor population of iridophores are located within the lateral stripe. In addition, leucophores are very closely associated with melanocytes and are located within the ventral head and in the dorsal stripe (Lamoreux et al. 2005; Nagao et al. 2014). The neural crest specifier SRY-related HMG-box 10 (Sox10) has been shown to control the neural crest non-ectomesenchmal cell fate and specifically influence the development of all three major pigment cell types in Zebrafish (Kelsh & Eisen 2000).

1.5.1 Melanocyte development

Mammals and birds develop only one kind of neural crest derived pigment cells, the melanocyte. Those black or brown melanocytes in colour produce two kinds of pigment: black/brown eumelanin and red/yellow pheomelanin (Kinoshita et al. 2009). However lower vertebrates such as Zebrafish and Medaka only synthesise eumelanin (Kelsh et al. 2000). Melanocytes develop from melanoblasts, an unpigmented precursor. Their migration away from premigratory neural crest positions leads them onto two pathways, the dorsolateral and the medial pathway. While they migrate towards their final destination within the embryo they differentiate and begin to produce melanin packed into organelles called melanosomes (Kelsh et al. 2000).

The transcription factor SRY-related HMG-box 10 (Sox10) is one of the melanocyte specifiers in Zebrafish (Kelsh & Eisen 2000; Dutton et al. 2001). The receptor tyrosine kinase Kit and its ligands may play a role in melanocyte proliferation as well, as mice studies have shown that homozygous mutations in *kit* led to decreased fur colouration as well as germ cell and haematopoietic cell defects (Mackenzie et al. 1997). Kit regulates the phosphorylation status of *microphthalmia transcription factor* (*mitf*) via the Ras-Raf-Map kinase pathway in mammalian melanoma cell cultures (Hemesath et al. 1998; Price et al. 1998) making it therefore an essential factor during melanocyte development in Zebrafish (Van Otterloo et al. 2010). Supporting this, the Zebrafish c-kit homologue mutant sparse (spa) suggests a conserved role for *kit* in melanophore survival, proliferation and dispersal (Parichy et al. 1999; Kelsh et al. 2000b). The *microphthalmia transcription factor (mitf)* is known to be the master regulator of melanocyte development (Uong & Zon 2010). *Mitf*, a basic helix-loop-helix leucine zipper (BHLH-Zip) transcription factor, regulates the expression of melanogenic enzymes including *dopachrome-tautomerase (Dct*), *tyrosinase-related protein 1 (tyrp1),* the melanosome structural protein *silver (si)* and *tyrosinase (tyr),* which is a transmembrane protein in melanosomes controlling oxidation levels and production of melanin (Hodgkinson et al. 1993; Lister et al. 1999). The melanocyte-specific *dopachrome tautomerase* (*Dct*) has been used in this study to label melanocyte precursors and track melanoblast migration *in vivo*. *In vitro* studies in mouse melanoma cells have shown that *dopachrome tautomerase* (*Dct*), also known as *tyrosinase-related protein 2*

(*Trp-2*) resides in the melanosome plasma membrane part of the eumelanin biosynthetic pathway by catalysing dopachrome to 5,5-dihydroxyindole-2-carboxylic acid (DHICA) in melanogenic cells (Körner & Pawelek 1980). *Dct* transcription is regulated directly or synergistically by Pax3, Sox10 and microphthalmia transcription factor (Mitf) through a responsive sequence site on its promoter (Jiao et al. 2006; Kelsh & Schmid et al. 2000). It is known as one of the earliest markers labelling the melanocyte lineage in Zebrafish. *Dct* presence is notable at around 16 hpf (14-19 somites), first in progenitors of the early pigmented retinal epithelium (PRE) in the developing eye and then 5 hours later througout the outer layer of the retinal epithelium and within trunk and tail melanoblasts (Kelsh et al. 2000). In contrast, Medaka studies report *Dct* expression at 75 hpf (st.30) (Nagao et al. 2014). Earlier stages have not yet been described.

1.5.2 Xanthophore development

Xanthophores migrate exclusively on the dorsolateral pathway (Parichy et al. 2000; Kelsh 2004). They contain pteridine and carotenoid pigments, giving them a yellow-orange appearance. Pteridine pigments are visible by autofluorescence under UV light around 35 hpf and are visibly abundant by 42 hpf in the trunk of Zebrafish embryos (Greenhill 2008; Kelsh 2004). Published lineage markers for xanthophore development and differentiation are the enzymes *GTP-cyclohydrolase I (gch)* and xanthine dehydrogenase (*xdh*), both required for pteridine synthesis. *Gch* converts guanosine triphosphate (GTP) to dihydroneopterin triphosphate and then into tetrahydrobiotin (BH4), a source for sepiapteridine pigments in xanthophores (Pelletier et al. 2001). BH4 also functions in eumelanin synthesis and helps to convert phenylalanine to tyrosinase as a co-factor for phenylalanine hydroxylase. Thus *gch* is also expressed within early melanoblasts of Zebrafish (Parichy et al. 2000). The main pathway in which xanthine dehydrogenase (*xdh*) is involved is not yet characterised in detail. However, it seems that *xdh* transforms and degrades pterins and is involved in molecular changes during pteridine synthesis (Ziegler 2003).
In Medaka differentiated xanthophores are scattered over the trunk region with more cells dorsally than within the lateral stripe. They are first observable at 6 dpf, but can be seen earlier under UV light. Unlike in Zebrafish, *gch* and *xdh* are markers for both xanthophores and leucophores and appear not to be in melanoblasts (Nagao et al. 2014).

1.5.3 Leucophore development

Leucophores are of dull to cream-white appearance (Lamoreux et al. 2005). When exposed to wavelengths oflight between 488 and 600nm they are visible by autofluorescence (personal

ovservation). As far as we know, in Medaka, the migration pathway of leucophores has not been described.. However, leucophores are closely associated with melanocytes on the dorsal midline similar to iridophores in Zebrafis, therefore it is possible that leucophores migrate on the medial pathway as well (Nagao et al. 2014). Their appearance results from intracellular uric acid organelles based on similar purine-related substances such as guanine and hypoxanthine in iridophores (Hama 1975). Later in development leucophores seem orange/gold because of an accumulation of drospterin (Oliphant & Hudon 1993). They first appear in the ventral head of 2 days old Medaka around stage 23 (personal ovservation), then form six bilaterally symmetrical spots at stage 25. By 5 dpf they have formed a continuous lateral stripe in close association with melanocytes (Lamoreux et al. 2005). Medaka leucophores also express the xanthophore markers *gch* and *xdh* (Nagao et al. 2014), which supports observations that both of these cell types contain pteridine pigments (Braasch et al. 2007). So far, it has been shown that on the genetic level, *slc2a15* and *slc2a11b* play an important role for pteridine synthesis as Medaka mutants *lf (slc2a15b)* and *wl (slc2a11b).* Both show defects in pteridine containing xanthophores and leucophores (Kimura et al, unpublished data Nagao et al. 2014). Recent studies by (Nagao et al. 2014) demonstrated that xanthophores and leucophores share a common progenitor, in which sox5 can act as a regulator to control the fate switch between those two lineages.

1.5.4 Iridophore development

We mention iridophores here only very briefly since they are not a focus for this thesis. Iridophores migrate within the medial pathway to their final destination - predominantly the dorsal stripe with some scattered cells above the eye as well as in the lateral and ventral stripe (Kelsh 2004; Greenhill & Kelsh 2008). Their shiny iridescent appearance results from reflective guanine platelets visible around 40 hpf in Zebrafish (Kelsh 2004). In Medaka, Iridophores are not as abundant as in Zebrafish. At 5 dpf, the first patches of iridescent cells appear above the eye and within the lateral stripe. They increase in cell number until hatching stage and overlap partly with xanthophores resulting in a golden yellow appearance (Lamoreux et al. 2005). In Zebrafish, they can be detected by markers such as *leukocyte tyrosinase kinase* (*ltk*), which play vital roles in this cell type (Parichy et al. 2000; Lopes et al. 2008). Iridophore specification is promoted by *foxd3* repressing *mitfa* expression, which indicates melanocytes and iridophores originate from a common precursor in Zebrafish (Curran et al. 2011).

1.6 Migration of neural crest cells

The migration of neural crest cells is largely controlled by factors directing migration and permissive factors of the extra-cellular matrix such as fibronectin, laminin and collagen which help to guide migrating cells along their respective pathways (Perris & Perissinotto 2000; Singh et al. 2010; McKeown et al. 2013). Neural crest cells migrate in large numbers, with multiple mechanisms regulating their route and terminal location, including chemotaxis, contact-inhibition locomotion and cell sorting.

1.6.1 Signals guiding NC migration in the head

The cranial neural crest (CCNC), including the cardiac NC, form in the neural plate from the diencephalon to the fourth somite (Mayor & Theveneau 2013). They contribute to a vast range of derivatives in the face and neck including the periocular skeleton around the eye, cartilage, a subset of pigment cells and the trigeminal ganglia (Le Douarin et al. 2004). In the hindbrain, neural crest emerges in an alternating fashion adjacent to rhombomere 2, 4 and 6 from which they form 3 discrete migratory streams. These ventrally-migrating neural crest cells either accumulate to form the cranial ganglia or they invade the branchial arches adjacent to rhombomere 2, 4 and 6 and form craniofacial jaw bones, as well as giving rise to cardiac ganglion and the outflow tract of the heart (Le Douarin & Kalcheim 1999).

The Ephrin (Eph) subfamily of the receptor tyrosine kinases (RTKs) and their ephrin ligands have been described as regulators during CNCC migration. Migrating cranial NCCs have been shown to express Eph receptors, which are directed to their target sites by branchial arch expressing ephrin-B2 cells (Adams et al. 2001). Neural crest cell migration towards the second branchial arch is impaired in mouse mutants, lacking ephrin-B2, indicating a NC delamination defect within the neural tube of rhombomer 4/6 (Adams et al. 2001). The ligand ephrin-B1 has also been shown to have a role in directing NC migration into branchial arches as ephrin-B1 mouse mutants display a cleft palate (Davy et al. 2004).

In addition, neuropilin-1 knockdown in chick NCCs results in a complete failure to invade the branchial arches, although the cells remain organised into distinct streams (McLennan & Kulesa 2007). Another study has shown that neuropilin-2 receptor is expressed in neural folds and migrating cranial neural crest. Its repulsive semaphorin-3 ligand is expressed in a rhombomeric alternating pattern in mice. Both are essential to guide neural crest cells through the cranial mesenchyme dorsal

to branchial arch 1 and 2 to form the trigeminal ganglion (Gammill et al. 2007). In addition semaphorin 3C has been shown to be involved in cranial neural crest migration towards the outflow tract of the heart as highlighted in mutant mice (Feiner et al. 2001).

To guide and direct cranial neural crest, several studies suggest the involvement of positive guidance cues such as stromal cell-derived factor 1 (Sdf1 also named Cxcl12), vascular growth factor (VEGF), FGFs and glial cell-derived neurotrophic factor GNDF).

Chemoattraction through stromal cell-derived factor (Sdf1) within the pharyngeal arch endoderm and optic stalk is a necessity for craniofacial development in *Xenopus* embryos (Theveneau et al. 2010). Whereas in Zebrafish it seems that a localised source and strict balance of Sdf1b signalling is required solely for directed and organised cranial NCC migration and not for overall cephalic NCC development (Killian et al. 2009).

Studies in chick have shown that cranial neural crest requires vascular growth factor (VEGFA) to migrate adjacent to rhombomere 2 to populate the 2nd branchial arch. However, it remains open how VEGFA functions adjacent to other rhombomeres (McLennan et al. 2010). Another group of factors controlling cranial NC migration are members of the fibroblast growth factors (FGF). *In vitro* organ plant cultures suggest that FGF2 functions as chemoattractant for mesenchephalic neural crest cells (Kubota & Ito 2000).

Lastly, hindbrain vagal neural crest cells form the majority of enteric neurons throughout the entire gut - in mice, they populate the entire gut within 5 days. In parallel, sacral trunk NCC's delaminate and migrate ventrally to form extrinsic pelvic ganglia next to the hindgut from where they enter to contribute to enteric neurons and glia (Sasselli et al. 2012). One of the factors regulating this process seems to be the glial cell-derived neurotrophic factor (GDNF). Cultures of mouse tissue explants demonstrated the chemoattractive properties of GDNF promoting colonisation of enteric neural cells as well as directed axon outgrowth within the gastrointestinal tract (Young et al. 2001).

1.6.2 Signals guiding NC migration in the trunk

Trunk neural crest arises caudal to the fourth somite and form pigment cells, dorsal root and sympathetic ganglia of the peripheral nervous system and the endocrine cells of the adrenal gland (Mayor & Theveneau 2013). As mentioned earlier trunk neural crest cells delaminate from the embryonic neuroectoderm and disseminate onto two distinct pathways through the trunk region

namely the dorsolateral and ventromedial pathways to form the peripheral nervous system as well as pigment cell pattern (Kelsh et al. 2009). The dorsolateral pathway is exclusively used by pigment cells and the ventromedial pathway by pigment cells and neural crest cells forming the peripheral nervous system (Kuo & Erickson 2010).

1.6.2.1 Ventromedial pathway

Studies in mice have shown that neuropilin (NRP) 1 or 2 receptors and their ligands class 3 semaphorin (SEMA3) play an important role in restricting peripheral neural crest neurons to their designated ventromedial pathways in mouse and chick. In detail, the NRP1 and SEMA3A prevent a first wave of trunk NCCs from entering an intersomitic niche and restricting them to the ventromedial pathway (Schwarz & Maden et al. 2009). During a second wave, the receptor NRP2 is expressed to the anterior part of the neural crest, whereas the ligand SEMA3F is located within the posterior somitic region, which results in NC repulsion from the posterior half and limits them to the anterior part of the sclerotome (Gammill et al. 2006; Schwarz & Maden et al. 2009).

In addition, Ephrin receptors and their ligands seems to have an inhibitory role in neural crest guidance in the trunk regions. Studies in chick, mouse and rat embryos showed that EphB3 receptors are expressed by NCCs in the anterior half of the somites, whereas the transmembrane ligand ephrin-B1 and –B2 are expressed within the posterior region of the sclerotome (Theveneau & Mayor 2012). This pattern leads to NCCs entering the anterior half, but avoiding the posterior half of each somitic sclerotome during migration on the medial pathway (Krull et al. 1997). The repulsive ability of ephrin-B1 and -2 was confirmed *in vitro* where NCCs explicitly avoided lanes coated in ephrin-B1. In addition *in vivo* studies confirmed that ephrin-B1 addition in ectopic positions disrupts segmental migration of NCCs within the sclerotome (Krull 1998).

Furthermore, endothelin-3 is expressed by the endoderm and dermomyotome, whereas endothelin receptor EDNRB is expressed by neural crest cells stimulating ventral migration through somites and inhibiting early entry to the dorsolateral pathway at the same time (Kuo & Erickson 2010).
The ventromedial pathway also expresses stromal-derived factor-1 (Sdf1), which is required for neural precursor expressing the receptor CXCR4 to migrate and coalesce into dorsal root ganglia (DRG) within the mouse spinal cord region (Belmadani et al. 2005). In comparison, in chick it is only expressed by DRG precursors of the sympathetic ganglia.

Lastly, trunk neural crest cells expressing Robo 1 and 2 receptors and are exposed to Slit ligands in the ventral mesenchyme acting as chemorepellents. The combination of both has the potential to selectively inhibit caudal NC from populating the gut, while stimulating vagal NC to do so during the first wave of the ENS formation (De Bellard et al. 2003). Slit expression within the dermomyotome also seems to repel NCCs form early migration onto the dorsolateral pathway. When Robo receptors were upregulated neural crest cells were able to choose the dorsolateral pathway prematurely or ectopically (Jia et al. 2005).

1.6.2.2 Dorsolateral pathway

The migration of neural crest cells on both pathways in mice seem to happen at the same time, whereas in chick the migration onto the dorsolateral starts with a 24 h and in Zebrafish with a 5 h delay after first NCCs enter the ventromedial route (Kelsh et al. 2009). Regulators, including ephrin/Eph and endothelin signalling control the migration of neural crest cells along the dorsolateral pathway lying beneath the ectoderm.

In chick, melanocytes have been shown to express EphB2 receptors, resulting in melanocytes being attracted to ephrin-B1 ligands along the dorsolateral route in contrast to the ventromedial pathway in which NC gets repelled (Santiago & Erickson 2002). Therefore, ephrin-B seems to be bifunctional as it first repels neural crest cells from migrating along the dorsolateral pathway too early, and later promotes this same migration.

Neural crest cells migrating ventrally express EDNRB preventing simultaneous entry onto the dorsolateral pathway. Later, neural crest cells within the melanocyte lineage downregulate EDNRB and upregulate EDNRB2. This switch in receptors allows them to migrate along the dorsolateral route (Kuo & Erickson 2010). In 2008 Harris et al. demonstrated through shRNA knockdown experiments that the level of receptors expressed by melanocytes on the dorsolateral pathway is important to overcome repulsive and non-permissive cues. Consequently, the specific presence of either EphB2 or EDNRB2 is not the crucial factor as either of them is redundant when the other one is overexpressed. Finally in mouse, melanocytes migrate along the dorsolateral pathway between the dermatome and the overlying ectoderm following the invasion of the dermis and accumulation in hair follicles (Slominski & Paus 1993). To do that, they require the combination of chemokines, for example CXCR4 receptors in melanoblasts are attracted by Sdf-1 ligands which are abundant in the dermis, and thus act in guiding migration (Belmadani et al. 2009).

1.6.3 ECM components and adhesion molecules affecting neural crest migration

Collective studies from mouse and chick suggest that the main ECM components influencing cranial and trunk neural crest migration are laminins, fibronectin, collagen I and collagen IV, proteoglycans, vitronectins, versicans and hyaluron (Duband & Thiery 1987; Sternberg & Kimber 1986; Trainor 2013). The importance of the ECM during neural crest cell migration and advances of the research in this particular field is highlighted below.

Laminin isoforms 1 and 8 seems to be important for the onset of neural crest migration, whereas fibronectin might be an overall important soluble component for NC migration shown by *in ovo* blocking with antibodies or shRNA inhibition (Perris & Perissinotto 2000). However, cranial and trunk neural crest in *Xenopus* seem to prefer fibronectin above laminin as substrate, although both permissive molecules can efficiently support adhesion during migration (Alfandari et al. 2003).

Integrin receptors have been studied extensively *in vitro* in regards to their cell adhesion ability. This revealed that migrating crest cells express at least 7 integrins: $\alpha3\beta1$, $\alpha4\beta1$, $\alpha5\beta1$- $\alpha8\beta1$, $\alpha v\beta1$, $\alpha v\beta3$, $\alpha5\beta5$ and $\beta8$ (McKeown et al. 2013). The relevance for integrins *in vivo* is less well understood and has mostly been studied in chick embryos. For example integrin $\alpha7\beta1$ is expressed within a subpopulation of trunk neural crest cells which mediates migration on substrates such as fibronectin, laminin and vitronectin (Kil & Bronner-Fraser 1996). The exact functional partnership of integrins with other ECM components have been shown as follows in chick: integrin $\alpha v\beta3$ binds to fibronectin, vitronectin and laminin; $\alpha5\beta5$ binds to vitronectin and overall the $\beta1$ subunit interacts with $\alpha4$, $\alpha3$ and $\alpha8$ to promote migration on fibronectin and laminin-1 (reviewed by McKeown et al. 2013). However, alpha and beta subunits as well as different isoforms are possibly functionally redundant as knockout of $\alpha1$ and $\beta1$ integrin subunits in mice had no neural crest migration defect (Gardner et al. 1996).

Additionally, recent studies have demonstrated that a number of Metalloproteases (MMPs) and ADAMs could play an important role in cell adhesion. Specifically a gradient of MMP-2 has been observed in migrating cranial neural crest in chick, in which only leading cells express MMP-2 (McLennan et al. 2012). Another member, MMP-9 seems to play a role in delamination and migration events as well, since decreased levels reduced migration; conversely overexpression in *in vitro* cultures enhanced it. Substrates for MMP-9 included laminin and to a lesser degree, N-Cadherin (Monsonego-Ornan et al. 2012). Functions of ADAM-13, an ADAM family member, include cleavage of Cadherin-11 and fibronectin, therefore remodelling the extracellular matrix for efficient cell

migration. Studies have shown that the nuclear translocation domain of ADAM-13 in *Xenopus* seems to be essential for promoting cranial neural crest migration *in vivo* but could not be replicated *in vitro* indicating that ADAM-13 could be required for remodelling the ECM environment for neural crest cells (Cousin et al. 2012). Supplementary to this, ADAM-13 and ADAM-19 might share redundant functions as knockdown of both components together caused a stronger defect in NC migration in mouse compared to inhibiting them individually (Cousin et al. 2011).

The chondroitin sulfate proteoglycans versican, mainly isoform variant V0 and V1 have been shown to be expressed within the caudal region of the sclerotome acting in a repulsive manner towards early neural crest migration whilst directing them to their appropriate target tissue (Dutt et al. 2006; Perissinotto et al. 2000; Landolt et al. 1995). One example of the effect versican has on neural crest migration can be found in the Pax3 mouse mutant (Moase & Trasler 1992). The Pax3 mouse mutant *splotch* is associated with a defect in neural crest migration leading to pigmentation abnormalities, altered number or size of dorsal root ganglia and a defect in the outflow tract of the heart (Serbedzija & McMahon 1997). Splotch mice also show increased levels of versican V1 and presumably V2, which seems to correlate with the absence of NC migration (Henderson et al. 1997). Controversially, isolated neural crest cells are able to migrate *in vitro* and minor population of cranial NCCs forming small streams still remains *in vivo*, which might suggest that decreased cell migration is not cell autonomous to the lack of Pax3, but rather is due to the extracellular environment (Conway et al. 1997). In addition, overexpression of Pax3 in a human medulloblastoma cell line increased levels of spliced V2 and a decreased V3 variant (Mayanil et al. 2001). The correlation of versicans and Pax3 might explain the *splotch* mutant phenotype; and provides evidence for the regulatory importance of low levels of versicans within the extracellular matrix surrounding migrating neural crest cells.

Furthermore recent morpholino knockdown studies have shown that hyaluron synthase XHas2 influences directionality and motility of trunk neural crest cells *in vivo* of *Xenopus* embryos (Casini et al. 2012) and has been shown to play a role for CNCC migration through binding to the cell surface marker CD44 (Ori et al. 2006).

Lastly, transmembrane protein cadherins type I and II, which classically interact intracellularly with catenins, have been implicated in neural crest development and migration. For instance, cadherin6 is found to be expressed in mouse NCCs during delamination and migration (Inoue et al. 1997), whereas in chick cadherin7 is expressed mainly in migrating trunk neural crest cells forming dorsal root ganglia (Nakagawa & Takeichi 1995). In addition cadherin11 is expressed in *Xenopus* cranial

neural crest where inhibition led to a failure of NCCs invasion beyond the second branchial arches (Kashef et al. 2009).

1.7 Models of human neural crest diseases

1.7.1 Teleost models of Melanoma

NCCs migrate extensively during embryogenesis in a manner similar to metastasis. Indeed cancers of NC-derived cells may be particularly prone to metastasis since embryological origin predisposes them to express migratory properties. On the other hand, they might reverse to a more progenitor cell state and therefore exhibit full potential for cell transformation properties. One highly metastatic disease with a cell type originating from neural crest progenitors is melanoma (Uong & Zon 2010). Malignant melanoma is the most aggressive form, which can be cured if excised at an early stage. However once melanoma metastasises to distant organs, the median survival of melanoma patients drops below 9 months (Gogas et al. 2007). Although melanoma accounts for only 4 percent of all dermatological cancers, it is responsible for 80 percent of deaths from skin cancer; only 14 percent of patients with metastatic melanoma survive for over five years (Miller & Mihm 2006). Melanocyte transformation can occur either from *de novo* single melanocytes or from an already existing naevi, such as dysplastic or giant congenital naevi (Clark et al. 1984). The severity and progression of melanoma is pathologically described in thickness by the Clark level or Breslow thickness, but is commonly described as a step-wise categorisation: nevus, dysplasia, melanoma with radial growth phase, vertical growth which is associated with the invasion of the basal membrane and subsequently metastasis (Clark et al. 1984). Melanocytic transformation is thought to occur through sequential accumulation of genetic and molecular alterations. The transformation itself is thought to happen on a cellular level through either genetic (gene mutations, deletion, amplifications or translocation) or epigenetic (a heritable change other than in the DNA sequence, generally transcriptional modulation by DNA methylation and/or by chromatin alteration such as histone modification) (Gruber et al. 2008). As a result, melanocytic clones acquire a growth advantage over surrounding cells.

Several molecular signalling pathways have been shown to either regulate melanoma tumour growth or be required to initiate primary melanocyte transformation. One of the main pathways is the MEK pathway, which is constitutively activated by a mutation of either BRAF or NRAS leading to constitutive phosphorylation of cytoplasmic serine–threonine kinases. Substitution of glutamic acid to valine at residue 599 (referred to V600E) in BRAF is the most frequently mutated defect and seen in 50-60% in melanoma tumours (Davies et al. 2002). Somatic N-Ras mutations occur in around 15%-

25% of melanomas usually in form of substitution of leucine for glutamine at residue 61 of NRAS (Albino et al. 1989). This alteration leads to an inhibition in GTP hydrolysis and constitutive protein activation (Dahl & Guldberg 2007). However, in human BRAF and NRAS mutations have also been found in naevi, which suggests that BRAF and NRAS is necessary for the initial melanocytic development and/or maintanance, but not for the actual transformation into a cutaneaous melanoma. This implies that the activation of MAPK signalling is a necessary event for melanoma development, but this does not initiate malignant transformation (Kumar et al. 2004).

Zebrafish and Medaka provide an excellent model for studying cancer because of advantages such as genetic modifications and easy husbandry. The first teleost melanoma model was reported in the 1920s when certain hybrids of *Xiphosphorus maculatus* and *Xiphosphorus hellerii* were backcrossed and developed spontaneous melanoma (Mione & Trede 2010; Dimitrijevic et al. 1998). Subsequent gene mapping yielded the *Xiphophorus melanoma receptor kinase (Xmrk),* which is homologous to the human epidermal growth factor (EGF) receptor (Wittbrodt et al. 1989). The oncogenic potential of Xmrk results from an altered 5' upstream sequence harbouring two mutations causing receptor activation and ligand-independent intracellular signalling (Meierjohann & Schartl 2006).

Several teleost melanoma models have been established since which mostly rely on overexpression of oncogenes under tissue-specific or ubiquitous promoters (Mione & Trede 2010). Most of these are tabulated below (Table 1.1).

Table 1.1: Melanoma teleost models

Melanoma model	**NC promoter**	**Gene**	**Onset of melanoma**	**Reference**
Zebrafish	Mitf promoter	$BRAF^{V600}$ transgenic in $p53^{-/-}$ background required	4 months	Patton et al. 2005
Zebrafish	Mitf promoter	$HRAS^{G12V}$	6 months (can be accelerated with $p53^{-/-}$	Michailidou et al. 2009
Zebrafish	Kita promoter	(eGFP)-HRASV12 transgenic	3-4 weeks	Anelli et al. 2009; Santoriello et al. 2010
Medaka	Mitf promoter	Xmrk (oncogenic receptor tyrosinase	2-6 weeks	Schartl et al. 2010

		kinase), mutated EGF receptor		

1.7.2 Mammalian and teleost models of Neurocristopathies

Problems of neural crest cell fate specification and migration form the basis of a variety of congenital diseases either including pigmentation and hearing loss called Waardenburg syndomes type I-IV or defects of the colon and rectum, such as in Hirschsprungs's disease (Mayor & Theveneau 2013). Neural crest deficiencies resulting in abnormalities of pigmentation and deafness are called Waardenburg syndrome, which can be categorised into four types (Table 1.2), some of which include additional syndromes of Hirschsprung's disease. Hirschsprung's disease (HD) was described in 1888 by Harald Hirschsprung and affects 1 in 5000 live births today. It is characterised by aganglionosis in the submucosal and myoenteric plexus due to a failure of neural crest cell migration, proliferation, differentiation or survival during the development of the enteric nervous system (ENS). The impaired enteric nervous system leads first to malfunctional contraction, whereas a complete lack causes permanent closure of terminal bowel largely within the proximal rectum that results in widening of the bowel, hence the term 'congenital megacolon' associated with HD.

Table 1.2: Types of Waardenburg syndrome with phenotypic and genetic characteristics as well as main animal models

Type	**Characteristic features**	**Genetic mutations**	**Animal model**	**Reference**
Waardenburg syndrome type I (WS1)	Pigment abnormalities, Appearance of a widened nasal bridge due to a lateral displacement of the inner eye canthi (dystopia canthorum), deafness	Pax3 (autosomal-dominant)	*Splotch* mice (*sp* – Pax3 gene)	(Moase & Trasler 1992; Serbedzija & McMahon 1997)
Waardenburg syndrome type II (WSII)	Pigment abnormalities, deafness (due to loss	Mitf, Slug, Sox10 (autosomal-	*Nacre* Zebrafish (*mitf*) *Slug-/-* mice	(Tassabehji et al. 1994; Nobukuni et al. 1996; Lister

	of melanocytes within the ear)	dominant)	(possibly)	et al. 1999; Bondurand et al. 2007)
Waardenburg syndrome type III (WS III; Klein-Waardenburg syndrome)	WS I defects and additional musculoskeletal abnormalities such as Upper limb defects ,hypoplasia, flexion contractures, fusion of the carpal bones, syndactyly	*PAX3* $^{-/+}$; $^{-/-}$ mutations described in human (autosomal-dominant)	- (maybe Pax3 mouse?)	(Tremblay et al. 1998; Zlotogora et al. 1995)
Waardenburg syndrome type IV (WS IV; Waardenburg-Shah syndrome)	WS4 or Waardenburg-Shah syndrome has features of Hirschsprung's disease in addition to WS2	*Sox10, Edn3* and *Ednrb*	*Colourless* Zebrafish (*cls* – Sox10); Piebald-lethal mice (s^1- Ednrb gene); *Lethal spotting* mice (*ls*- Edn3 gene); Dominant megacolon mice (Dom –Sox10 gene); Japanese Fancy mouse 1 (JF1 – Ednrb gene) (autosomal recessive or dominant depending on the gene)	(Bondurand et al. 2007; Edery et al. 1996; Carney et al. 2006; Kapur et al. 1995; Tachibana et al. 2003; Koide et al. 1998; Kikkawa et al. 2001; Herbarth et al. 1998; Dutton et al. 2001; Elworthy 2003; Elworthy et al. 2005)

1.8 Mutant screen and identification of *hirame* phenotype

To date, the majority of large-scale genetic studies have been confined to forward genetics in Zebrafish (Driever et al. 1996; Kelsh et al. 1996; Haffter et al. 1996), in which the genetic basis of a given phenotype is characterised, whilst in reverse genetics, the phenotype associated with a given allele is characterised. Zebrafish has several advantages such as cost-effective husbandry, large quantities of offspring and easy micro-manipulation of translucent fish embryos; benefits found in the Japanese rice fish Medaka (*Oryzias latipes*) as well. Yet Medaka is evolutionary distant from Zebrafish, and differences in functional overlap of genes between the two species permits identification of mutations as yet unknown in Zebrafish.

In 2004, Furutani-Seiki et al. published mutants established in a random mutagenesis screen using a forward genetics approach. This was the first large scale mutagenesis screen in Medaka (*Oryzias latipes*). As in the Zebrafish screen, mutagenesis was induced in sperms using N-ethyl-N-nitrosourea (ENU), which were then cryopreserved and progressively screened for distinct phenotypes such as organ malformations induced by the resulting point mutations in the DNA sequences. Resulting from this large screen, a unique mutant named *hirame* with a mutation on allele j50-20C was first described (Furutani-Seiki et al. 2004; Watanabe et al. 2004; Kitagawa et al. 2004). Furutani-Seiki describes *hirame*$^{j50\text{-}20C}$ as mutant with a defective converging subset of cells towards the dorsal axis in which the cellular movement in the hypoblast is drastically impaired resulting in reduced dorso-ventral thickness of the tissue along the body axis. In parallel, Watanabe describes *hirame*$^{j50\text{-}20C}$ mutants as phenotypically flat with coinciding liver defects and terminally embryonic lethality. A general failure to develop the correct liver size possibly resulted from initial misalignment of the epithelium. This in turn might have caused a defect in the primary endodermal convergence causing a misconstruction of the endodermal rod. The mutant also exhibits mislocated tissues such as the heart and the lens. Lastly, Kitagawa defines *hirame* as a mutant with differentiation defects; flattened CNS, forebrain dysmorphology and a beating heart located next to the ears as well as compressed general body morphology in their screen for mutants with forebrain malformations. Because its unique phenotype is unlike any other mutant previously described in Medaka and Zebrafish (Taniguchi et al. 2006; Watanabe et al. 2004), Furutani-Seiki went on to make this mutant his main focus of research. After intensive work using positional cloning, he identified a non-sense point mutation within the first WW domain in the Yes-associated protein 1 (YAP1 -1 out of 2) exchanging leucine to a stop codon in the 164th position in allele j54-20C (L164X) (

Figure 1.4A). Medaka yap1 (out of 2) is a homologue for the two WW domain-containing human YAP1 (YAP65) and is referred to in this thesis as “yap”, whereas yap 2 (out of 2) corresponds to the single WW domain human TAZ. YAP is a transcriptional co-activator downstream of the Hippo Signalling Pathway which promotes cell survival, proliferation and maintenance of the 3-dimensional tissue structure (Jiang et al. 2009; Sudol et al. 1995; Lian et al. 2010; Huang et al. 2005). YAP itself is widely expressed in embryonic and adult tissue, and in mammals YAP loss-of function mutants are embryonic lethal and difficult to study *in utero*. In contrast, the *hirame (hir)* embryo can survive until 4 days post fertilisation (dpf) during embryogenesis (corresponding to Iwamatsu’s stage 32), which can be monitored in real-time under a microscope. In *hirame* the patterning along the anterior-posterior and dorsal-ventral axes up to 34 hpf (st.21) mid-neurulation develops normally, thanks to the maternal and zygotic YAP contribution, as indicated by Zebrafish YAP knockdown experiments (Jiang et al. 2009). However, from stage 21 onwards the body of the *hir* mutant embryos gradually collapses, and mutant embryos exhibit a peculiar body flattening and dislocation of several tissues including retina, lens and heart (
Figure 1.4B). Since the *yap* mutation is a zygotic recessive mutation, all references to *hirame (hir)* in this thesis refer to homozygous mutants unless otherwise stated.

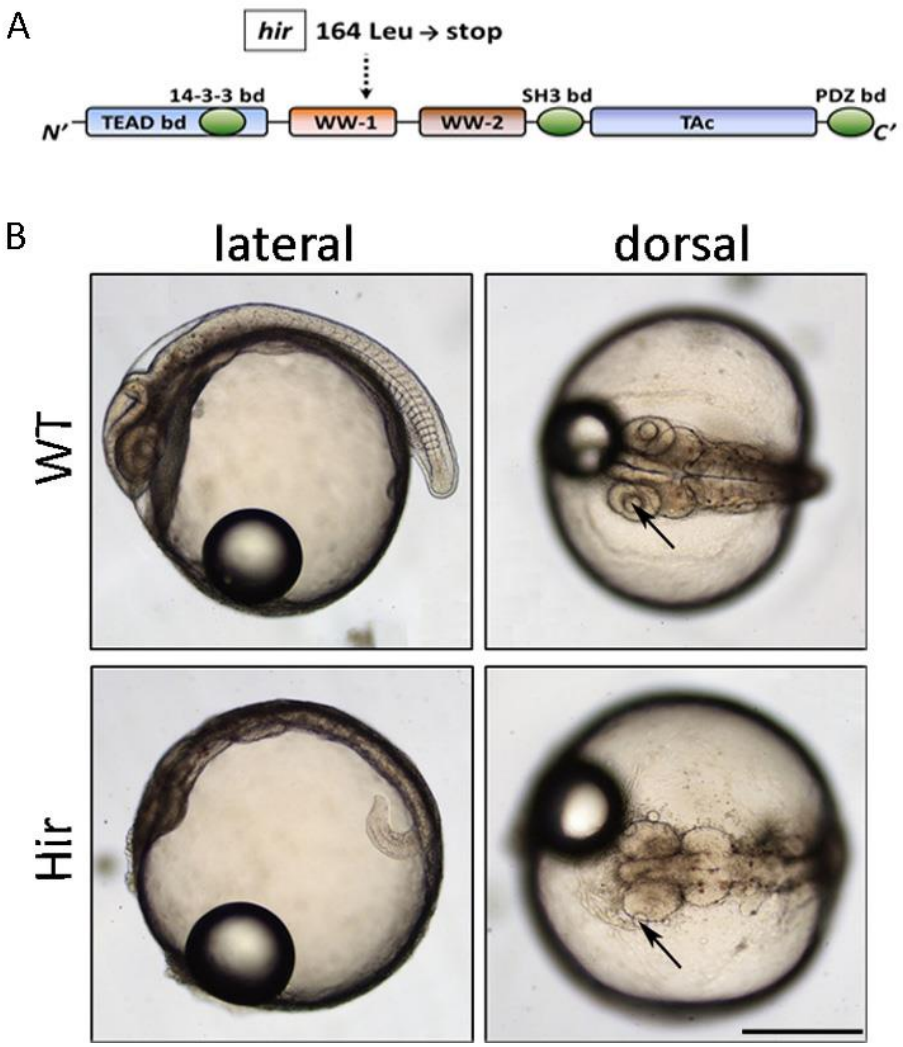

Figure 1.4 Schematic representation of YAP protein domains and images of wild type and *hirame* embryos at 2.5 dpf (st.26)

A) Schematic representation of YAP and its protein domains including TEAD binding domain, 14-3-3 protein binding site, two WW domains, SH3 binding site, transactivation coding region (TAc) and a PDZ binding site. The nonsense point mutation causing the *hirame* phenotype is a leucine to stop amino acid codon exchange in the amino acid 164 within the first WW domain (L164X). **B)** Comparison between wild type (top row) and *hirame* mutant (bottom row) at 54 hpf (st. 26). Lateral view shows the flattened body morphology in *hirame* from st. 22 onwards as described in Watanabe et al, 2004 and Kitagawa et al., 2004. Note the tail of *hirame* embryos is sometimes seemingly grown inside the yolk sac due to soft yolk layers. Dorsal view onto embryos highlights organ abnormalities such as the dislocation of lens compartments of the eye (arrows). Anterior (head) is left. Scale bar = 500µm.

1.9 Hippo pathway signalling and its main regulators

YAP is a downstream effector of the recently discovered Hippo pathway. The core kinase cascade of the Hippo pathway was originally found in a genetic screen for *Drosophila melanogaster* overgrowth mutants (Wu et al. 2003). In this study, the discovery of additional upstream component Hippo (Hpo) could be linked to previous studies that have already established a connection between Salvador (Sav) and the downstream-most factor Warts (Wts) in regulating organ size through cell proliferation and modulation of downstream effectors cell cycle regulator CycE and apoptosis inhibitor Diap1 (Tapon et al. 2002). They also demonstrated that a dysfunctional Hippo pathway consistently led to tissue overgrowth such as enlarged eye imaginal discs, and excess head epidermis (Udan et al. 2003). Subsequent studies have revealed additional members of the Hippo pathway including the upstream Expanded (Ex), Kibra and Merlin (Mer) components (Hamaratoglu et al. 2006), the core kinase component Mats (Lai et al. 2005) and downstream transcriptional co-activator Yorkie (Yki) (Huang et al. 2005). The pathway is evolutionary conserved in vertebrates and the majority of research has been carried out in mammals. In humans the equivalent core kinase cascade consists of mammalian sterile 20 -1 and -2 (Mst1/2) which is the homologue of *Drosophila* Hpo, while Salvador 1 (Sav1) is homologous to Sav, Large tumour suppressor 1 and 2 (Lats1/2) correlates to Wts and the scaffold protein Msp-one binder Mob1 is Mats (Figure 1.5). Subsequent studies revealed upstream components Kibra and Merlin (NF2) (Saucedo & Edgar 2007; Pan 2010), in which Kibra has been shown to regulate Lats1/2 directly (Xiao et al. 2011).

When the Hippo pathway is active, Mst1/2 forms a complex with the scaffolding protein Sav1 and together with Mob1 they phosphorylate the large tumour suppressor protein Lats1/2. Activated Lats1/2 subsequently phosphorylates and inactivates the transcriptional co-activator Yes-associated protein (YAP) at Ser127 and its human paralogue TAZ (also known as WW domain containing transcription regulator 1 (WWTR1)) (Hao et al. 2008; Kanai et al. 2000). Phosphorylation leads to cytoplasmic retention and hinders YAP and TAZ from entering the nucleus (Zhao et al. 2007). YAP (also known as YAP1 or YAP65) is characterized by two WW domains, whereas the paralogue TAZ only carries one WW domain and an additional PDZ domain (Sudol et al. 1995; Kanai et al. 2000). Additional phosphorylation of YAP at Ser381, and TAZ at Ser89 by 14-3-3 proteins leads to ubiquitin-mediated proteosomal cytoplasmic retention and degradation (Zhao et al. 2010). When the Hippo pathway is inactive, YAP/TAZ stays in an unphosphorylated state and both transcriptional co-activators translocate to the nucleus. Because YAP and TAZ do not have DNA binding domains they depend on TEAD family transcription factors (1-4) to induce downstream target genes (Vassilev et al. 2001; Zhao et al. 2010). The nuclear activity of YAP and TAZ induces expression of a variety of genes concerned with proliferation, cell migration, cell cycle division and suppression of anoikis, a special

form of apoptosis in which cells first detach from the surrounding extracellular matrix (ECM) substrate and then initiate programmed cell death (Pan 2010). Comprehensive expression profiling studies have revealed target genes of YAP, including IAP family member BIRC5 (Dong et al. 2007), the secreted Cystein-rich protein connective tissue growth factor (CTGF) (Zhao et al. 2007), FGF1, GLI-2 and amphiregulin (AREG), which is an EGF family member. Other proteins, such as BDNF, ITGB2, IGFBP3, PDGFβ and CyclinD are upregulated by YAP overexpression, whereas p57, RASSF4, prolactin and BMP2 are down regulated (Zhao et al. 2007; Hao et al. 2008).

Other regulatory elements influencing the activity of the Hippo pathway are regularly found and added to the core network. For instance the adaptor protein Ajuba has been shown to inhibit the Hippo pathway by physically interacting with Lats and Sav1, thus blocking YAP phosphorylation (Thakur et al. 2010). Ajuba normally localises to adherens junctions through an association with α-catenin during the establishment of cell contacts. This implies that recruitment of Ajuba to the cell membrane may contribute to contact dependent inhibition of YAP and TAZ (Marie et al. 2003). α-catenin has also been shown to be regulated independently of the activity of the Hippo pathway by recruiting phosphorylated YAP to adherens junctions (Schlegelmilch et al. 2011). In addition, Merlin has been found to competitively complex with Angiomotin (Amot) at tight junctions. This binding releases Rich1 from the inhibitory Angiomotin complex and allows Rich1 to activate Rac1 (Yi et al. 2011). Angiomotin also seems to directly regulate YAP activity by sequestering it into the cytoplasm or through Lats1/2 phorshorylation, therefore excluding it from the nucleus and blocking its transcriptional activity (Zhao et al. 2011; Paramasivam et al. 2011).

Furthermore RASSF1 which usually binds to Ras-GTPs, has been shown to interact and activate Mst1 (Khokhlatchev et al. 2002), resulting in apoptosis which can be abrogated through Raf-1 (Neill et al. 2004). Another study demonstrated that upon DNA damage RASSF1 is phosphorylated by ATM; a main sensor of double stranded DNA breaks. This interaction results in apoptosis through activation of MST1 and Lats1 (Hamilton et al. 2009). Another factor influencing and controlling the Hippo pathway are stress signals induced by contact inhibition. Thereby YAP translocates into the nucleus when epithelial cells are cultured in low density, whereas cytoplasmic YAP was found predominantly when cultured in high density (Ota & Sasaki 2008). Additionally, cell-surface hyaluron receptor CD44 has been placed upstream of the Hippo pathway as upon activation of CD44 or stress induced oxidation with H_2O_2, Mst1/2 was found to be phosphorylated, activating downstream kinases (Xu et al. 2010). Lastly, Mst1/2 seem to associate with, and monitor changes in actin polymerisation and regulates downstream effectors *c-Jun N-terminal kinase* (*JNK)*/stress-activated protein kinase (SAPK) and *cyclin-dependent kinase inhibitor 1 (p21)* (Densham et al. 2009). As well as that, hormonal cues are received by a G-protein-coupled receptor (GPCR), mediated through F-actin to stimulate the activity of Lats1/2 which inhibit YAP and TAZ depending on the kind of GPCR involved (Mo et al.

2014). This would indicate that the Hippo pathway responds to cytoskeleton disruption, mechanical stretching and/or shear stress.

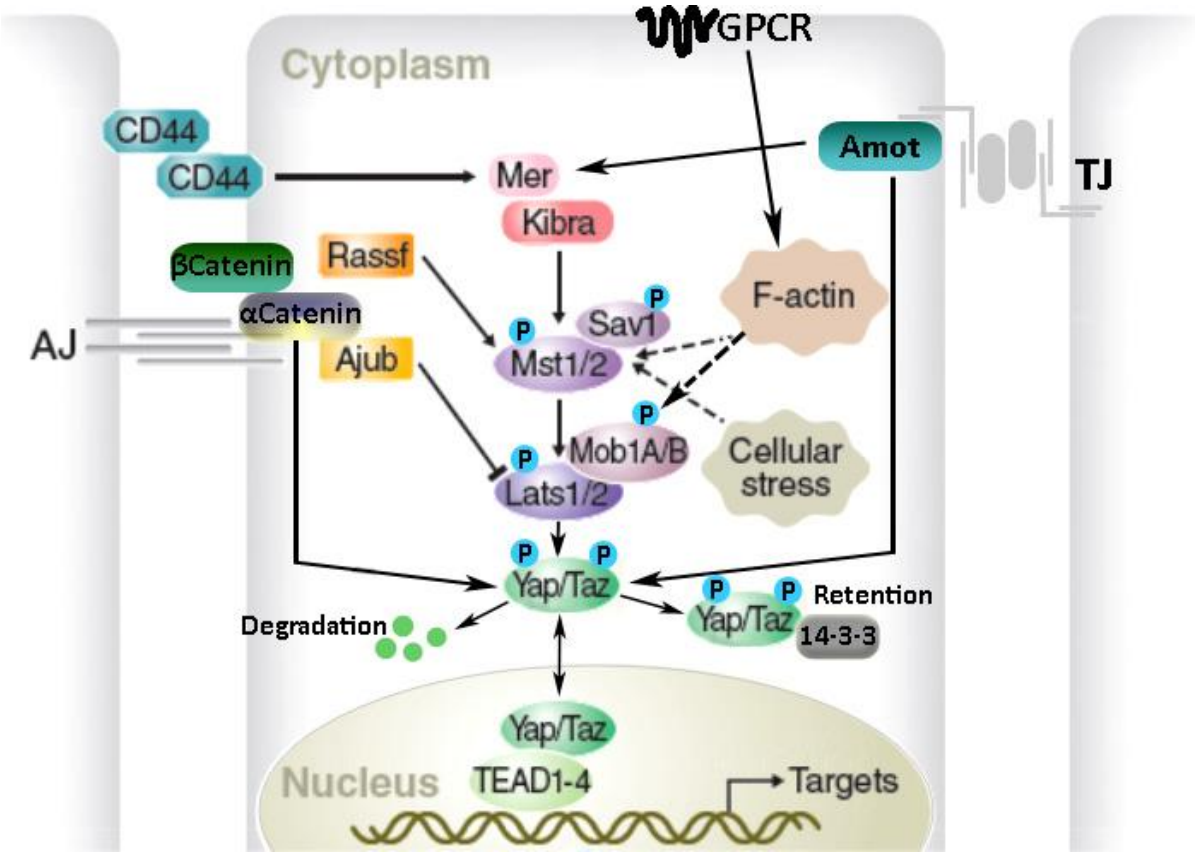

Figure 1.5: Schematic of the mammalian Hippo pathway and some of its components

Core features of the mammalian Hippo kinase cascade and some of its effectors influencing nuclear localisation and transcriptional activity of co-activators YAP and TAZ within the nucleus. The signalling pathway includes Merlin (Mer); Kibra; Salvador 1 (Sav1); mammalian sterile 20 like 1 and 2 (Mst1/2); Large tumour suppressor 1 and 2 (Lats1/2); Msp1 binder 1 (Mob1A/B); Yes-associated protein (YAP) and its paralogue TAZ; TEA domain transcription factor TEAD as well as cell-surface hyaluron receptor CD44, Ajuba (Ajub), αCatenin, Angiomotin (Amot), Ras-associated factor Rassf and the G-protein-coupled receptor (GPCR). Cytoskeleton changes and induced cellular stress levels also influence the Hippo pathway. TJ, tight junctions; AJ, adherens junction. Pointed arrows indicate activation; blunt arrows show inhibitory function (modified after Halder & Johnson 2011).

Overall, the discovery of the Hippo pathway provided a chance to address enduring questions about how organ size is established, controlled and maintained throughout life.

1.10 Effects of Hippo-YAP signalling on tissue physiology

1.10.1 Dysregulation of Hippo pathway components cause cell transformation and cancer growth in mammals

In humans, amplifications of the 11q22 locus causing *yap* overexpression has been reported in several tumour types, such as oral and esophageal squamous cell carcinoma, cancer of the liver, breast, pancreas and lung (Lorenzetto et al. 2014). TAZ/WWTR1 has been found to be overexpressed in papillary thyroid carcinoma possibly controlled by the RAS/RAF/MEK (mitogen-activated protein kinase)/ERK (extracellular-signal-regulated kinase) signalling pathway (Cristofaro et al. 2011). Specific mutations in members of the Hippo pathway are rare in human cancers (Pan 2010) and have only been found in Merlin (*neurofibromin 2*, NF2) in neurofibromatosis type 2 and in cDNA of Mob1 isolated from human melanoma and mammary carcinoma (Lai et al. 2005). Additionally, gene deletions of *salvador1* were detected in two renal cancer cell lines (Tapon et al. 2002). And strong YAP protein expression was found in various cancer types, for example ovarian serous cystadenocarcinoma, esophageal squamous cell carcinoma, colonic, lung, pancreatic, hepatocellular and prostate adenocarcinoma (Steinhardt et al. 2008). Interestingly, there are reports describing hypermethylation events in Hippo pathway members, which suggest that epigenetic silencing could be another mechanism by which core components regulate tissue homeostasis. For instance, Mst1/2 in soft sarcoma (Seidel et al. 2007) and Lats1/2 in breast cancer (Takahashi et al. 2005) as well as astrocytomas (Jiang et al. 2006) have been described to be hypermethylated. Also, upstream regulator RASSF is frequently hypermethylated in wide range of human cancer (Richter et al. 2009), which might affect Mst1/2. Furthermore miRNA-mediated silencing of Lats2 through miR372 and miR373 has been described in testicular germ cell tumours (Voorhoeve et al. 2006).

Hippo pathway signalling has been shown to control tissue growth in mammals. Remarkably, transgenic mice with tissue specific YAP induction developed enlarged livers which after prolonged YAP exposure advanced into hepatocellular carcinoma (Camargo et al. 2007; Dong et al. 2007). This effect was partly reversible through repression of *yap* expression, confirming that the Hippo signalling controls organ size by inhibiting nuclear function of oncogenic YAP. In addition to regulation of cell growth in various cell types, YAP expression is known to modulate cell differentiation capacity. YAP, together with its transcriptional binding partner TEAD2, has been reported to maintain self-renewal properties and prevents mouse ES stem cell differentiation (Tamm et al. 2011). In mouse intestine, expression of endogenous YAP was shown to be restricted to the progenitor/stem cell compartment and overexpression of *yap* expanded the multipotent

undifferentiated progenitor cell population (Camargo et al. 2007). In addition, overexpression of YAP or TAZ can induce anchorage-independent growth and epithelial-mesenchymal transition (EMT) of immortalized mammary and pancreatic epithelial cells *in vitro*, which are hallmarks for cancer progression and the onset of metastasis (Overholtzer et al., 2006; Zhao et al., 2008; Zhang et al., 2009a; Chan et al., 2009; Dong et al., 2007).
In contrast, YAP can also induce apoptosis in response to DNA-damage by binding to the transcription factor p73, a p53 family member (Strano et al. 2001). Thereby, the pro-apoptotic role of YAP seems to depend on the regulation of its upstream components (Hamilton et al. 2009; Oka et al. 2008).

1.10.2 YAP as regulator of cell migration

Active cell migration is a feature of the neural crest cells and is a main hallmark of cancer progression and metastasis. As mentioned above overexpression of YAP induced EMT in non-cancerous cell cultures (Overholtzer et al. 2006). *In vivo* studies confirmed the oncogenic potential of YAP to transform cell behaviour. The constitutively active form of YAP (5SA) being mutated in five phosphorylation sites, increased the overall proliferation and migration of ovarian cancer cells *in vitro* and *in vivo,* possibly by increasing epithelial-mesenchymal transition leading to accelerated cell motility. Promoted cell migration was assessed *in vitro* by both a colony forming transwell migration assay and a wound-healing assay, and *in vivo* by metastasis formation within lungs after caudal vein injection (Xia et al. 2014). In addition, increased YAP levels were found in adult granulosa cell tumours, whereby increased expression levels correlated with an incline in cell proliferation. Further tests concluded that overexpression of constitutive active YAP in isolated granulosa tumour cells resulted in increased proliferation and motility of individual cells *in vitro* (Fu et al. 2014).
Lamar et al. in 2012 provided the first report suggesting YAP involvement in the melanocyte transformation. Their mouse *in vivo* studies showed that through interaction with the DNA-binding domain TEAD, YAP mediated a 60% increase in melanoma tumour growth after sub cutaneous injection and enhanced the number of lung metastases following tail-vein injection. The effect observed included cell invasion and migration, highlighting pro-metastatic potential in melanoma cells (Lamar et al. 2012). In agreement, in 2014 Nallet-Staub's functional studies showed that overexpression of YAP increased the anchorage-independent growth in cutaneous melanoma cultures in soft agar. Conversely, specific knockdown of either of these Hippo effectors led to reduced clonogenic and invasive capacity *in vitro*, and reduced their tendency to metastasise to lungs following tail-vein injection in nude mice. This could implicate YAP in contributing to the invasive and metastatic capacity of melanoma cells.

These studies provide an indication of the importance of Hippo-YAP signalling as driver for *in vivo* cell growth and migration.

1.10.3 Connecting YAP with neural crest development

Because our study focuses on the analysis of YAP within the neural crest development, we were intrigued to find out about existing experiments implying regulation of neural progenitor cell proliferation and/or differentiation via the Hippo-Pathway. In mouse TEAD2 transcription factor binds to the Pax3 neural crest enhancer sequence NCE2 which promotes its activity during neural crest cells development (Milewski et al. 2004). Overexpression of a dominant negative form of Tead2 under a Wnt1 promoter reduced Pax3 expression within the neural crest derivatives and resulted in smaller dorsal root ganglia. They also showed a remarkable overlap of PAX3, Tead2 and YAP in the dorsal neural tube ventricular zone, which suggests that co-transcriptional partner YAP together with TEAD DNA binding might act to positively regulate *Pax3* expression (Milewski et al. 2004).
In 2008 Cao et al. demonstrated that the YAP-TEAD interaction mediated by the upstream kinase cascade regulates the Sox2 positive neuronal progenitor population of the neural tube during chick embryogenesis. Thus, the Yap expression domain correlated with the ventricular progenitor zone and co-localised with neural progenitor marker Sox2 and theTEAD transcription factor. Overexpression of constitutive active YAP within the neural tube decreased neuronal differentiation and increased the number of Sox2 positive progenitor cells. This suggests that YAP could maintain the neuronal stem cell population, increases proliferation and depresses neuronal differentiation. Increased proliferation of neural progenitor cells also caused overgrowth in a rosette-like fashion, resembling Homer-Wright rosettes present in various neurological tumours (Dyer 2004). To confirm if TEAD mediates its function through YAP, a transcriptionally active version of TEAD was expressed to recapitulate the YAP phenotype described above. The increased transcriptionally TEAD activity resembled the YAP overexpression outcome, including expansion of progenitor cells, reduced differentiation and tumour-like overgrowth, confirming their interaction (Cao et al. 2008).
Supporting data came from *Xenopus* studies. Gee et al. showed that YAP gain-of-function expands the $Sox2^{+}$ progenitor cells within the neural plate and inhibits neuronal differentiation. It also enlarged the $Pax3^{+}$ neural plate border cells during late gastrulation, which inhibited markers required for neural crest development (*zic1, foxd3*), pre-placodal ectoderm and hatching gland differentiation. The regulation of Pax expression and neuronal cell fate by YAP was shown to be through an interaction with TEAD transcription factors (Gee et al. 2011).
Dysregulation of Hippo signalling upstream components, specifically fat cadherin family members, have also been proposed to control the neural tube progenitor pool through the regulation of YAP. In

Drosophila transmembrane receptor Fatd has been shown to regulate tissue size and planal cell polarity by deregulating Hippo target genes such as cyclin E and diap1 (Willecke et al. 2006; Matakatsu & Blair 2004). In mice, the deletion of Fat4 (also called FatJ) led to a consistent increase in neural tube progenitor cell number within the neural tube causing a widening of the spinal cord, but did not inhibited neuronal differentiation. The authors suggest a link to Hippo-YAP as simultaneous knockdown of *YAP* and *Tead4* rescued the FatJ phenotype, indicating a functional connection (Van Hateren et al. 2011).

So far the most relevant report tying together aspects of neural crest development to the Hippo pathway comes from Jiang et al. published in 2009. Therein *yap* knockdown in Zebrafish embryos caused reduced numbers of *elavl3*$^{+}$ cells in mid- and hindbrain and fewer abnormally distributed craniofacial cartilages in the branchial arches. Analysis of the neural crest marker crestin revealed weaker expression throughout the embryo, whereby some periocular located cranial NC accumulated near the developing retina and the lens mesenchyme (Jiang et al. 2009). However, the outcome and quality of the data might have been masked by embryonic developmental defects caused by high morpholino dosages.

Therefore, the question still remains open whether the Hippo pathway is essential to neural crest development in general or if it has limited requirements to some of its derivatives.

1.11 Aims

As outlined previously a failure of Hippo signalling has been linked to tumorigenic cell alterations, increased cancer growth, migration and metastasis in numerous cancer types *in vitro* and *in vivo*. Especially interesting for us are investigations concerning melanoma development, as melanoma metastasis is characterized by features such as epithelial-mesenchymal transition (EMT) and intensive migration over long distances thought to recapitulate some of the neural crest cell properties found during embryogenesis. Furthermore, there are reports linking the Hippo pathway directly to a neural crest cell progenitor population within the dorsal tube, which seemed to be regulated by precise levels of Hippo downstream effector Yes-associated protein (YAP). In parallel, a mutagenesis screen carried out in the Japanese rice fish Medaka led to the discovery of a mutant named *hirame* with astonishing developmental abnormalities (Furutani-Seiki et al. 2004). Further investigations revealed that *hirame* carries a non-sense point mutation in *yap* resulting in a non-functional protein (Fututani-Seiki unpubl. data). One of *hirame*'s characteristics is a decrease in differentiated melanocytes observed in late stage embryos.
Together, this seemed like a fantastic opportunity to investigate the role of Hippo downstream effector YAP in neural crest development in this Medaka loss-of-functional YAP mutant. We aimed to:

1.) analyse the abnormal melanocyte phenotype at different stages to highlight when and where the abnormality starts during embryogenesis.
2.) establish and carefully characterise a Medaka melanocyte specific promoter, with which we could potentially address questions concerning cell behaviour, proliferation and melanocyte survival in *hirame* embryos.
3.) overexpress YAP and validate its cell autonomy within the melanocyte lineage in an attempt to rescue the *hirame* phenotype. The melanocyte specific expression could also confirm YAP's oncogenic potential *in vivo*.
4.) characterise a wider range of unpublished Medaka neural crest markers spanning different neural crest derivatives. First describing those markers in wild type embryos, we would then move on to analyse them in *hirame* mutants to reveal whether YAP causes changes to other neural crest cell lineages as well.

Together, these results could shed light on the role of YAP during Medaka neural crest development. During the course of experiments, we expect to establish and verify new tools such as neural crest specific promoter fragments or *in situ* hybridisation probes that could be useful to the wider Medaka research community.

2 Chapter: Material and Methods

2.1 Materials

Materials used and sources are listed below in categories.

2.1.1 Chemical Reagents

UltraPure™ Agarose	Invitrogen Life Technologies, UK
Low Melting Agarose	Invitrogen Life Technologies, UK
IPTG	Melford Labs Ltd, Suffolk, UK
Luria Agar/Broth Base	Invitrogen Life Technologies, UK
Methylcellulose	Sigma Chemical Co, St Louis, MO, USA
Phenol/Chlorophorm/isoamyl alcohol	Sigma Chemical Co, St Louis, MO, USA
Tricaine (Ethyl 3-aminobenzoate methanesulfonate)	Fluka Analytical, Sigma Aldrich, Germany
Tween 20	Sigma Aldrich, Germany
Luria Agar	Sigma Life Science, Germany
Luria Broth	Sigma Life Science, Germany
Formaldehyde	Sigma Aldrich, Germany
Ethanol	Sigma Aldrich, Germany
Methanol	Fluka Analytical, Sigma Aldrich, Germany
PBS	Fisher Scientific, UK
DPX mounting medium	Fisher Scientific, UK
Heparin	Sigma, Aldrich, Germany

2.1.2 Kits and Miscellaneous Materials

Technovit 8100 Cold-curing resin kit	Kulzer, Germany
DIG RNA labelling kit SP6/T7	Roche Diagnostics GmbH, Germany
NucleoBond® Xtra Midi	Macherey-Nagel, Germany
Gel DNA Recovery kit	Zymo Research, USA
DNA Clean & Concentrator (PCR purification kit)	Zymo Research, USA
mMESSENGER RNA synthesising kit SP6	Ambion Inc Texas, USA

2.1.3 Antibodies

Anti-DIG	Roche Diagnostics, Germany
Anti-Fluorescein	Roche Diagnostics, Germany

YAP1 polyclonal (rabbit) #13584	Proteintech (ptglab), UK
YAP1 polyclonal (rabbit) #4912	Cell Signalling, UK

2.1.4 Antibiotics, Indicators and Dyes

Ampicillin	Sigma Chemical Co, St Louis, MO, USA
Ethidium Bromide	Sigma Chemical Co, St Louis, MO, USA
Kanamycin	Sigma Chemical Co, St Louis, MO, USA
Phenol Red	Sigma Chemical Co, St Louis, MO, USA
X-gal	Sigma Chemical Co, St Louis, MO, USA
Neutral Red	Sigma Chemical Co, St Louis, MO, USA
Histo-Clear (Xylene substitute)	National Diagnostics, UK
Harris Haematoxylin	Raymond A Lamb Ltd, UK
Mayer´s Heamatoxylin	Sigma-Aldrich Chemie GmbH, Germany
Eosin 1% Aqueous	Raymond A Lamb Ltd, UK
Fast Red tablets	Roche Diagnostics, Germany
NCB/BCIP	Roche Diagnostics, Germany

2.1.5 Enzymes

Proteinase K	Fisher Scientific, UK
RNase A	Promega, UK
RNase Inhibitor	Promega, UK
Pronase	Sigma Aldrich, Germany
Shrimp Alkaline Phosphatase	Promega, UK
T4 Ligase	Promega, UK
Go Tag Polymerase	Promega, UK
KOD Hot Start DNA Polymerase	Novagen, USA

Restriction enzymes were supplied with specific buffers and reactions were done according to manufacturer's inctructions (Promega, UK or New England BioLabs, UK)

2.1.6 Nucleic Acids

dNTP mix	Promega, UK
Yeast tRNA	Invitrogen Life Technologies, UK

DIG labelled digoxygenin	Roche Diagnostics, Germany
DNA ladder 100bp	New England BioLabs, UK or Promega, UK
DNA ladder 1kb	New England BioLabs, UK

2.1.7 Bacterial Strains and Cloning Vectors

The MAX Efficiency® DH5α™ Competent Cell bacterial strain used for general plasmid preparation and cloning was originally purchased from England BioLabs. From there all following stocks of competent cells were made in-house following the protocol given by Dr. K.Kaji (Appendix 2) in which transformation efficiencies up to 1×10^9 transformants/µg plasmid DNA can be achieved. DH5α™ competent cells containing the *rec*A1 and *end*A1 mutations increase insert stability, improve yield and quality of plasmid DNA preparion as well as blue/white screening capability (*lac*ZΔM15) (England BioLabs, Life technologies, Cat# 18258-012.

2.1.8 Frequently used cloning vectors

Cloning vectors used in this thesis are tabulated (Table 2.1) and illustrated below.

Table 2.1: Cloning plasmids used throughout this thesis

Plasmid name	Supplier
pGEM®T-Easy	Promega, Madison, WI
pEGFP-1	obtained in-house, but can also be purchased from BD Bioscience Clontech
$pCS2^+$	obtained in-house, but can also be purchased from Addgene
pEGFP-C3	obtained in-house, but can also be purchased from addgene, BD Nioscience Clontech

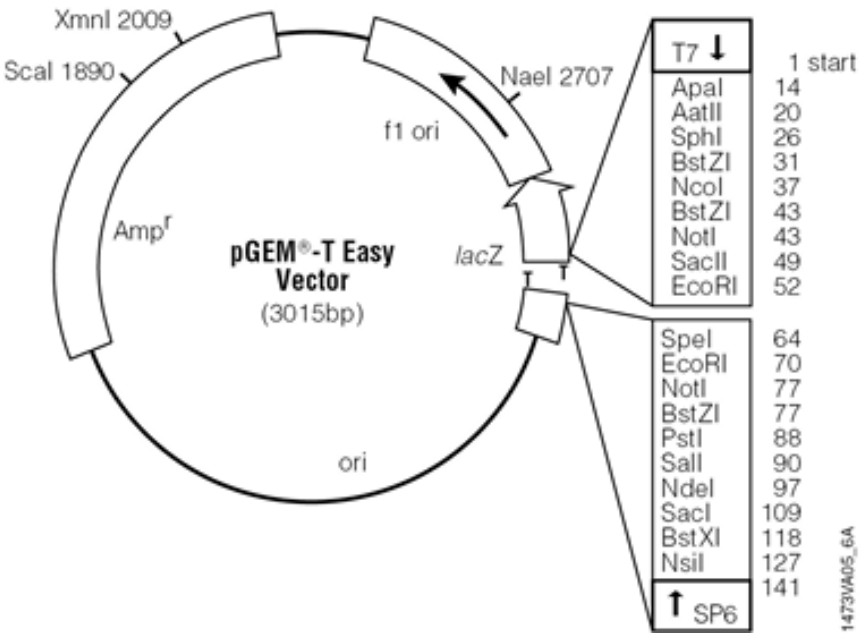

Figure 2.1: pGEM®-TEasy vector map

A plasmid map of pGEM®-T Easy Vector featuring the TA-nucleotide overhang for TA-cloning of PCR products enclosed by a multiple cloning site (MCS) with common restriction enzyme recognition sites for further cloning approaches. It also features the T7 and SP6 polymerase recognition sites frequently used for in-vitro transcription of RNA probes. The pGEM®-T Easy Vector carries a Ampicillin resistant genes. The handling protocol was obtained from Promega.

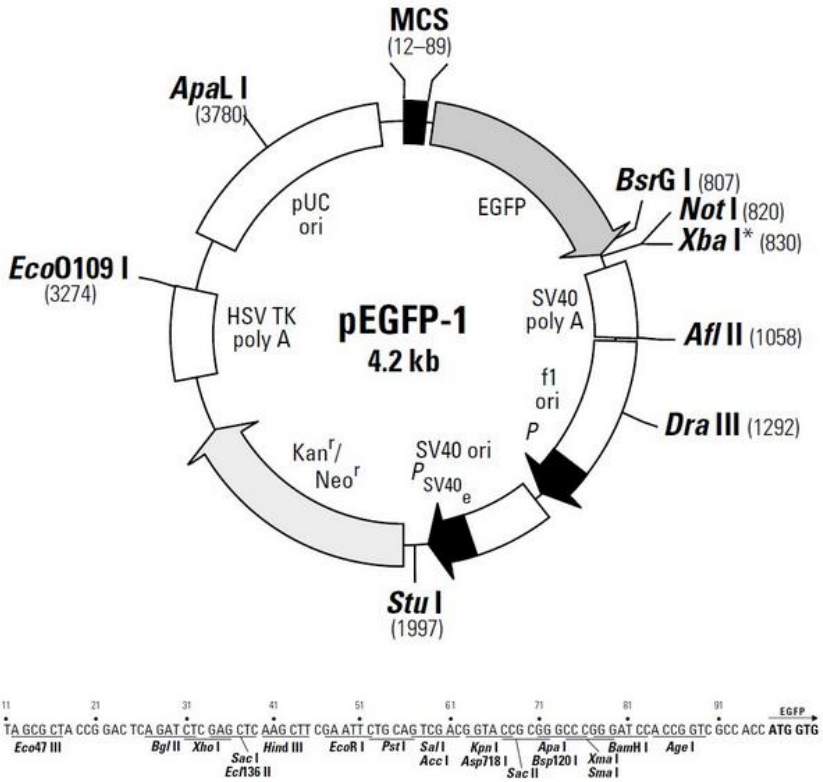

Figure 2.2: Map and MCS sequence of pEGFP-C1

Restriction map (top) and multiple cloning site (bottom) of pEGFP-1. All restriction sites shown are unique. pEGFP-1 is a promoterless eGFP vector used to monitor transcription from different enhancers/promoters. Desired sequences are inserted into the MCS located upstream of the EGFP coding sequence. pEGFP-1 encodes a red-shifted variant of wild-type GFP (1-3) which has been optimised for brighter fluorescence (Excitation maximum= 488nm; emission maximum= 507nm). A bacterial promoter confers kanamycin resistance in E.coli. The backbone also provides a pUC origin of replication in E.coli and an f1 origin for single-stranded DNA production (BD Bioscience Clontech product website).

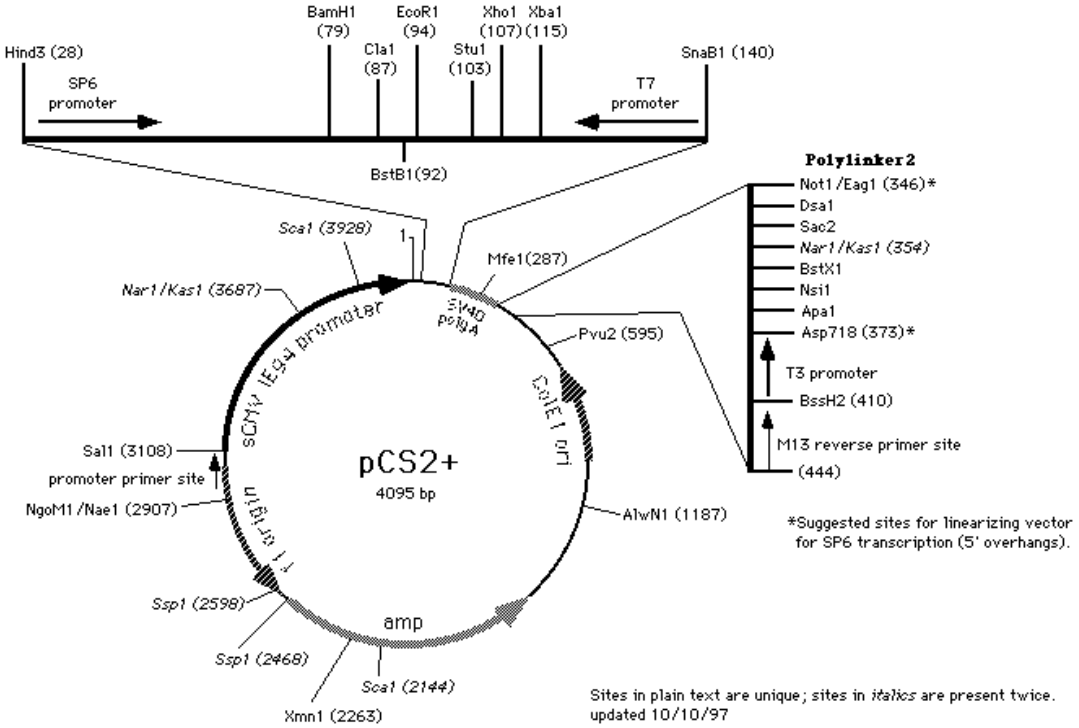

Figure 2.3: Map of pCS2^{+} plasmid

Restriction map of the 4095bp pCS2+ multipurpose expression vector. A strong CMV IW94 promoter is coupled to the first polylinker followed by a SV40 late polyadenylation site. Within that polylinker there is a 5'-3' SP6 promoter at the start and and reverse oriented T7 promoter at the end. A second polylinker follows with more unique restriction enzyme sites and a T3 promoter region used for RNA in-vitro transcription and translation. The vector backbone itself includes an ampicillin resistance gene and an f1 origin to produce single stranded DNA (D.Turner website, University of Michigan; ttp://sitemaker.umich.edu/dlturner.vectors/home).

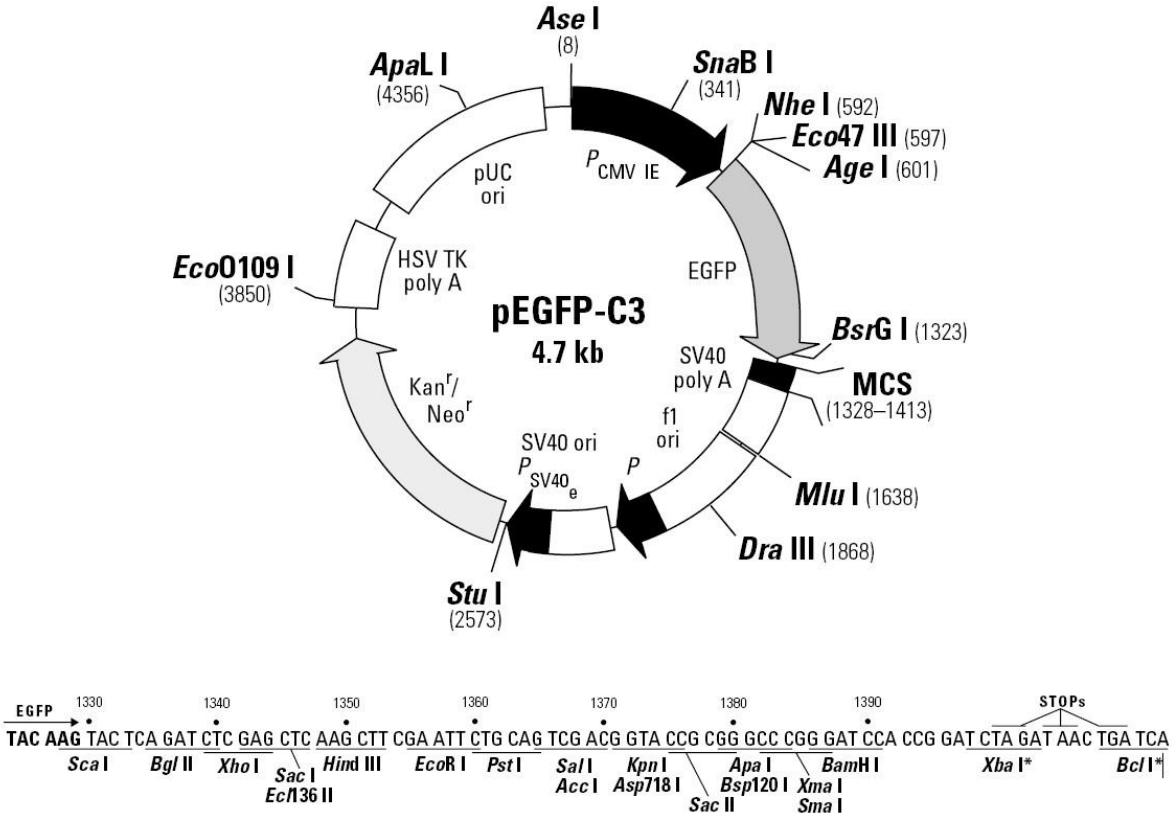

Figure 2.4: Map of EGFP-C3 plasmid

Plasmid restriction map of the 4.7kb pEGFP-C3 vector enabling insertion of DNA fragments in C-terminally to EGFP with help of a multiple cloning site (MCS) followed by a SV40 late polyadenylation site. A strong CMV promoter drives expression of EGFP or the EGFP fusion gene. Other regulatory elements within the backbone are an F1 origin, SV40 origin and Kanamycin/Neomycin resistance gene expression cassette followed by HSV poly A and pUC origin sequence. (map from http://www.biosubway.com/?product=pegfp-c3)

2.1.9 Solutions and Buffer

Phosphate buffered saline (PBS)

2.7 mM KCl

137 mM NaCl

In distilled water

Tween phosphate buffered saline (PBST)

0.1 % (v/v) Tween20 in PBS

Pronase

20 mg/ml stock solution of Pronase (Protease from Streptomyces griseus, Sigma-Aldrich, England, Cat# P8811) in PBS

Paraformaldehyde (PFA)

4 % (w/v) paraformaldehyde in PBS

Autoclaved PBS is firstly warmed to 60°C and then PFA is added, pH adjusted to 7.0 and immediately frozen in aliquots to prevent degradation.

SSC 20X

3M NaCl

300 nM sodium citrate

Dissolve in Milli-Q water and adjust pH to 7.0 with 1M HCl

Hybridisation mix (HM)

50 % (v/v) Formamide

5X SSC

50 ng/ml Heparin

500 ng/ml yeast tRNA

Antibody Blocking solution

0.2 % BSA

2 % Goat serum

In PBS

Alkaline phosphatase (AP) buffer

100 mM Tris-HCl pH 9.5

100mM NaCl

In distilled water

1x TAE

40mM Tris HCl

20mM sodium acetate

2mM EDTA

In distilled water

Adjust to pH 7.8 with glacial acid

Tricaine stock solution (3-amino benzoic acidethylester)

400mg tricaine powder

87.9ml dd water

~2.1ml 1M Tris (pH 9). Adjust pH to ~7

To use tricaine as an anesthetic combine the following in a 250ml beaker:

4.2ml tricaine solution

~ 100ml clean tank water

Embryo medium (50X stock solution)

0.5 µM NaCl

0.17 µM KCl

0.33 µM CaCl

0.33 MgSO4

0.1 % methylene blue

In distilled water

SOB (Super Optimal Broth)

0.5% (w/v) yeast extract

2% (w/v) tryptone

10 mM NaCl

2.5 mM KCl

20 mM $MgSO_4$

Per liter:

5 g yeast extract

20 g tryptone

0.584 g NaCl

0.186 g KCl

2.4 g $MgSO_4$

Adjust to pH 7.5 prior to use. This requires approximately 25 ml of 1M NaOH per liter.

SOC (Super Optimal broth with Catabolite repression)

1l SOB

20 mM glucose solution (20ml)

Luria Agar (L-agar)

3.7% (w/v) Luria agar base in distilled water, autoclave

Luria broth (L-broth)

2.5% (w/v) Luria broth base in distilled water, autoclave

Lysis Buffer

5ml 1M TrisHCl pH 8.0

2ml 5M NaCl

0.5ml 10% SDS

0.5ml 0.5M EDTA

- fill up to 50ml with dH_2O

Transformation buffer (TB) for competent cells

1.5g PIPES

1.1g $CaCl_2$-$2H_2O$

9.3g KCl

Put PIPES, $CaCl_2$-$2H_2O$ and KCl into 400ml ddH_2O

Adjust pH to 6.7-6.8 using 5N KOH

Add 5.45g $MnCl_2$-$4H_2O$

Fill up to 500ml and filter sterilise

SOB (competent cells)

200ml LB

0.5ml 1M KCl

2ml 2M $MgCl_2$ (sterilise using filter)

Mix LB and KCl – sterilise using autoclave, add $MgCl_2$ solution

2.2 Methods

2.2.1 Preparation of DNA samples

2.2.1.1 Bacterial Growth

Glycerol stocks or agar stabs of bacterial stocks were propagated by streaking on LB-agar plates containing appropriate selective antibiotics and incubated overnight at 37°C.
Bacterial cultures were grown in LB-medium supplemented with required antibiotics. Antibiotic concentrations used were as follows: Ampicillin: 50µg/ml and/or Kanamycin: 25µg/ml. After inoculation with a single colony, the culture was incubated overnight at appropriate temperature in a shaking incubator.

2.2.1.2 Plasmid Preparation

Plasmid preparation for multiple colony screening through digestion or PCR was either accomplished by using an in-house protocol (Appendix 2) or using an industrial high quality Plasmid and DNA purification kit such as the NucleoBond® Xtra Midi (Macherey-Nagel, Germany). Thereby bacterial pellet was lysed by alkali and loaded onto the provided column. Following extensive washing of the column, the plasmid DNA was eluted in water and DNA concentration was measured with the IMPLEN DNA spectrophotometer (Geneflow, UK).

2.2.1.3 Isolation of genomic DNA from Medaka *fish embryos for cloning*

Medaka genomic DNA was isolated from 30 - 50 anaesthetised wild type HB32C embryos at early 9 dpf by incubating them overnight at 37°C in 1ml of lysis buffer supplemented with 20µl of 20mg/ml ProteinaseK. This step was repeated ending up with 2ml in total. Solution was carefully taken up and phenol/chlorophorm followed by ethanol precipitation was carried out. Note: when starting ethanol precipitation, genomic DNA can be seen as white aggregates after ethanol addition to the solution. Take up the DNA carefully with a blunt glass needle and transfer in new tube. Carry on with 70% ethanol wash step within precipitation protocol. Air dry the pellet and dissolve in 20µl TE or water.

2.2.1.4 Isolation of genomic DNA from Medaka *fish embryos for PCR genotyping*

Single embryos before hatching stage were washed in PBS and dissociated by boiling in 60µl of 100mM NaOH for 20min. After cooling down solution was neutralised in 10µl of 1M TrisHCl pH8.5 and 1µl was taken for PCR reaction.

2.2.2 Molecular Techniques

2.2.2.1 Restriction Digests

Digestion of DNA by restriction enzymes was performed in a minimal volume, using reaction conditions recommended by the manufacturer. Five/one units of restriction enzyme were added per one µg of DNA, ensuring that the volume of enzyme never exceeded 1/10 of the total reaction volume. When required, BSA was added to a final concentration of 100µg/ml respectively. Where required, heat inactivation at 65°C was carried out or the reaction was cleaned up by running on an agarose gel or Phenol/Clorophorm precipitation.

2.2.2.2 Separation of DNA molecules through Agarose electroporation

Size fractionation of DNA was performed by submarine gel electrophoresis on 0.8-1.5% (w/v) agarose gels in 1x TAE supplemented with ethidium bromide to 100mg/ml. Samples wereloaded with 1x loading buffer and electrophoresed at 120V. The gel was exposed to UV light to visualise DNA, which could then be photographed with a gel documentation system connected to a camera and computer.

2.2.2.3 Recovery of DNA from Agarose Gel

The band of interest was cut out from the gel and DNA isolated using the Gel DNA Recovery kit (Zymo Research, USA) according to manufacturer instructions. Briefly, the agarose block was dissolved by heating for 5-10 min at 55°C in the provided buffer, and the resulting mixture loaded onto the supplied column. Following washings of the column, the DNA was eluted in water and ready to use.

2.2.2.4 Purification of DNA

Using Phenol/Chloroform Extraction

DNA solutions were made up to a minimum volume of 100µl with water and adding an equal volume of phenol/chloroform/isoamyl alcohol (25:24:1 with 10mM Tris, pH 8.0, 1mM EDTA). The emulsion was centrifuged at 1300x rpm for 5 min and the upper aqueous phase transferred into a new 1.5 ml centrifuge tube. Next, and equal volume of chloroform was added to the remaining solution and centrifuged for another 5 min at 1300x rpm. The upper aqueous phase after in the tube was transferred into a new tube and ethanol precipitation was undertaken.

Using DNA purification kit

To purify DNA from enzymatic reactions the DNA Clean & Concentrator (Zymo Research, USA) was employed as per manufacturer instructions. Briefly, the reaction mix was diluted with water or provided buffer and applied onto the provided column. The column was then washed with the provided buffer and DNA eluted in water.

Ethanol precipitation of DNA and RNA

DNA and RNA samples were precipitated by adding 2.5x volume of 100% ethanol and of 3M sodium acetate pH 5.2 to a final concentration of 0.1M. The DNA or RNA was then centrifuged at 1300x rpm for 30min at 4°C. The supernatant was removed and the DNA/RNA was washed with 70% ethanol by centrifugation at 1300x rpm for 15min. The remaining pelleted was air dried and DNA eluted in water and RNA eluted in water plus 1µl of 100µg/ml RNAse.

2.2.2.5 Determination of DNA and RNA concentration

DNA and RNA concentrations were determined by UV Nanospectrophotometry at a wavelength of 230nm, 260nm and 280nm to determine the quality of DNA and RNA sequences. Thus a ratio of $A_{260/280}$ around 2.0 indicates that the sample is "pure". If this ratio is lower it may indicate the presence of protein, phenol, change of pH or other contaminants with strong absorbance at or around 280nm. Values between 2.0-2.2 from the $A_{260/230}$ output suggest high purity of nucleotide molecules. Lower ratios may be a result of EDTA, carbohydrate, TRIzol or phenol contaminations, all absorbing at 230nm (Nano & Drop Technologies website 2007). DNA and/or RNA concentration and purity was either tested on the Genflow Nano spectrophotometer or BioRad Nano spectrophotometer.

2.2.2.6 Messenger RNA (mRNA) synthesis

mRNA was synthesised using the mMESSENGER RNA kit with SP6 polymerase (Ambion Inc Texas, USA) followed by Phenol/Chloroform and subsequent ethanol precipitation. Precipitated RNA was eluted in a small amount of RNAse free ddH_2O and kept at -80°C until use.

2.2.2.7 Polymerase Chain Reaction (PCR)

PCRs were performed in a 15µl sample reaction volume containing the following supplements: 0.2mM each of dATP, dCTP, dGTP and dTTP; 1x PCR reaction buffer containing the optimal $MgCl_2$ concentration specifically for the used Polymerase enzyme; 0.5-1µM of each forward and reverse

primer; 2.5 U of GoTaq or Kod polymerase and DNA template. Amplification was performed in a heat-controlled PCR amplification cycler (G-Storm, GRI Ltd, England). PCR programme consists of an initial template denaturation at 94°C for 2min, followed by 35-40 PCR cycles including denaturation at 94°C for 30s, primer annealing for 1min at a primer specific temperature and final extension at 72°C for 23-90s depending on the expected band product length, followed by one-off final extension at 72°C for 5min after all cycles are completed.

Primers were purchased either from SourceBioscience, Eurofins or ThermoScientific and some major ones are listed in Table 2.2.

Table 2.2: Primer sequences frequently used or essential for some experiments

Primer description	Primer sequence
FW_MF_*Dct* pro	5‘- ACA TTG TAG TAG GTG TAA GGG CTG T -3‘
RV_MF_*Dct* pro	3’- CTT AGC GGT CAA TTA GTT CCT CTT A -5’
FW_ClaISpeI_gfp	5’- ata tct agt CGC CAC CAT GGT GAG CAA GGG -3’
RV_egfpFLClaI	3’-taa tcg atg gct tcc gcc gcc acc gga ccc acc tcc gcc aga gcc acc gcc acc aga CTT GTA CAG CTC GTC CAT GCC -5’
Genot FW_inner_hir	5’- ACG CAA AGC CCT GCT CCA GTA -3’
Genot RV_ inner_wt	3’- TAC TGG GAG GGG TAG CCT GGT TCA -5’
Genot FW_common1	5’- ACA GGG ATT GAT TTC ATC AAG GAG TC -3’
Genot RV_common1	3’- TAC GCC TGA GTC TTA CAT CAC CTA G -5’
FW_MF_YAP1	5’- ATT CCA GAC AAG CTA GCA CTG ATG C -3’
RV_MF_YAP1	3’- CAT CTG CTG CAG CCT CAT CTG GT -5’
FW_EGFP(470)	5’- GCA GAA GAA CGG CAT CAA -3’
RV_YAP(786)	3’- CAT CTG CTG CAG CCT CAT CTG GT -5’

2.2.2.8 Genotyping with Tetra-primers ARMS-PCR amplification

Genotyping was carried out using a similar approach to the tetra-primer ARMS-PCR amplification system (Figure 2.5) (Ye et al. 2001; Piccioli et al. 2006) to detect the single nucleotide polymorphisms (SNPs) in Medaka $^{j50\text{-}20C}$ embryos. This multiplex PCR facilitates two primer pairs amplifying two different alleles around a SNP, therefore amplifying both the wild type and mutant allele in a single reaction. The region flanking the *hirame* mutation at 491bp exchanging thymine to adenine is amplified by 2 common outer primers (Genot FW_common1, Genot RV_common1) resulting in a none-allele specific fragment for wild type and mutant alleles. Then, two allele-specific inner primers for *hirame* mutation (Genot FW_inner_hir) and wild type nucleotide (Genot RV_ inner_wt) simultaneously amplify inner regions of the allele in combination with outer primers. The two inner

amplicons from wild type and *hirame* are easily distinguishable because of their different fragment length. This particular PCR method was applied to genotype mRNA injected single embryos after *in situ* hybridisation. Size fractionation after genotyping will then indicate in three bands which genotype the individual embryo harboured. For example, the upper fragment represents the non-specific allele amplified by outer primers, the middle band indicates the *hirame* allele with primers recognising the SNP and the lower band shows the wild type allele (Figure 2.6). If the embryo was heterozygous carrier for *j50-20C,* we would find all three bands at once.

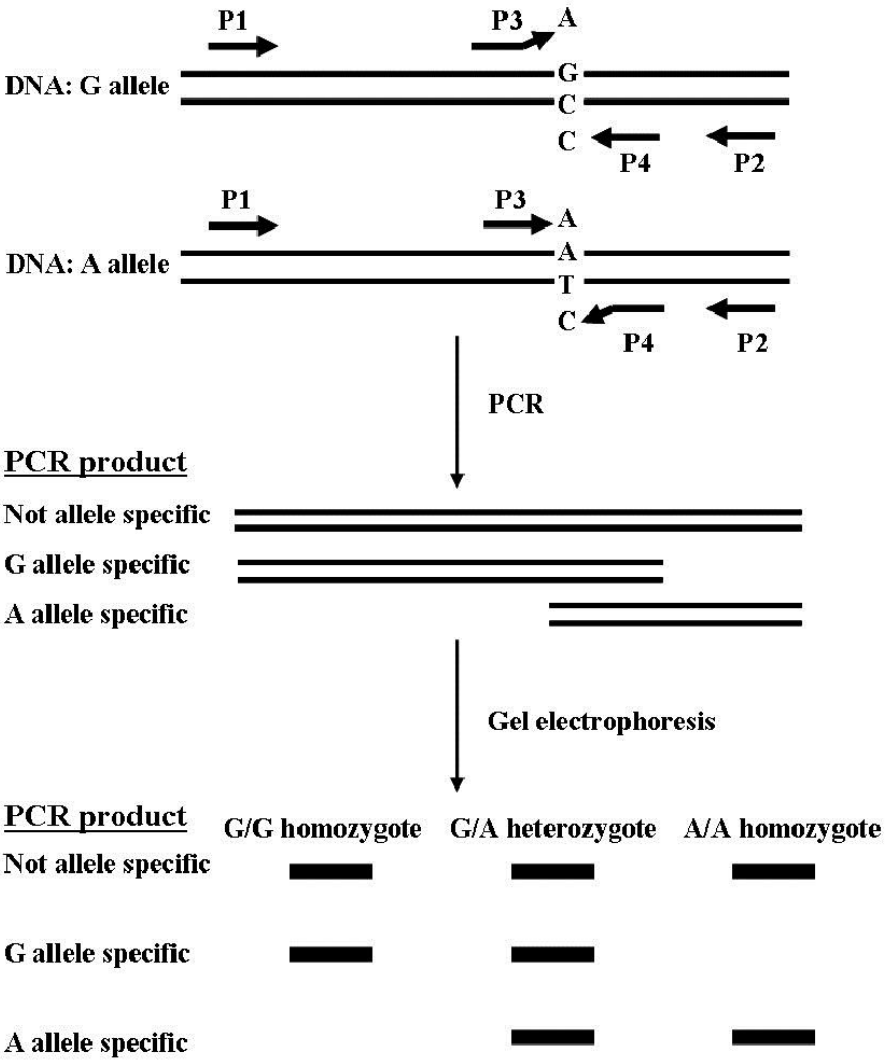

Figure 2.5: Schemata of adapted Multiplex tetra-primer ARMS-PCR amplification used for genotyping
Schematic presentation of the tetra-primer ARMS-PCR method in which an outer primer pair amplifies a non-allele specific bigger amplicon. The asymmetrically located inner primers simultaneously produce an amplicon from either the wild type or the *hirame* SNP allele in combination with the outer primer set. This results in a middle and smaller fragment. Redrawn after Yang et al. (2006).

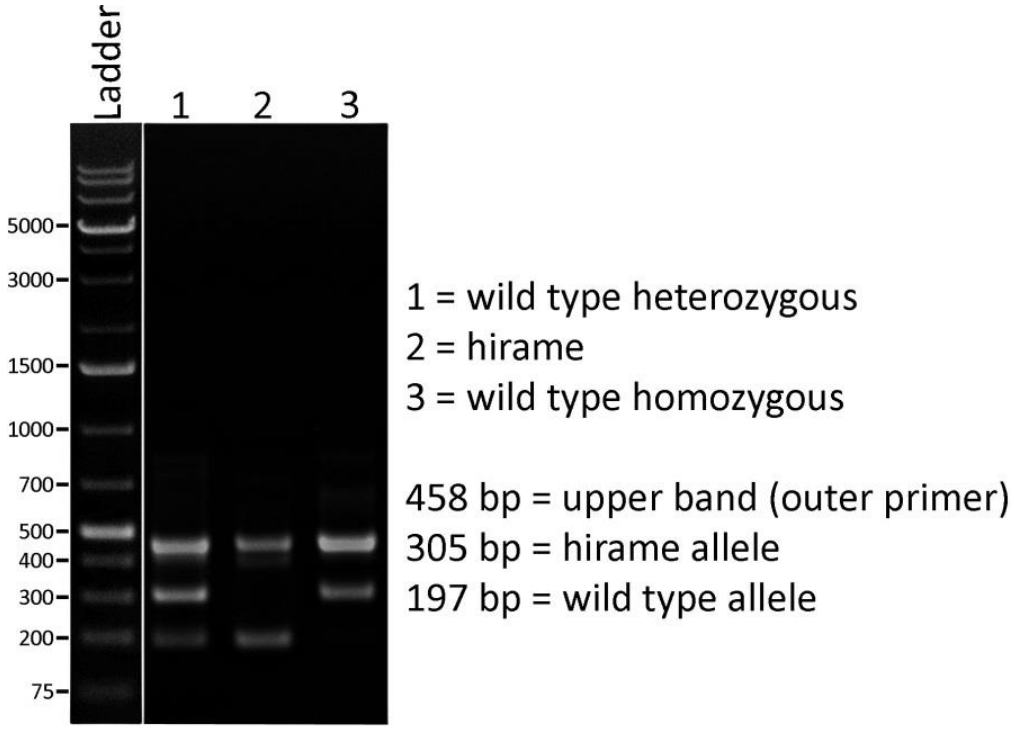

Figure 2.6: Example of tetra-primer ARMS PCR with Medaka embryos

Example of tetra-primer ARMS-PCR to genotype Medaka$^{j50\text{-}20C}$ sibling embryos at any stage of development to examine their genotype. Both primer pairs were designed to result in distinguishably different amplicon lengths after agarose gel electrophoresis. Outer primers give upper band with at 458bp, middle band represents *hirame* allele present in *hirame* mutants only and wild type heterozygous siblings and lower band highlights the wild type allele in heterozygous and homozygous wild type siblings. Ladder = 1KB (Thermo Scientific).

2.2.2.9 DNA Sequencing and sequence analysis

General DNA sequencing runs were performed through Thermo Fisher Scientific and Eurofins in-house next-generation sequencing (NGS) platforms. Analysis of raw sequences and chromatograms, compilation of contigs and sequence comparisons were performed using the free online download software package ApE.

2.2.2.10 In-situ probe synthesis

Prior to probe synthesis 5µg of midi-prep plasmid DNA containing the cDNA of interest was linearised by digesting the 3´end of the antisense sequence. The reaction is cleaned using phenol/chloroform/isoamyl alcohol (25:24:1 with 10mM Tris, pH 8.0, 1mM EDTA) extraction followed by ethanol precipitation.

In vitro RNA probe synthesis used to label the in-situ hybridisation probes either with digoxigenin using the DIG RNA Labelling Kit (Roche, Mannheim, Germany, Cat# 11175025910).

Probe fractionation was performed to optimize probe permeabilisation and performance within the specimen following the Parichy laboratory protocol. Therefore an alkaline hydrolysis was used to fragment probes of length greater than 300 nucleotides (nt) with adding 1/5th of 0.4M sodium bicarbonate, 1/5th of 0.6M sodium carbonate and a 60°C heat incubation. The length of the heat step is calculated as follows:
Time (min) = (starting kb – desired kb) / (0.11 x starting kb x desired kb).
Calculated examples of hydrolysis times were taken out of the ISH protocol from the Parichy laboratory at the University of Washington at Seattle (Parichy 2011) and is tabulated within the appendix (Appendix 7).

2.2.3 Cloning strategies

DNA fragments for ligation were generated by complete restriction, followed by heat inactivation of the restriction enzyme where possible. Dephosphorylation of DNA ends, when required, was achieved by adding 2 units of Shrimp Alkaline Phosphatase directly to the restriction enzyme reaction. If required, the desired fragment was purified by recovery from an agarose gel.
Vector DNA for use in ligations was digested with the appropriate restriction enzymes and purified through either Phenol/Chlorophorm precipitation or a manufacturer column with DNA Clean & Concentrator (Zymo Research, USA).

2.2.3.1 Ligations

Ligations were performed using 50-100ng of vector DNA and a three molar excess of insert DNA, catalysed by 10 units of T4 DNA ligase in 10µl reaction volume (following manufacturers instruction). Ligations were incubated at 4°C overnight or 2h at RT. PCR products were mostly cloned into pGEM-T Easy vector following Promega instructions.

2.2.3.2 Preparation and Transformation of Competent E.coli

Competent cells of the DH5α E.coli strain were prepared in-house following the protocol from Dr K. Kaji (Appendix 2), which yields transformation efficiencies up to 1×10^9 transformants/µg plasmid DNA. Introduction of plasmid DNA into E.coli was performed by the calcium chloride method as per Sambrook (SAMBROOK et al. 1989). Thereby a maximum plasmid DNA volume of 1/10 was incubated with DH5α competent cells for 20min on ice followed by a 45s heat shock at 42°C. Following transformation bacteria cells were incubated in 1ml SOC for 1h at 37°C with gentle shaking before

spreading on LB-agar plates containing required antibiotics. Plates were incubated upside-down overnight at 37°C. Where colour selection of colonies was necessary (e.g. p-GEM T-EASY cloning) prior spreading, plates were prepared with 200µg/ml X-gal and 160µg/ml IPTG was added.

2.2.4 Medaka Fish and Zebrafish Methods

2.2.4.1 Aquarium System, water and room conditions

The water condition of our fish facility is pH 6.8-7.5, 200-450mS/cm, 26-28°C, NH_4 <0.2mg/L, NO_2 <0.05mg/L, NO_3 <20mg/L. Whilst Medaka is more tolerant of varying water quality than Zebrafish, weak inbred strains, such as the transparent strain HNI prefer soft water (300µS/cm) compared to Zebrafish (700µS/cm). As the natural habitats of Medaka are rice fields and streams with little water flow, Medaka are stressed in a strong water flow such as that in which Zebrafish are kept. Thus, water flow to tanks needs to be adjusted to a minimum.
Since Medaka is native to regions of East Asia with four seasons, it tolerates wide ranges of temperature (4-38°C) and salinity. The fish room is kept at 25-28°C, with 14 hours of light and 10 hours of darkness. Medaka spawns better in relatively strong light (at least 100 lux).

2.2.4.2 Fish husbandry of Medaka *fish and* Zebrafish

Embryos were obtained through crosses of wild type, mutant and transgenic fish lines kept in the University of Bath Zebrafish facility. Breeding Zebrafish adults were kept separate from soft shelled eggs falling down to the bottom of the tank. Medaka pairs can be kept together in mouse cages as eggs are hardy and stay close to the female's body and do not fall down immediately. Refer to HO Project license: PPL30/2937.

2.2.4.3 Raising of Zebrafish *embryos*

Zebrafish embryos were raised and stages according to Kimmel et al. 1995 (Appendix 4). Dechorionation was either performed with Watchmakers' No.5 forceps or with 20µg/ml Pronase for embryos older than 18hpf. For further manipulation of embryos older than 15hpf, tricaine was added to the embryo medium to a final concentration of 0.2% v/v to immobilise the specimen. Note hatching period in Zebrafish is around 48 hpf and free feeding is after 72 hpf.

2.2.4.4 Raising of Medaka *embryos*

Medaka fish lay their eggs in clusters held together by filaments, which are attached on the egg chorion. Eggs are cleaned up by unclustering with forceps. To determine the embryonic development of Medaka fish embryos after fertilisation, eggs are incubated at 27°C and staged according to the Iwamatsu's staging (Iwamatsu 2004) (Appendix 5). To accelerate the growth temperature shifting can be done occasionally to facilitate experimental procedures. Hence, the Temperature-Stage-Correlation matrix (provided by Dr M. Furutani-Seiki) (Appendix 6) needs to be taken into consideration so that embryos can be incubated between a temperature range of 4°C and 33°C, without compromising their health.

2.2.4.5 Injection of Zebrafish *and* Medaka *embryos*

To calculate the micropipette injection volume I placed one drop on a micrometer slide (Fisher, 12-561-SM1) and measured the diameter of the drop. The value 100 on the micrometer slide corresponds to 1mm ($1mm^3$ = 1µl). We have measured our drop to be 15, which means $0.15mm^3$. Taking the formula of a spherical object, we would result in $V(\mu l) = (4/3)\pi (d/2)^3 = (\pi \times d^3)/6 = (\pi \times 0.15^3)/6$ = 1.76nl injected into 1-cell stage embryos.

Before starting injection an agarose plate was prepared to hold individual eggs. Hot 1.5% agarose was poured into a 10cm petri dish in which a custom made ridged plexiglass mould was dropped in. After the agarose solidified, the mould is removed to reveal the sketch shape of the mould to hold the embryos.

Injection of Medaka embryos was carried out with borosilicate glass capillaries 1.0mm O.D. x 0.58mm I.D. (standard wall without filament) from Harvard Apparatus Ltd, UK. For injections into Zebrafish embryos I used thin walled filamentous glass capillaries 1.0mm O.D. x 0.75mm I.D. (World Precision Instruments, Inc., USA). Needles for injection were made by pulling glass capillaries on a Micropipette puller (Narishige model PC-10, Japan). Injections were performed under a dissecting microscope using a WPI Pneumatic PicoPump Nanoinjector into the cytoplasm on 1-cell stage Medaka embryos or the yolk sac of Zebrafish embryos. Occasionally, 0.1% Red was added to the DNA solutions if needed.

2.2.4.6 Removing the chorion of Zebrafish *and* Medaka *embryos*

Freshly layed and fertilised eggs in Medaka differ in appearance to Zebrafish eggs. Filaments on the chorion which can be cleaned up by unclustering using forceps hold them together. The chorion of Zebrafish embryos is much softer and can be removed manually with forceps or by incubation in

20µg/ml Pronase. Medaka embryos however are surrounded by a much harder chorion consisting out of a soft inner layer and a harder outer layer, meaning that manual dechorionation is impossible when the embryos morphology has to stay intact.
It is necessary to dechorinate embyros for detailed observation of embryogenesis or for other protocols like cell transplantation, in-situ hybridisation or antibody staining, resulting in better imaging quality and accuracy. To achieve this, unclustered eggs are transferred onto fine waterproof sandpaper (p2000) and gently rolled, using the forefinger to remove any filaments on the chorion. Embryos can either be incubated for 40 min in pronase (20mg/ml) to remove the inner softer layer of the chorion, followed by quick washes in embryo medium or directly placed into freshly made hatching enzyme. Hatching enzyme is obtained from late stage embryos and is necessary to remove the outer chorion, which can take up to 30min on living specimen.
For further manipulation of dechorionated embryos older than stage 23, tricaine was added to the embryo medium to a final concentration of 0.2% v/v. A low concentration of tricaine in this case allowed experimental procedures such as live-imaging due to anaesthetised immobile embryos.

2.2.5 Whole-mount in-situ hybridisation(WISH)

Dechorinated embryos are fixed in 4% PFA for 1-10 days at 4°C depending on its developmental stage, whereby older embryos are fixed for a longer period. After fixation, embryos are washed three times in PBST before dehydrating through a Methanol series beginning with 25%, followed by 50%, 75% and 100% Methanol in PBST. Dehydrated embryos can be stored at -20°C until needed. All washes were done under gentle agitation in 2ml round bottom centrifuge tubes throughout the protocol.
The first step of the in-situ hybridisation protocol is to rehydrate the embyros in a reverse Methanol in PBST series of 75%, 50% and 25% for 5 min each, followed by three 5 min washes in PBST only. Embryos are then incubated in Proteinase K (10µg/ml) 10µg/ml Proteinase K/PBST to permeabilise cell walls to allow effective probe penetration before commencing with *in situ* hybridisation (WISH) technique. Thereby the incubation time with Proteinase K depends on individual developmental stages as well as spatial and temporal projection of the specific anti-sense probe used for each WISH in Medaka embryos (Table 2.3).

Table 2.3: ProteinaseK incubation times for Medaka embryos at different developmental stages

Developmental stage	Incubation time with ProteinaseK
Stage 20 - stage 22	Rinsing
Stage 23 - stage 24	3 min
Stage 25 - stage 27	5 min
Stage 28 - stage 29	~ 8 min
Stage 30 - stage 32	~ 10 min
Stage 33 - stage 34	~ 15 min
Stage 35- stage 36	~ 20 min
Stage 37	~ 30 min
Stage 38	~ 40 min
Stage 39	~ 45 min

To stop the kinase reaction fixed embryos are washed twice in PBST and re-fixed in 4% PFA for 2 hours at RT. To remove the samples from PFA three washes in PBST are applied. Embryos are then pre-hybridised for 1.5 hours in a 100% hybridisation mix (HM) at 65°C before incubating them overnight at 65°C in approximately 200µl of pre-heated synthesised probe in 100% hybridisation mix. The next day, embryos are washed with 66% HM in 33% 2X SSC, then 33% HM in 66% 2X SSC, followed by 2X SSC washes for 10 min each in 65°C before leaving them twice for 30 min at 65°C in 0,1% 2X SSC in Milli-Q water. Afterwards embryos are washed twice in PBST for 5 min to remove traces of SSC. Blocking solution is added for one hour at RT, before resting the embryos overnight at 4°C with anti-DIG antibodies (1:500d dilution in blocking solution).

The following day, embryos are periodically washed in PBST over duration of 5 hours under gentle agitation. After the last washing step, embryos are rinsed three times in freshly prepared AP buffer. To accomplish purple staining samples are transferred to NBT/BCIP (Roche, Mannheim, Germany Cat# 11681451001) solution until the signal was strong enough or background started to appear. The reaction can be stopped by rinsing twice with PBST and re-fixation for 2h in 4% PFA at RT. For storage at 4°C samples undergo a glycerol series of 30%, 50% and 80% glycerol in water.

For *in situ* double staining embryos had to be incubated simultaneously with a DIG and Fluorescein anti-sense probe. After development of the first staining, the active alkaline phosphatase from anti-

DIG was inactivated by acid treatment with 0.1M glycine-HCL pH 2.2 for 30min. This was then followed by extensive washing with PBST. Another blocking step was carried out and the anti-Fluorescein antibody was incubated overnight at 4°C, before clearing the samples up from any residues of that by washing them with PBST. The anti-fluorescein can either be imaged directly or incubated with NBT/BCIP or Fast Red prepared using manufacturer's instruction.

2.2.6 Whole-mount Antibody Staining of Medaka embryos

Embryos were fixed for 2h at RT or overnight at 4°C. The following day samples were cleared of PFA by washing them in PBST three times for 10min, followed by a permeabilisation step in 0.5% Triton X-100/PBS overnight at 4°C with gentle shaking. Traces of Triton were removed by washing the embryos in PBST three times for 10min at RT. A blocking step was carried out in blocking solution (49ml PBST, 1ml 2% sheep serum, 0.1g BSA) for 2 hours at room temperature before incubation with the primary antibody in blocking solution at 4°C overnight (usually in a 1:100-1:2000 dilution). First antibody was removed by washing the samples three times in PBST, 10min each at RT. The secondary antibody diluted in blocking solution was applied and left overnight at 4°C. After removing the second antibody samples were washed with PBST as outlined before. The embryos can then be mounted and visualised depending on the wavelength of the fluorescent dye.

2.2.7 Resin embedding and section of Medaka embryos

Resin sections have been prepared using Kulzer Technovit® 8100 Cold-curing resin kit (Germany). This HEMA-based plastic embedding system is suitable for producing uniform sections up to 1 micron thin revealing a clear morphology of the tissue and cell structures, observable under light microscopy. The cold polymerisation process during embedding prevents sample shrinkage, thus decrease dye leakage after *in situ* hybridisation has been carried out. The resin polymerisation step is oxygen sensitive, therefore the embedding process must be performed fast and must be sealed for the final hardening (Emgrid Pty 2013). A detailed in-house protocol from Dr T. Sambe-Adachi is laid out in Appendix 2. Resin sections were placed onto Superfrost Plus glass slides (Menzel, Germany) as these have been tested to be of much greater adherence during subsequent staining procedures (Appendix 3). Some sections have been counterstained with 1% Neutral Red to label and highlight nuclei within the tissue structures (Appendix 2).

2.2.8 Embryo mounting and microscope techniques

Low power microscopic analysis and general embryo handling was mostly performed under an MZ12-FL dissecting microscope (Leica). Anaesthetised embryos were placed either in 3% methylcellulose or 100% glycerol on a cavity slide and orientated with forceps to prevent rolling. Snap shot imaging was performed either on the Eclipse E800 (Nikon) microscope using Nomarski optics and a colour SPOT digital camera (Diagnostic Instruments) or the Zeiss fluorescence dissecting microscope using bright field or fluorescence combined with a black and white Zeiss camera.
For static Z-stack imaging embryos had to be immobilised in 1% low melting agarose to prevent rolling and movements and subsequently imaged on the Zeiss microscope.
All images were analysed, contrasted and enhanced using Photoshop™ edition CS3 (Adobe) obtained with a personal licence.

2.3 Statistical Methods

2.3.1 2-Sample t-Test

To determine significance of counted melanoblasts and melanophores a Student´s 2-Sample t-Test was conducted with the Minitab statistics programme. Herein, T-values compare responses between two independent groups such as *hirame* and wild type with normal distributions (dt) (tested with dt plot). Herein $p<0.05$ is indicated by one *, $p<0.01$ = ** and $p<0.001$ = ***.

2.3.2 Chi-Square Test

The Chi-Square (X^2) test investigates in general whether distributions of variables in different categories differ from one another. It compares the actual counts of categorical outputs between two (or more) independent groups. This for example was used to determine the distribution of melanoblast counts within the same set of resin sections within different categories.

2.3.3 Bonferroni-correction

This statistical test is used to take into consideration multiple comparisons. It adjusts the *P* values of several dependent or independent concurrent statistical tests on a single set of data by dividing the *P* value by the number of comparisons being made, thus increasing the probability of a significant output. It therefore reduces the chance of false-positive results on statistical comparisons on a single

set of data. The Bonferroni correction was also used to determine statistically the distribution of melanoblast counts within resin sections and significant values were indicated as follows: $p<0.01$ = *, $p<0.001$ = **.

3 Chapter: Characterisation of the melanocyte lineage in wild type and *hirame* and establishment of a Medaka *dct* promoter

3.1 Background

3.1.1 Importance of YAP in melanocytes

In humans, melanocytes are found in a number of locations including the eyes, ears, and particularly in the skin, at the junction of dermis and epidermis. In humans, they populate the basement membrane in a density of around 1000 cell per square millimeter. Their function is to synthesise melanin and transport it in melanosomes the upper epidermal keratinocytes, which helps to protect underlying layers from cell damaging ultraviolet light (UV) (Kim et al. 2013). In teleosts, especially Zebrafish and Medaka, melanin producing melanocytes can be found in three distinguishable stripes on the embryonic body, the dorsal, lateral and ventral stripe (Lamoreux et al. 2005; Kelsh & Schmid et al. 2000). Next to protection, melanin or the pigment cell patterning in fish has also the function of camouflage (Kelsh 2004). Several of the genetic requirements for neural crest embryonic melanocyte pattern, have been demonstrated to be important in melanoma, a deadly highly pro-metastatic cancer originating from melanocytes, such as ECM, migration, proliferation and growth (Uong & Zon 2010).

One hypothesis is that the Hippo pathway is a key regulator in melanocyte growth, transformation and/or migration. Supporting data comes from melanoma studies investigating the contribution of Hippo signalling in regard to melanoma transforming properties.

The first study reporting about YAP involvement in the transformation of melanocytes into cancerous melanoma cells was provided by Lamar et al. in 2012. Their *in vivo* studies showed that through interaction with the TEAD DNA-binding domain, YAP mediates tumour growth and metastasis, including invasion and migration in a cell-autonomous fashion. The activated version of YAP S127A, in which LATS mediated phosphorylation is hindered by exchanging serine to alanine at position 127aa, enhanced the growth of transplanted melanoma cell lines *in vivo* and increased the number and size of metastases after tail-vein injection to 60% (Lamar et al. 2012). In addition and supporting these findings Nallet-Staub et al. showed in 2014 that overexpression of YAP increased the anchorage-independent growth in cutaneous melanoma cultures in soft agar, thus identifying YAP´s metastatic potential (Nallet-Staub et al. 2014). Furthermore, they carried out knockdowns of YAP and TAZ *in vitro* through small hairpin RNA, which specifically repressed melanoma cell tumorigenicity and invasiveness, represented by decreased colony formation in anchorage-independent growth assays on soft matrigel. Here YAP had a greater effect than TAZ without inhibition of cell proliferation. I*n vivo* analyses revealed that knockdown of *yap* and *taz* reduced the depth of invasiveness into the basal layer after xenotransplantation and also dramatically inhibited not only the occurrence, but also the actual size of lung metastases after tail-vein injections with melanoma cultures. Out of 6

injections 1-2 mice formed metastases compared to five out of six in the positive control. Knockdown of YAP and TAZ directly decreased the transcriptional levels of CTGF encoded by CCN2, a TEAD mediated transcription factor target gene, while overexpression had the opposite effect (Zhang et al., 2009). Herein downregulation of TAZ had a much greater effect than YAP on its downstream target genes (Nallet-Staub et al. 2014). Therein, observed differences in individual melanoma cell cultures might be due to dissimilar endogenous expression levels of YAP and TAZ, both factors have been shown to act redundantly. Therefore, overexpression of one component might not have an effect on transforming cell properties in mammalian studies, if the paralogue is already present in high levels. To summarise, these studies link higher transcript and protein levels of YAP and activated variants of YAP to an increased cell migration potential. Thus, we suggest that intrinsic YAP might be required for normal melanocyte migration within vertebrates. To investigate this, we utilised the unique Medaka *hirame* mutant. Observations made from 3 dpf *hirame* embryos indicated a melanocyte defect, specifically in form of reduced numbers on the yolk sac area. We speculated that the loss of YAP might do the opposite and slow cell movement to the extent that individual melanocytes might struggle to escape from the embryo and move on the yolk sac. In this chapter, we analyse thoroughly the melanocyte phenotype in *hirame* from its arising until embryonic death.

3.2 Results

3.2.1 Crossing Cab$^{j50\text{-}20C}$ into HB32C to enhance melanogenesis

The mutagenesis screen in Medaka lead by Furutani-Seiki 2004, was mainly carried out in the Cab, Heino and Kaga strains. The Cab strain originated from a Southern population of Medaka and was once obtained from the Carolina Biological supply, North Carolina (Kinoshita et al. 2009) After that it was maintained as an inbred strain at the Wittbrodt laboratory in Germany (Loosli et al. 2000). It was used for that particular screen in Japan. The Kaga strain originated from a Northern population and was used for genetic linkage analysis in Furutani-Seiki´s study, whereas the albino Heino strain was mainly used for specific locus tests (Furutani-Seiki et al. 2004). *Hirame* $^{j50\text{-}20C}$ is maintained in the Cab strain, exhibiting weakly melanised to amelanotic melanocytes due to its homozygosity for the recessive b' allele at the B locus. The B locus encodes for *solute carrier family 45 member 2 (slc45a2)* gene, a Membrane-associated transporter protein also known as melanoma antigen AIM1 which mediates melanin synthesis through microphthalmia-associated transcription factor. The original Cab strain contains a mutation within the promoter region of *slc45a2* leading to a pale skin phenotype only, whereas other pigment mutants are characterised by coding changes within the *slc45a2* gene sequence (Fukamachi et al. 2008). The phenotype named hiMedaka, associated with that strain is

orange-red as xanthophore differentiation is unaffected. In comparison the HB32C strain is a wild type strain in which the melanocyte lineage synthesises high amounts of melanin. This strain was originally collected near Chiba City and first bred at Chiba University around 1970. It was then established as an inbred strain by Hyodo Taguchi at the National Institute of Radiological Sciences (NIRS) (Hyodo-Taguchi 1996).

Initial microscopic observations of 3 dpf (st.28) *hirame* embryos bred in the Cab background hinted towards a defect in the melanocyte neural crest lineage due to reduced numbers of melanocytes on the yolk sac compared to its wild type siblings (RN Kelsh personal communication,
Figure 1.4). However, in this particular strain fully differentiated melanocytes are weakly melanised, which makes it more difficult to identify and quantify this cell type by light microscopy. Therefore, I crossed heterozygous *hirame* carrier onto the HB32C wild type background in which melanocytes produce an increased amount of melanin, resulting in darker grey-brown and more distinguishable differentiated melanocytes. When bred onto the HB32C background, and selected for B, we observed that *hirame (hir)* mutants indeed had fewer melanocytes on the body and yolk sac in 3 dpf embryos compared to its wild type sibling (Figure 3.1C,D).
This simple observation confirmed the validity of our hypothesis that melanocyte differentiation was disrupted in *hirame* mutants. Differentiated melanocytes can be directly identified after 9 somites (st.22) through their accumulation of melanin in melanosomes (Lamoreux et al. 2005). In order to assess their unmelanised progenitor melanoblasts prior to stage 28, I analysed the pigment cell marker *dopachrome tautomerase* (*Dct)* expression pattern in sequential developmental stages. This would provide us insights about asked when melanocyte patterning first becomes distinguishable from wild type (WT) siblings.

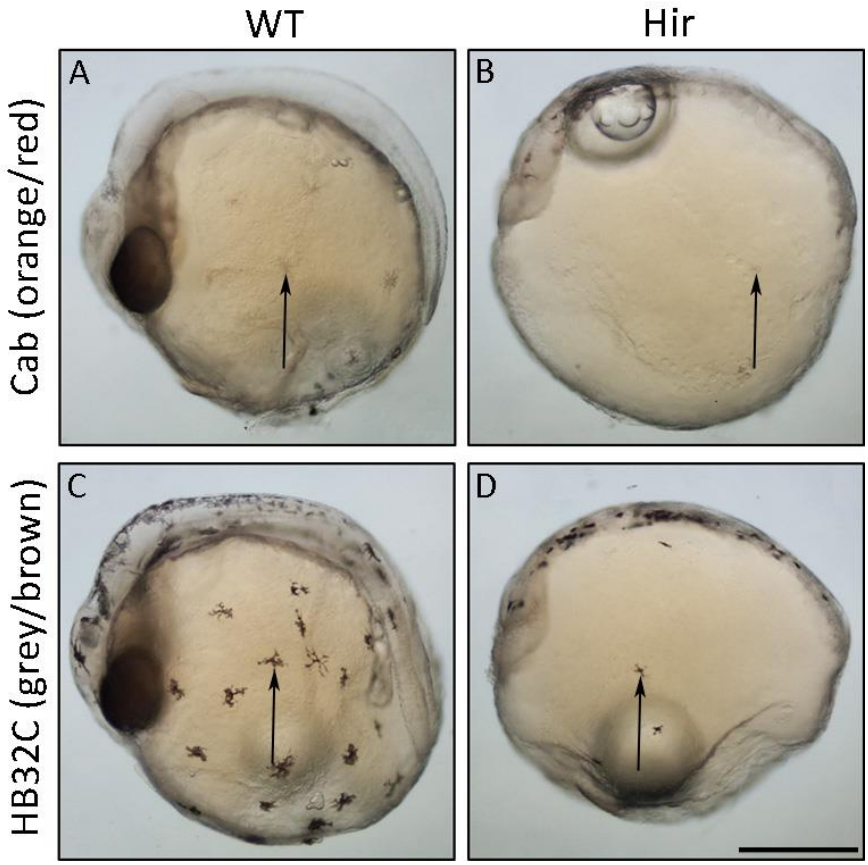

Figure 3.1: Comparison of 3 dpf (st.28) wild type and *hirame* embryos in Cab with weakly melanised melanocytes and in HB32C with strong dark brown melanophores

A,B) Melanocytes are hardly distinguishable and unquantifiable under normal light microscopy in wild type and *hirame* with Cab background. **C,D)** *Hirame*$^{j50\text{-}20C}$ was crossed into HB32C background to visualise differentiated melanin-rich melanocytes. Now, numbers of melanocytes in HB32C wild type embryos could easily be quantified and the defect in *hirame* (D) pigment cells is readily seen. Scale bar = 500µm.

3.2.2 Analysis of *Dopachrome tautomerase (Dct)* expression in wild type and *hirame* embryos

3.2.2.1 Observing the melanocyte pattern through in situ hybridisation (ISH)

Dopachrome tautomerase (*Dct*), also known as *tyrosinase-related protein 2* (*Trp-2*) acts downstream of tyrosinase and collaborates in the biosynthetic pathway of eumelanin by catalysing the conversion of dopachrome to 5,5-dihydroxyindole-2-carboxylic acid (DHICA) in pigment cells (Kelsh et al. 2000). Studies in Zebrafish and mouse have shown *Dct* to be one of the earliest markers of the melanocyte lineage (Kelsh et al. 2000; Steel et al. 1992). In Zebrafish it was shown that *dopachrome tautomerase* transcriptional levels can be detected as early as 16 hpf (14-19 somites) within progenitors of the

early pigmented retinal epithelium (PRE) in the developing eye. Then over the next 5 hours *Dct* expression was detected throughout the outer layer of the retinal epithelium and within melanocyte precursors (melanoblasts) in the trunk and tail of 21 hpf embryos (Kelsh et al. 2000). In comparison to Zebrafish, Medaka studies have reported *Dct* expression only at 75 hpf (4dpf, st.30) (Nagao et al. 2014). Nagao et al. published a *Dct in situ* probe showing no overlap with the xanthine dehydrogenase (*xdh)* expression pattern, a marker for early xanthophores and leucophores in Medaka. They classified the *Dct* anti-sense probe as melanocyte cell specific, because it matched the *Dct* pattern and distribution comparable to published work in Zebrafish (Van Otterloo et al. 2010). With this background and probe information, we asked the question, "how early can we see a melanocyte patterning defect in *hirame* embryos compared to normal wild type embryos?" To answer that I examined a series of developmental stages starting from stage 20 (1 dpf 7.5h and 4 somites) to stage 32 (4 dpf 5h and somite completion), in which I used *in situ* hybridisation (ISH) with an anti-sense probe against *Dct,* detecting early unmelanised melanoblasts in whole-mount embryos. Appendix 8 shows all individual stages analysed in this series, whereas detailed analysis was carried out for stage 21, 24 and 28 only representing the embryonic melanocyte development (Figure 3.2).

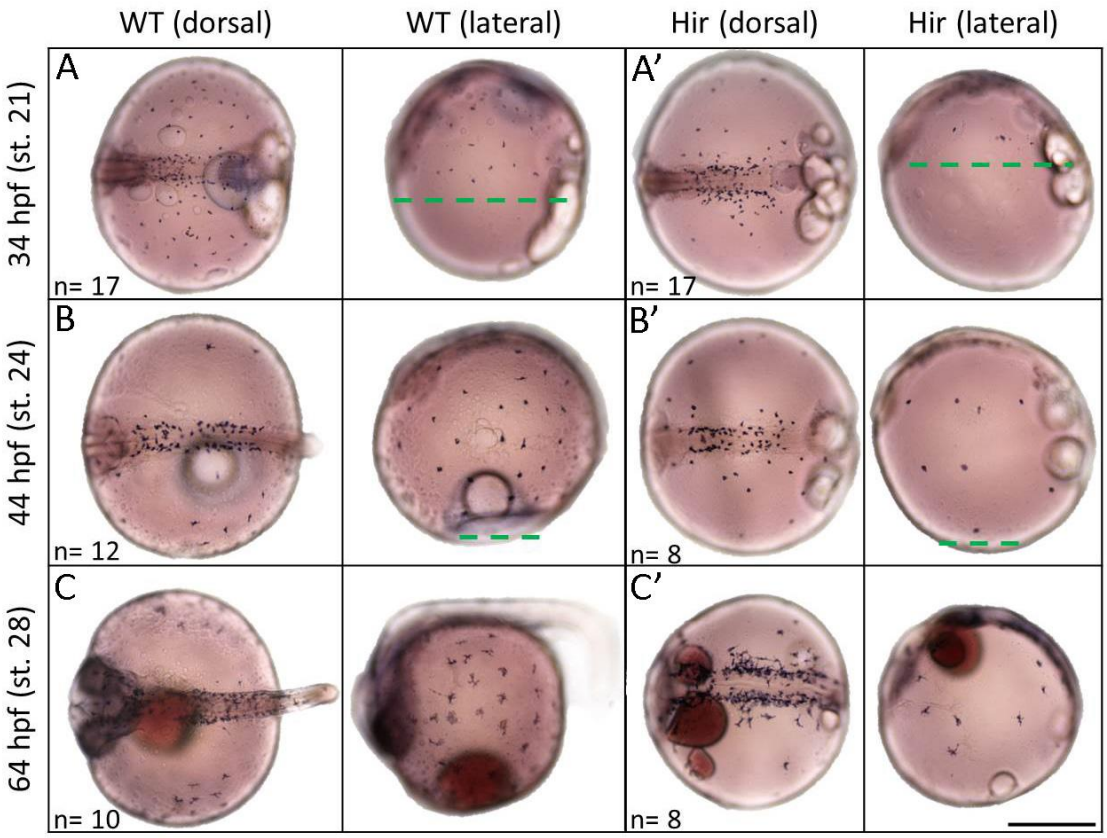

Figure 3.2: ISH of *Dct* in st.21, 24 and 28 wild type and *hirame* embryos showing the early melanoblast and later differentiated melanocyte patterning defect

Dopachrome tautomerase (*Dct*) WISH to highlight the melanocyte lineage in wild type and *hirame*. Series of embryonic stages (st. 21, st. 24, st. 28) are represented in panels A/A', B/B' and C/C' with embryos in dorsal and lateral view and anterior to the left. The overall pattern seem to indicate that unmelanised melanoblasts in early stages (st.21) and melanised melanocytes in later stages (st.24, st.28) are present within the body and on the yolk sac. The overall amount of cells seem to be reduced on the yolk sac throughout. Melanoblast location on the yolk sac of st.21 and st.24 embryos suggest a slower migration of remaining *Dct*+ cells in *hirame* compared to wild type siblings (indicated by dashed green lines). Scale bar = 500µm.

We observed that early in embryonic development and prior to melanisation (st. 21, 1d 10 hpf), wild type embryos exhibited melanoblasts within the body as well as migrating melanoblasts dispersed on the dorsal part of the yolk sac (Figure 3.2A, A'). At that stage *hirame* melanoblast numbers within the body appeared normally (A' dorsal) whereas numbers on the yolk sac (A' dorsal, sagittal) seemed to be reduced. In addition wild type melanoblasts dispersed progressively more ventrally on the yolk, but this process appeared delayed in *hirame* mutants where both the numbers and the ventral spread of melanoblasts were decreased (indicated by dashed green lines). At higher magnification it is more obvious that melanoblasts in *hirame* embryos accumulated alongside the body axis (Figure 3.3B) compared to wild type embryos (Figure 3.3A).

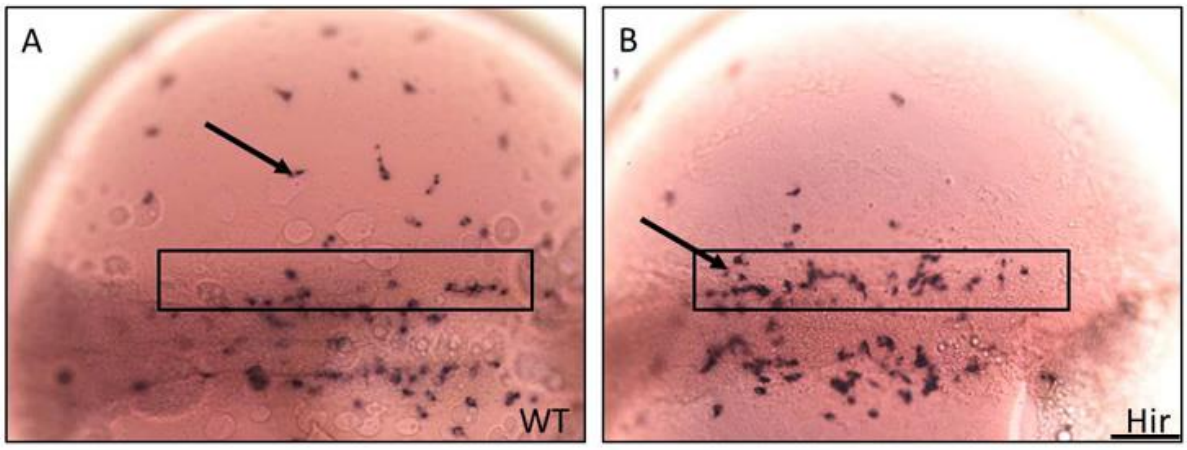

Figure 3.3: Melanoblasts in *hirame* reside in close proximity to the body axis at st.21

Close-ups of st.21 wild type (WT) and *hirame* (Hir) whole-mount embryos after *in situ* hybridisation for *dopachrome tautomerase (Dct).* Black rectangles enclose the area in which melanoblasts (arrow) seem to be accumulated in *hirame* embryos (B) compared to wild type embryos (A). Note also the increased numbers in yolk sac melanoblasts in WT embryos. Scale bar = 100µm.

Over the next 10 hours up to stage 24 wild type *Dct* expressing melanoblasts increased in numbers and migrated ventrally away from the body. In contrast, in *hirame* the melanoblast numbers on the yolk sac remained dramatically reduced; although some more Dct^{+} cells migrated further away from the body. This ventral progression was still slower than in wild type (indicated by dashed green lines, Figure 3.2B' sagital). Meanwhile melanoblasts differentiated and synthesised visible melanin. Melanocyte migration onto the yolk sac was completed by stage 28 in wild type (Figure 3.2C) (2d 16 hpf), but numbers in *hirame* embryos still remained low (C'). To further characterise these effects, I carried out cell counts in both, *hirame* and wild type embryos after *Dct* ISH.

3.2.2.2 Quantification of melanocytes in wild type and hirame

Cell counts in *hirame* mutants and wild type siblings were carried out under the dissecting microscope and were noted separately for both, body and yolk sac (Graph 3.1).
These data revealed that the number of *Dct* positive cells on the body (Graph 3.1 A) of *hirame* was significantly higher than in wild type siblings at stage 21, and those on the yolk sac fewer, although the total number of cells were comparable. The increased number in the body of *hirame* remained at stage 24, but was reversed by stage 28, in which body melanocytes in *hirame* showed a dramatic reduction to 126.8 cells compared to its wild type siblings with around 301.1 cells.

Concerning melanoblast numbers on the yolk sac (Graph 3.1 B), cell counts confirmed our initial observation that in *hirame* an overall melanoblast and later melanocyte reduction on the yolk sac existed throughout all featured embryonic stages.
Surprisingly, in *hirame* the total cell number presented within the third section (Graph 3.1 C) indicated no significant difference in melanoblast numbers from wild type siblings at early stage 21. In contrast, beyond st.21 *Dct+* cell numbers were persistently lower in *hirame* compared to wild type.

These counts affirmed that before stage 21 wild type and *hirame* embryos exhibited the same quantities of melanoblasts. This changed from stage 21 onwards when total numbers of melanoblasts in *hirame* were significantly reduced throughout. Interestingly, even so at st.21 there is no quantitative difference in Dct^{+} cell numbers, melanoblasts resided more within the body, which was supported by visual examination of melanoblasts located in close proximity alongside the body axis.
However, the transition from body mesoderm to yolk sac epidermis can be difficult to distinguish when counting *Dct* positive cells under a dissecting microscope, which means that cell counts might not represent actual numbers in those two areas of interest at st.21. To obtain accurate quantities of melanoblasts at stage 21 within the body and on the yolk sac of *hirame* and wild type, I carried out consecutive resin sections showing the spatio-temporal position of cells within different tissue structures.

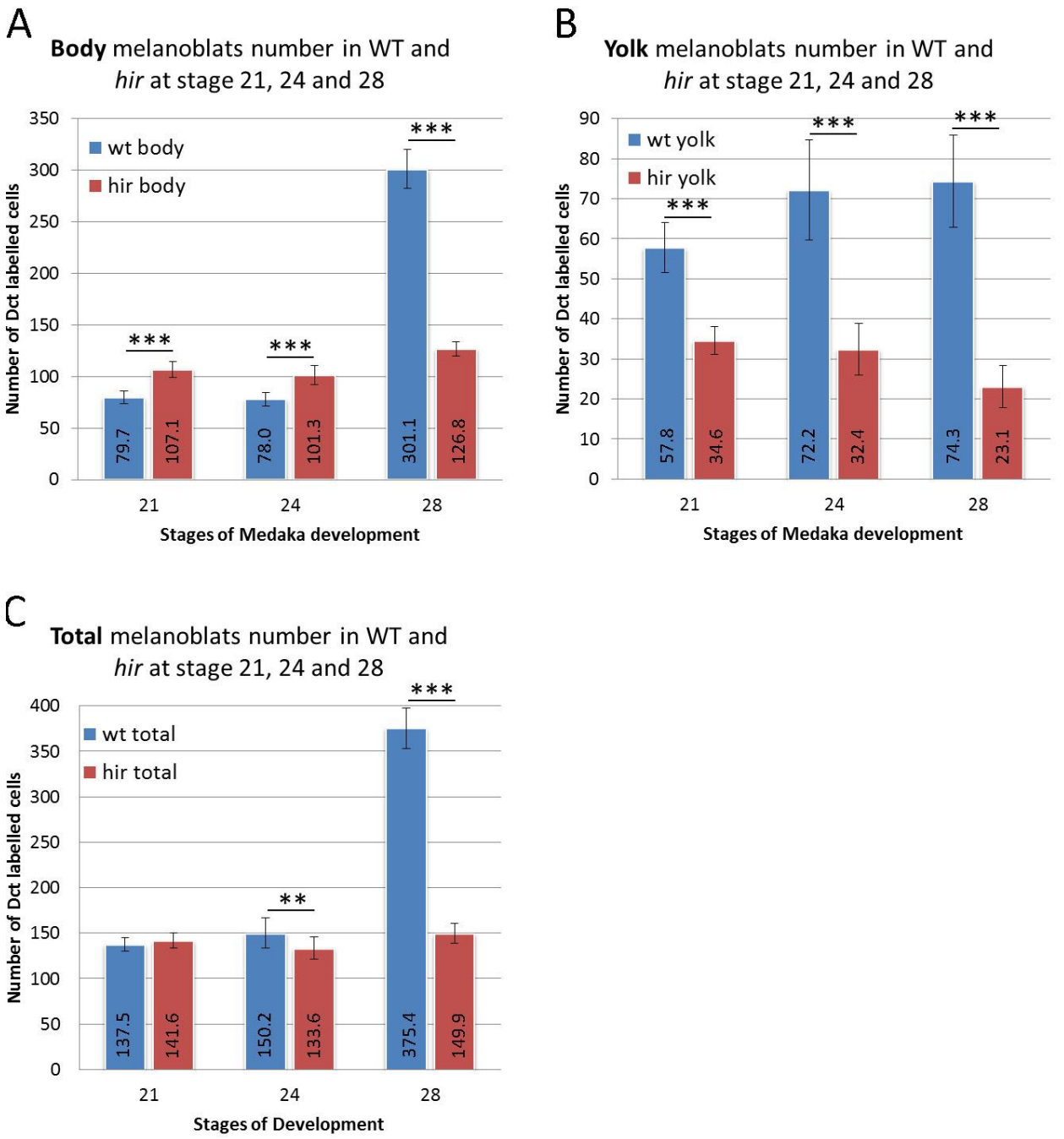

Graph 3.1: Numbers of melanoblasts and early differentiated melanocytes of wild type and *hirame* embryos counted at stage 21,24 and 28 after *in situ* hybridisation with *Dct*-antisense probe

A) *Hirame* exhibited more melanoblasts in the body compared to wild type at stage 21 (N=17) and stage 24 (N=12). In contrast, at st.28 in wild type (N=10) melanoblast numbers have risen up to around 300 cells, whereas *hirame* (N= 8) retained around 150 cells. **B)** Throughout embryonic development *hirame* possessed significantly lower quantities of yolk sac melanoblasts compared to wild type siblings. **C)** Despite the differences in cell number distribution, the total number of *Dct* positive cells at stage 21 in *hirame* and wild type is the same. At later stages (24, 28) the total number of melanoblasts is lower in *hirame.* All data are means ± SEM. 2-Sample-t-test: *p<0.05 , **p<0.01 or ***p<0.001; numbers within bars represent the average melanocyte counts within each stage .

3.2.2.3 Distribution of MC within the body of stage 21 embryos

Our WISH data suggested that at least initially during early stages of embryogenesis melanoblast distribution, specifically migration onto the yolk sac, may be defective. In order to determine the location of individual *Dct* positive melanoblasts within the embryo and whether those cells are accumulated within a specific area, consecutive cross sectioning from resin embedded embryos were performed. With that approach we set out to determine where within the body and whether melanoblasts can be found on the ventromedial or the lateral pathway. As we know, the neural crest precursors arise dorsally within the neural tube as premigratory neural crest from where cell commitment begins and melanocyte precursors can be detected. From this pre-migratory position melanoblasts migrate throughout the body initially on a medial pathway towards ventral position through mesodermal tissue laterally alongside the neural tube. Some melanoblasts then migrate from those ventral locations laterally along the outside of the mesoderm towards the top and migrate onto the yolk sac. A second wave of melanoblasts arising from pre-migratory positions migrate on a dorsolateral pathway to final positions within the body as well as contributing to yolk sac patterning (Raible & Eisen 1994). The schematic (Figure 3.4) illustrates anatomical features found in cross sections of the trunk region of an embryo at stage 21 (31 hpf), including the migration pathways of neural crest cell precursors and differentiated melanocytes.

Embedding tissue in resin has several advantages compared to frozen or paraffin embedding. Sample tissue retains a better morphology with less shrinkage, and the width of an individual section may be thinner; benefits we aimed for when planning this experiment. We generated 15 consecutive 8µm trunk sections starting from somite 2 onwards from 19 wild type and 18 *hirame* individual resin-embedded embryos to obtain a significant sample size. Single *Dct* positive cells were scored in 5 positions as outlined in Figure 3.4A; premigratory, medial/ventral/intra-somitic, dorso-lateral, contact with yolk/epidermis/mesoderm, and melanocytes on the yolk sac itself.

Graph: 3.2 represents those cell counts for each area. In total, four of five areas indicate significant statistical differences of melanoblasts between wild type (left columns) and *hirame* (right columns) either with *p<0.01 or **p<0.001 obtained after Chi-Square test, Mann-Whitney test and Bonferroni-Correction. We observed a decline in melanoblasts on the yolk sac in *hirame* mutants, which was accompanied with elevated numbers in close proximity to the lateral mesoderm of the body axis reaching out to the yolk sac epidermis (area of named yolk/epidermis/mesoderm). In addition, we could detect a significant difference in pre-migratory and dorsolateral positions. Within the pre-migratory location, numbers were lower in *hirame*, whereas on the dorsolateral pathway Dct^{+} cells were higher.

Taken together, at stage 21 melanoblasts accumulated within the mesodermal tissue and presented a dramatic decrease on the yolk sac itself. These counts support our previous melanoblast cell counts

in WISH showing an increase of numbers within the body. The asymmetry of cell distribution unaffected by total cell numbers, suggest a failure of melanoblast migration on the yolk sac in *hirame* embryos at stage 21.

Our next hypothesis was that the loss of YAP could also affect cell differentiation, especially in melanocytes. To further investigate this idea, we decided to carefully dissect the onset of melanisation during early stages of development.

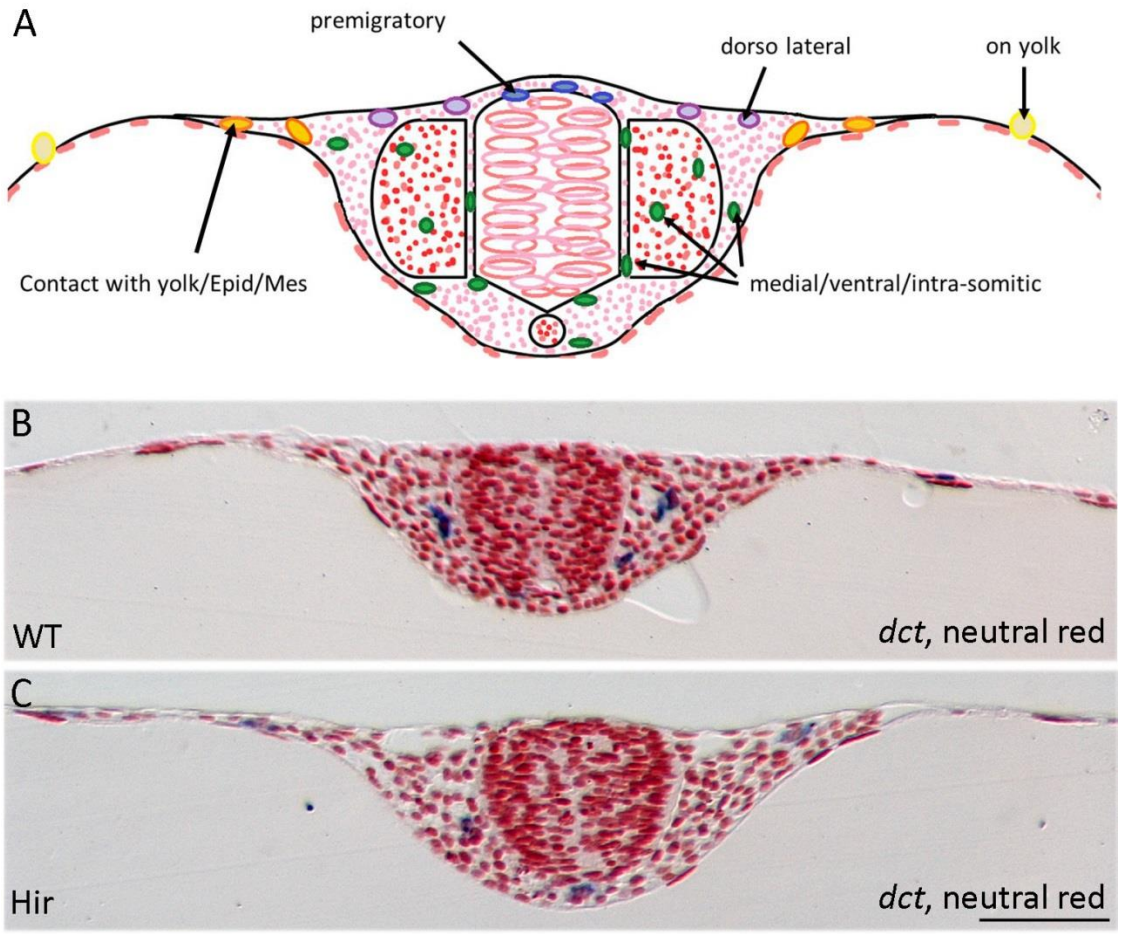

Figure 3.4: Schematic representation of internal and external melanoblast locations used for scoring and representative images of wild type and *hirame* resin cross sections at st.21

A) Schematic of a resin cross section of Medaka embryos at st.21 to indicate possible melanoblast locations distinguished and referred to in our analysis. Five categories were set to score melanoblast presence within 15 consecutive section in wild type and *hirame*: premigratory, medial/ventral/intra-somitic, dorso-lateral, contact with yolk/epidermis/mesoderm and melanocytes on the yolk sac itself. Taken this outline, melanoblasts from cross sections were then identified and placed in those categories to analyse their distribution within the embryo. **B/C)** Representative resin sections for wild type (B) and *hirame* (C) at st. 21 after *in situ* hybridisation with *Dct* as melanoblast marker and neutral red staining to label cell nuclei. Scale bar = 50µm.

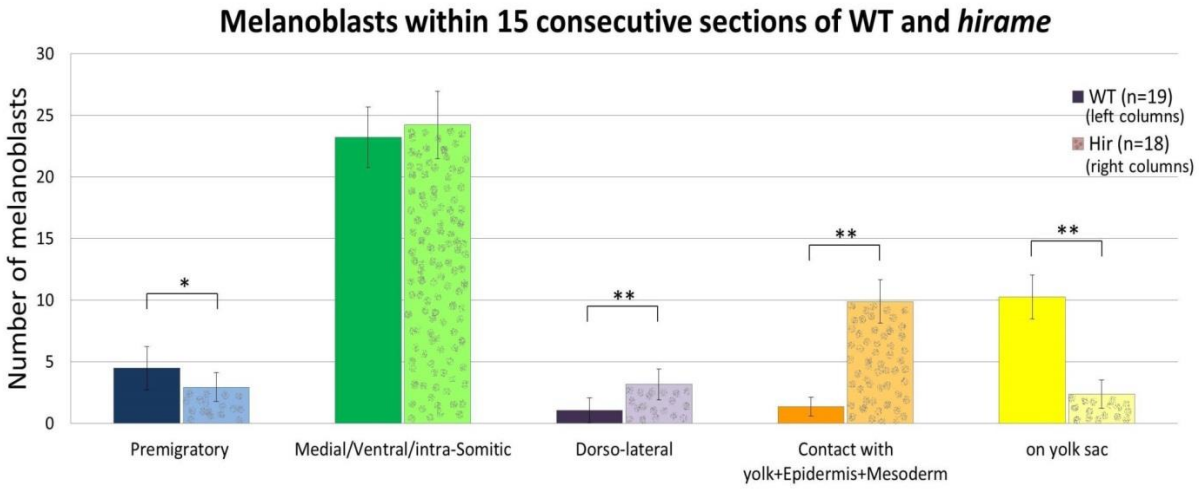

Graph: 3.2: Single cell quantification of melanoblasts in *Dct* st.21 embryos sections

Single cell quantifications of melanoblasts within 15 consecutive resin sections of 19 wild type (left plain columns) and 18 *hirame* (right speckled columns) st.21 embryos after *in situ* hybridisation with *Dct* followed by neutral red nuclei staining. Cells were separated and quantified in those 5 categories displayed in Figure 3.4A. 4 categories presented significant differences after Chi-Square test, Mann-Whitney test and Bonferroni-Correction *p<0.01; **p<0.001. The data indicates an asymmetric distribution of melanoblasts in *hirame* towards the edge of the mesoderm. The incline in Dct^{+} cells corresponds with the decrease on the yolk sac making this a specific migration defect at stage21. All data are means ± SEM.

3.2.3 Evaluating the onset of melanocyte differentiation

As previously noted *hirame* embryos develop differentiated melanocytes in late stages beyond 2 dpf. However, we do not know if the beginning of the differentiation process is happening in a similar fashion to wild type embryos with functional YAP protein present. Therefore, I investigated if the loss of functional YAP protein in *hirame* is affecting the onset of melanisation by scoring the overall presence of visible melanin in melanosomes synthesised during melanocyte cell differentiation. Offspring from HB32C heterozygous and homozygous carriers for the *hirame* allele j50-20C were staged carefully at 7 somite to 14 somite stages and photographed after fixation. As seen in Figure 3.5 and Figure 3.6 visible brown melanin accumulated in melanosomes and is first detectable at the 8 somite stage in wild type increasing until the 10th somite. Melanisation was also observed in *hirame* mutants during the same time window. Furthermore, consistent with our studies of *Dct* positive cells, we saw similar defects in dispersion of pigmented melanocytes on the yolk sac of *hirame* mutants from 8 somites onwards wherein melanocytes reside in close proximity to the lateral body axis compared to wild type siblings. Taken together, these data suggest that while migration of melanoblasts onto the yolk sac is impaired in *hirame* mutant, the timing of differentiation is not. However, to confirm this statement, we were determined to affirm the staging my analysing the circadian clock.

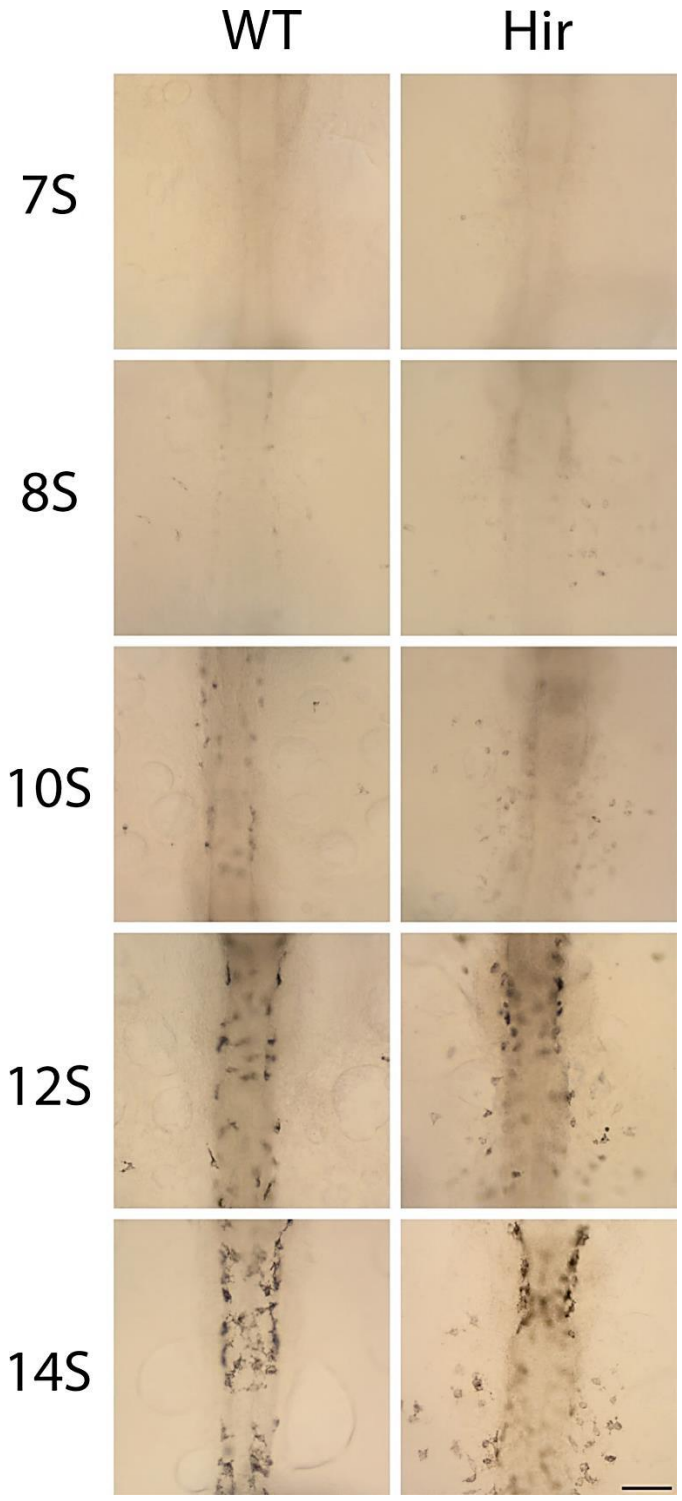

Figure 3.5: Onset of melanisation in wild type and *hirame* in differentiating melanocytes in both begins during 8 somite stage

Magnified brightfield images of fixed Medaka embryos at 7 somite stage up to 14 somites to investigate the onset of melanisation upon melanin detection in wild type (top row) and *hirame* (bottom row) embryos. Differentiation of melanoblasts into melanocytes occurs between 8 and 10 somite stage in wild type as well as *hirame* embryos. Although in *hirame* melanocyte distribution is abnormal and their localisation is close to the lateral body axis compared to wild type in which they spread away from the body. Again the onset of melanisation is normal. Scale bar = 100µm.

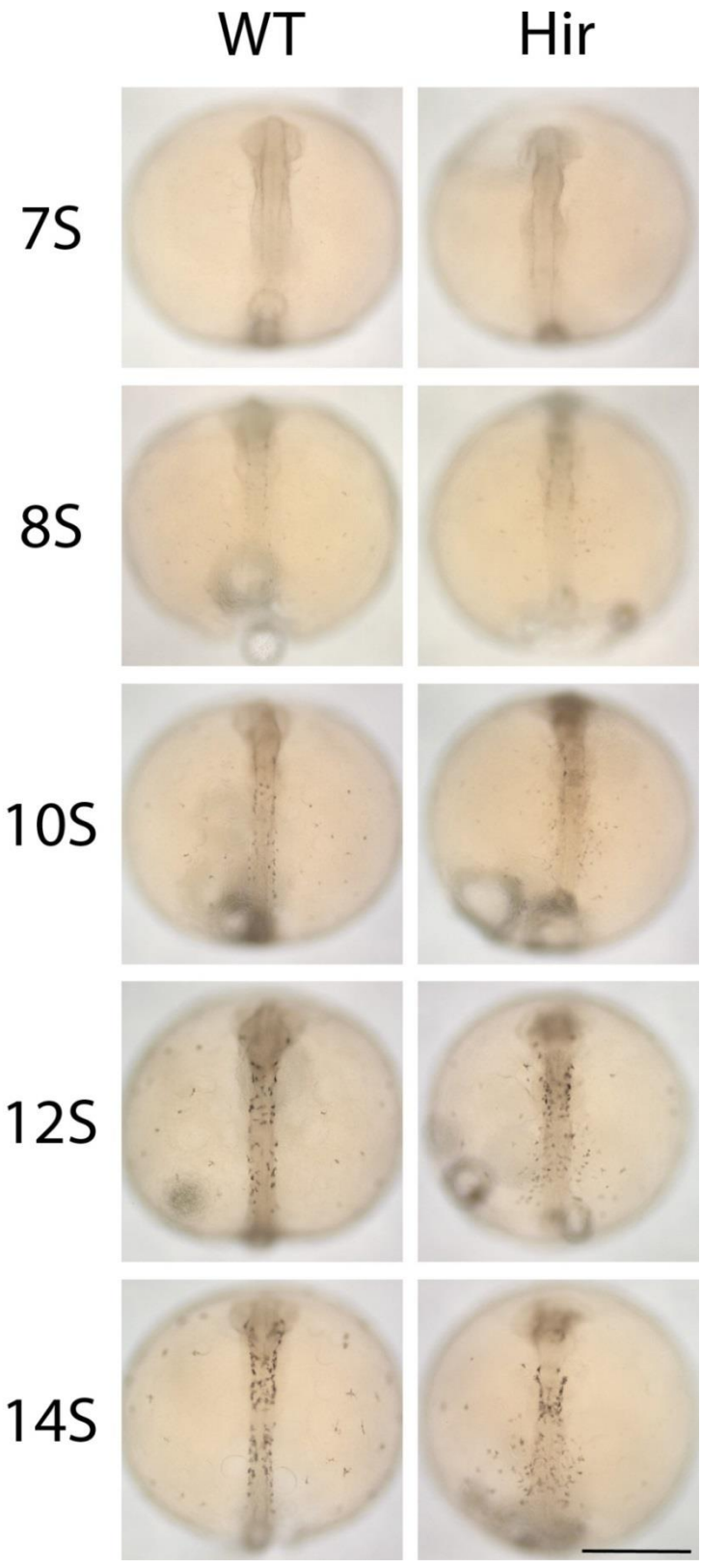

Figure 3.6: Onset of melanisation in wild type and *hirame* in differentiating melanocytes (whole-mount)

Lower magnified images of embryos as in Figure 3.5, in which onset of melanisation in wild type (left) and *hirame* (right) occurred between somite 8 and 10. Note, melanocytes disperse onto the yolk sac in wild type, but stay close to the body in *hirame* embryos. Scale bar = 500µm

3.2.3.1 Somite staging to investigate developmental progress

One ongoing concern throughout these studies was the possibility that melanocyte developmental defects could be a secondary effect resulting from general retardation of embryonic developmental mechanisms. *Hirame* mutants do not show general retardation and dislocation of organs prior to stage 22 (1d 17 hpf), however internal structural analysis has not been carried out to exclude this possibility.

Typically, in mouse the number of somites is used as a reference for age in a developing embryo. Somites are transient structures and give rise to the vertebrae, cartilage, tendons, skeletal muscle and the dermis in vertebrates during a process called somitogenesis. Established during gastrulation somites segregate from an unsegmented presomitic mesoderm (PSM) also called paraxial mesoderm which runs lateral to the neural tube of the neurulating embryo. They are formed by "budding off" as somitomeres of paraxial mesodermal cells. Around each developing somite the outer cells undergo a mesenchymal–epithelial transition (MET) to form an epithelium also known as the dermomyotome, while the inner cell mass remains mesenchyme. The immature somites are then compacted and separated into distinct parts. Somites are formed sequentially and simultaneously from head to tail of the developing embryo on the caudal side of an already existing somite. Their tight regulated formation depends on a temporal periodicity controlled by a molecular oscillator, the segmentation clock. Phenotypically they are bilaterally paired blocks of mesoderm along the embryos anterior-posterior axis. However the number of somites is only given as a guide to what might be expected of typical embryos as the true range of development can be wider depending on minute time intervals (Downs & Davies 1993). In addition, mutations affecting segmentation could cause a wide range of symptoms including complete or partial absence of whole somite structures or incomplete somite boundaries.

For our purpose, we decided to use the segmentation clock as general criterion to evaluate developmental retardation in *hirame* mutants. Analysis of somitogenesis and somite quantification was carried out on age-matched *hirame* and wild type sibling embryos after *in situ* hybridisation with a mixture of *pax3* and *foxd3* anti-sense probes (hand gift of Dr H Hashimoto) to label mesodermal somite structures. The paired-domain transcription factor Pax3 was shown to play an important role for normal myogenesis and neural crest development in the developing embryo (Nelms & Labosky 2010b). It activates several *Myogenic factor 5* (*myf5*) enhancers and is thought to control the transcription factor *myogenic differentiation1 (myoD)* expression (directly or indirectly); both *myf5* and *myoD* are early markers for myogenic differentiation. Pax3 is expressed in the unsegmented paraxial mesoderm (UPM) and epithelial somite, being confined first to the dermomyotome and later to its ventrolateral half (Tajbakhsh et al. 1997; Rawls & Olson 1997). *Fork head domain 3 (fkd3)* also known as foxd3 is expressed early on in the neural plate border during gastrulation, as well as in the

mesoderm of the posterior and ventral tail bud and briefly in the developing floor plate (Odenthal & Nüsslein-Volhard 1998). It specifies premigratory neural crest cells for several lineages such as neuronal, glial or cartilage fate and represses melanogenesis, by regulating lineage-associated transcription factors (Nelms & Labosky 2010a). In later stages *foxd3* can be monitored in premigratory neural crest cells of the head and trunk, in forming somites and in newly formed peripheral glia in Zebrafish (Kelsh et al. 2000).

In Medaka, foxd3 shows mild expression during early somite myogenesis, but is strongly expressed in mature somites (data not shown). By combining pax3 and foxd3 anti-sense probes during *in situ* hybridisation, the detection level and clarity of somatic structures was improved and therefore used to assist somite counting. Figure 3.7 represents the same embryos used in Figure 3.6 labelling *pax3* and *foxd3* mRNA to highlight paired somitic structures (indicated by asterisks). The staging between 7 and 14 somites is based on nominal somite counts in wild type siblings before fixation. The results show that the number of somites in *hirame* is the same as in wild type embryos in all developmental stages during somitogenesis between 7 and 14 somites. This indicates that *hirame* is not developmentally retarded at stage 21 (6 somites).

We concluded that, although mesodermal somite structures seem to be irregularly sized and shaped in *hirame* and some somite boundaries are not very clear compared to wild type siblings, the process of somitogenesis follows a normal course in terms of somite segmentation up to at least 14 somites.

To summarise, although the onset of melanocyte differentiation in *hirame* is not impaired, the migration onto specific areas of the embryo i.e. yolk sac is. For a sophisticated approach to record cell migration and survival, we aimed for a transgenic line during our next step in which we could label and follow melanocytes in real-time starting from its progenitors until the death of *hirame* embryos.

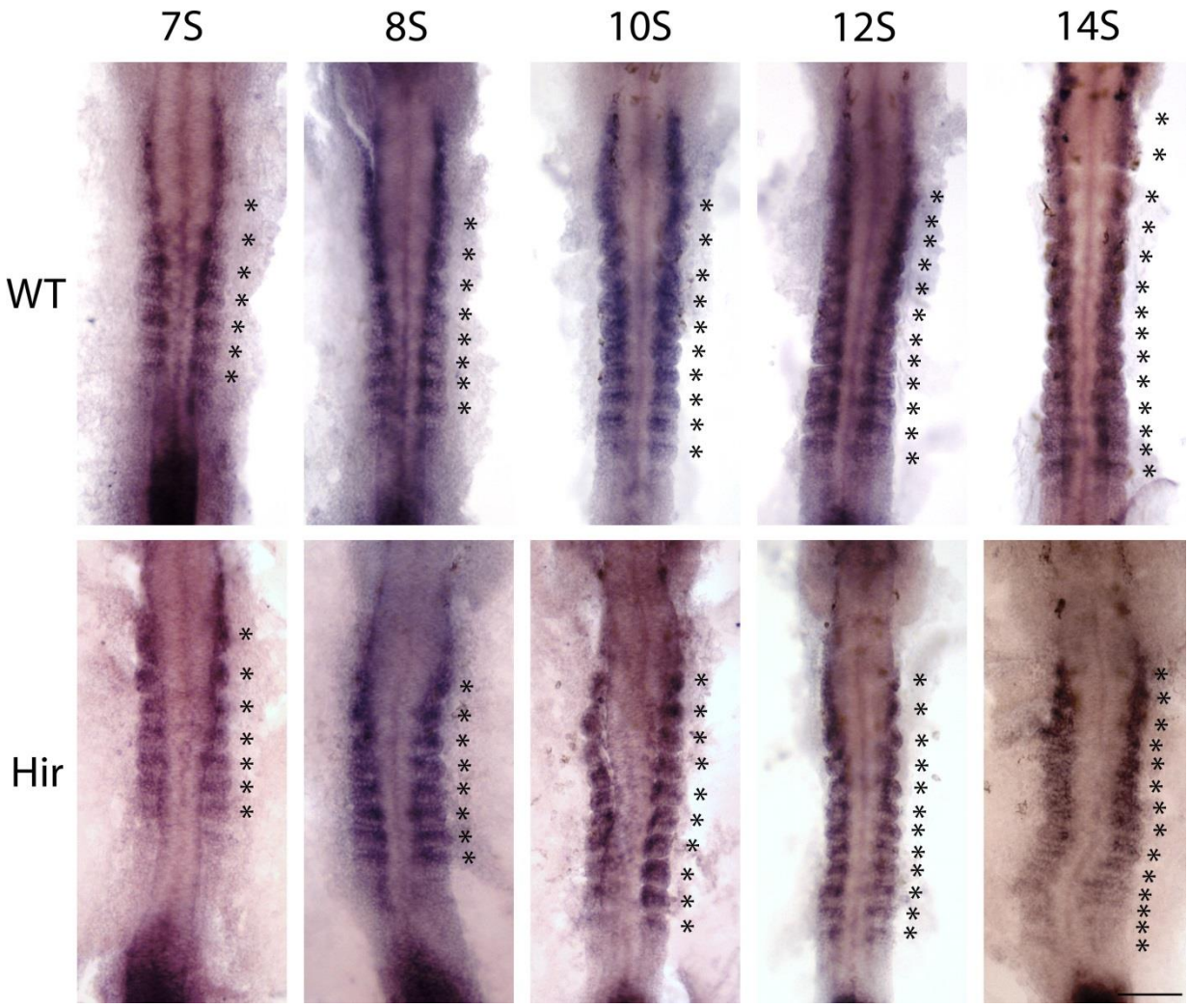

Figure 3.7: Developmental progress in *hirame* and wild type is non-different revealed by ISH of somite structures

In situ hybridisation (ISH) with *pax3* and *foxd3* anti-sense probes to visualise somite structures and quantify their numbers used for staging in 3.2.3. Asterisks indicate individual horizontal pairs of somites. The number of somites in wild type matches the number in *hirame* embryos despite morphological differences in width and length. Scale bar = 100µm.

3.2.4 Cloning the Medaka *Dct* promoter

To better understand the Medaka melanocyte lineage, its origin, migration behaviour, proliferation and survival, I desired a transgenic line in which melanocyte lineage cells were readily detectable at all stages during embryogenesis.

Although, a previous study carried out by Martinez-Morales et al. in 2009 established a 3kb long Medaka tyrosinase promoter fused to GFP (tyr:gfp), which seemed to be melanocyte specific beyond 3dpf, it had not been characterised in any more detail (Martinez-Morales et al. 2009). Using the already established tyrosinase promoter was one possibility to carry out functional studies of YAP within the melanocyte lineage. However, due to uncertaintly about the *tyr* promoter at earlier stages

and the inpurity of the *tyr* probe itself, we decided not to pursue with this option. In addition, the *Dct* probe we already established and analysed was overwhelmingly clear and lineage-specific to melanoblasts at early stages as well as melanocytes beyond 3dpf (Dr H. Hashimoto, (Nagao et al. 2014). Moreover, *Dct* expression was first detected in early melanoblasts within the body as early as st.18-19 (1-2 somite, data not shown), which has not been reported yet.

These are the reasons why I decided to clone the Medaka *Dct* promoter to use it for future melanophore studies in regards to YAP protein functionality. I aimed to clone the promoter and couple it to a fluorescence marker, the enhanced green fluorescence protein eGFP to be able to trace the melanocyte lineage during embryogenesis.

As starting point, I decided to use the amino acid sequence from the 1884 bp Zebrafish *dopachrome tautomerase* (*Dct*) mRNA (actual size is 1538bp from first ATG to stop codon) found on chromosome 9 annotated in NCBI with NM_131555.2. Using BLASTX in search of *Dct* against the Oryzias latipes genome on the ensemble.org website, I identified a region which is most likely the Medaka homologue for the Zebrafish *Dct* coding region, which also matched the construct for the *Dct* anti-sense probe obtained by Dr H. Hashimoto (Nagao et al. 2014). This region on chromosome 21 defined in ensemble as *dopachrome tautomerase* (25,518,211-25,522,729 / ENSORLG00000017760) with a transcript of 1714bp and protein length of 518aa. I increased the 5' flanking region before the first ATG by 3700bp only as previous promoter studies have demonstrated that a promoter length of 3-5kb is likely to contain sufficient promoter regulatory elements (Martinez-Morales et al. 2009; Carney et al. 2006). We obtained the Medaka *dopachrome tautomerase* (*Dct*) promoter as genomic DNA fragment by polymerase chain reaction, allowing us to isolate a 3607bp genomic DNA fragment using a specific primer pair (Figure 3.8). After amplifying the desired region from the Medaka genome, the purified PCR product (Figure 3.9A) was then cloned into a pGEM T-Easy vector (Figure 2.1) via the TA-cloning strategy after an extra adenylation step. I decided to introduce the promoter into the pEGFP-1 vector containing a multiple cloning site (MCS) allowing insertion of enhancer or promoter sequences, which consequently drives the enhanced GFP reporter gene. This would allow me to assess the promoter cell specificity easily by fluorescence analysis *in vivo*. To achieve that, I had to re-amplify the *Dct* promoter region with the same primer set previously used. However those primers contained additional unique restriction enzyme sites matching the target vector's MCS Eco47III (also called AfeI) was added to the forward primer and SalI to the reverse primer. The full map of the 7692bp MF_*Dct*:eGFP is shown in Figure 3.9B.

Figure 3.8: Medaka *dopachrome tautomerase* promoter and its cloning primers

Nucleotide sequence of the 3607bp long Medaka *dopachrome tautomerase* (*Dct*) with 5' and 3' flanking regions resulting from an ensemble BLASTX search with the Zebrafish *Dct* protein amino acid sequence. The matching sequence of *Dct* from Zebrafish chromosome 9 is found on chromosome 21. Forward and reverse primers to clone the promoter region are indicated in green. First ATG (red) of *Dct* codon region (pink, incomplete) is indicated.

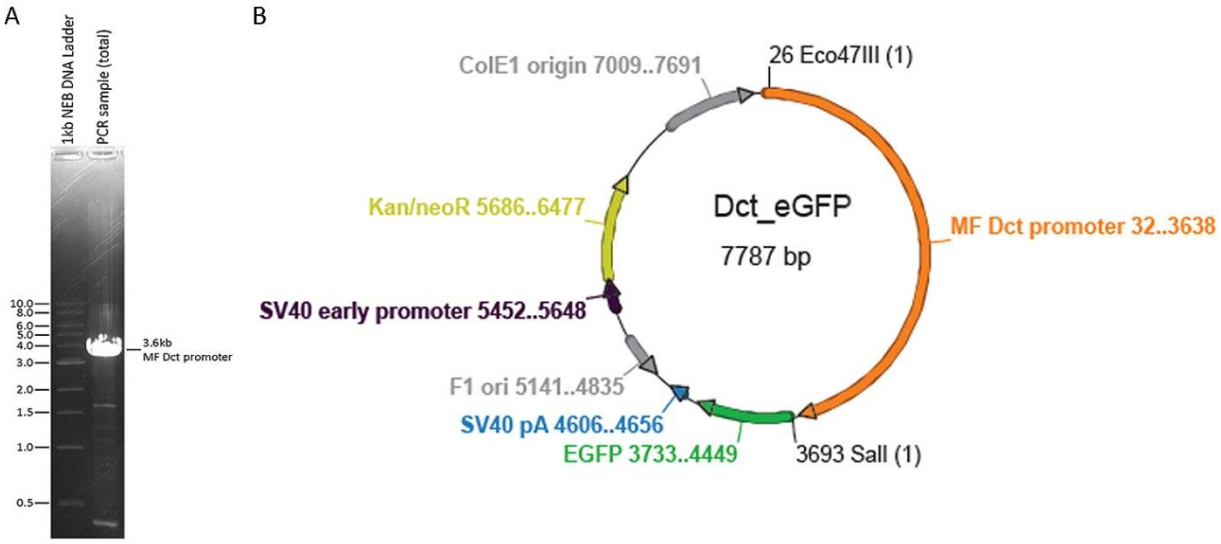

Figure 3.9: Medaka *Dct* genomic DNA amplification and cloning into target vector to obtain Medaka ***Dct*:eGFP**

A) Total PCR product on 1% agarose gel visualised under UV with ethidium bromide before gel extraction. Amplified DNA band shows approximately the expected band size of 3.6kb.
B) Map of the Medaka *Dct*:eGFP plasmid featuring the Medaka *dopachrome tautomerase* 3.6kb promoter sequence (orange) transcribing eGFP (green). Other regulatory elements are the simian virus SV40 polyA signal (blue) for termination of transcription, F1 bacteriophage origin (grey) for DNA replication of viral strand synthesis and termination allowing synthesis of single-stranded DNA (not needed in my case) and ColE1 origin (grey) for double-stranded bacteria vector replication. SV40 promoter driving expression of selectable marker kanamycin resistance gene in *E.coli*. Restriction enzymes Eco47III (AfeI) and SalI were used for direct cloning of the Medaka *Dct* promoter PCR fragment into the pEGFP-1 plasmid backbone.

To test the construct, we purified the plasmid by plasmid midiprep and injected it as 20ng/µl working solution into one-cell stage embryos to obtain 20-40pg total amount of intracellular DNA. Through live observation in transient transgenics, I could verify its transient expression within the melanocyte lineage (data not shown). This meant that our promoter could be used for further usage to establish a *Dct*:eGFP transgenic line in Cab$^{j50\text{-}20C}$ strain.

3.2.5 Establishing the *Dct*:eGFP Medaka transgenic line

The Medaka *Dct*:eGFP construct described and verified within Chapter 3.2.4 was now used to establish stable transgenic Medaka strains. This plasmid was linearised with BglI and 20ng/µl working solution (total amount of 20-40pg DNA) was injected directly into cells of one-cell stage embryos of Cab *hirame*$^{j50\text{-}20C}$.

Injecting it into this strain meant that it was most likely to obtain hemizygous founders for the j50-20C allele after transgenesis voiding having to backcross founders. We obtained compatible results from 20 separate sets of injections (data combined in
Table 3.1). In total 2301 eggs were injected from which 662 were viable after 72hpi (3dpi). This high death rate of 71% was expected due to the high concentration of injected DNA used to maximise DNA integration into the genome of chimeras. However, the process of microinjection of any kind of solution into Medaka one-cell stage embryos itself is a delicate procedure. When not carefully handled, it can lead to disruption of the yolk syncytial layer through either the injection of too much volume or the damage of the egg chorion, which then changes pressure conditions for the oil containing egg leading to leakage and death. Another reason for the high death rate might be the breaking of the syncytial layer with the capillary needle itself.

From those 662 embryos, 121 eGFP positive chimeras were selected prior to 8 dpf hatching stage as putative founders and consequently grown up. These transient chimeras exhibited an overall high amount of visible eGFP expression either exclusively in melanocytes, which was mostly the case, or they represented some additional ectopic epidermal skin cell expression. However, this observation did not concern us, as previous studies reported about ectopic cell expression whilst establishing transgenic lines as well (Carney et al. 2006; Thummel et al. 2006). In addition Medaka *Dct* is not expressed in epidermal cells, which might suggest that the transgene was located near an epidermal enhancer resulting in eGFP expression in ectopic locations.

Only 66 larvae hatched after 9 dpf and could be transferred into growing tanks. In general, it is not uncommon that Medaka embryos do not survive until 9 dpf. Such an outcome depends on various negative factors such as bacteria or fungal contamination in the embryo media, developmental retardations or difficulties with motor skills required during the hatching process.

From those, 50 survived the first month and were raised to sexual maturity. After three months, 48 adult fish remained from which 44 were fertile. These adult chimera were set up with Cab wild type or Cab heterozygous $^{j50\text{-}20C}$ of similar age to test for germline transmission of the transgene. The offspring, mostly 2-15 eggs daily, was then screened under a fluorescence microscope for cellular eGFP expression. If none of the F1 embryos scored had any eGFP positive expression, the parental generation was deemed not to be transmitting through their germline and were subsequently euthanized. If, however, some of the embryos did display eGFP expression we knew that the outcrossed parent was able to transmit the transgene and so was selected as a founder. These embryos were then grown up as the hemizygous F1 generation for the transgene and named as separate Tg(*Dct*:eGFP) lines depending on the parental gender and number. Through fluorescence microscopy we identified eGFP positive offspring out of 10 individual founders showing expression within melanocytes. 8 out of those 10 founders carrying the transgene were selected for further

evaluation and detailed characterisation. The remaining two founders gave offspring with very high ubiquitous background expression and therefore excluded from further analysis. The total number of founders obtained though injection of linearised DNA indicate a transgene transmission rate of up to 22.7%.

Table 3.1: Summary of the F0 Medaka **fish *Dct*:eGFP generation from microinjection up to the finding of founders of the transgene**

Experimental process in G0 founder generation	Corresponding number of individual chimeras
Injected embryos	2301
Survival after 3dpi	662
Grown up to 8 dpf after eGFP selection	121
9 dpf hatchlings	66
Survived 1st months	50
Survived till adulthood	48
Screened for eGFP if fertile/laying	44
eGFP positive	10

3.2.6 Characterising *Dct*:eGFP transgenic lines for melanocyte specificity

3.2.6.1 Initial characterisation of Cab Dct:eGFP founders

The selection, maintenance and characterisation of those 8 out of 10 founders mentioned in 3.2.5 is described below. Normally it is not necessary to grow up all founders to decide which strain to keep for further experiments. However, the low germline transmission, short time frame of fertility and low number of progeny made it risky to examine the F1 generation immediately in detail. Therefore, I attempted to grow up around 50 transgenic offspring from each of those 8 individual founders as a necessary precaution and analyses the F2 generation instead. In reality, this could not be achieved and a quantity of 2 to 33 progeny of each individual founder was obtained and raised. Table 3.2 summarises the total number of transgenics being transferred as juvenile into the fish facility system from separate transgenic *Dct*:eGFP lines. They were inbred with each other if possible depending on

male and female ratio. The F2 offspring of each new line was then analysed as regards to melanocyte cell specificity. Appendix 9 shows the gender and description of the original founder and referral to the new line name.

Table 3.2: Number of germline transmitting transgenics in F1 pool of offspring after 1 month growing period. When the ratio of progenies was low as in the case of line 4 or line 5 and the gender ratio was not suitable, then F1 adults were backcrossed to adult wild type Cab for further analyses.

Tg(*Dct*:eGFP) line individually	Number of transgenic F1 progeny grown up
Line 1	33
Line 2	5
Line 3	17
Line 4	3
Line 5	2
Line 6	32
Line 7	27
Line 8	28

Prior to choosing which lines to maintain and use for further experiments, I performed *in situ* hybridisation on 4 dpf (st.32) wild type embryos to highlight the melanocyte, xanthophore and leucophore cell distribution at that chosen stage of development (Figure 3.10A,B and Figure 3.12A,B). This was done as a comparison to the prospective eGFP expression driven by the Medaka *Dct* promoter. The melanocyte lineage was labelled using *dopachrome tautomerase* (*Dct*) and the xanthophore/ leucophore cell lineage through a *GTP cyclohydrolase 1* (*gch*) anti-sense probe. The melanocyte pattern seen in Figure 3.10A is very similar to the characteristic pattern seen in Zebrafish featuring the characteristic dorsal, lateral and ventral stripes (Kelsh et al. 2000) as well as a minor subpopulation of differentiated melanocytes on the yolk sac itself. In contrast, the *gch* pattern is readily distinguishable (Figure 3.10B). As reported by Nagao et al. in 2014 *gch* (XM_004085058) is expressed in unpigmented and pigmented xanthophores and in ventral head leucophores only. It does not overlap with the melanophore marker expression of *dopachrome tautomerase* (*Dct*, XM_004081789) (Nagao et al. 2014). Close-ups of the dorsal head epidermis show again the difference in cell distribution and number of melanocytes and xanthophores at stage 32 (Figure 3.12 A,B). Therefore, we were confident that we could identify and ascribe eGFP positive cells to the melanocyte lineage when analysing the *Dct*:eGFP transgenic lines for the expected patterning. One found consideration is that leucophores exhibit autofluorescence in the head and dorsal stripe when excited by 488 to 546nm, emitting green and red light resulting in orange-red colouration, which

needs to be taken into account when analysing the transgenic lines. We note that leucophores show signals in both the red and green channels, whereas eGFP is only detectable in the green channel enabling us to distinguish them from each other. The autofluorescence of leucophores appears when light reflects from crystal of uric acid, purine-related intracellular organelles similar to iridophore guanine and hypoxanthine in Zebrafish (Hama 1975). Figure 3.10C and Figure 3.12C/D represent z-stack images of wild type embryos emitting autofluorescencing leucophores in the head and dorsal stripe when excited by 488 to 546nm, emitting green and red light, which as mentioned needs to be taken into account when analysing the transgenic lines.

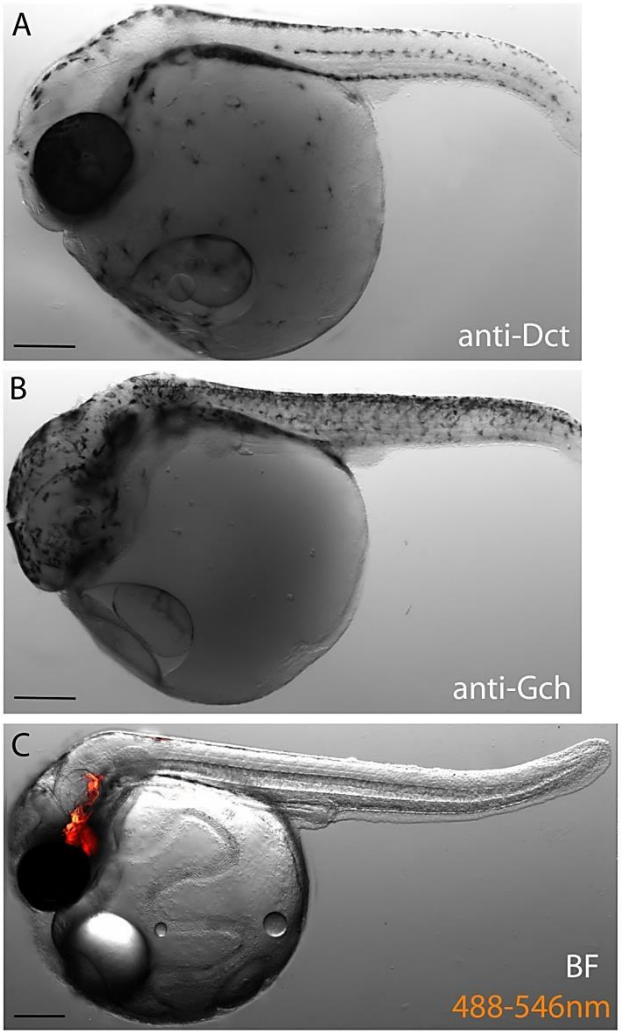

Figure 3.10: Representation of pigment cell patterns and negative control as non-transgenic in 4 days old embryos (st.32)

A-B) *In situ* hybridisation (ISH) for pigment cell markers, **A)** *dopachrome tautomerase* (*Dct*) anti-sense probe labelling melanocyte lineage **B)** *GTP cyclohydrolase I (gch)* anti-sense probe marking laterally migrating xanthopores together with leucophores in the ventral head region **C)** Merged image of Differential interference contrast (DIC) microscopy (Nomarski) and excitation range of autofluorescence leucophores displayed as orange cells, a combination out of green and red emitting channels mainly in the ventral head and some in the dorsal stripe. Scale bar = 200µm.

Dechorionated, agarose embedded embryos from F1 incrosses were scored for the expected melanocyte pattern at 4 dpf (st. 32). Incrossing also checks for recessive effects, such as death and malformation rates, but we did not see any evidence of these effects in our transgenics. Outcrossing to Cab $^{j50\text{-}20C}$ was performed when the male/female ratio was not suitable. Of those 8 transgenic lines incrossed or outcrossed into wild type Cab adults, all of them gave eGFP positive embryos within progeny of F1. Although the levels of eGFP expression under the *Dct* promoter were variable between those 8 Tg(*Dct*:eGFP) transgenic lines, the emission intensity was generally strong and cells were easily detectable. 6 lines exhibited similar expression patterns, containing eGFP expression seemingly within the melanocyte lineage (Figure 3.11A-F). Two lines had an incomplete pattern (Figure 3.11G,H) and were not expressed in all differentiated melanocytes, which could indicate a silencing effect in proliferating melanophore clones. Figure 3.12 shows a close up of the dorsal head and the melanocyte distribution in the epidermis, which highlights the difference between individuals with complete patterning in Figure 3.12E-J, and the incomplete patterning in Figure 3.12K/L. However, direct assessment of eGFP in melanised melanocytes is not possible in the Cab background due to its recessive b allele causing in amelanotic melanocyte phenotype. Therefore I conducted further analyses after crossing one Tg(*Dct*:eGFP) line originated from founder "line 1" onto the HB32C background where the b allele in the B locus is normal, resulting in strong melanin synthesis in melanosomes (Kinoshita, M., K. Murata, K. Naruse 2009).

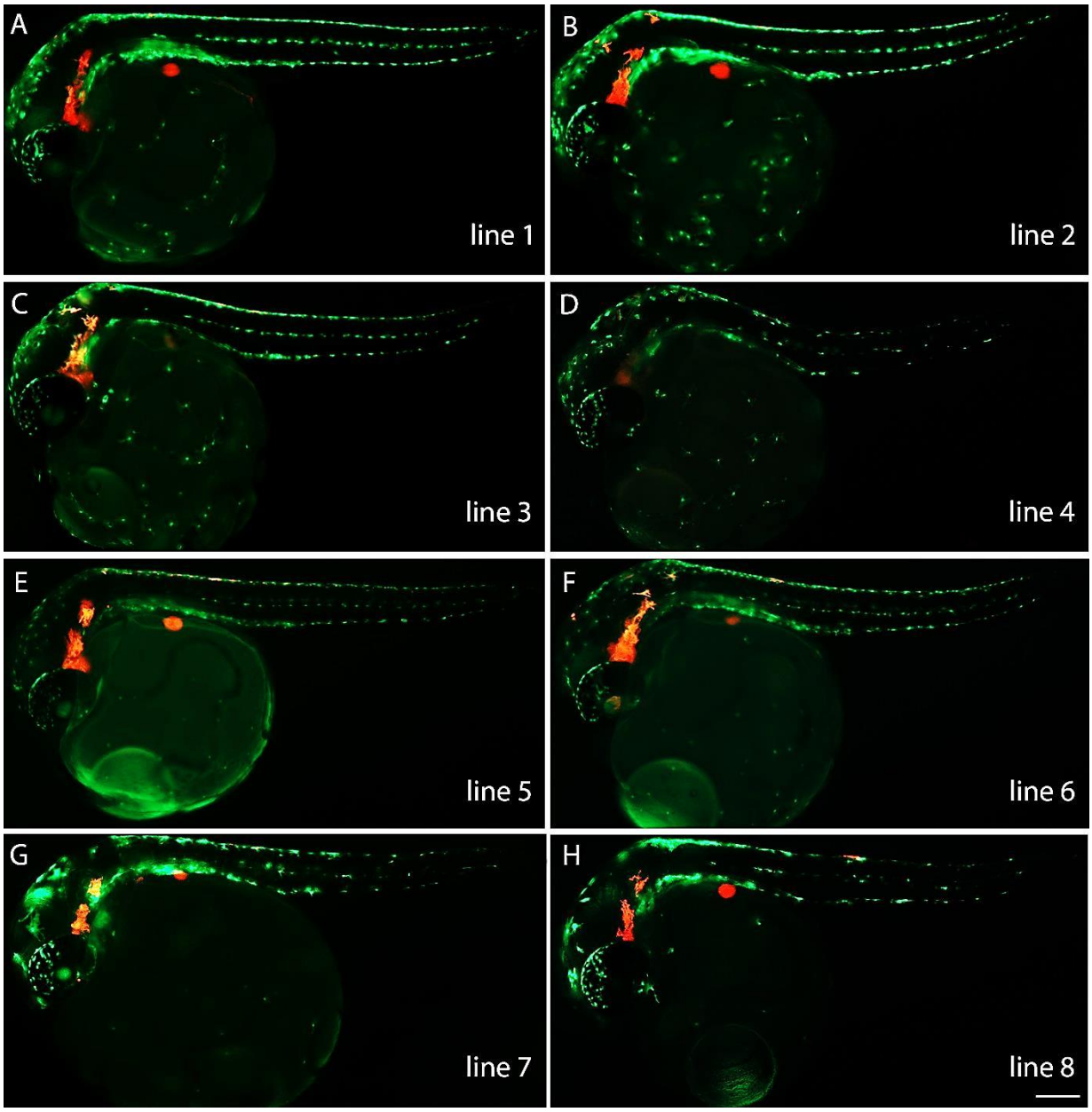

Figure 3.11: eGFP expression in Tg(*Dct*:eGFP) transgenic lines is consistent with sites of endogenous *Dct* expression

Lateral view of 4 days old whole embryos (st.32). **A-F)** represent individuals of Tg (*Dct*:eGFP) F1 progeny matching the desired melanocyte pattern shown in figure Figure 3.10A and not the xanthophore cell distribution. **G-H)** are transgenic lines with incomplete eGFP expression in some melanocytes in various locations within the body. Scale bar = 200µm

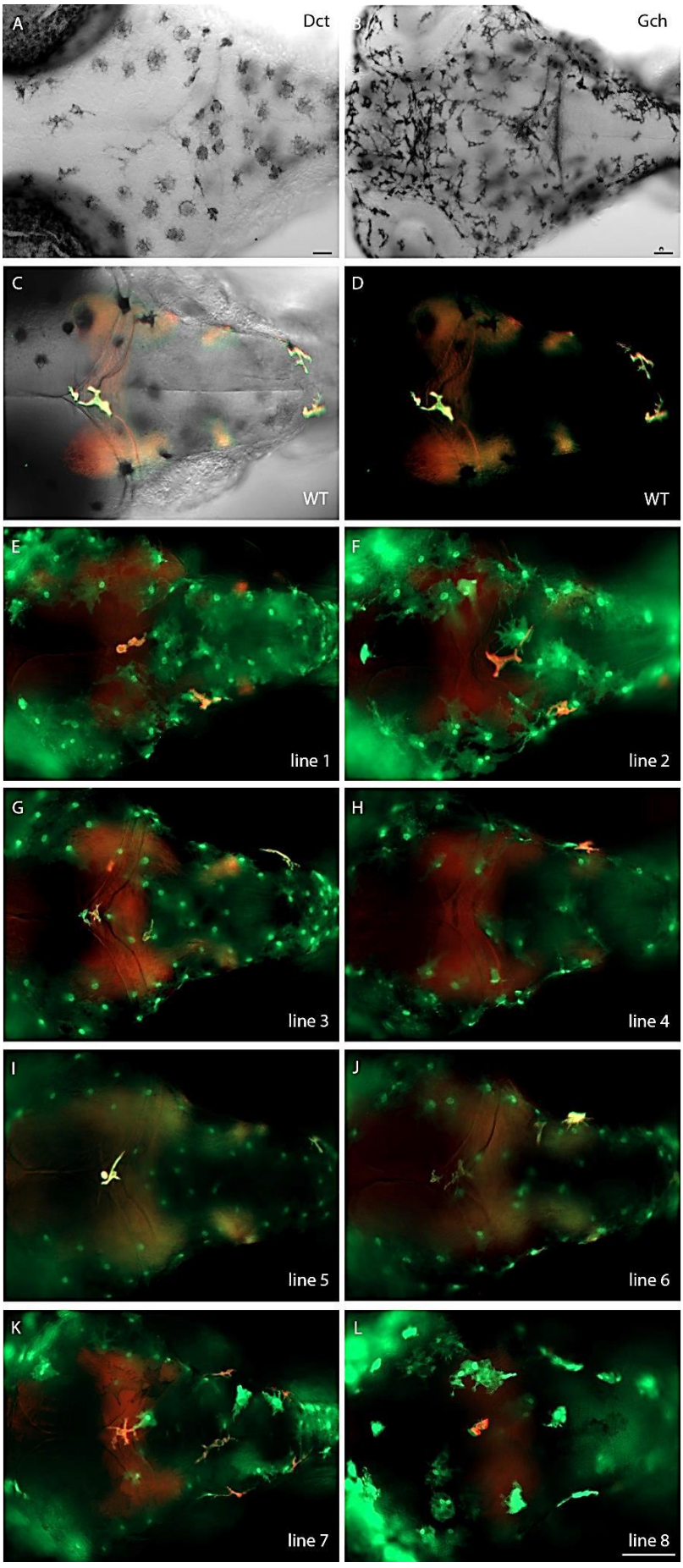
A
Dct
B
Gch
C
WT
D
WT
E
line 1
F
line 2
G
line 3
H
line 4
I
line 5
J
line 6
K
line 7
L
line 8

Figure 3.12: eGFP expression in Tg(*Dct:eGFP*) transgenic lines is consistent with sites of endogenous *Dct* expression

Dorsal view of heads of 4 days old embryos (st.32). **A-B)** ISH of *Dct* and *gch* showing the chromatophore arrangement on the head **C-D)** non-transgenic wild type embryos highlighting the endogenous excitation of autofluorescent leucophores in the ventral head. (**C)** bright field, **D)** 488-546nm excitation) **E-J)** 6 out of 8 Tg(*Dct*:eGFP) transgenic lines characterised show distinct melanocyte specific patterning, whereas two (K,L) show melanocyte specific expression, but with missing eGFP levels in some melanocyte positions. Scale bar A-B= 50µm, C-L= 100µm.

3.2.6.2 Extended characterisation of the Dct:eGFP pattern in melanised HB32Cto proof cell specificity

To make valid conclusions about the cell specificity of the Medaka *Dct* promoter and the obtained transgenic lines described in 3.2.1, I crossed adults from the F1 generation of Tg(*Dct*:eGFP) line 1 with individuals of HB32C wild type. The HB32C strain exerts a higher amount of melanin production resulting in a phenotype with darker differentiated melanised melanocytes. This approach would show precisely if eGFP co-localises with those strongly melanised cells. Figure 3.13 shows a wild type embryo at 3 dpf in a lateral view as a whole (upper panel) and dorsal view of the head region (lower panel). The *Dct* promoter controlled eGFP co-localised with melanised melanocytes in a very cell specific manner in all positions such as on the head, yolk and dorsal stripe (Figure 3.14). It is also persistent throughout embryonic development until 9 dpf, the time where embryos hatch out of their chorion and begin free swimming (Figure 3.15). The weaker emission signal at later stages is explained by increased amount of melanin which is produced and accumulates within differentiated melanocytes, masking the signal of green fluorescence proteins. Importantly, I saw no ectopic cell expression in any embryo at any developmental stage throughout these experiments. From our obtained data we concluded that the Medaka promoter demonstrates correct spatio-temporal expression properties and would be highly suitable for visualising Medaka melanocytes development.

In summary, our data demonstrates successfully the construction and characterisation of a novel Medaka *dopachrome tautomerase* (*Dct)* which is cell specific to the neural crest melanocyte lineage throughout embryogenesis. Because Medaka represents a wide range of natural pigmentation mutants (Kelsh et al. 2004) providing this promoter offers a valuable tool for the Medaka community to study pigment cell development in more detail. One of the possibilities and questions still to answer in *hirame* would be, if the remaining melanocytes on the yolk sac do migrate in a directed and polarised fashion or not as well as the speed of cell movement towards the ventral side of the yolk sac. Queries which could be attempted by real-time analysis on live embryos as eGFP fluorescence aids directly as melanoblast marker as early as 2 somite stage.

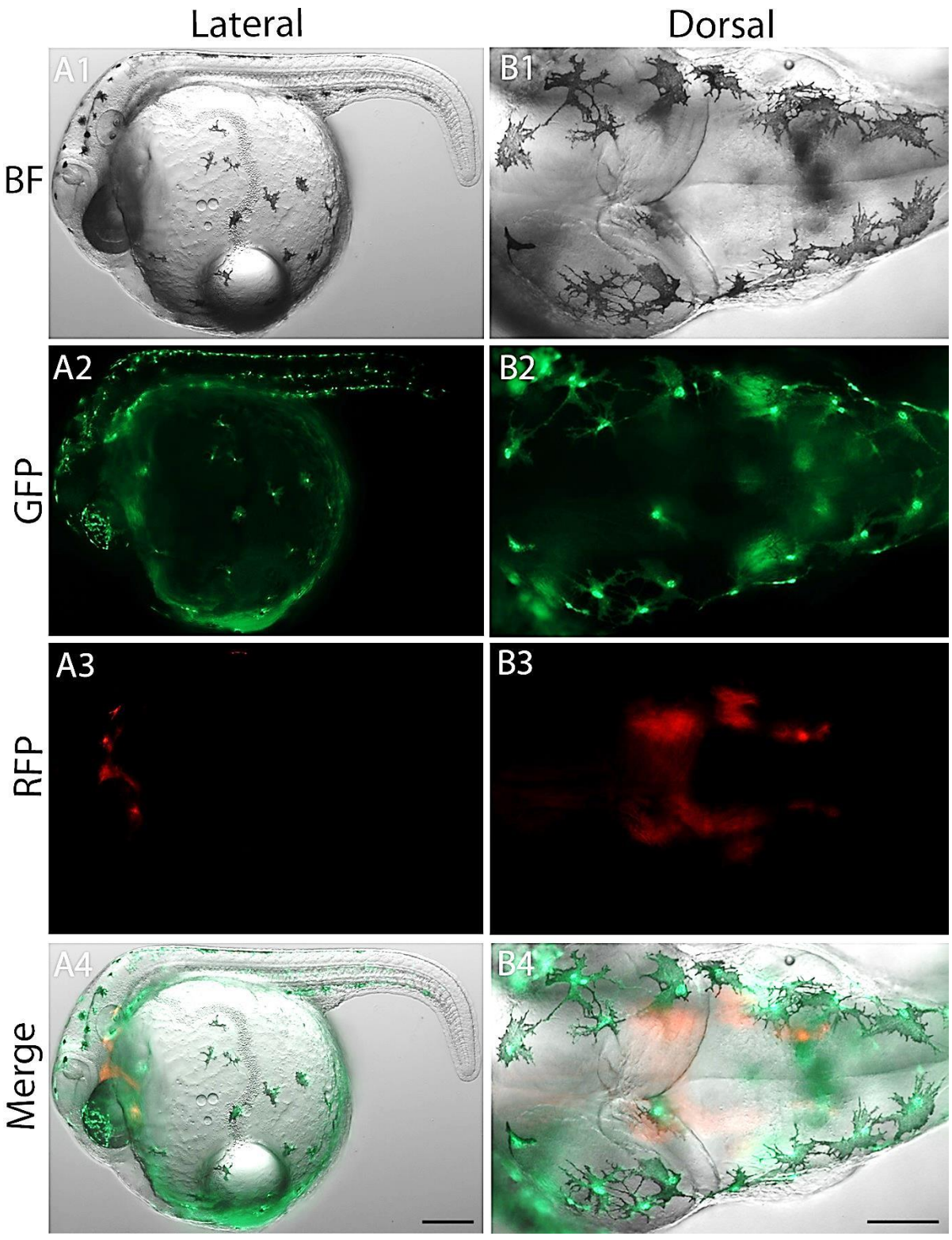

Figure 3.13 Embryos of Tg(*Dct:eGFP*) in HB32C background after 3 dpf showing co-localisation of eGFP in all melanised melanocytes

No ectopic cell expression could be observed meaning the tissue specificity of the *dopachrome tautomerase* (*Dct*) promoter and its final validation. Upper panel **A1-A4)** shows a lateral view of whole embryos and lower panel **B1-B4)** a dorsal view onto the head in bright field (BF), under green fluorescence (GFP) and red fluorescence (GFP) filter as well as all channels merged (Merge). Autofluorescent leucophores mainly positioned in the ventral head emit green and red light, but do not express eGFP as seen in melanocytes only. Scale bar = 100µm

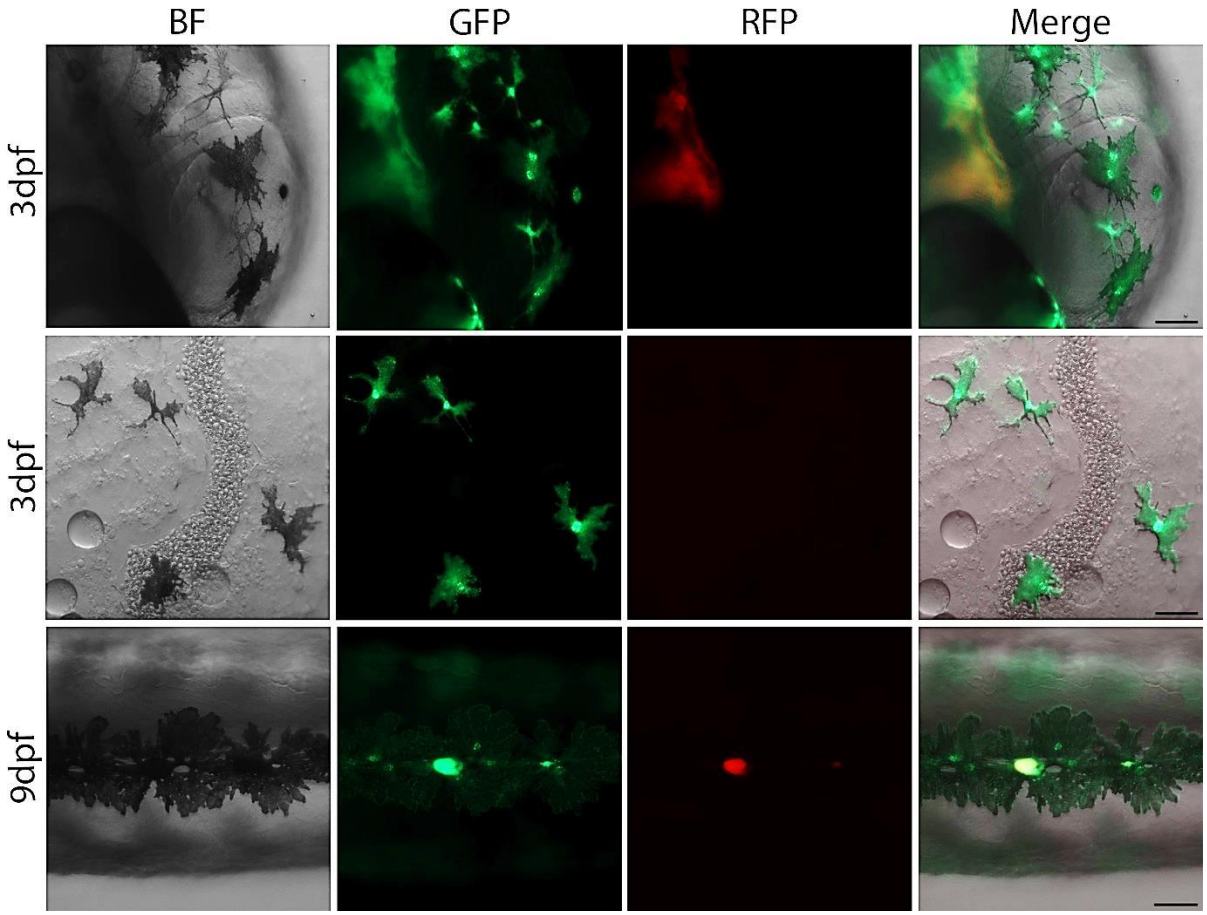

Figure 3.14 eGFP expression is specific to the melanocyte lineage

Strong overlap of eGFP in melanocytes on the head (**A1-A4**) and the yolk (B1-B4) of 3 dpf embryos as well as on the dorsal stripe (**C1-C4**) of 9 dpf embryos could be detected. Autofluorescence leucophores emit within the green and red spectrum resulting in an orange-red combined cell colour within merged images. However, they do not express eGFP as seen in melanocytes under the control of the *Dct* transgene promoter. Scale bar = 50µm

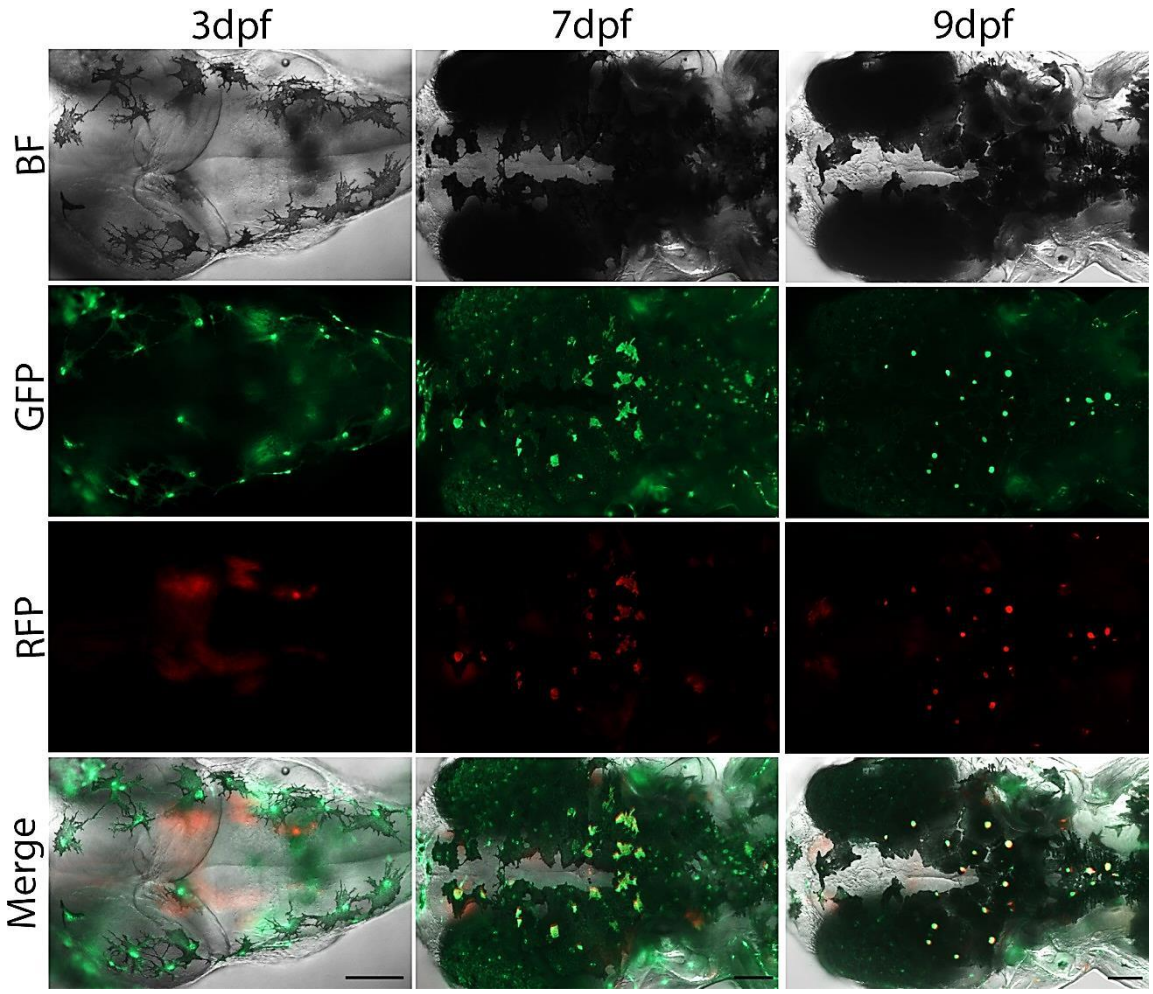

Figure 3.15 Co-localisation of eGFP within melanocytes throughout embryogenesis

Expression pattern of eGFP is tissue specific and co-localises with the melanocyte lineage throughout embryonic development until 9 dpf hatching stage without any ectopic cell expression. Strong expression of melanin in later stages 7 dpf and 9 dpf is masking the eGFP slightly, therefore the observed intensity is lower, but not diminished. Scale bar = 100µm.

3.2.7 Tg(*Dct*:eGFP) as tool for melanoblast time-lapse studies

One of the advantages when establishing this unique *Dct*:eGFP Medaka transgenic line is that we can monitor melanocyte and even early melanoblast behaviour. To test this hypothesis I carried out a pilot study in which real-time snapshots were taken from one wild type and two *hirame* embryos of Tg(*Dct*:eGFP) line 1 progeny. Briefly, dechorionated and agarose embedded embryos were incubated at 28°C and subsequently z-stacked images were taken on the Zeiss dissecting microscope every 30min. Although fluorescence signals become apparent at stage 18-19 (data not shown), I decided to choose stage 20 (1d 7h 30min, 4 somite stage) because the distance of melanoblast migration can be imaged without having to rotate the embryo manually and intracellular eGFP is sufficiently accumulated and strong. In addition, embryo epiboly is completed and most, if not all, convergence-extension cell movements should have been completed. Figure 3.16 shows merged snapshots of those images in real-time. As indicated in circles (red in wild type, top panel and purple in *hirame*, bottom panel) individual green fluorescent melanoblasts can be observed and monitored during active migration from a location close to the body at the 4 somite stage (0 min) to areas further away from to the body at 6 somite stage (180 min). Our results suggest that in *hirame* first melanoblasts migrating ventrally are slower compared to wild type melanoblasts. However, more cells need to be analyses and the distance of migration needs to be measured accurately. However, it would be interesting to analyse progeny of characterised F3 transgenic *Dct*:eGFP$^{j50\text{-}20C}$ lines for either real time studies under a dissecting or high magnification confocal live microscope. A series of images could then be taken and analysed for cell movement activities using for instance cell tracking software. Investigating living embryos also opens up possibilities to measure the actual speed of migration, the spacial distribution in this area, individual cell morphology and polarisation during directed cell migration.

Even so, this pilot study could yield interesting results, the practicalities of handling living Medaka embryos makes live imaging complex, numerous and complicated. One reason for that is, the yolk fluid in Medaka embryos is constantly in circulation, and this flow causes a yolk contraction and therefore movement of the yolk sac membrane. This makes it difficult to perform z-stack imaging precisely, because cell locations change from a viewer´s point. This means, numerous pictures have to be obtained from several embryos to get significant data showing actual melanoblast migration on the yolk sac membrane.

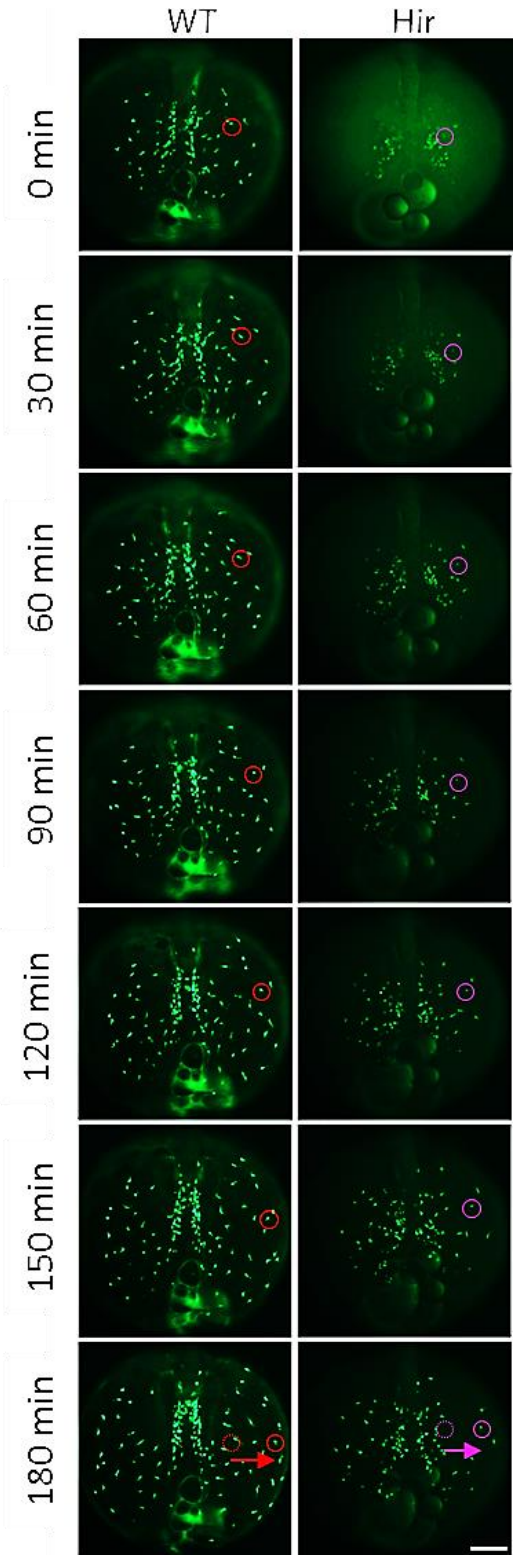

Figure 3.16 Time-lapse analysis of Tg(*Dct*:eGFP) reveals delayed melanocyte migration in *hirame*

Merged images of fluorescence z-stacks of time-lapse analysis of Tg(*Dct*:eGFP) line 1 from 4 somite to 6 somite stage to track melanoblast migration in wild type (left column row left to right) and *hirame* (bottom row) embryos. Pictures were taken every 30min starting from 4 somite to 6 somite stage. Coloured circles, red in wild type and purple in *hirame*, highlight the distance of an individual melanoblast through active cell migration. Scale bar = 200µm

3.3 Discussion

3.3.1 Abnormal cell distribution of melanoblasts in *hirame*

Our initial observations in 3 dpf embryos suggested a neural crest defect in the differentiated melanocyte lineage. To investigate this phenotype we performed a series of whole-mount *in situ* hybridisations for an early marker for melanocyte precursors, *dopachrome tautomerase (Dct).* We demonstrated that the abundant absence of functional Yes-associated protein 1 (YAP1) affects the melanoblast distribution in different locations within the embryo, whereas our initial experiments suggested a major reduction of Dct^{+} cells on the yolk sac. Cell quantifications in *hirame* embryos revealed a dramatic decrease in melanoblast numbers, especially on the yolk throughout all developmental stages, and in the body itself beyond 2 dpf. Cross sections of stage 21 embryos revealed that an increased number of melanoblasts reside and accumulate within the mesodermal tissue lateral to the anterior-posterior bodyline, which contrasted to decreased numbers on the yolk sac area. In addition, few melanocytes did migrate towards the ventral side of the yolk sac, which was however delayed compared to wild type siblings. It strongly suggests that individual melanocytes lacking YAP migrate slower than wild type sibling embryos expressing functional YAP protein. Interestingly, our melanoblast cell quantifications confirmed that despite local differences, the total amount of Dct^{+} cells is similar between *hirame* and wild type siblings at stage 21. Beyond that, a permanent decrease of total melanocytes was seen in *hirame* mutants on the yolk sac.
The reason for the quantitative change of MCs on the yolk sac at stage 21 despite the overall similarities in total MC numbers, and the sudden decrease afterwards could be explained first with a decrease in mRNA levels. Porazinski described in his thesis that maternal *yap* transcript levels in *hirame* mutants drop after stage 20 and are absent by stage 22 compared to ubiquitous mRNA *yap* levels in wild type siblings (Porazinski 2013). Undetectable *yap* transcript levels might be due to a mechanism called nonsense-mediated mRNA decay (NMD), which allows the elimination of mRNA transcripts containing premature stop codons, which is the case in the *hirame* allele after the amino acid exchange of leucine to a stop codon in position 164 within the first WW domain. In principal the maternal to zygotic mRNA transition during *hirame* embryonic development is suddenly disrupted by a loss of functional YAP protein; thereby impairing important developmental processes such as organogenesis. This explains why *hirame* exhibits organ dislocation such as failure of both lens invagination and Cuvierian duct endothelial vessel formation, or the general thickness of the embryonic body after 2 dpf (Watanabe et al. 2004; Kitagawa et al. 2004; Porazinski 2013), which corresponds with a dramatic decrease of MCs after our analysis.

It could mean that low levels of YAP or even a lack of functional YAP protein beyond stage 21 in *hirame* is likely to cause a melanoblast migration defect affecting melanoblast distribution, as fewer melanoblasts migrate onto the yolk sac and the once which do seem to be slower.

We have also shown that the *Dct* patterning defect starts as early as stage 20 (1d 7.5h) and even as early as stage 18-19 (1d 3.5h, 2 somites) (data not shown). However, during that time maternal *yap* transcripts are still present and detectable (Porazinski et al.2003), which could mean the quantity of YAP influences first MC migration and then development and/or proliferation at later stages. One possibility during stage 21 is that maternal transcript levels are just about to drop and the threshold is not sufficient to maintain neural crest cell migration. It seems that this drop has not been picked up as the regular RT-PCR-amplification product of the *yap* transcript at stage 20 is still relatively strong before total loss at stage 22. It might have been that the product within the conventional RT-PCR reached its plateau, which can be between 20-40 cycles and therefore is unreliable when it comes to representing the maternal mRNA decrease accurately. A better and much more accurate approach would be quantitatively real-time quantitative polymerase chain reaction (qPCR), in which the targeted product gets amplified and simultaneously measured either by absolute or relative quantification. Absolute quantification detects exact numbers of target cDNA molecules by taking DNA standards through calibration curves into consideration, whereas relative quantification is in reference to a control housekeeping gene and is determined in fold-changes. QPCR measures in-depth the accumulation of fluorescent signals emitted when a DNA-binding fluorophore is activated upon binding to the double stranded DNA produced during the exponential phase of qPCR, leading to a much more precise and objective analysis.

Furthermore, we have shown that beyond st.21 when a lack of *hirame* transcripts is abundant, melanoblasts are persistently reduced in total numbers. This might also be a result of either a lack of melanoblast proliferation or survival. Supporting data for the requirement of YAP for cell proliferation comes from several overexpression studies. As outlined earlier, tissue expands when *yap* is overexpressed in a tissue specific manner, which can be seen as the opposite effect of our observation in *hirame*, indicating a requirement for YAP in cell growth. Increased levels of YAP, for instance, was able to expand liver tissue (Camargo et al. 2007; Dong et al. 2007) and neural progenitor populations within the neural tube (Milewski et al. 2004; Dyer 2004; Gee et al. 2011; Cao et al. 2008). The question if YAP restricts melanocyte proliferation in *hirame* could be determined by BrdU proliferation assay. One the other hand the decrease in melanocyte numbers might be due to decreased melanocyte survival. Studies have shown that c-Abl directly binds phosphorylated YAP resulting in protein stabilisation which caused selective binding to p73, which is required for induced apoptosis (Levy et al. 2008). To test for cell apoptosis we could either perform terminal transferase dUTP nick end labelling (TUNEL) and analyse for co-localisation within melanoblasts. Furthermore,

we could perform antibody staining for anti-caspases, because caspases play a major role for intracellular apoptotic signals concerning their induction, transduction and amplification of intracellular apoptotic signals (Fan et al. 2005).

In summary, this capital implies that a lack of functional protein YAP has an influence on specific melanoblast migration on the yolk sac, which might implicate that YAP is required in a cell-autonomous fashion for the development of correct melanocyte patterning in vivo. This idea is investigated within the next chapter in this thesis.

3.3.2 Differences in transgene integration results in varied melanocyte lineage specificity and GFP intensity

When generating multiple *Dct*:eGFP transgenic lines, we observed a germline transmission rate of 22.7%, which is thought to be high for transgenesis attempts where circular or linear DNA fragments normally reach up to 16% (Thermes et al. 2002). However transgenic progeny obtained from founders were only few in numbers making it sometimes difficult to establish individual transgenic lines from different chimeric founders. This is down to mosaicism of germline integration (Stuart et al. 1988; Gaiano et al. 1996). Over the range of 9 founders only between 2 and 33 individuals could be grown up to adulthood for those lines and maintained as F1 generation for detailed studies. This was sometimes laborious and risky, as we cannot predict female to male ratios when growing the embryos needed for future incrossing. This raises the question of whether another technique might have generated transgenesis more efficiently yielding a higher number of founders and their offspring.

In recent years, the two most common methods of creating transgenic Zebrafish lines with a gene of interest are 1) transposon mediated transgenesis and 2) I-*SceI* meganuclease-mediated transformation. Tol2 is a transposable element. It was first identified as an autonomous and naturally active regulatory component in the Japanese Medaka fish, *Oryzias latipes* genome. Transposition techniques are widely used in the Zebrafish, chick and mouse communities. The transposon constructs requires a 5' 200bp and 3' 150bp DNA flanking region of the Tol2 sequence used as recognition sites for the coinjected transposase. The transposase is encoded as synthetic mRNA, which gets translated within the embryo and integrates foreign DNA up to 11kb as single-copy entries. The Tol2 insertion becomes stable once the injected transposase mRNA degrades and the protein activity declines. Studies have shown germline transmission of 12-16% (Parinov et al. 2004; Kawakami 2007), and some report from 3-100% germline transmission (Kawakami 2007). However, in Medaka fish itself the transpositional activity of exogenously introduced Tol2 is found to be far

more inefficient and therefore has not been established as a sophisticated genetic tool for transgenesis. It was suggested that the Tol2 transposase may have an extranuclear localization signal only active in Medaka cells which hinders its nuclear transpositional function (Kawakami 2007) or the endogenous Tol2 transposase might actively displace the transgene continuously within the genome, exerting an effect on reporter gene expression (H. Hashimoto, personal communication). Because of that reason, we did not consider using a Tol2 transgenesis approach for establishing the *Dct*:eGFP lines.

Conversely, the other approach is based on the *I-Sce* technique. Studies have claimed that coinjection of the I-*SceI* meganuclease with a reporter construct including I-*SceI* flanking regions increases transgenesis frequency up to 45% in Zebrafish compared to 5% or less without, as well as promising earlier transgene integration in F0 with up to a 50% increase in germline transmission frequency in their progeny (Soroldoni et al. 2009). In addition, the 18bp long endonuclease I-*SceI* sequence originally from *Saccharomyces cervisiae* allows a single integration of the transgene at low copy numbers. The mechanism is based on the coinjection of I-*SceI* meganuclease and a reporter vector with I-*SceI* flanking sites, in which the endonuclease remains attached to its flanking regions counteracting concatamerisation by blocking endogenous ligases within the early embryo. This might be the cause for lower transient mosaicism and a higher transgenesis frequency in F0 chimeras (Soroldoni et al. 2009). Indeed some Medaka researchers do make use of the I-*SceI* meganuclease approach. In 2002, Thermes tested the meganuclease as tool specifically for Medaka, where they present two lines in which the transgenesis frequency could be raised to 30.7% with half of the progeny expressing the transgene in F0 generation due to early integration of the transgene into the embryo. When injected as linear and circular vector DNA the germline transmission rate was between 5.9 and 15.6% with about 15% of offspring being germline transmitters (Thermes et al. 2002). Furthermore, the Schartl laboratory used I-*SceI* when establishing the mitf::xmrk melanoma model in Medaka fish (Schartl et al. 2010). His paper describes a germline transmission into 8 individual adult F0 founders out of 105, which is a transmission frequency of 7.6% (Schartl et al. 2010). In contrast, the *Dct*:eGFP transgenesis conducted and described in this thesis had a germline transmission of frequency 22.7%, which is 3-times higher achieved without an *I-Sce* site. This might be due the careful selection of strong GFP positive chimeras which were placed aside to be grown up, thus increasing the chance of transgene integration into germline precursor cells. 6 out of 8 analysed *Dct*:eGFP transgenic lines recapitulate the endogenous *Dct* expression pattern with eGFP. It seems that some researchers do obtain promising results with I-*SceI* technology and some do not and further analysis of this transgenesis technology might be one of the useful options to clarify its compatibility and advantages for the Medaka research field.

If our approach not to use any I-Sce meganuclease is right or wrong, is debatable. To our understanding in the Zebrafish community, the conventional microinjection of coiled or linearised plasmid DNA is now seen to be outdated, because of its drawbacks such as mosaic distribution of the injected transgene with long concatamer DNA formation, late transgene integration during late cleavages, low transgenesis frequency). However, this approach is still used frequently in the Medaka field (personal communication Furutani-Seiki 2011, Hashimoto & Adachi 2013), which justifies our approach to exclude a Tol2 or I-Sce sequence in our target vectors.

In addition we have observed an incomplete eGFP expression pattern within the melanocyte lineage in two of our transgenic *Dct*:eGFP lines. One hypothesis is that it might be due to silencing in early clonogenic melanocytes, which might be associated with short multi-copies of the inserted transgene often seen in mice transgenics (Calero-Nieto et al. 2010). Gene silencing is an epigenetic mechanism to regulate gene expression either during transcription or translation. However, in our case it needs to be investigated if this silencing effect happened in clonogenic melanocytes on a transcriptional or translational level, which might be possible by carrying out *in situ* hybridisation against the eGFP transcript in F2 offspring.

We also observed minor variation in eGFP intensities between those 8 *Dct*:eGFP transgenic lines, which might be due to different chromosomal insertion points of the transgene. Supporting, Day et al. have shown that expression level can vary up to 10-fold difference depending on the insertion site (Day 2000) . This strengthens the view that the chromosomal integration site can have an effect of the level of gene expression and that reproducible insertion into the same chromosome position is capable of generating the same expression levels.

Importantly, I saw no ectopic cell expression in any embryo at any developmental stage throughout these experiments in those 8 characteristic lines. From this data set we concluded that the Medaka promoter had the correct spatio-temporal expression properties and would be highly suitable for use in visualising Medaka melanocytes. It would also be an excellent choice for manipulating gene expression within melanocytes.

3.3.3 Summary

We aimed to explore the melanocyte pattern of *hirame* mutants in detail and draw conclusion about the timing when this patterning defects is established. We have shown in this chapter that *hirame* embryos lacking functional Yes-associated protein 1 (YAP1) exhibit an abnormal melanocyte patterning as early as stage 20. In fact, the melanoblast numbers are particularly reduced on the yolk sac indicating a migration defect. To broaden our analysis of melanoblast behaviour, we elected to establish transgenics using the *Dct* promoter we made ourselves mimicking the endogenous

melanocyte pattern. After successfully establishing several transgenic *Dct*:eGFP lines, one had been backcrossed into a wild type HB32C strain expressing strong levels of melanin in melanocytes. This presented us with the chance to analyse co-expression of eGFP in the melanocyte lineage and confirmed that our isolated Medaka *dopachrome tautomerase* promoter is melanocyte specific. In addition we could detect and monitor melanoblasts as soon as somitogenesis began, allowing real-time observations of individual cell migration, potentially also of cell division and survival. Careful exploration of a particular promoter also enables researchers to use it to its full potential with respect to other neural crest derivatives.

4 Chapter: Designing, testing and establishing *yap* overexpression constructs to test YAP cell autonomy within melanocytes

4.1 Background

4.1.1 Cell autonomy or non-cell autonomy as classical approaches to study gene function

In the previous chapter, we reported about the dramatic reduction of melanocytes with a strong melanoblast migration defect in *hirame* embryos, particularly during early embryogenesis. However, the question remains if this melanocyte defect is cell-autonomous or non-cell autonomous with regards to missing YAP activity. Cell-autonomy describes a genetic trait, which changes the phenotype and/or cell behaviour of a mutated individual or a subpopulation of cells. These changes are only present in mutated cells, and they cannot be found or transferred to surrounding normal cells. Conversely, a non-cell autonomous trait describes a situation in which genotypically mutant cells are able to transform surrounding cells, regardless of their genotype, to display a mutant phenotype. In other words, mutant cells can transform normal neighbouring cells to exhibit altered cell behaviour. However, the opposite can occur as well, wherein a normal environment can re-normalise the behaviour of genotypically altered cells, for instance, after transplantation experiments into normal wild type hosts. Characterisation of cell autonomy and non-cell autonomy is classically described as mosaic analysis and has been carried out in a wide range of organisms such as *Caenorhabditis elegans*, *Drosophila melanogaster*, mice and Zebrafish to study individual gene function (Carmany-Rampey & Moens 2006). An example of cell autonomy was delivered in 1990 by Ho & Kane in which the phenotype of Zebrafish spt-1^{b104} (spadetail) mutants express an important genetic trait solely autonomous to the paraxial mesoderm trunk precursors, which failed to converge during gastrulation (Ho & Kane 1990). Likewise, cell autonomous expression of the receptor neuropilin 2 (Npn2) in mouse trunk neural crest cells is required for the repulsion of crest cell migration by the posterior half of the somites in which the ligand semaphorin 3F (Sema3f) is expressed. Npn2 signalling forces NCCs to migrate separately through the mesoderm instead of remaining as a uniform cell sheet (Gammill et al. 2006).

To our knowledge, there are no publications concerning about the cell autonomous function of the Hippo pathway in particular tissues during development. However, unpublished data from a previous colleague working with the *hirame* mutant suggests a non-cell autonomous role for YAP during cuvier´s duct formation and the invagination of the lens into the retina of the developing eye (Porazinski 2013). The cuvier´s duct is an early circulatory system defined by a superficial vasculature sitting on top of the yolk sac, which plays an important role in yolk absorption to provide nutrients during early teleost embryogenesis (Fujita et al. 2006). It consists out of two merged sets of endothelial progenitor cells. The primary stream originates posteriorly near the developing somites

and the secondary population arises anteriorly close to the otic vesicle rudiment. Both streams unite at around stage 23. Porazinski not only observed that in *hirame* both cell streams were truncated and did not fuse to form an entire cuvier's duct, he also showed that as little as 15 wild type cells transplanted into *hirame* could partly rescue the endothelial cell migration and extend the anterior stream. Conversely, transplanted *hirame* cells into wild type embryos integrated fully in into the cuvier's duct endothelial structures. Another example came from the same thesis, when as few as 5 wild type cells were transplanted in the a region of the *hirame* developing eye, the lens, which normally is not invaginated within the retina tissue, could be rescued and resembled the wild type phenotype. This rescue was up to 100% when at least one cell was present within the lens and others remained in the retina (Porazinski 2013). These experiments suggest that at least in cuvier's duct and eye formation, YAP has a non-cell autonomous role, as wild type cells are able to exert a rescue in *hirame* mutants and *hirame* mutant cells are behaving somewhat normal when transplanted into wild type hosts.

Whereas most mosaic studies have been carried out by creating chimeric embryos through transplantation of tissue grafts or individual cells from a mutant into a wild type host or vice versa, cell autonomy can also be tested by overexpressing a target gene under a cell specific tissue promoter and examining whether phenotype is rescued. Similarly, non-cell autonomy can be assessed by overexpressing a gene of interest in a neighbouring tissue and investigating the behaviour of the mutant cells for instance after cell transplantation or YAP expression in other tissue. In this chapter we aimed to investigate if Yes-associated protein (YAP) plays a cell autonomous role within the melanocyte lineage. To test this hypothesis, I planned to establish transgenic lines overexpressing functional YAP protein under the Medaka *dopachrome tautomerase* (*Dct*) promoter, which would not only answer the question of the cell autonomy, but also provide a tool for monitoring cell behaviour through a fluorescent reporter eGFP in the future. Conversely, *yap* mRNA injections into the yolk sac were carried out as a complementary approach to test if melanoblasts can be rescued in a YAP non-cell autonomous fashion.

4.1.2 Choice of eGFP as fusion tag reporter

To investigate if Yes-associated protein (YAP) plays a cell autonomous role in melanocyte migration in embryos, I planned to increase the levels of YAP in MC protein and track this cell lineage with a fluorescent reporter. To accomplish this, I fused either wild type or an activated version of *yap* C-terminally to the enhanced green fluorescence protein (eGFP). In Medaka, the activated version of YAP, S87A, corresponds to the designed mutation S127A in human *yap,* which abolishes phosphorylation; thereby increasing YAP presence level within the nucleus (Basu et al. 2003). I

decided to use eGFP not only because it is available in the background pEGFP-1 plasmid generated in Chapter 3, which was suitable for expressing this fusion protein within melanocytes, but also because of its molecular properties.

The wild type green fluorescent protein (GFP), an important marker in research, was originally derived from the jellyfish *Aequorea victoria.* The original sequence and its derived protein structure were below the *sensitivity* of standard reporter systems such as β-galactosidase which enzymatically amplifies colour labelling to a visual level. By substituting the amino acid threonine for serine at position 65 within the GFP sequence, the chromophore intensity could be improved by 35 times in mammalian cells (Zhang et al. 1996). The excitation was shifted to 490nm and emission to 509nm (Gines et al. 2014). This enhanced version of GFP (eGFP) is one of the brightest proteins available, and it exhibits both high photostability and low cell toxicity. One of many properties is that the enhanced GFP can be detected as early as 10-12h after infection of *in vitro* cultures when driven by a basal promoter (Ma et al. 2000). Others report signals later than 16-24h (Zhang et al. 1996) after infection of mammalian cell cultures. The protein half-life has been estimated to be around 26h (Corish & Tyler-Smith 1999). EGFP is predominantly monomeric, but has a weak tendency to dimerise (Arpino et al. 2012). Although eGFP can be sensitive to pH (Piston et al. 2013), it has not been shown to significantly affect cell physiology in many numerous studies that have used eGFP for establishing transgenic lines in Zebrafish and Medaka (Jung et al. 2010; Nakamura et al. 2007; Carney et al. 2006). Furthermore, the majority of publications describing *yap* fusions, also fused eGFP directly to the N-terminal of the human *yap* sequence to monitor its subcellular location within *in vitro* cell cultures (Dong et al. 2005; Zhang et al. 2010; Liu-Chittenden et al. 2012; Zhao et al. 2011). Taken together, this means we could be confident in using the eGFP as a reporter for our N-terminal fusion with the *yap* gene.

4.2 Results

4.2.1 Constructing the fusion protein eGFP-YAP1

The first step was to fuse a flexible linker to the cDNA of *egfp* that will later be connected to the *yap* gene. Linker sequences generally provide the fusion protein with structural flexibility, improve protein stability or increase biological activity. I decided to use a 15 aa repetitive sequence glycine- and serine-rich linker $[GGGGS]_3$ Table 4.1), which had previously been shown to be a good linker sequence for fusion proteins used in various mammalian *in vitro* cell cultures (Trinh et al. 2004; Delacôte et al. 2013; Ito et al. 2011).

Table 4.1: Table: Sequence of the $[GGGGS]_3$ glycine-serine-rich flexible linker in eGFP-YAP fusion protein

Nucleotide sequence 5'- 3':	ggtggcggtggctctggcggaggtgggtccggtggcggcggaagc
Amico acid sequence N-C-terminus:	GGGGSGGGGSGGGGS

In theory, the *egfp*-linker sequence was then to be inserted into the pCS2 backbones (Figure 2.3) containing the wild type and activated version of Medaka *yap1.* The Medaka *yap* cDNA was present in its wild type (pCS2_*yap*(wt)) plus a mutated activated version S87A (pCS2_*yap*(S87A)) with an amino acid exchange in position 87aa that replaces serine with alanine. The activated version of *yap1* corresponds with the human S127A mutation, which in the mammalian context hinders the upstream kinase LATS and also Akt to phosphorylate YAP protein, thus increasing nuclear localisation and activity as a transcriptional co-activator (Dong et al. 2007; Basu et al. 2003). pCS2 constructs were kindly provided by Dr M. Furutani-Seiki.

To achieve this, first, I designed primers which amplified *egfp* and would attach the $[GGGGS]_3$ flexible linker (FL) sequence simultaneously on eGFP's C-terminus during the amplification process. The eGFP stop codon sequence was removed to maintain the open reading frame (ORF) between *egfp* and *yap*. In addition I added the restriction enzyme sequence of ClaI and SpeI to the N-terminus of the forward primer and another ClaI site after the flexible linker to its reverse primer set (Table 2.2), which helped to subclone it into the pCS2_yap(wt/S87A) constructs afterwards. The exact expected sequence order included the 5' restriction sites followed by *egfp* connected to a flexible linker with another restriction site attached (Figure 4.1). Finally, using the pEGFP-1 vector as a template (Figure 2.2), the PCR amplified *egfp* sequence was then ligated into the pGEM®-T Easy vector resulting in pGEM_*egfp*FL (Figure 4.2).

Figure 4.1: 5' and 3' nucleotide sequence of the egfpFL sequence

One-step PCR amplification in which ClaI and SpeI endonuclease restriction sites were added 5' to *egfp* and the flexible $[GGGGS]_3$-rich linker plus an additional ClaI restriction site was added 3' to the *egfp* gene. All supplementary nucleotides to *egfp* were added within the PCR through a specially designed forward and reverse primer pair. Note, *egfp* sequence does not contain a stop codon to maintain the reading frame of the fusion gene.

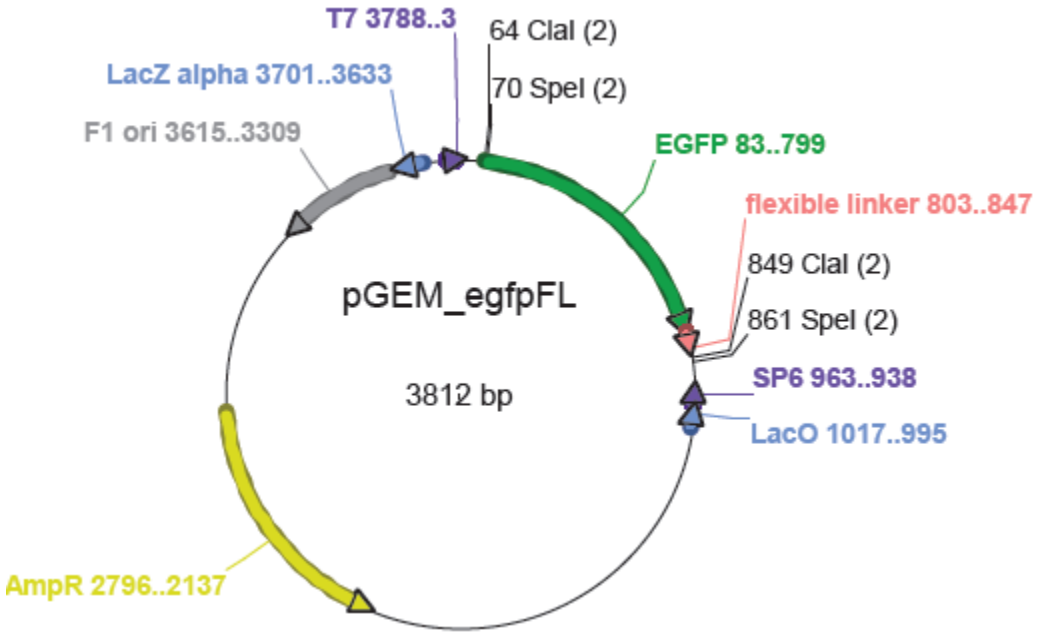

Figure 4.2: Plasmid map of pGEM_egfpFL

PCR amplified *egfp* fused to the $[GGGGS]_3$-rich linker nucleotide sequence inserted into pGEM®-T Easy cloning vector readily for subsequent cloning. Map features eGFP (green), followed by flexible linker (pink), and additional endonuclease enzyme recognition sites 5' and 3' of the PCR fragment. Other regulatory elements are the T7 and SP6 promoter (purple), ampicillin resistance gene (yellow), remaining LacO and LacZ alpha selection cassette (blue), F1 bacteriophage origin (grey) for DNA replication of viral strand synthesis and termination allowing synthesis of single-stranded DNA (not needed in my case) and ColE1 origin (grey) for double-stranded bacteria vector replication.

Next, I digested the pCS2_*yap*(wt) and pCS2_*yap*(S87A) with ClaI to open the backbone. Alkaline phosphatase incubation was carried out to remove the overhanging phosphate groups on the 5'end to prevent backbone self-ligation. In parallel, I digested pGEM_*egfp*FL with ClaI enzyme to extract the *egfp*-flexible linker sequence. Basically, I exploited the opportunity to insert my designed *egfp*FL sequence into the single-cut pCS2_yap vector through ClaI restriction site lying in front of the *yap* gene. Importantly, this left the open reading frame intact, thus creating a functional fusion protein. I then loaded the digestion onto agarose gels, extracted appropriate sized fragments, ligated together and transformed into DH5α. The purified construct was then analysed with SpeI/XbaI double digestion to check the orientation of the inserted *egfp*FL sequence on an agarose gel. In theory if self-ligation occurred, I would expect to see a linear 5403bp backbone band, because pCS2_*yap*(wt) or (S87A) only contains the XbaI restriction site. If the *egfp*FL sequence was inserted in the right direction and the construct is digestible, I would expect a 4072bp and 2116bp band. In the event of an inverted insertion, the fragments size of 4843bp and 1345bp would be present. Figure 4.3 represents a gel image taken after loading 18 digestions from 10 pCS2_*egfp*FL*yap*(wt) and 8

pCS2_egfpFLyap(S87A) mini-preps. Sample 2, 4, 7, 16, 17 and 18 represent constructs having *egfp*FL inserted in the right direction, whereas samples 1, 3, 5, 9, 10, 12 and 15 represent inverted inserts. In contrast, sample 6 and 14 represent double insertions of *egfp*FL where the first sequence is inserted in the right orientation and sample 8 and 13 picture double insertions of *egfp*FL where the first sequence was in the wrong orientation. Number 11 shows a linearised pCS2_yap backbone only. Clone 2 pCS2_egfpFLyap(wt) and clone 16 pCS2_egfpFL(S87A) were consequently chosen as successfully constructed plasmids, verified by sequencing and used for further experiments. A representative plasmid map is shown in Figure 4.4.

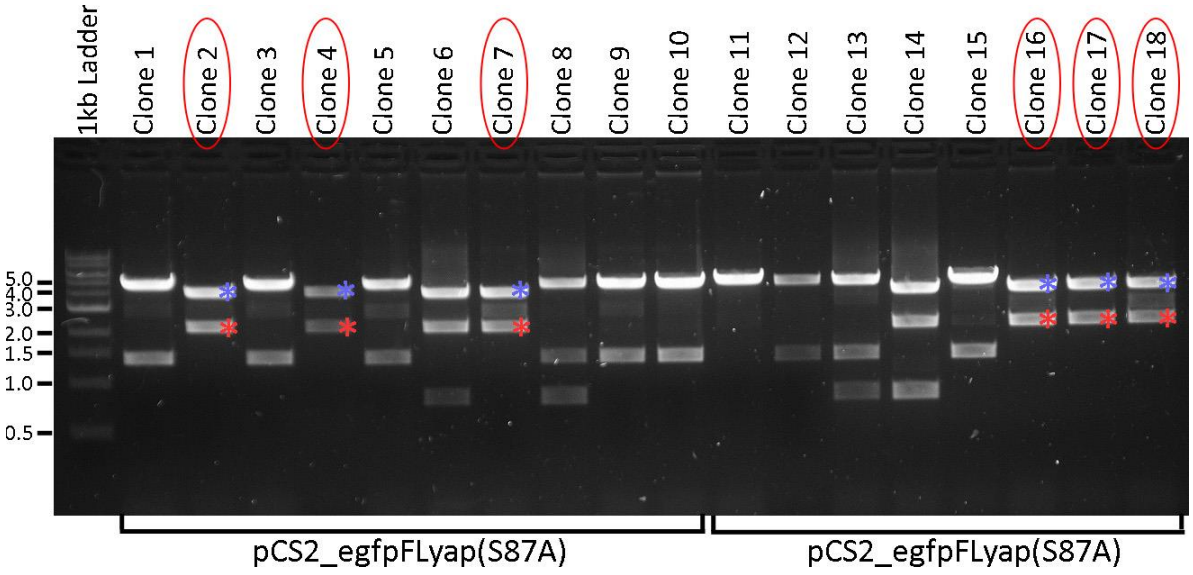

Figure 4.3: Identification of *egfp*FL*yap*(wt/S87A) colonies in PCS2 backbones

Agarose gel after electrophoresed DNA digests to check for egfpFL fragment insertion into both backbones, pCS2_yap(wt) and pCS2_yap(S87A) to create the fusion sequence egfpFLyap(wt or S87A). Seen are 10 digest reactions of pCS2_*egfp*FL*yap*(wt) and 8 of pCS2_egfpFLyap(S87A). The correct fragment size should show DNA bands at 4072bp (backbone, blue asterics) and 2116bp (insert, red asterics) band, which is the case with sample 2, 4, 7, 16, 17 and 18 (red circled). Other bands show either self-ligation, double insertions or reverse insertion of the desired construct (see explanations in text).

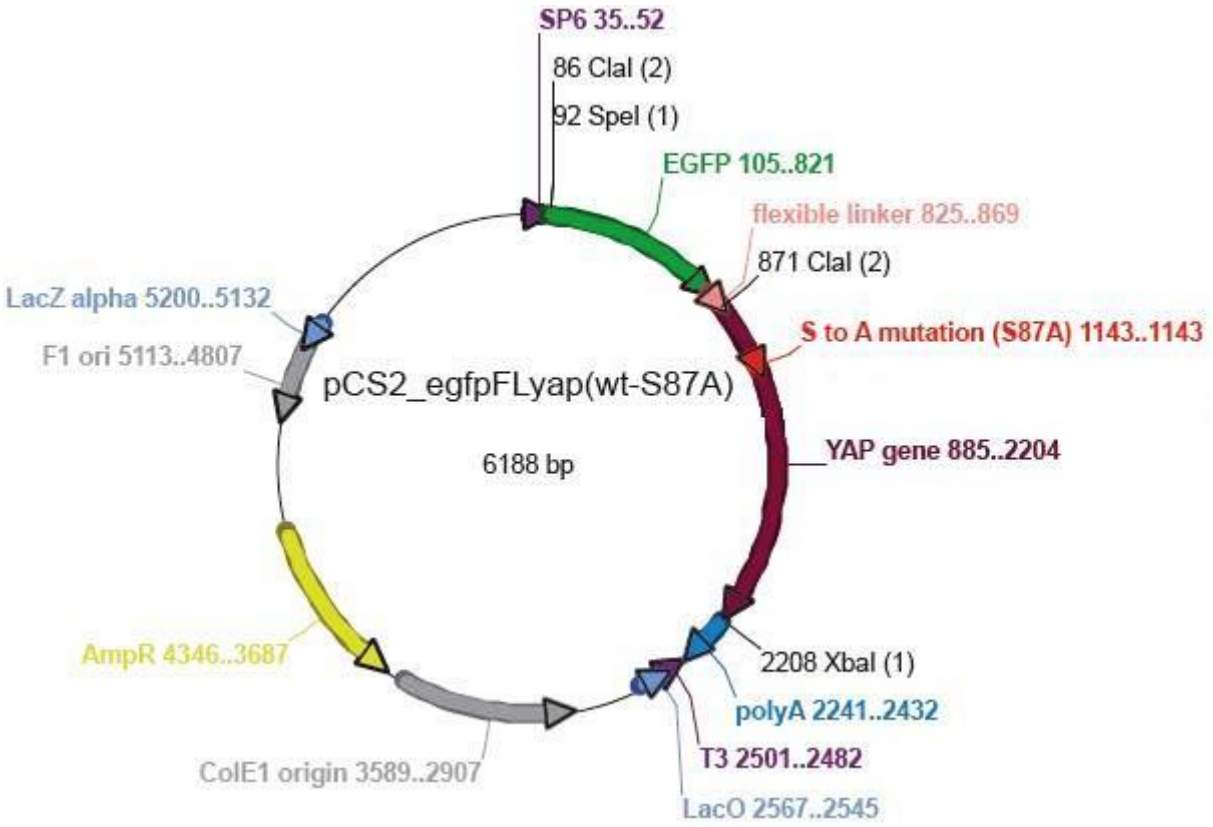

Figure 4.4: Representative map of pCS2_*egfp*FL*yap* (wt or S87A) plasmids

The fusion sequence egfpFL (green, pink) was inserted via ClaI restriction enzyme sites into the pCS2_yapwt/S87A) backbone infront of the Medaka *yap* (dark red) cDNA sequence. The representative map of verified plasmid clone 2 of pCS2_egfpFLyap(wt) and clone 16 of pCS2_egfpFL(S87A) is shown above. The S87A mutation and the putative *hirame* single nucteotide exchange is indicated within the *yap* gene sequence. Other regulatory elements within the pCS2 plasmid backbone include the SP6 promoter and T3 (purple), ampicillin resistance gene (yellow), remaining LacO and LacZ alpha selection cassette (blue), F1 bacteriophage origin (grey) for DNA replication of viral strand synthesis and termination allowing synthesis of single-stranded DNA (not needed in my case) and ColE1 origin (grey) for double-stranded bacteria vector replication.

As a positive control, a separate pCS2 vector was constructed with *egfp* cDNA only. The *egfp* gene was extracted from pEGFP-C3 (Figure 2.4) with a double restriction enzyme digest of NheI and HpaI. In parallel, an empty pCS2 destination vector (Figure 2.3) was opened up with XbaI and SnaBI. The *egfp* insert was ligated into the pCS2 backbone as NheI and XbaI remained compatible cohesive ends after digestion and could be ligated together. HpaI and SnaBI form blunt ends which were also compatible. After ligation, transformation and colony screening with HindIII digestion, all 9 mini-preps tested were positive for the right *egfp* insert orientation and number within the pCS2 host vector. Therefore I decided to purify clone 2 from pCS2_egfp in larger DNA quantities for further studies. A summary of this cloning process is reproduced in Figure 4.5. The complete fusion sequence of both pCS2_egfpFLyap(wt) and pCS2_egfpFLyap(S87A) was sequences to confirm the correct

nucleotide arrangements, but still needs to be tested in regard to its functionality *in vivo*. To accomplish that I aimed to assess synthesised synthetic messenger RNA of those two *yap* fusion genes in *hirame* mutant embryos. The presence of functional YAP would rescue mutants as would be revealed by analysing the melanocyte patterning.

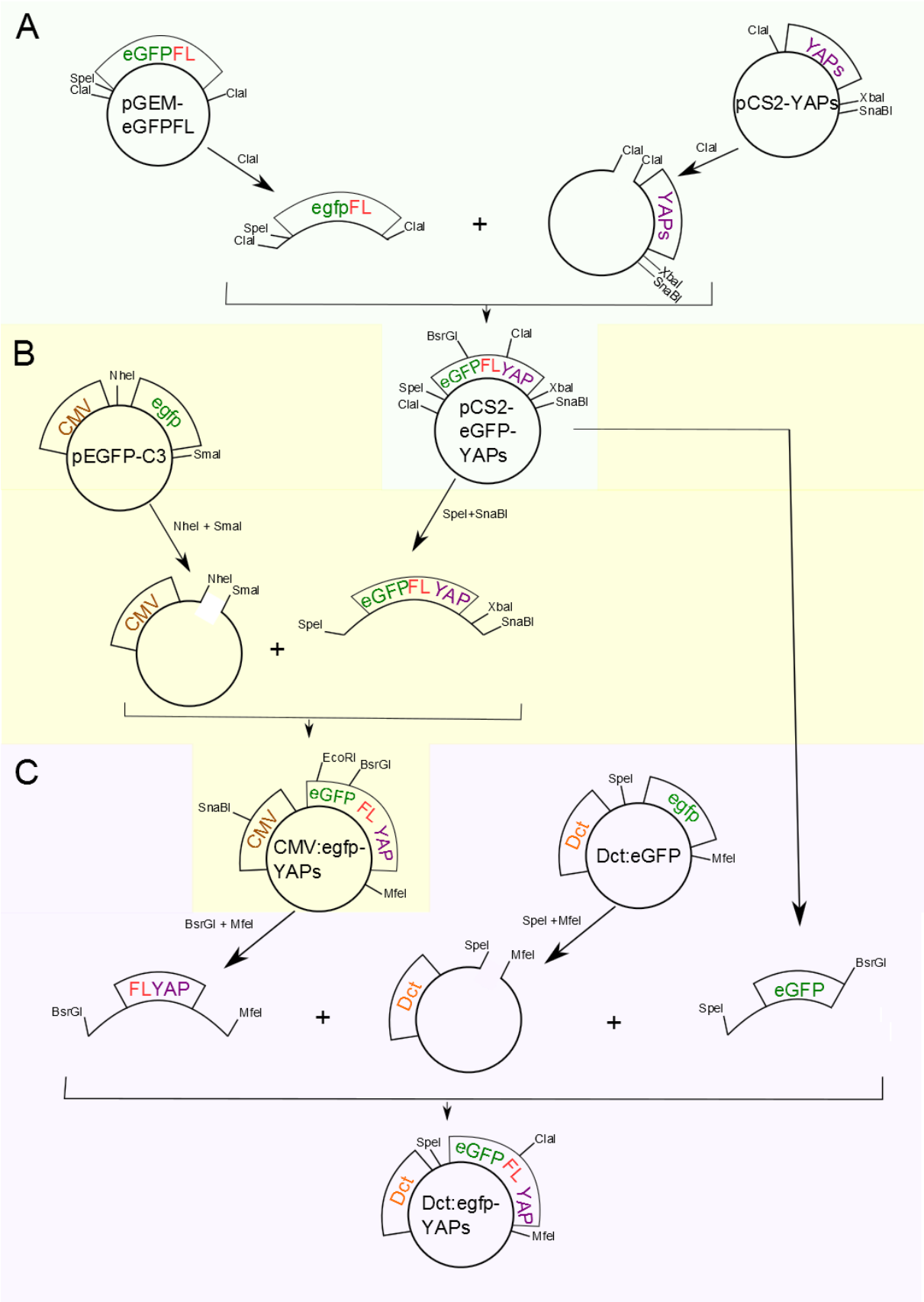

Figure 4.5: Schematic summary of the cloning strategy featuring the *egfp*FL*yap*(wt/S87A) fusion sequence

Each component has and retains the same colour definition related to the map featured in each section and throughout the whole thesis. Section A-C features different stages in constructing plasmids containing the *egfp*FL*yap*(wt/S87A) fusion sequence. **A)** Isolation of the *egf*FL sequence from pGEM_*egfp*FL, which was fused to wild type (wt) or an activated version (S87A) of *yap* (both included in description "YAPs") within the pCS2 backbone. This construct was taken for subsequent cloning as well as *in vitro* transcription to produce messenger RNA which verified the functionality of the YAP fusion proteins. **B)** Insertion of *egfp*FL*yap* fusion sequence into pEGFP-C3 backbone to obtain ubiquitous cell expression *in vivo* as positive control vector regards protein fluorescence and stability. **C)** Combining DNA fragments from A, C and *Dct*:eGFP (Chapter 3) to create the *Dct*:eGFP-YAP(wt/S87A) (here described as *Dct*:egfp-YAPs) constructs used for transgenesis and later analysis of YAP cell-autonomy within the melanocyte lineage.

4.2.2 mRNA rescue of *hirame* with egfpwtYAP1 and egfpS87A fusion proteins

Rescue of mutant phenotypes either by DNA constructs or synthetic mRNA injections into the embryo mutants allows for rapid testing of gene identity and functionality. Whereas injected foreign DNA is spread in a chimeric fashion, mRNA and other small nucleotide sequences such as morpholinos are distributed more evenly throughout early embryonic development. When injected into the cytoplasm of 1-2 cell Medaka embryos RNA maintains its activity only up to 1.5 dpi making the rescue of later defects difficult and sometimes impossible (Wittbrodt et al. 2002).

4.2.2.1 In vitro synthesis of messenger RNA

One disadvantage of transient mRNA (or cDNAs under a ubiquitous promoter) is that the abundant manifestation is ectopic. This can either lead to developmental defects or unintended tissue rescue, which may obstruct estimates of the rescue rate. In addition, RNA is less stable than DNA and thus needs to be handled with more care to avoid degradation (Gilmour et al. 2002).
Capped messenger RNAs of the *egfp*FL*yap* fusion sequences of wild type *yap*, activated *yap,* and *egfp* as a negative control were produced by *in vitro* transcription with the Ambion messenger kit. Firstly, pCS2_*egfp*FL*yap*(wt or S87A) and pCS2_egfp (all three vectors from section 4.2.2 were linearised with NotI restriction endonuclease cutting in its specific recognition site located after the SV40 polyA signal which follows the *yap* or *egfp* cDNA sequence. Genes of interest were transcribed *in vitro* with the SP6 RNA polymerase using the purified and linearised constructs and the Ambion messenger RNA kit (manufacturer's instruction). The resulting RNA was measured with an RNA Nano spectrophotometer and diluted to a working concentration of 500ng/µl. For quick visual testing, 1µl of RNA working solution was loaded onto bleach containing agarose gel in a bleached gel chamber to prevent RNA's degradation. The gel was loaded with the 3 different messenger RNA´s: firstly *egfp*,

secondly *egfp*FL*yap*(wt) and lastly *egfp*FL*yap*(S87A) . The actual RNA size starting from the SP6 signal and ending with the NotI cut for the egfpFLyap(wt/S87A) fusion was 2387bp and for the *egfp* RNA 1192bp, exactly what we see on the gel picture. Additionally, I re-measured the RNA concentration and purity with the Nano spectrophotometer to exclude the possibility of overlooked salt or protein contaminants as well as degenerated RNA. When measuring RNA, a ratio of $A_{260/280}$ with an absorbance of around 2.0 is classified as "pure" RNA. Lower ratios may indicate the presence of protein, phenol, change of pH or other contaminants with strong absorbance around 280nm. The $A_{260/230}$ represents a second value of nucleic acid and RNA purity and "pure" samples would be expected to reach values between 2.0-2.2. Lower ratios may be the result of EDTA, carbohydrate, TRIzol or phenol contaminations, all absorbing at 230nm (Nano Drop Technologies website 2007). Table 4.2 shows that all RNA concentrations were around 500ng/µl and that all RNA samples produced with *in vitro* transcription were very pure as indicated by the $A_{260/280}$ and $A_{260/230}$ ratios.

Table 4.2: Duplet measurements of RNA with Nano spectrophotometer concentration and emission data to indicate quality ratios

RNA sample	Concentration [c]	A260/280 ratio	A260/230 ratio	Quality
egfp	554 ng/µl	2.022	2.216	Pure
	546 ng/µl	2.053	2.238	Pure
egfpFLyap(wt)	544 ng/µl	2.045	2.230	Pure
	538 ng/µl	2.023	2.261	Pure
*egfp*FL*yap*(S87A)	520 ng/µl	1.985	2.222	Pure
	550 ng/µl	2.022	2.218	Pure

Further to the above, I measured the RNA purity on a BioRad Experion™ Automated Electrophoresis System as the purity of messenger RNA is an extremely important factor for any mRNA injection experiments. I measured the concentration of diluted mRNA of all three samples on the BioRad following manufacturer´s instructions (Figure 4.6). The electropherogram in each of the of the three samples, *egfp* (A) *egfp*FL*yap*(wt) (B) and *egfp*FL*yap*(S87A) (C), revealed only a single mRNA peak indicating that the samples were very pure, did not include any RNS degradation, and therefore suitable for *in vivo* studies.

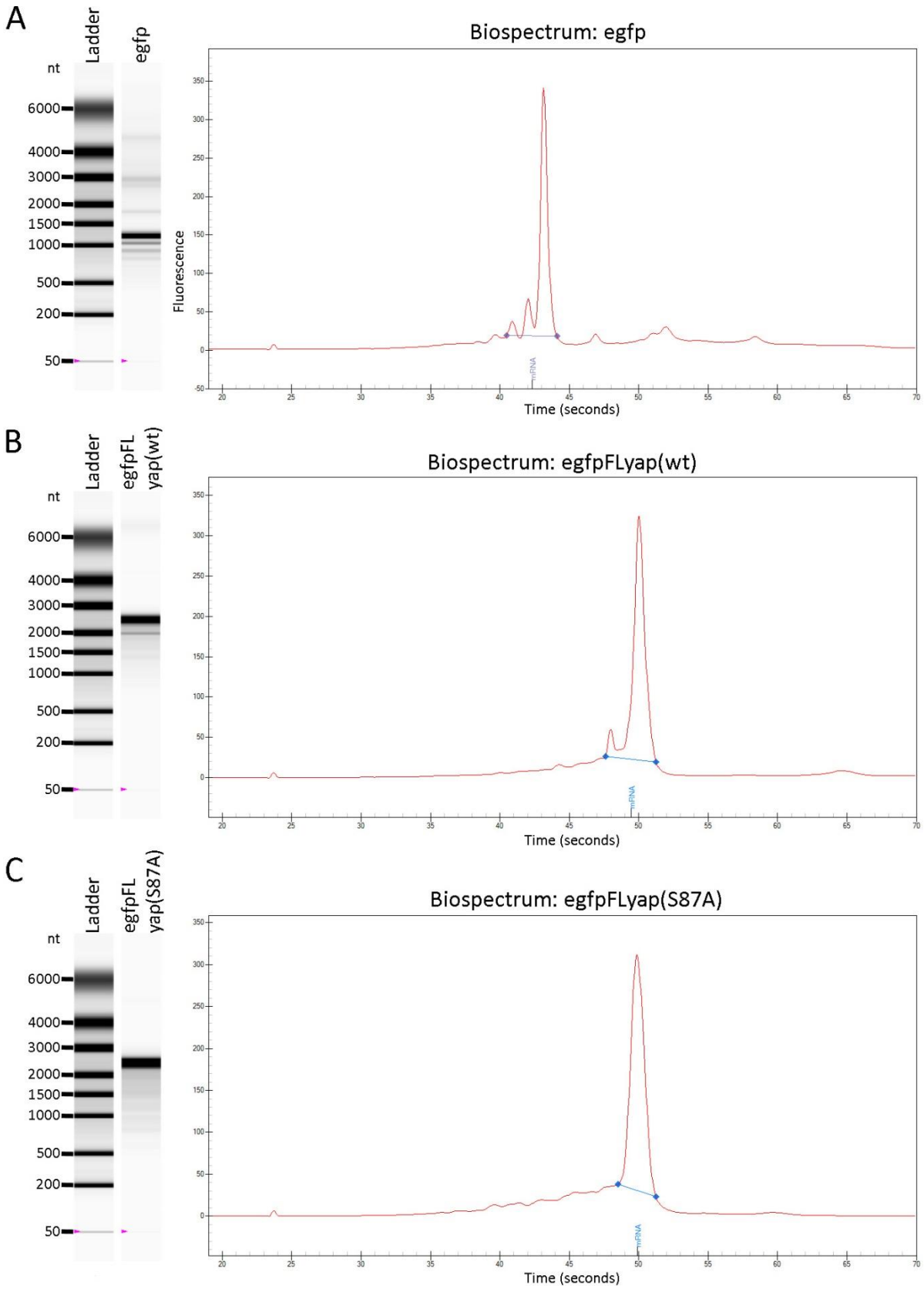

Figure 4.6: BioRad data of analysed *egfp*, *egfpFLyap(wt)* and *egfpFLyap(S87A)* mRNA samples

Bioanalysis of synthesised capped mRNA for egfp (A), egfpFLyap(wt) (B) and egfpFLyap(S87A) (C) was carried out on the BioRad spectrophotometer and imaged gel electrophoresed RNA

molecule (left panel) and the relevant biospectrum (right graph) was obtained. All samples show a very low degree of RNA degradation shown by a straight mRNA peak within the spectrum as well as a very clear RNA fragment band on the RNA gel.

4.2.2.2 Yap mRNA injection into the one cell stage rescues hirame mutants

Our aim was to evaluate the functionality of our *egfp*FL*yap* fusion protein *in vivo* and proof that the fusion of eGFP to YAP does not interfere with each other. The first approach I took was mRNA injection, which would show that the assembled final protein is able to rescue the *hirame* phenotype. Functional mRNA injected into the cytoplasm of an embryo at one to two-cell stage can be active from the time of injection up to early organogenesis, which is roughly 1.5 dpf (Wittbrodt et al. 2002). Theoretically, a total rescue would include a restoration of the abnormal organogenesis, flattened body morphology, dislocation of several organs and defects in neural crest melanocyte pattern. The early degradability means that a phenotypic evaluation of any rescue in *hirame* body morphology, as described in Chapter 3 section 3.2.2 of 24-28 stage embryos, would be difficult. This is because 1.5 dpf embryos still lack visual organ compartmentalisation such as lens and optic cup tissue as well as defined fore-, mid- and hind-brain structures. Therefore, precise distinctions between wild type and *hirame* embryos at stage 21-22 can be tricky especially after injections that might disrupt some developmental features. Because of these reasons, I decided to judge the rescued phenotype in *hirame* with the melanocyte patterning defect present on the yolk sac detectably via *dopachrome tautomerase* (*Dct*) *in situ* hybridisation, observed and described previously in *hirame* in great detail. A total of around 200-250pg *egfp*, *egfp*FL*yap*(wt) or *egfp*Fl*yap*(S87A) mRNA was injected into 1-2 cell-stage Cab$^{j50\text{-}20C}$ embryos, which were subsequently raised to stage 22 (9 somites, 1d14 hpf) and fixed in 4% paraformaldehyde. Fixed embryos were then hybridised with a *Dct*-antisense probe to visualise melanoblasts and early differentiated melanocytes in the body and on the yolk sac. Numbers of labelled cells in individuals were then counted, recorded and a random selection imaged. All embryos were then genotyped using the tetra-primer ARMS-PCR method to distinguish homozygous *hirame* and wild type sibling embryos.

Visual examination of injected embryos at stage 22 showed no obvious sign of the *hirame* MC phenotype i.e. putative *hirame* mutants were indistinguishable from their wild type sibling embryos after injection with *egfp*FL*yap*(wt) (second column) and *egfp*FL*yap*(S87A) (third column) RNA (Figure 4.7). In contrast, *hirame* embryos injected with the negative control RNA *egfp* exhibited typical abnormal melanocyte distribution as characterised previously, possibly due to the lack of functional YAP protein. This first impression provides an indication that the fusion constructs of *egfp* and yap variants leads to functional protein that are able to rescue the affected *hirame* melanocyte phenotype.

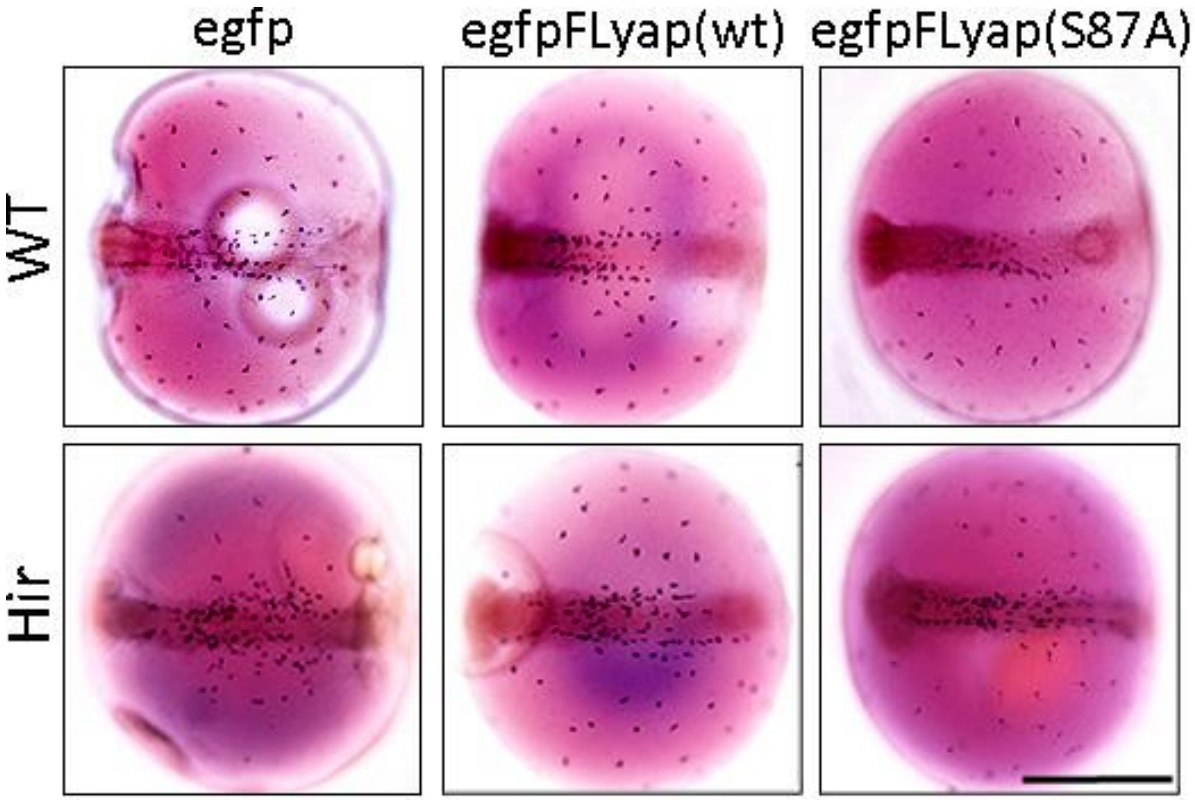

Figure 4.7: Injection of *egfp*, *egfp*FL*yap*(wt) and *egfp*FL*yap*(S87A) mRNA into 1-cell stage embryos rescues the *hirame* melanocyte defect

Dopachrome tautomerase ISH was carried out on st. 22 embryos after injection of *egfp*, *egfp*FL*yap*(wt) and *egfp*FL*yap*(S87A) mRNA injection into 1-cell stage embryos to visualise the *Dct* melanoblast pattern within body and on yolk sac of *hirame* mutants and wild type sibling. Wild type siblings injected with *egfp*FL*yap*(wt) (n=57) and *egfp*FL*yap*(S87A) (n=37) resemble the same normal melanoblast pattern as siblings injected with negative control mRNA *egfp* (n=43). However, *hirame* embryos injected with the *egfp*FL*yap*(wt) (n=13) and *egfp*FL*yap*(S87A) (n=11) show wild type melanoblast patterning especially on the yolk sac area which remains affected in *egfp* (n=7) injections only indicating a functional rescue with the YAP fusion protein *in vivo*. Scale bar = 500µm.

Manual cell counts of *Dct* positive melanoblasts were carried out after taking images and before PCR genotyping was performed for individual embryos. In total 168 embryos were injected in triplicates within each RNA group, 50 embryos were injected with the negative control RNA *egfp*, 70 embryos were injected with the *egfp*FL*yap*(wt) fusion gene and 48 embryos were injected with the activated version of *yap* in form of *egfp*FL*yap*(S87A) RNA. Our first observation reflects the ratio of homozygous recessive *hirame* mutants to its wild type siblings. Theoretically, we should expect around 25% *hirame* in each group as per Mendelian genetics. In fact, within the *egfp* category 7 embryos turned out to be *hirame* resembling 14% of its total injections after genotyping. In the *egfp*FL*yap*(wt) population, 13 embryos were *hirame* which is 18.6%. Within the *egfp*FL*yap*(S87A) pool, 11 (20.8%) embryos were identified to be of *hirame* genesis. While at first glance, it seems

surprising that the *hirame* mutants were underrepresented in our sample, there is a simple explanation. During the experimental procedures, the eggs were scratched with sandpaper to aid dechorionation, incubated in hatching enzyme followed by fixation, which led to decreased survival rates in especially *hirame* embryos due to its soft and fragile tissue structure. This would adequately explain the deviation from Mendelian expectations for the homozygous recessive *hirame* mutant population.

Table 4.3: *Dct* cell of *egfp*, *egfp*FL*yap*(wt) and *egfp*FL*yap*(S87A) wild type and *hirame* embryos

	egfp (n = 50)	**egfpFLyap(wt) (n = 70)**	**egfpFLyap(S87A) (n = 48)**
WT # of embryos	43	57	37
Body MC #	81.8	82.9	87.6
Yolk MC #	54.2	59.3	51.6
Total MC #	133.2	142.3	139.2
Hir # of embryos	7 (14% out of 50)	13 (18.6% out of 70)	11 (20.8% out of 48)
Body MC #	102.7	97.5	105.4
Yolk MC #	36.6	**61.5**	**53.5**
Total MC #	130 (**% baseline**)	158.9 (**22.2% increase**)	158.8 (**22.15% increase**)

Our second observation and analysis focuses on the *Dct*$^{+}$ cells in the body and on the yolk sac of embryos in each individual injection group respectively. Hereby cell counts are represented in Graph 4.1 which are based on the data shown in Table 4.3. The three left groupings represent wild type genotypes in the body, on the yolk sac and total numbers, whereas the three right units signify *hirame* in those same classes. Each section comprises RNA injections either of *egfp*, *egfp*FL*yap*(wt) or *egfp*FL*yap*(S87A) and is analysed in regards to melanocyte numbers.

Within wild type embryos we did not observe any significant changes in terms of melanocyte patterning or numbers after injection of *egfp*FL*yap*(wt) or *egfp*FL*yap*(S87A) compared to *egfp* mRNA negative control in any of these three areas, body, yolk sac and total *Dct* cell numbers. Both *yap* injections show that increased levels of abundant YAP protein in wild type embryos did not have any significant effect on melanoblast numbers within the body nor on the yolk sac itself, therefore total numbers were unaffected. All values for the body location were between 81.8-87.6 *Dct* positive cells and 51.6-59.3 for the yolk sac region, showing no significant differences within those categories (Table 4.3). Again, there were no alterations seen in any of those three categories in embryos overexpressing *yap* in comparison to the negative control of *egfp* RNA injections.

On the other hand, mRNA injection of functional YAP protein into *hirame* embryos resulted in an altered and seemingly rescued phenotype as melanocytes were able to migrate away from the body axis onto the yolk sac. All *hirame* embryos injected, either with wild type (wt) or the activated version of YAP (S87A), exhibited increased numbers of *Dct* positive cells in which between 53.5-61.5 melanoblasts/melanocytes were located on the yolk sac itself. In comparison with 36 cells in *egfp* injected *hirame* where the melanocyte pattern remained abnormal. This meant that the injection of *yap* genes translating into functional YAP protein could restore the number of *Dct* positive cells on the yolk sac to normal wild type levels. Inevitably, the incline in *Dct* cells on the yolk sac resulted automatically in a 22% rise in total cell quantities within the *yap*- injected group. The data implies that our fusion produced a functional protein capable of rescuing the *hirame Dct* patterning defect.

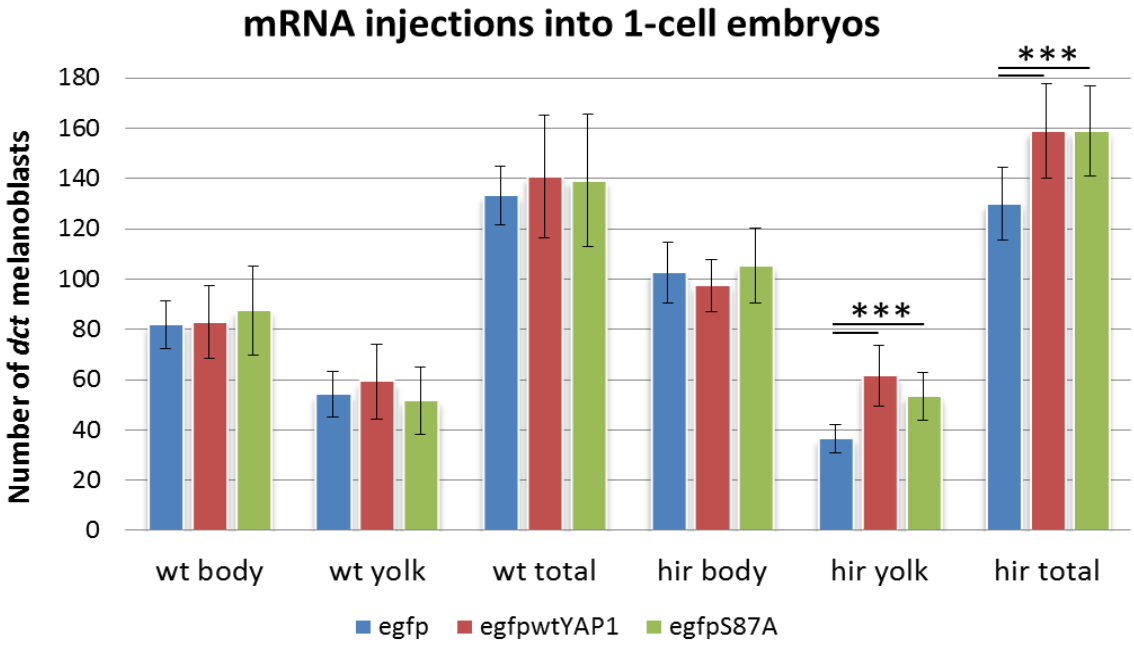

Graph 4.1: Melanoblast quantification in body and on yolk sac in st.22 embryos after *Dct* ISH of egfp, egfpFLyap(wt) and egfpFLyap(S87A) injected 1-cell stage embryos
Manual cell counts of *Dct* positive cells in stage 22 embryos after *egfp*, *egfp*FL*yap(*wt) and *egfp*FL*yap*(S87A) mRNA were carried out to evaluate the rescue achieved by YAP fusion protein. None of the overexpressed form of YAP had an effect on normal wild type melanoblast pattern in the body nor on the yolk sac in wild type siblings resulting in no difference in total *Dct* positive cell numbers. However, wild type and activated YAP´s did increase significantly the cell number of melanoblasts on the yolk sac of *hirame* embryos compared to negative control mRNA egfp, ultimately leading to an incline in total *Dct* positive cell numbers. This means that sufficient levels of YAP fusion protein in a transient ubiquitous fashion are able to rescue the *hirame* melanoblast defect when administered at one-cell stage. All data are means ± SEM. 2-Sample-t-test: *p<0.05, **p<0.01 or ***p<0.001 .

After demonstrating that the fusion of eGFP to YAP does not interfere with YAP's functionality *in vivo*, we were ready to carry on and use this fusion of *egfp*FL*yap*(wt/S87A) for our non-cell autonomous and cell autonomous studies. Non-cell autonomy was tested by injecting the mRNA into the yolk sac, whereby the cell autonomy was assessed by expressing *yap* under the *Dct* melanocyte-specific promoter.

4.2.3 Analysis of YAP cell-autonomy within the yolk sac environment

As mentioned earlier we hypothesised that a non-cell autonomous function of YAP within the syncytial layer could rescue the failure of melanocyte migration on the yolk sac of *hirame* embryos. Our idea was based on previous findings whilst carrying out melanoblast cell counts within consecutive resin sections presented in chapter 3 section 3.2.2.3, whilst observing those resin sections, we found numerous fragmented nuclei in the yolk sac membrane of st.21 *hirame* embryos not present in wild type siblings. In normal embryos, approximately two to three 15-40µm oval shaped nuclei are spread over a distance of 100µm within the yolk sac membrane (Figure 4.8 left panel). In *hirame,* while we observed a similar distribution, some of those were fragmented, spot-like neutral red stained nuclei (Figure 4.8 right panel).

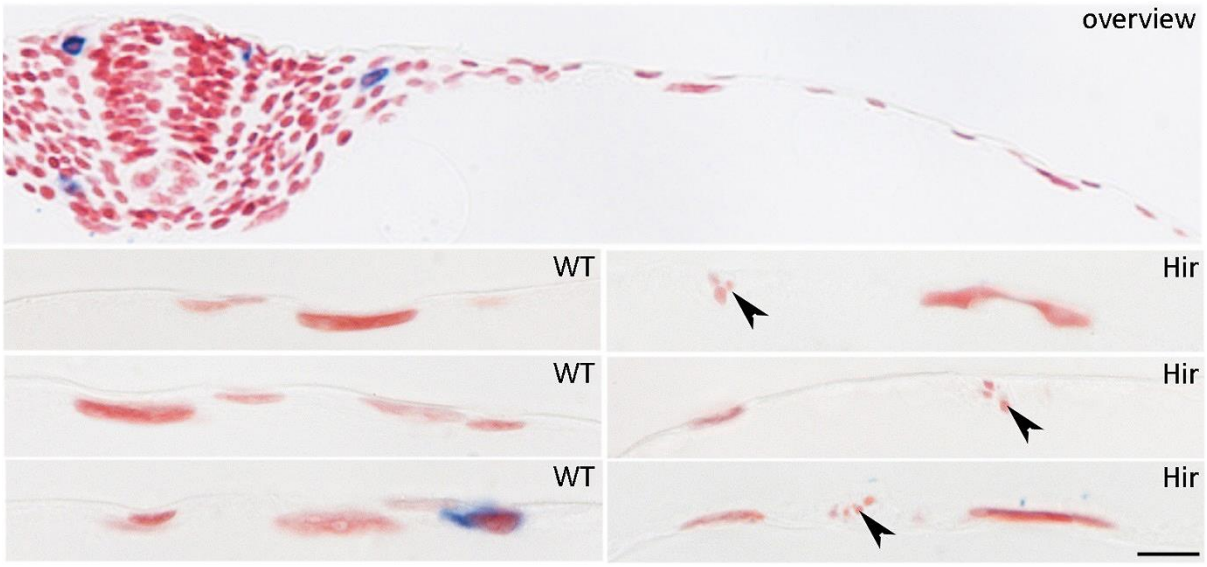

Figure 4.8: Fragmented nuclei within the yolk sac membrane of st.21 *hirame* embryos

Neutral Red labels nuclei in resin sections carried out after *Dct* WISH at st.21 in wild type (n=19) and *hirame* (n=18). **Top)** represents a cross section of a WT embryo to give a broad overview of the tissue morphology and scale. **Bottom)** pictures represent nuclei of wild type (left panels) and *hirame* (right panels). Note, in *hirame* a subset of nuclei are fragmented (arrow head) compared to wild type siblings in which all nuclei are oval and stretched in shape. Scale bar = 20µm.

We were wondering if those anatomical features might contribute or may even be the cause for the melanoblast migration defect in *hirame*. Our hypothesis was that injection of *yap* mRNA may rescue those dying membrane cells and re-establish a suitable environment required for successful cell migration. However, to that date we did not knew anything about the structure of the yolk sac membrane in Medaka. What we knew was, that the yolk sac membrane must consist of at least two different membranes: the inner yolk syncytial and the outer enveloping layer (EVL), thoroughly described during early gastrulation (Carvalho & Heisenberg 2010). Yet, images taken from those stained resin sections could not produce high enough magnifications to provide a conclusive answer about the layer in which those abnormal nuclei reside. Neither could it provide an answer about the state in which they are in; for instance, if they are apoptotic or necrotic as light microscopic appearance of nuclear structure staining may be seen in both (Corcoran et al. 1994). Therefore, we performed transmission electron microscopy of st. 21 wild type and *hirame* embryos to solve the yolk sac structure and identify abnormal cell structures in *hirame*.

TEM images showed that first of all the Medaka yolk cell is surrounded by three membranous layers, possibly the inner yolk syncytial layer, a middle epidermal and an outer enveloping layer (EVL) in which individual cell nuclei are inherent (Appendix 10). In regard to *hirame*, residing nuclei appeared to be oval wave-like, an indication of nucleus condensation (pyknosis) (Figure 4.9B, arrows, n=7) compared to more smooth and stretched-like nuclei in wild type siblings (A, n=7). Interestingly, we could indeed find three examples of fragmented nuclei (karyorrhexis) (Figure 4.9C, asterics) in *hirame* seemingly surrounded by apoptotic bodies in which organelles such as mitochondria remained. We could also see condensed chromatin in form of apoptotic nuclear inclusions (Figure 4.9D, arrows) found in late stage apoptotic cells within one cell residing within mesodermal tissue just beyond the somites. Despite these remarkable differences, there were similarities as well, for instance protruding tight junctions in the EVL as well as inclusions and lipid droplets within the yolk cytoplasm facing the yolk syncytial layer (Appendix 11).

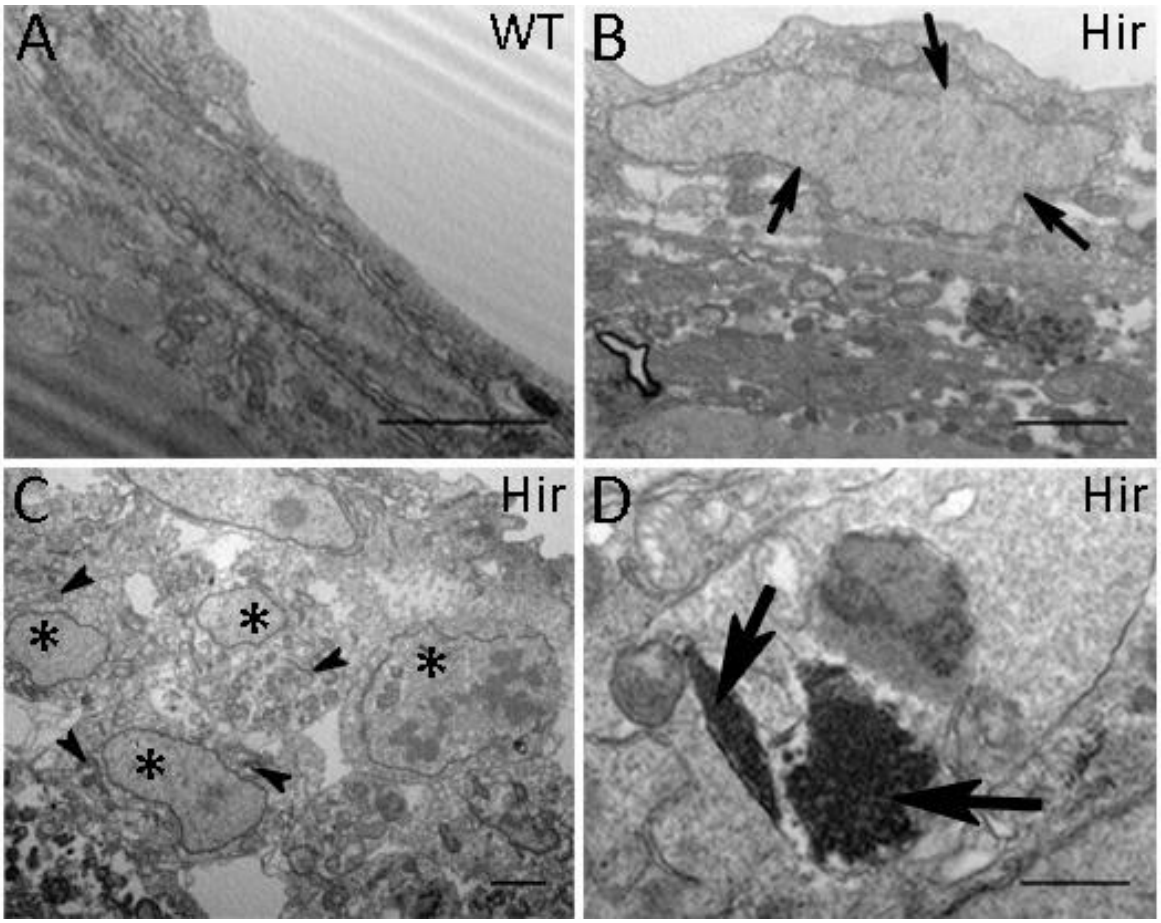

Figure 4.9: TEM of nuclei in wild type and *hirame* embryos

Transmission electron microscopy (TEM) highlighting the differences in nuclear shape. **A)** wild type embryos represent oval stretched nuclei with a smooth surrounding membrane. **B-D)** Nuclei in *hirame* present a variety of shapes including those found wild type siblings. **B)** Condensation of chromatin leads to shrinkage of nuclei (pyknosis) indicated by wave-like membrane (arrows). **C**) Fragmentation (asterics) of nuclei into small apoptotic bodies in which cell organelles such as mitochondria remain (arrow heads). **D)** Densely compact chromatin shown as dark inclusions (arrows) within the actual nuclei of an apoptotic cell. Scale bar: A-C = 2µm, D = 1µm

These data would link to the method of injecting *yap* mRNA directly into the yolk sac. The idea behind it is, that injected *yap* mRNA would be taken up by the most inner membranous layer during the processes of yolk absorption whilst "feeding" the embryo with nutrition (Fujita et al. 2006). Through this uptake, it might rescue dying cells and influence melanoblast migration indirectly in a non-cell autonomous manner. To test our hypothesis, we needed to be sure that our injected mRNA solely localises to the yolk sac and is excluded from any other embryonic tissue. As described earlier, injections into Medaka differ from Zebrafish. To manipulate gene expression or establish transgenic lines in Zebrafish, microinjection of RNA, DNA, morpholino oligonucleotides or tracer dyes can be carried out by injecting solutions deep into the yolk cytoplasm of 1-8-cell embryos (Detrich et al. 1998). The easier method of inserting the capillary into the yolk sac instead of into the cell directly is

possible because cytoplasmic streaming pushes components within 15 min completely from the yolk sac into the cell cytoplasm. The reason behind this is the fact that until the 8-cell stage, there is no physical barrier between the blastoderm and the yolk, thus solutions can be exchanged. The first membrane separating the developing blastomers completely from the yolk appears at 16-cell stage (Kimmel et al. 1995). However in Medaka, microinjection has to be carried out through the chorion directly into the cytoplasm of the 1-cell stage embryo rather than the yolk, as yolk cytoplasmic streaming has not been seen in Medaka early embryogenesis (oral communication with Dr M. Furutani-Seiki, Kinoshita et al. 2009). Although the chorion hardens after fertilisation, injections performed up to 64-cell stage are possible with great care (Porazinski et al. 2010). However, injections between 1-2 cell stage is not as variable and more accurate, because the hard chorion at later stages is likely to break the needle which then alters the injection volume after each injection attempt.

We first wanted to test if it was true that Medaka does not exhibit any cytoplasmic streaming within the yolk sac pushing substances towards the embryonic cells, as this could lead to an exchange with the one cell cytoplasm once we inject RNA into the yolk. To assess this, we injected rhodamine dextran either into the cell cytoplasm or into the yolk sac cytoplasm of one-cell stage embryos. Indeed, when rhodamine was injected purely into the yolk, we could not observe any exchange of dye at any stage during embryonic development (Figure 4.10, 2nd row) and rhodamine dextran retained well distributed within its specific destination up to 9 somite stage. When we injected the dye into the 1-cell, we noted a red glow around the yolk sac, which was not observed in the other experiment (Figure 0.8, 1st row). Higher magnifications indicated that when rhodamine dextran was administered into the embryonic cell, the dye distributed throughout some of the yolk membrane layers (Figure 4.11) surrounding the entire yolk sac. It means the layer surrounding the yolk cell is directly connected to the blastoderm and acquires the same DNA or RNA after injections. Whereas in the yolk sac injected embryos, this particular part of the yolk sac membrane remained separate and unlabelled.

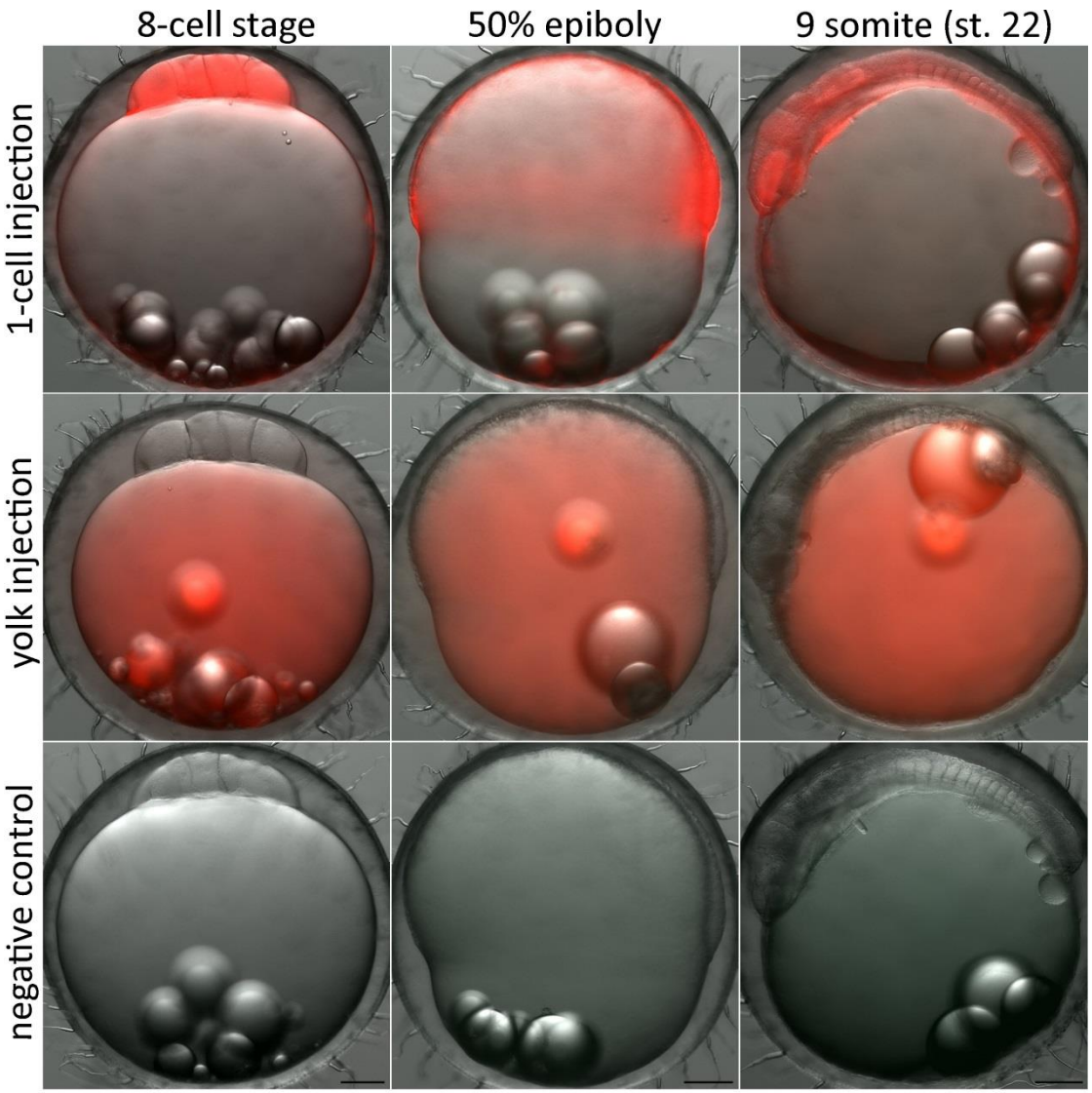

Figure 4.10: Visualisation of dye diffusion of injected one cell or yolk sac exclusively through rhodamine dextran dye

One-cell cytoplasm or yolk sac were exclusively injected to test cytoplasmic yolk streaming in Medaka embryos. Up to 9 somite stage red fluorescence stays uniformly distributed within either the embryonic cells (upper row) or yolk sac exclusively (middle row) and did not fuse with each other. However, when injected into the embryo we could observe a fluorescence shine surrounding the yolk sac that remained until 9 somite. Scale bar = 100µm

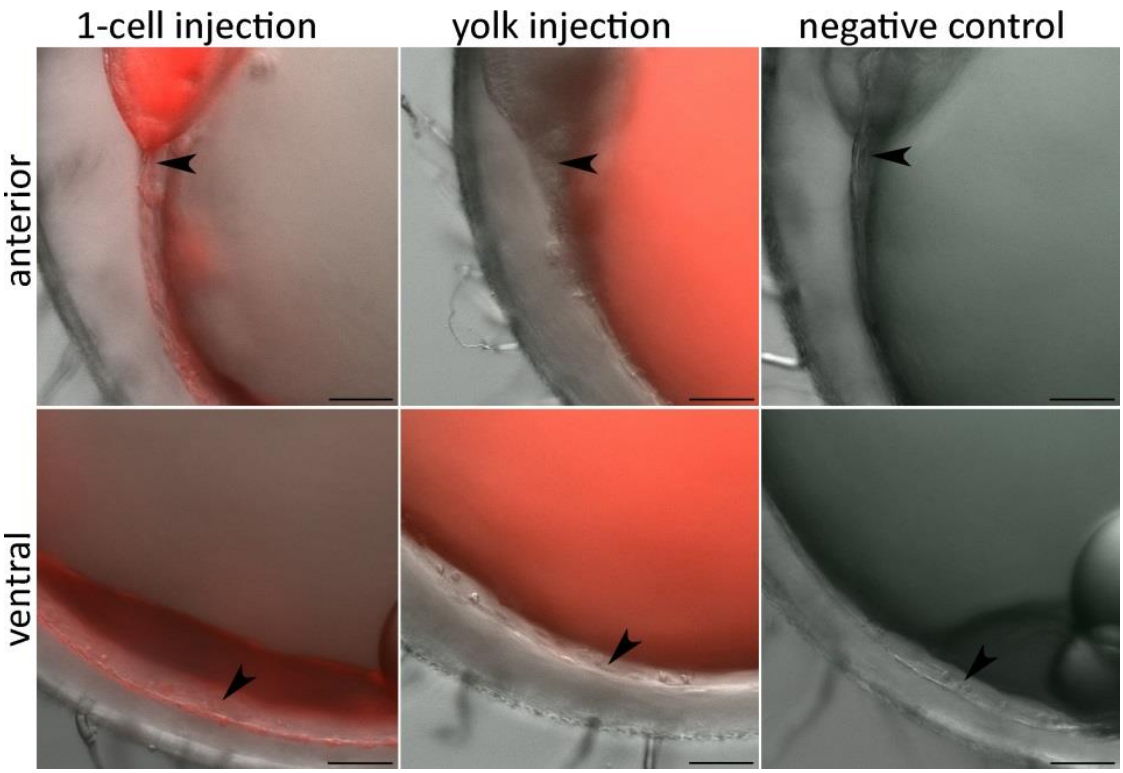

Figure 4.11: Rhodamine dextran does not diffuse in neighbouring body and cell compartments

Higher magnification revealed that the most outer layer of the yolk sac was labelled with rhodamine dextran dye when injected directly into the one-cell embryo (arrow heads). This was not found in others. Scale bar = 50µm

Next, we attempted injection of *yap* mRNA into the yolk sac to finally test if it could rescue the *hirame* melanoblast patterning defect on the yolk by restoring an environment in which melanoblasts can migrate. For injections we utilised the capped mRNA of *egfp*, both fusions *egfp*FL*yap* (wt) and *egfp*FL*yap* (S87A) which we have previously synthesised in section 4.2.1 and tested successfully its functionality in section 4.2.2. A total of around 200-250pg was injected solely into the yolk sac of 90 one cell stage Cab$^{j50\text{-}20C}$ embryos. 32 embryos were injected with the negative control RNA *egfp*, 27 embryos were injected with the *egfp*FL*yap*(wt) fusion gene and 31 embryos were injected with the activated version of yap in form of *egfp*FL*yap*(S87A) RNA. Those embryos were then raised to stage 22 (9 somites, 1d14hpf) and fixed in 4% paraformaldehyde. Subsequently, fixed embryos were hybridised with the *dopachrome-tautomerase (Dct)* anti-sense probe to visualise melanoblasts and early differentiated melanocytes in the body and on the yolk sac. Numbers of labelled cells in individuals were then counted, recorded and imaged.

When we examined those embryos, we could not see any phenotypic difference between wild type embryos injected either with the wild type or activated version of *yap* compared to the negative control *egfp* only (Figure 4.12 upper row). There was no noticeable decrease or increase neither in cell number nor in the distance of migration towards the ventral pole. When observing *hirame*

embryos we came to the same conclusion as we could not identify any obvious difference of *yap* injected embryos compared to the negative control (Figure 4.12 lower row). All embryos developed in a *hirame*-like fashion with abnormal body morphology. Melanoblasts did not populate the yolk sac in normal numbers and remained close to the body comparable to the negative control injected with *egfp* only. In summary, there was no effect on the melanoblast migration on the yolk sac and the *hirame* phenotype was not rescued when we injected *yap* mRNA exclusively into the yolk sac.

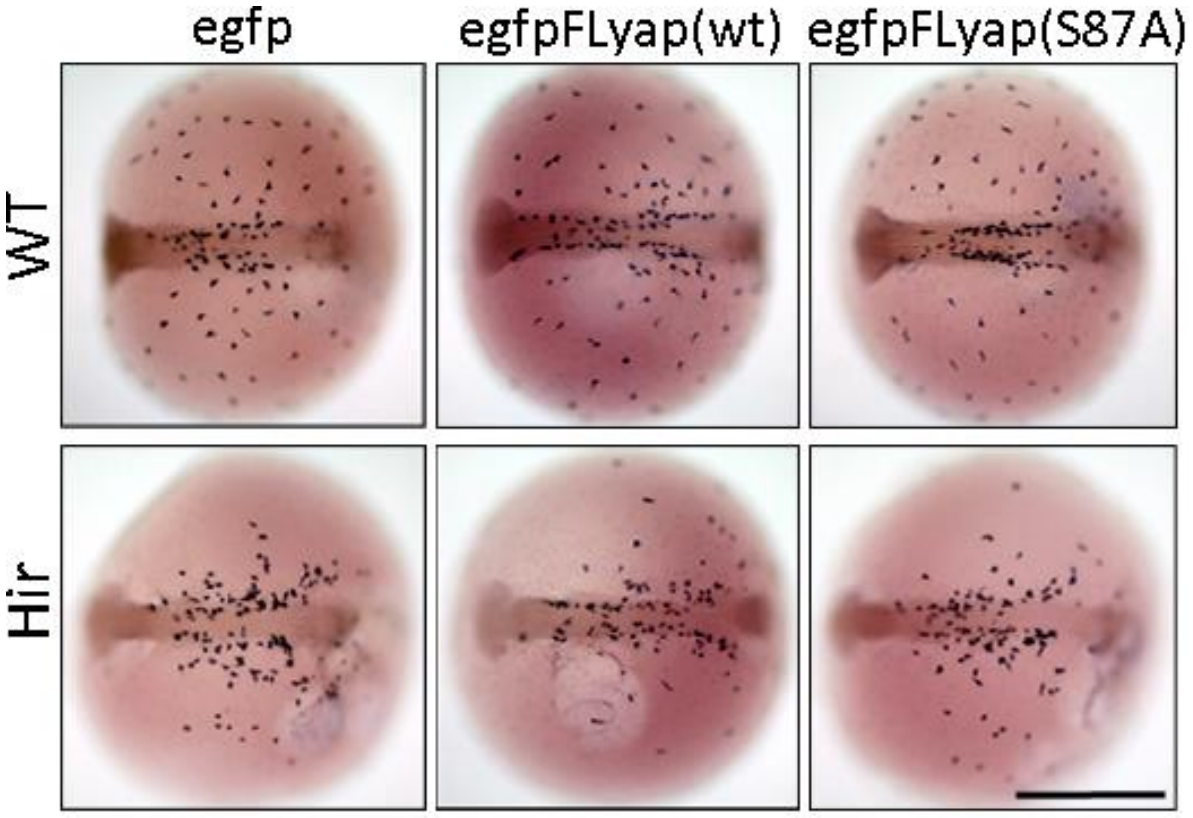

Figure 4.12: *egfp*, *egfp*FL*yap*(wt) and *egfp*FL*yap*(S87A) mRNA injection into the yolk sac does not rescue hirame and/or increase the melanocyte population in wild type embryos

Dct ISH was carried out on st. 22 embryos after injection of *egfp*, *egfp*FL*yap*(wt) and *egfp*FL*yap*(S87A) mRNA directly into the yolk sac of one cell stage embryos. This visualised the melanoblast pattern within the body and on yolk the sac of *hirame* mutants and wild type sibling. Wild type siblings injected with *egfp*FL*yap*(wt) (n=22) and *egfp*FL*yap*(S87A) (n=27) mimicked the normal melanoblast pattern as siblings injected with negative control mRNA *egfp* (n=28). The same takes effect in *hirame* embryos when injected with either *egfp*FL*yap*(wt) (n=5) or *egfp*FL*yap*(S87A) (n=4) as they remained the melanoblast patterning defect comparable to the negative control section of *egfp* (n=4) injectants. Scale = 500µm

Manual cell counts of *Dct* positive melanoblasts were carried to quantify cell numbers within the body and on the yolk sac of each mRNA group (Graph 4.2.). Graph 4.2 represents cell counts in which the three left groupings represent wild type genotypes in the body, on the yolk sac and total numbers, whereas the three right units signify *hirame* in those same classes. Each section comprises

RNA injections with *egfp*, *egfp*FL*yap*(wt) and *egfp*FL*yap*(S87A) and are evaluated in regards to melanocyte numbers respectively. While we could not detect any obvious phenotypical difference in melanoblast distribution in wild type embryos injected with *yap* fusion RNA, there was a statistical significant decrease in melanoblast numbers on the yolk sac of embryos injected with *egfp*FL*yap*(S87A) compared to the *egfp* negative control injection ($p<0.001$, 2T-test). Similar phenotypical and statistical results were obtained for *hirame* embryos. Again, we could not observe any phenotypical rescue (as described above), but *Dct*$^{+}$ cell quantifications revealed significant changes. Melanocyte numbers on the yolk sac of *egfp*FL *yap*(wt) injected embryos were significantly lower compared to the negative control *egfp* only. This change caused a significant decrease of total melanoblasts for *egfp*FL*yap*(wt) embryos as well ($p<0.05$). Unexpected, rather than increasing the cell number, *yap* injection into the yolk sac decreased the melanocyte number statistically in both, wild type and *hirame*. A possible explanation for the mathematical significance could be caused by low sample repetitions as no hirame mutants seemed visually rescued.

Either those changes are not visible by eye or it is an artefact of low embryo numbers in each category. The latter possibility is perhaps more likely, because phenotypically none of the *hirame* embryos seemed to be rescued.

This could mean that at least in this particular experiment YAP is not able to act non-cell autonomously to influence upper layers or maybe the assembly of extracellular matrix through the yolk syncytial layer to facilitate melanoblast migration.

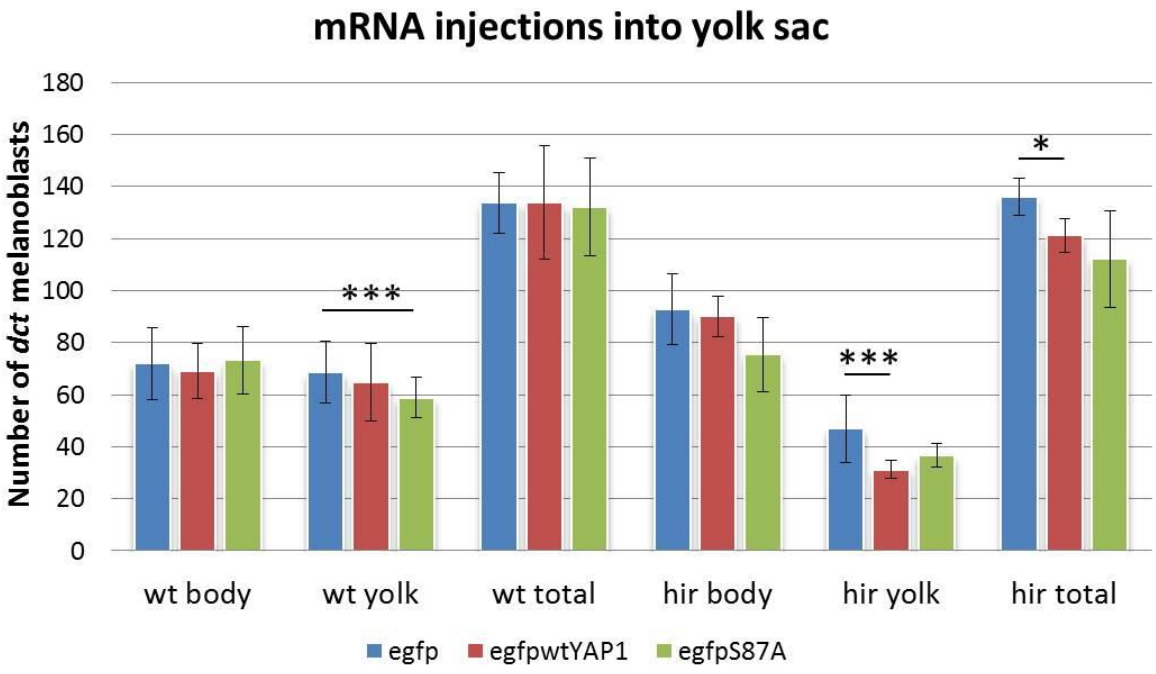

Graph 4.2: Melanoblast quantification in body and on yolk sac in st.22 embryos after *dct* ISH of egfp, egfpFLyap(wt) and egfpFLyap(S87A) injected directly into the yolk sac of embryos

Manual cell counts of *Dct* positive cells in stage 22 embryos after *egfp*, *egfp*FLyap(wt) and *egfp*FL*yap*(S87A) mRNA were carried out to assess Dct^{+} cell quantifications. Overall, yap overexpression in either form, wt or S87A did not increase melanoblast cell numbers nor their migration in wild type or *hirame* embryos. Despite the fact that no visual difference in each group was observed, a significant decline in melanoblast numbers was obtained on the yolk sac of wild type embryos injected with egfpFLS87A and on the yolk sac of *hirame* embryos injected with egfpFLyap(wt). The latter resulted in decreased total numbers as well. All data are means ± SEM. 2-Sample-t-test: *p<0.05, **p<0.01 or ***p<0.001 .

After we have demonstrated that our fusion protein is functional *in vivo* and rescues the *hirame* phenotype, we wanted to test if it also retained eGFP fluorescence properties, which we intended to do with a promoter yielding widespread tissue expression.

4.2.4 Making the positive control vector CMV:eGFP-YAP(wt/S87A)

To validate the functionality and capability of our fusion protein *egfp*FL*yap*(wt/S87A), I now wanted to evaluate whether the fused eGFP is able to emit a fluorescent signal *in vivo.* To proof that, I created a CMV:eGFP-YAP(wt/S87A) construct, in which the human cytomegalovirus (CMV) immediate early enhancer and promoter can drive its target gene expression. The human cytomegalovirus (CMV) is a member of the herpesvirus superfamily and causes different diseases including encephalitis, gastrointestinal diseases, pneumonitis, hepatitis, and retinitis (Mella-Alvarado et al. 2013). The immediate early gene of the human cytomegalovirus is essential to the viral replication in its host. This constitutively active promoter is commonly used for transient expression of transgenes by *in vitro* and *in vivo* research in mouse, stem cell, Zebrafish and Medaka fish, but less common for stable transgenesis approaches (Barrow et al. 2006; Hasegawa et al. 2009; Iwai et al. 2009; Langenau et al. 2005). However, in an attempt to validate the spatial and temporal activity of the cytomegalovirus in Zebrafish transgenesis Mella-Alvardo et al. discovered in 2013 that the CMV:eGFP construct was expressed in a tissue-restricted manner. These expression sites corresponded to targeted sites resulting from CMV infections usually found in humans such as the spinal cord, olfactory organs, central nervous system, retina, skeletal muscles and hepatocytes (Mella-Alvarado et al. 2013). The strength and nearly ubiquitous expression profile gave us enough confidence to use the CMV promoter as a widespread transcriptional driving element. The CMV:eGFP-YAP(wt/S87A) constructs would also work as positive control vector in further promoter studies.

The construction of the CMV:eGFP-YAP(wt/S87A) vectors was achieved by a two-step cloning process. Again, a summary of the whole cloning process outlined in this chapter is presented in Figure 4.5. Firstly, the fusion sequence either of clone 2 pCS2_*egfp*FL*yap*(wt) or clone 16 pCS2_*egfp*FL*yap*(S87A) described in Chapter 4.2.1 (Figure 4.4) was extracted in a double digest with SpeI and SnaBI restriction endonucleases. At the same time a pEGFP-C3 (Figure 2.4) plasmid was double-digested with NheI and SmaI to obtain the backbone including the CMV promoter sequence upstream of the cut. This resulted in a loading pattern (Figure 4.13 A), where digested pCS2 constructs end up with 4049bp backbones and 2139bp *egfp*FL*yap* inserts and the pEGFP-C3 plasmid with a desired 3936bp backbone containing the CMV promoter and an excised 791bp *egfp* sequence. After DNA extraction, the appropriate fragments were ligated together, whereby the backbone underwent dephosporylation to prevent self-ligation. However, this step can be ignored in this case because each double digest produces non-compatible ends, which cannot be ligated to each other. The straightforward ligation was possible, because NheI and SpeI restriction endonucleases produce compatible cohesive ends for each other that can be ligated together. SmaI and SnaBI restriction enzymes both cut blunt end and can therefore be bound to each other. The ligation product was transformed into E.coli DH5α, plated out onto an antibiotic resistant medium and individual colonies were tested the correct plasmid and insert orientation. All colonies picked and tested with a double digest of SnaBI and EcoRI were found to be positive and inserts were rightly placed without forming concatamers. Therefore one of each CMV:eGFP-YAP(wt) and CMV:eGFP-YAP(S87A) was amplified and purified as Midi-preps. The final map of the CMV:eGFP-YAP(wt/S87A) is shown in Figure 4.13 B.

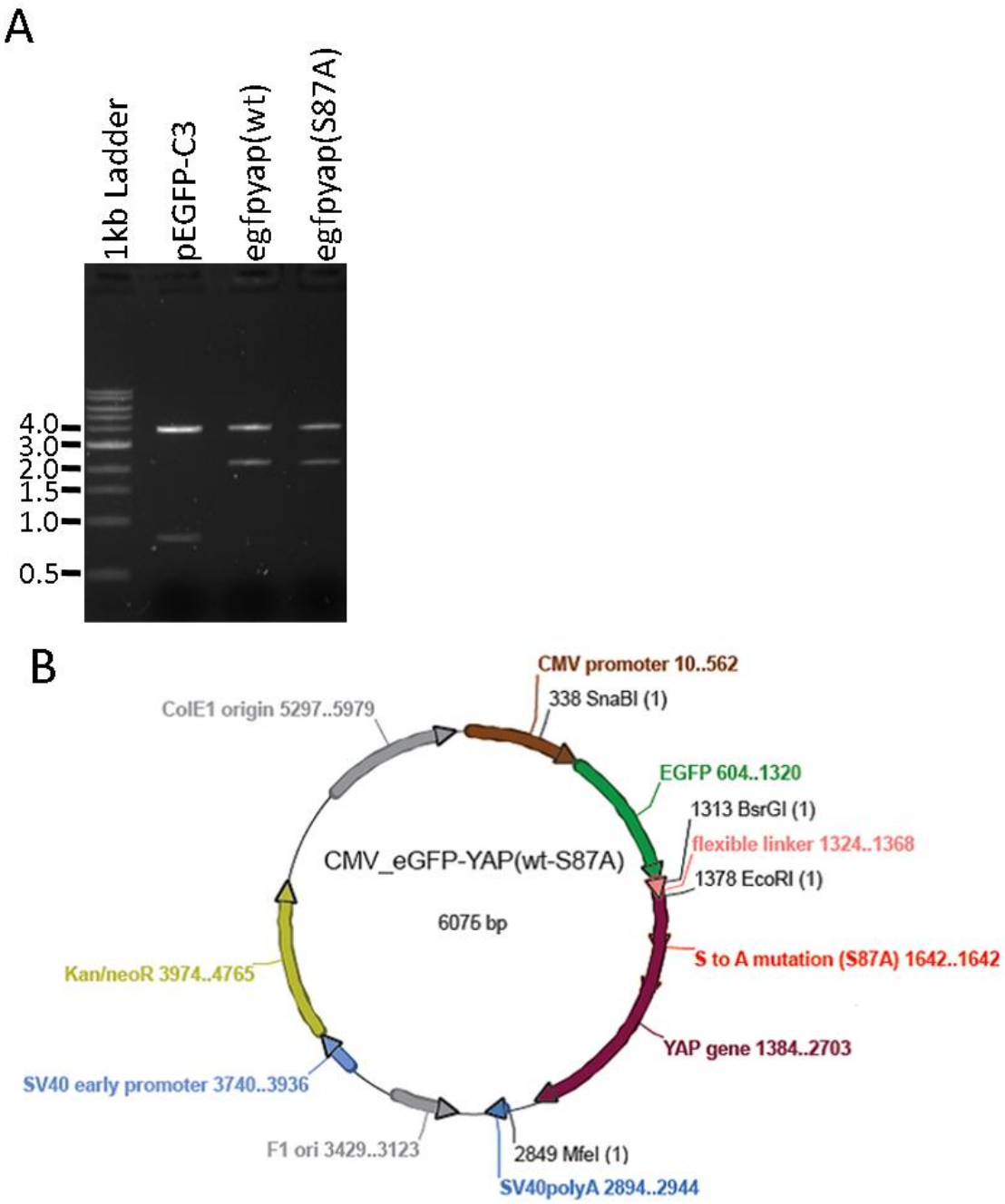

Figure 4.13: Plasmid backbone and DNA inserts on agarose gel (left) and complete map of CMV:eGFP-YAP(wt/S87A) construct

A) Agarose gel showing DNA digests of pEGFP-C3 (third lane), pCS2_egfpFLyap(wt) (fourth lane) and pCS2_egfpFLyap(S87A) (fifth lane), an intermediate step of the cloning process. Digestion reaction produces the 4049bp backbone containing the CMV promoter and the 2139bp *egfp*FL*yap* DNA fusion inserts for subsequent ligation step.
B) Representative complete map of CMV:eGFP-YAP(wt/S87A) showing the CMV promoter (brown) driving EGFP (green), flexible linker (pink) and YAP together as fusion protein. Other regulatory elements of the plasmid are the simian virus SV40 polyA signal (blue) for termination of transcription, F1 bacteriophage origin (grey) for DNA replication of viral strand synthesis and termination allowing synthesis of single-stranded DNA and ColE1 origin (grey) for double-stranded bacteria vector replication. SV40 early promoter driving expression of selectable marker kanamycin resistance gene in *E.coli*.

To test the construct, I injected both plasmids as 15ng/µl working solution in a volume of 1-2nl estimated to contain 15-30pg total DNA. Out of 39 embryos injected with CMV:eGFP-YAP(wt) 18 individuals survived and could be examined. In those chimeras eGFP was expressed in various cell types such as retinal and muscle but mainly in epithelial cells (data not shown). The intracellular fluorescent molecules could be seen within the nucleus and cytoplasm, whereas the nuclear signal was slightly stronger than the surrounding cytoplasm in epithelial cells on the body or yolk sac. When injecting the CMV:eGFP-YAP(S87A) construct, out of 38 embryos 22 survived and the transgene expression pattern could be analysed. The majority of cells identified expressing eGFP were again body and yolk sac epithelial cells (data not shown). This time the nucleus exhibited a much stronger nuclear signal than the cytoplasm, which was only faintly detectable by visual observation under the microscope. I also detected a high number of circled shaped GFP conclusions and aggregates in unknown cell types within the body. Those aggregates disappeared one by one after 3 dpf leaving no visual trace of enhanced green fluorescent protein behind. From this injection experiment we concluded that the egfpFLyap(wt/S87A) sequence fusion is capable of folding into a secondary protein structure able to emit green fluorescence and could therefore be used for subsequent studies . Table 4.4 summarises this short study.

Table 4.4: Summary of CMV:eGFP-YAP(wt/S87A) plasmid injection into one-cell stage embryos to verify the eGFP signal of YAP fusion protein in vivo to confirm its functionality

Injected construct	Embryo survival/injected ratio	Fluorescence pattern observed
CMV:eGFP-YAP(wt)	18/39	Medium nuclear + weak cytoplasmic fluorescence mainly in small epithelial cells on body + large epithelial cell on yolk sac; other cell types include retinal optic cup epithelial and internal muscle cells
CMV:eGFP-YAP(S87A)	22/38	Strong nuclear + very weak cytoplasmic fluorescence only in epithelial cell on body and yolk sac observed; mainly GFP aggregates detected seemingly in and on the body which disappear after 3 dpf

4.2.5 Designing the overexpression construct *Dct*:eGFP-YAP(wt/S87A)

Our final goal of this chapter was to overexpress both wild type and mutated activated versions of *yap* in melanocytes. This should yield insights into the cell specific autonomous role of YAP within the melanocyte lineage by showing whether *yap* can rescue melanocyte migration in a cell-autonomous fashion in *hirame* embryos. To establish this construct, I again decided to use a classic subcloning strategy. All steps are depicted within the summary Figure 4.5, in which the *egfp* and *yap*(wt or S87A) sequence including the flexible linker sequence connecting both genes were inserted together into the *Dct*:eGFP-1 destination vector created in chapter 3.

In detail, I tried to avoid PCR amplification of the egfpFLyap(wt/S87A) fusion gene in pCS2 from chapter 4.2.1 as I was sure that this sequence is exactly as required. Therefore, I aimed for a cloning strategy using restriction endonucleases. In general, PCR-based cloning carries a much higher risk for mutation than restriction enzyme based cloning. DNA replication by PCR has error rates that range from roughly 1 per 500bp to 1 per 10 million base pair depending on the polymerase used. Because of this, no matter which *taq* polymerase you use, it is important that you sequence the final product (Addgene 2014), which is more time consuming.

I carried out a two-step cloning process in which I digested out the *egfp* gene with SpeI and BsrGI from Clone 2 pCS2_*egfp*FLyap(wt) and clone 16 pCS2_egfpFL(S87A) (section 4.2.1). In parallel I isolated the FLyap(wt/S87A) sequence from both CMV:eGFP-YAP (section 4.2.4) constructs with the restriction enzymes BsrGI and MfeI. The destination vector *Dct*:eGFP was cut with SpeI and MfeI, extracting the *egfp* sequence and opening up the vector downstream of the Medaka *dopachrome tautomerase* vector (*Dct*). In this way, *egfp*-BsrGI can be re-ligated to BsrGI-FL-*yap*(wt/S87A) and SpeI upstream of *egfp*-BsrGI can get re-ligated to SpeI within the destination vector. Also, MfeI downstream of BsrGI-FL-*yap*(wt/S87A) can be ligated to the compatible ends of the MfeI digest in the open *Dct* promoter backbone. This digest had to be done in this way, because the destination vector *Dct*:eGFP itself contained two BsrGI restriction enzymes sites, one in *egfp* and the other one within the promoter sequence itself, which meant a straightforward insertion of the FL*yap*(wt/S87A) sequence of either plasmid was not possible. Because the backbone was cut with two different restriction endonucleases producing non-compatible cohesive ends, it did not need further alkaline phosphatase treatment to prevent self-ligation. Following the digestion reaction, all desired fragments were extracted from the gel and purified. Therefore the ligation reaction contained one backbone *Dct*-SpeI-MfeI and two inserts, SpeI-*egfp*-BsrGI and BsrGI-FL-*yap*(wt/S87A)-MfeI.

10 colonies of each version of yap were screened with a triple restriction digestion of ClaI, SpeI and MfeI to identify the correct insert orientation and reveal any double insertions. Briefly, if both inserts were ligated once and in the correct orientation we would see a 6860bp, 1479bp and 779bp band. If

only *egfp* was inserted the SpeI enzyme would linearise the fragment leaving a 7639bp band. If Fl-yap was only inserted we would obtain a 6917bp and 1479bp band. Contamination in our backbone with undigested *Dct*:eGFP-1 plasmid it would result in a 6874bp and 913bp double band when screening such colonies. I screened 10 colonies from each ligation containing either the wild type or activated form of *yap*. In both cases I got 5 positive colonies containing both inserts in the correct orientation evaluated from its digestion pattern. The remaining 10 colonies were proven to be the original undigested *Dct*:eGFP-1 backbone with its specific two 6874bp and 913bp bands, indistinguishable from the backbone control, which was linearised only. I decided to purify Clone 3 of *Dct*:eGFP-YAP(wt) and Clone 5 of *Dct*:eGFP-YAP(S87A) and use those two constructs for further studies. The map of *Dct*:eGFP-YAP(wt/S87A) is shown in Figure 4.14.

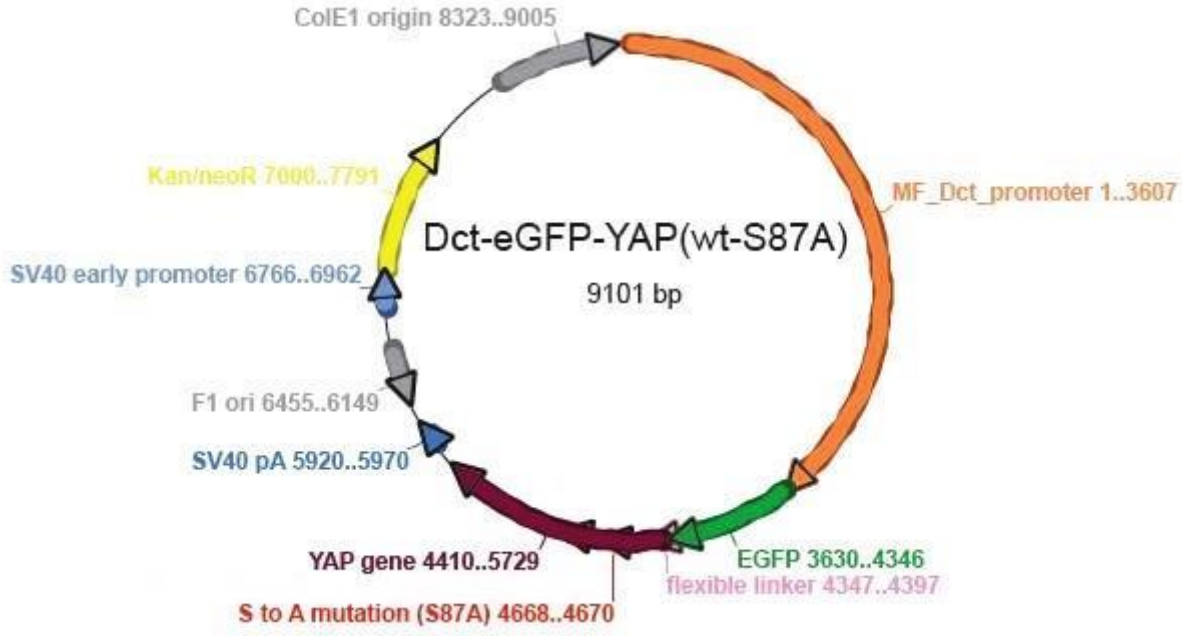

Figure 4.14: Representative map of Medaka *Dct*:eGFP-YAP(wt/S87A)

Dct:eGFP-YAP(wt/S87A) plasmid featuring the fusion protein of Medaka YAP wild type and the activated version S87A) with fluorescence reporter EGFP under the control of the Medaka melanocyte lineage specific *dopachrome tautomerase* promoter. Other regulatory elements of the plasmid are the simian virus SV40 polyA signal (blue) for termination of transcription, F1 bacteriophage origin (grey) for DNA replication of viral strand synthesis and termination allowing synthesis of single-stranded DNA and ColE1 origin (grey) for double-stranded bacteria vector replication. SV40 early promoter driving expression of selectable marker kanamycin resistance gene in *E.coli*.

With the final plasmid, we decided to establish transgenic lines in which cell-autonomy of wild type and activated YAP within the melanocyte lineage can be assessed.

4.2.6 Establishing and screening *Dct*:eGFPwt and *Dct*:egfpS87A Medaka transgenic lines

We attempted to establish transgenic lines overexpressing the wild type form of Medaka *yap* and an activated version. Again, the mutated form of *yap* leads to an serine-to-alanine amino acid exchange hindering cytoplasmic YAP protein phosphorylation by Lats1 and degradation though 14-3-3 proteins; therefore increasing nuclear co-transcriptional activity of Hippo pathway downstream target genes. In chapter 3 we have shown that the Medaka *dopachrome tautomerase* (*Dct*) promoter drives reporter genes such as eGFP exclusively in the melanocyte neural crest lineage without any ectopic expression in any other cell type. Furthermore, in chapter 4 section 4.2.2 we have shown that the fusion proteins of *egfp*FL*yap*(wt) and *egfp*FL*yap*(S87A) translate into functional proteins capable of rescuing the *hirame* mutant melanocyte phenotype by stage 22 (1d 14h). On account of those two substantial experimental findings, we were confident in using the created *Dct*:eGFP-YAP(wt) and *Dct*:eGFP-YAP(S87A) transgene constructs (section 4.2.6) to establish our transgenic lines.
The plasmid backbone was first linearised with BglI to increase the chance of sequence integration into the genome as we did before for the Tg(*Dct*:eGFP) lines. This was done because, if not linearised at a specific point away from our fusion gene and promoter region, endogenous DNA nucleases may cleave within the region of our transgene. The cleaned construct was then injected as 15ng/µl working solution (total amount of 15-30pg DNA) into the cytoplasm of one-cell stage embryos obtained by crossing Cab heterozygous carrier for the *hirame* allele. All results are tabulated in Table 4.5 below. In total 1641 embryos were injected for *Dct*:eGFP-YAP(wt) from which 441 embryos survived the first 48hpf. This high death rate of 73% is comparable with the 71% death rate when establishing the *Dct*:eGFP transgenic lines. Surviving embryos showed no clear melanocyte eGFP pattern comparable to *Dct*:eGFP transgenic lines, but some did show green aggregates on and within the body (data not shown) comparable to the CMV:eGFP-YAP(S87A) transient expressions (section 4.2.4) which seem to disappear after 2 dpf and/or prolonged excitation. As the origin of this signal is not clear, I selected 99 embryos out of 441 survivals expressing any eGFP signals and grew them up as chimeras out of which 98 larvae were transferred into the facility system. 75 chimeric fertile adults were screened after 4-5months from which only 1 founder visibly expressed enhanced green fluorescent protein within the melanocyte lineage. Two months after the initial fluorescence screening the same pool of F0 chimeras was taken and 47 adults were screened for offspring harbouring the *Dct*:eGFP-YAP(wt) transgene by targeted polymerase chain reaction (PCR). This genotyping approach revealed another 6 founders transmitting the transgene to their F1 progeny. However, the actual eGFP signal was not visually detectable by microscopy.

On the other hand when establishing the *Dct*:eGFP-YAP(S87A) line, I injected 1791 embryos of which 293 survived resembling a slightly higher death rate than previously at 83.6%. The minority of surviving embryos seem to express or accumulate eGFP in the same aggregate-like fashion as described in CMV:egfpFLyap(S87A) transient expression. Here however it lasted for less than 2 dpf before disappearing. Because of this peculiar expression profile, I decided to grow up all surviving embryos, from which 97 survived. I decided to immediately genotype the pools of progeny of F0 adults and managed to do so in 77 adults. At the end 3 founders were positive for the *Dct*:eGFP-YAP(S87A) transgene, but did not show any sign of eGFP within the melanocyte lineage. However, I did observe a small amount of tiny GFP aggregates appearing only around 1d 7h up to 1d 14h in a fraction of offspring in one founder (data not shown). This was however difficult to visualise and evaluate further, because the signal seemed to photobleach rapidly.

All offspring of founders with the *Dct*:eGFP-YAP(wt) and *Dct*:eGFP-YAP(S87A) were grown up to F1 generation. F1 adults must be genotyped again, backcrossed into heterozygous Cab *hirame* allele carriers and offspring grown up. The pool of genotyped F2 adults will need to be analysed in future for any yap cell-autonomy within the melanocyte lineage and evaluated for rescue and restoration of *hirame* melanoblast and melanocyte patterning.

Table 4.5: Summary of the F0 Medaka **fish *Dct*:eGFP-YAP(wt/S87A) generation from microinjection until the finding of founders carrying the transgene**

Experimental process in G0 founder generation	Chimeras of *Dct*:egfp-yap(wt)	Chimeras of *Dct*:egfp-yap(S87A)
Injected embryos	1641	1791
Survival after 2dpi	441	293
Grown up to 8 dpf	99 (eGFP selected)	293 (all taken)
Survived 1st months	98	97
eGFP screened founder: founders/total screened	1/75	-
PCR screened founders: founders/total screened	6/47	3/77

4.3 Discussion

4.3.1 Testing fusion protein functionality via *hirame* MC pattern rescue after mRNA injection into one cell stage

In section 4.2.1 we designed a fusion protein of Medaka *yap* and an *egfp* reporter gene, which we intended to test and validate by mRNA injections into *hirame* 1-cell-stage embryos.
It is essential for any kind of fusion to maintain the open reading frame, which was achieved by deleting the stop codon from *egfp* and adding additional nucleotides to keep both genes in-frame. The connection of those two genes was done by designing a fragment of *egfp* via PCR amplification which included 5' and 3' endonuclease recognition sites plus an glycine-serine linker $(GGGGS)_n$ sequence on its 3' end. Subsequently this fragment could be ligated onto the pCS2_yap(wt/S87A) backbone without interfering with the reading frame. We managed to obtain high quality capped mRNA from both constructs, clone 2 pCS2_egfpFLyap(wt) and clone 16 pCS2_egfpFL(S87A), which was in the range of 1.985-2.053 for $A_{260/280}$ and 2.216-2.261 for $A_{250/230.}$ This indicated that our mRNA was of very high standard and purity as values around 2.0 for $A_{260/280}$ and 2.0-2.2 for $A_{260/230}$ are normally classified as "pure" RNA samples. Lower ratios can be due to contaminations in our case such as protein, phenol, EDTA or even change of pH (Nano Drop Technologies website 2007). Once high-purity mRNA was obtained, I injected around 200pg into the cytoplasm of 1-cell-stage embryos of heterozygous $Cab^{j50\text{-}20C}$.
As described in the previous chapter 3 section 3.2.2 *hirame* develops a specific melanoblast pattern, in which, as early as stage 20 (4 somites, 1d7h30min), some individual melanoblasts are not able to move away from the lateral body axis and onto the yolk sac. Because the *Dct* pattern is a reliable criterion for distinguishing *hirame* from wild type embryos throughout embryonic development, I decided to evaluate the functionality and effect of the fusion protein by analysing *Dct* after *in situ* hybridisation. The analysis of transient mRNA injections itself was aimed at early stages up to 1.5 dpf, as this is a time window where mRNA seem to be stable (Wittbrodt et al. 2002). Embryos identified genetically as *hirame* mutants injected with either *egfp*FL*yap*(wt) or *egfp*FL*yap*(S87A) fusion constructs, all seemed phenotypically like wild type embryos at stage 22, revealing a normal melanocyte pattern (Figure 4.7) compared to the negative control *egfp* RNA individuals.
Dct cell quantifications confirmed that melonoblasts in *hirame* mutants were indeed able to migrate away from the body axis onto the yolk sac area in similar quantities to its wild type siblings; supporting the notion that ubiquitous restoration of functional YAP protein to wild-type levels rescues the *hirame* phenotype. This confirmed that our designed fusion construct yields in functional YAP protein, which is able to rescue *hirame in vivo* and can therefore be used for further studies.

4.3.2 Analysis of YAP´s non-cell autonomous function within the *hirame* yolk sac layer on melanocyte migration

Our overall goal was to test the existence of a non-cell autonomous role for YAP to influence the migration of the yolk sac residing melanoblast population by injecting functional mRNA of *egfp, egfp*FL*yap*(wt) or *egfp*FL*yap*(S87A) directly into the yolk sac.

4.3.2.1 Characterisation of yolk sac membrane nuclei

Our approach of direct yolk sac injection was supported by previous observations we made in neutral red stained resin sections of wild type and *hirame* embryos. In *hirame* embryos, a set of mainly yolk membrane cells exhibited fragmented nuclei next to microscopically normal oval shaped nuclei (Figure 4.8). Such interesting finding led us wonder if those dying cells, either necrotic or apoptotic, may be one of the contributing factors to the melanocyte migration defect on the yolk sac. Our hypothesis was that those dying membrane cells could not contribute to environmental stability required for successful melanoblast movement. However, at that time we had very little understanding of Medaka yolk sac anatomy at stage 21 during embryogenesis. Numerous studies have described developmental processes occurring earlier during gastrulation. Scientists have documented in great detail on how the blastoderm engulfs the yolk sac during epiboly and how the hypoblast involutes and extends underneath the epiblast to set up the basic plan for the developing embryo (described in Introduction chapter 1 section 1.2). However, to our knowledge there are no existing studies describing which layers remain after gastrulation and neurulation. There must be at least two layers, the yolk syncytial and the enveloping layer. We wanted to solve the anatomical structure of the yolk sac and characterise those fragmented nuclei in *hirame*. To do so, we performed transmission electron microscopy in st. 21 wild type and *hirame* embryos. Our results conclude that the Medaka yolk sac consists of three layers: the most inner yolk syncytial, the middle epidermal and the outermost enveloping layer. We observed nuclei in all three layers. One of the questions we wanted to answer was if those fragmented nuclei in *hirame* are necrotic or apoptotic cells. Apoptosis is the programmed active cell death, a fundamental physiological process during development as it tightly regulates the number of cells within the whole organism. This controlled internal death is mediated by an intracellular proteolytic signalling where enzymes such as caspases are involved (Alberts et al. 2002). In marked contrast, necrosis is an uncontrolled cell death in which dying cells swell and burst for instance after viral infections (Pierce 2012). During that process, they spill their contents over neighbouring cells potentially triggering a local inflammatory response characterised

by, for instance, histamine producing white blood cells causing redness and pain (Alberts et al. 2002). Both processes apoptosis and necrosis are characteristically different. However, the initiation of each can have overlapping origin. Indeed, numerous *in vitro* culture studies have shown that a variety of events, which cause necrosis, can also lead to apoptosis. For example, severe insults to cells with injurious agents lead to necrosis whereas milder drug administration caused apoptosis (Lennon et al. 1991). This opens up the possibility that we could potentially observe necrotic and apoptotic cells in *hirame* embryos. Our TEM data revealed that in *hirame*, a large number of nuclei were irregular shaped indicating cell shrinkage compared to smooth-like oval nuclei in wild type siblings. Cell shrinkage is accompanied by chromatin condensation (pyknosis) which alters the form of the nucleus. In addition, we were able to find characteristic black inclusions within the nuclei in the form of dense chromatin. This particular example was found within the mesodermal tissue leading towards the yolk sac membrane just beyond the somite structures. More frequently, we would observe nuclear remnants retained in apoptotic bodies of varying size. These apoptotic bodies retained cell organelles such as mitochondria and were separated as small entities from each other. It presents a case for apoptosis in which the cell undergoes controlled disassembling into multiple pieces, each retaining cell organelles to control its further degradation (Corcoran et al. 1994). However, we could not determine in which layer those fragmented nuclei are located, because of our small sample size. Taken together, we conclude that those fragmented nuclei found in the yolk sac membrane would be either epithelial or yolk syncytial layer cells that had undergone programmed cell death.

Those findings strengthened our experimental approach of injecting *yap* mRNA directly into the yolk sac to test if it could rescue apoptosis and therefore re-installing melanoblast migration within those layers.

4.3.2.2 Yolk sac injection to test non-cell autonomous rescue of hirame melanoblast migration defect

To test a non-cell autonomous function for YAP within the yolk membrane, we needed to verify that cytoplasmic streaming as seen in Zebrafish does not occur in Medaka embryos (Detrich et al. 1998). Our additional tests confirmed that during Medaka embryogenesis yolk cytoplasmic streaming towards the blastoderm does not occur. It seems that a physical boundary appears between the embryonic cell and the yolk sac as soon as the egg is fertilised. This membranous separation separates injected solutions into the yolk sac from the embryo (Figure 4.11). With this knowledge in mind, we carried out injection of synthesised capped mRNA from *egfp*FL*yap*(wt), *egfp*FL*yap*(S87A) and a negative control *egfp* into the *yolk sac* and performed *Dct in situ* hybridisation on those st. 22

embryos. Surprisingly, injection of *yap* mRNA into the yolk sac did not alter the melanoblast pattern phenotypically in the wild type nor *hirame* embryos. However manual cell counts revealed statistically significant differences in terms of a decrease in melanoblast numbers on the yolk sac of embryos injected with *egfp*FL*yap*(S87A) compared to wild type siblings ($p<0.001$, 2T-test). It also revealed a profound decrease of melanocyte numbers on the yolk sac of *egfp*FL *yap*(wt) injected embryos and consequently a decline in total numbers in egfpFLyap(wt) embryos compared to the negative control *egfp* only. Although those quantifications revealed a significant difference in those categories, they are likely to be caused by deviations originating from variations of small sample sizes. Taken together, there was no biologically striking difference and phenotypical rescue of yolk sac melanoblast migration in *hirame* embryos, which could indicate that YAP does not exhibit any function within the yolk syncytial layer and therefore does not act non-cell autonomously towards melanoblast migration. However, our experimental approach has a major caveat. We are not certain if the injected mRNA was able to enter the yolk syncytial or other yolk sac layers in the first place which would be a fundamental requirement for translational processes and YAP functionality. One way would be to perform *in situ* hybridisation for egfp and microscopically dissect the pattern. However, the yolk sac cell layers are too small to distinguish. Therefore, another approach would be to test the mRNA integrity by quantitative real-time PCR. What we might be able to do is separating pieces of yolk sac at around stage 22 and isolate mRNA. We could then quantify and test for common YAP protein downstream target genes such as *itgb2* or *cyclinD* (Zhao et al. 2007; Hao et al. 2008), which would indicate activity of YAP within the yolk sac membrane.

Our results obtained in this experimental section could also explain the rescue of cell migration after mRNA injection into the cytoplasm one-cell embryos . As demonstrated with rhodamine dextran injected RNA, DNA or dye into the cytoplasm of the one cell embryo did not mix with the yolk sac, but distributed within the membranous layers surrounding the yolk sac. This could mean, that the rescue of yolk sac melanocyte migration might have occurred through rescuing the yolk epidermal layer configuration, as functional YAP protein was abundant throughout the whole body including the yolk sac epidermis. Specifically, YAP might have re-installed an extracellular environment suitable and required for successful cell movement. For instance, components such as laminins, fibronectin, collagen I and collagen IV, proteoglycans, vitronectins and hyalurons have all been shown to play important roles during neural crest migration (Duband & Thiery 1987; Sternberg & Kimber 1986; Trainor 2013)(detailed descriptions in introduction section 1.6.3). Supporting data comes from Porazinski`s thesis, in which he described that already as early as st.18 (26 hpf) fibronectin assembly was perturbed in *hirame* embryos. It seemed *hirame* formed either longer fibronectin fibrils or a shorter punctuated fibronectin pattern on the basal surface of the epithelia and mesenchyme

compared to the much finer fibrilious mesh found in wild type siblings (Porazinski 2013). Strikingly, when he performed knockdown experiments of 70kDa fibronectin, he could mimic the cuvier´s duct migration defect he observed in late stage *hirame* embryos, strongly suggesting that a defect in extracellular fibronectin polymerisation compromises directed cell migration through a non-cell autonomous role of YAP.

Taking his data into account, the rescue we have achieved might imply that extracellular matrix components such as fibronectin have been restored and guidance of neural crest cells re-installed. To test this possibility, we could perform whole-mount immunohistochemistry with an anti-fibronectin antibody to assess its polymerisation status before and after the *hirame* rescue. To widen our analysis, we could include other ECM components such as laminins, collagens and vitronectins to assess their functional status in our mutants. Knocking down individual ECM components via oligo-morpholino injection would if it could mimic the melanoblast migration defect on the yolk sac and confirm YAP's non-cell autonomous role.

4.3.3 Undetectable eGFP expression in newly established *Dct*:eGFP-YAP(wt/S87A) transgenic lines

4.3.3.1 Non-detectable eGFP levels as a result of intracellular toxicity levels

To evaluate YAP´s cell autonomy within the melanocyte lineage we attempted transgenesis with our designed constructs *Dct*:eGFP-YAP(wt/S87A) overexpressing either the wild type version or the activated form of Medaka *yap* under the Medaka *dopachrome tautomerase* (*Dct*) promoter. We expected a melanocyte specific expression pattern of the fusion protein with no ectopic cell expression elsewhere, as this was achieved in 6 out of 8 transgenic *Dct*:eGFP lines. In addition, we predicted a nuclear/cytoplasmic eGFP distribution similar to the results obtained from the CMV:eGFP-YAP transient expressions. As a reminder, wild type *yap* fusion resulted in weak cytoplasmic and moderate nuclear eGFP accumulation and the *yap* S87A version exhibited very weak cytoplasmic retention plus very strong nuclear presence. In addition, we expected a transgenesis frequency of around 23% similar to the obtained *Dct*:egfp transgenic line. With some difficulties I managed to obtain 7 founders within the *Dct*:eGFP-YAP(wt) population, in which one expressed eGFP strongly within the melanocyte lineage of some offspring, while 6 others were positively identified by PCR genotyping, yet fluorescence was not detectable in any offspring after 2 dpf. The second line produced using linear DNA injections of a *Dct*:eGFP-YAP(S87A) construct gave rise to 3 chimeric founders, only identifiable through genomic PCR genotyping approaches. Again, no fluorescent molecules could be detected after 2 dpf in any of the offspring descended from those parents. All

progeny of the founders identified were therefore grown up as F1 generation and will need in depth analysis once an F2 generation has been established from these.

Only in one *Dct*:eGFP-YAP(S87A) founder's progeny I could see weak but distinct tiny green fluorescent GFp aggregates between stage 20 and 22 (1d 7h to 1d 14h). It seemed that those fragments were sensitive to photobleaching and were undetectable after that period, making it difficult to image (mention in results section). The areas where conclusions of intracellular eGFP molecules occurred was only seen once before in the case of transient CMV:eGFP-YAP(S87A) DNA injection (section 4.2.4). One possibility is that this could have been a result of toxicity caused by high transgene levels. The strong human cytomegalovirus (CMV) promoter regulatory region drives constitutive protein expression levels as high as 1 mg/L in COS cells. For less potent cell lines, protein levels are typically ~0.1 mg/L (Sigma-Aldrich website 2014). Most basal promoters have fairly consistent strengths across different cell types, but the CMV promoter can vary considerably from cell type to cell type (Qin et al. 2010). Furthermore, the *dopachrome tautomerase* (*Dct*) promoter used in to transcribe *yap* fusion proteins is also thought to be a strong promoter in driving high levels of *Dct* expression in melanocytes (Kelsh unpubl. data). Therefore, strong promoter activity might explain the ectopic GFP aggregates due to toxic levels of *yap*S87A, which seem to either result in protein missfolding and subsequent damage of individual cells.

Overall, we could not clearly identify which cell type transiently emitted eGFP signals, but we expected from the start, that our transgene would be expressed within the melanocyte lineage. Therefore, one possibility could be that committed melanoblasts might have been affected and underwent apoptosis once they have acquired a toxic level of transgene. However, this would mean that embryos would lack melanocytes either completely or to a high percentage before hatching stage. A comparable phenotypical example might be the kit^{b5} Zebrafish mutant, in which the majority of melanoblasts fail to leave primary sites and undergo apoptosis (Parichy et al. 1999) resulting in a dramatic loss of melanocytes throughout the body. A more dramatic example is provided by the $sox10^{-/-}$ (colourless) Zebrafish mutant lacking melanocyte differentiation, migration and survival (Kelsh & Eisen 2000; Elworthy 2003). However, in our case, I could not observe a lack of melanocytes nor melanogenesis when growing up those individual embryos exhibiting eGFP aggregating, which dismisses the idea of early melanoblast death.

4.3.3.2 Changes of eGFP signals due to transcriptional errors through silencing

Another possibility for the seemingly complete loss of green fluorescent protein in the *Dct*:eGFP-YAP(wt/S87A) transgenic lines could be through silencing mechanisms. I previously mentioned partial silencing of melanocytic clones in 2 out of 8 *Dct*:egfp transgenic lines (chapter 3), which showed an

incomplete spatial eGFP-melanocyte pattern. Plant research demonstrated that in tobacco protoplasts insertion of transgenes could lead to an expected full or incomplete patterning resulting from partially silenced transgenes. Those studies showed that DNA methylation occurs specifically in newly inserted DNA resulting in low transcription levels through partial silencing (Day 2000). In this chapter, variable gene expression levels or a complete loss of gene activity might have occurred when the *Dct*:eGFP-YAP(wt/S87A) transgene was randomly inserted into regions with close proximity to heterochromatin instead of euchromatin, the latter of which is loosely packed chromatin associated with high transcriptional activation. Heterochromatin on the other hand is thought to be closely packed, thus inaccessible to the transcriptional machinery. It is also correlated with cytosine hypermethylation and specific histone hypoacetylation (Huck-Hui & Bird 1999). This would mean our transgene is either expressed at low levels and fluorescent molecules are not present in sufficiently detectable quantities, or our transgene is completely shutdown inside an inactive region of chromatin.

In addition to silencing mechanism of transgenes inserted into non-active chomatin regions, inverted short multi-copies or polymeric DNA concatemers of repeated transgene sequences can also cause gene silencing, which is often seen in mice transgenesis. Calero-Nieto encountered a subset of previously active transgenes that became specifically silenced, which was accompanied with epigenetic changes such as increased methylation and decreased acetylation of histone H3K9. Transgenic silenced lines also experienced a loss of DNase I hypersensitive sites and lacks the ability to recruit DNA polymerase II for DNA repair (Calero-Nieto et al. 2010). A proposed role for the repeat sequences is to induce DNA–DNA interactions that lead to changes in chromatin conformation and epigenetic silencing (Matzke & Matzke 1998). Unfortunately we have not been able to test copy numbers of the transgene in our transgenic lines, which can be done by southern-blotting.

In our case 5 out of 6 for *Dct*:eGFP-YAP(wt) and 3 out of 3 for *Dct*:eGFP-YAP(S87A) founders lacked detectable levels of fluorescent signals, which would indicate that the majority of transgene insertions became silenced. This would mean that the frequency of a silencing mechanism would be very high. Unfortunately, I cannot tell how frequently silencing normally happens in a Medaka transgenesis approach. Nor I cannot make any assumptions if I might have missed silenced founders in the non-eGFP expressing screened F1 offspring when I established the previous *Dct*:egfp transgenic line (chapter 3). Even so there are studies in which unexpectedly nearly half of the insertions failed to give a full spatial pattern of the transgene (Day 2000), my feeling is that our problem of non-detectable eGFP signals might be a consequence of other errors. As future tests of the silencing hypothesis, I would propose using *in situ* hybridisation with an anti-sense *gfp* probe in the F2 generation embryos of all *Dct*:eGFP-YAP(wt) and *Dct*:eGFP-YAP(S87A) lines showing no fluorescence signal to ask whether the transgene is transcriptionally active. A more unfavourable

option would be to amplify the eGFP signal histochemical with an anti-GFP antibody. The amplification of GFP signal has been routinely done in previous Zebrafish studies and antibodies are readily available from commercial companies such as Invitrogen and CellSignalling. However, despite being able to reach an amplification amplitude by 1000, the immunohistochemical protein amplification is based on the recognition of available GFP protein antigen, which is unlikely due to the lack of any GFP signal beyond 3 dpf as in our case.

4.3.3.3 Non-detectable eGFP levels due to post-translational errors

Another possible cause of undetectable eGFP might be at the translational levels. Fusion proteins have been constructed and used successfully for subcellular function analysis in the past, yet this does not mean that a successful fusion applies for every gene fused or tagged to a reporter gene. Therefore, the order in which both genes are fused could make a difference in gene stability and/ or intracellular localisation. It is conceivable that the N-terminal eGFP protein may destabilise YAP resulting either missfolding and/or rapid degradation leading to decreased fluorescence signals. Although, we did not expect this to be a problem, because most previous publications used not only eGFP, but also fused this reporter gene N-terminally to the YAP sequence (Dong et al. 2005; Zhang et al. 2010; Liu-Chittenden et al. 2012; Zhao et al. 2011) to monitor YAP's subcellular location in mammalian *in vitro* cultures. Palmer & Freeman (2004) approached a general analysis to test if the order of reporter fusions matters. They showed that tagging the GFP C-terminally to the gene of interest results in subcellular location more in accordance with previous studies and/or bioinformatics predictions. Fusing eGFP to the N-terminus of gene, which we did in our case, resulted in less than half of the fusion proteins localising incorrectly (Palmer & Freeman 2004). This imperfection or mislocalisation is because GFP emerges first from the ribosomal subunit followed by the amino acid sequence of our protein of interest. Then, cytoplasmic chaperones prevent the amino acid sequence from folding into a three-dimensional structure unless an amino acid chain of approximately 50-300aa has emerged. Therefore, when tagging GFP N-terminally to the gene of interest, it would cause GFP to get folded first, possibly disrupting correct folding and localisation of the second protein (Hartl & Hayer-Hartl 2002). It is possible, that the YAP protein disrupted the GFP folding itself giving rise to incomplete protein expression. Tagging the *yap* gene N-terminally to eGFP remains another possibility, which we could try.

Furthermore, the protein turnover and degradation of both fused genes might be different, leading to pre-mature degradation. Enhanced GFP has been reported to have a half-life of around 26h (Corish & Tyler-Smith 1999), whereas YAP1 seems to have a much shorter half-life of 3h, as tested in cycloheximide (CHX)-human embryonic kidney (Levy et al. 2008). Others show that the half-life of

wild type YAP is over 24h, much longer than a mutated activated version of YAP which halves below 24h when treated with cycloheximide (Liu-Chittenden et al. 2012), whereas its human paralogue TAZ is shown to have a half-life of 1-2h. The protein stability of both Hippo pathway members is dependent upon cell density levels. YAP as well as TAZ seem to be more stable in low densities in which hypophosphorylation seems to accumulate and stabilise both proteins (Oren & Aylon 2013). The true half-life of the YAP protein is yet to be determined in our model organism Medaka, but in the case of a short half-life of YAP we would need to try and overcome the difference in protein half-life of those fusion partners. For instance, I could use an eGFP version, which has a short maturation time and is suitable for fusion to transcriptional factors such as YAP. In that case the company evrogen supplies TurboGFP an improved variant of the green fluorescent protein CopGFP cloned from copepod *Pontellina plumata* (Evrogen 2014).

Finally, the use of protein linkers to link proteins can also harbour issues in protein folding. I decided to use a 15 aa repetitive sequence of the glycine-and serine-rich linker $[GGGGS]_3$. The $(GGGGS)_n$ linker provides structural flexibility and improved protein stability, and its biological activity for protein fusions has been successfully demonstrated in other studies, mainly mammalian *in vitro* culture systems (Trinh et al. 2004; Delacôte et al. 2013; Ito et al. 2011). However, stable peptide linkers do not allow separation of the two fusion proteins after translation. This can cause in some cases rigid secondary structures, leading to missfolding or wrong subcellular localisation of the fusion protein. Even so, we did not anticipated this to be happening in our case, because transient expression of our fusion protein egfFLyap under the CMV promoter resulted in widely distributed eGFP signal within endothelial cells, we cannot dismiss this possibility to 100%. It might still be an explanation for those intracellular eGFP aggregates seen in the F1 generation of *Dct*:eGFP-YAP(wt/S87A) transgenics.

To overcome the likelihood for such pitfalls, researchers are increasingly utilising gene linkage systems which ultimately lead to two separate individual proteins. The expression of more than one gene bicistronically or multicistronically under the control of one promoter can be achieved by using vectors comprising the internal ribosomal entry site (IRES) or the 2A-peptide. IRES is a nucleotide sequence added between two cistrons with an approximately 100bp-spacer after the first gene, which enables co-translation of two proteins from the same RNA transcript. Initiation of translation occurs exclusively at the 5’ cap in eukaryotic mRNAs; though with an IRES sequence from HTLV-1, poliovirus or encephalomyocarditis virus (EMVC) ribosomes are recruited simultaneously at a second internal site (Jang et al. 1988; Pelletier & Sonenberg 1988). However, recent advances point out that the yield of protein from the 3’ cistron is usually much lower than from the 5’ gene due to cryptic promoters or splice sites within various IRES sequences, and at around 500bg, the sheer size of the linker can cause complications during gene comparative studies (Kozak 2005). IRES motifs are

available as an *in vitro* tool expressing antibiotics or fluorescent reporter genes bicistronic with lower intensity (Clontech Takara Bio Company 2014), but are less commonly used in *in vivo* studies as they require additional experiments and controls (Sampath & Sudipto 2010, Nikaido & Kelsh unpubl. data). In contrast, the viral 2A peptide, a multicistronic gene expression system is starting to appear in Zebrafish and Medaka research (Sampath & Sudipto 2010). The 2A peptide is a self-cleaving motif with an average length of 18-22 amino acids first isolated from the foot-and-mouth disease virus (FMDV), a member of the picornavirus family (Ryan et al. 1991). Through creation of a transgene with a single, long open reading frame, stoichiometric expression of multiple proteins either side of the 2A peptide is achieved by ribosome skipping. Ribosomes skip the synthesis of the glycyl-prolyl peptide bond at the C-terminus of the 2A peptide, leading to cleavage between the 2A peptide and its immediate downstream peptide. As a result, the 2A peptide sequence remains C-terminally on the upstream protein and a proline amino acid at the N-terminus of downstream proteins (Donnelly et al. 2001). 2A peptide sequences have been used widely in the production of Induced Pluripotent Stem Cells (iPS cells or iPSCs) (Takahashi & Yamanaka 2006; Kaji et al. 2009), in gene therapeutic studies and mice *in viv*o transgenesis (Holst et al. 2006) or in *in vitro* bioimaging techniques co-expressing fluorescent proteins to target different sub-cellular sites (Amrani et al. 2004). However to date it has not been used widely in *in vivo* studies and detailed analysis of different 2A peptides used were missing until Kim et al. (2011) addressed this issue for the first time using human cell lines, Zebrafish embryos and adult mice. They generated and compared four different 2A peptide sequences from foot-and-mouth disease virus, equine rhinitis A virus, *Thosea asigna* virus and porcine teschovirus-1, respectively, and demonstrated the highest cleavage efficiency when using the porcine teschovirus-1 (P2A) (Kim et al. 2011). This means that one possibility could be to exchange the $(GGGGS)_n$ linker with a porcine teschovirus-1 (P2A) 2A peptide sequence between *egfp* and *yap* sequence to produce a bicistronic expression under the *Dct* promoter. In that way YAP would only carry the N-terminal additional proline amino acid and would not be constrained by a large upstream fusion 260 aa GFP-linker sequence, which harbours the possibility to inhibit YAP's accurate three dimensional folding. In summary, there are changes we could apply to our fusion protein. Firstly, we could swap the order of the fusion sequences itself and place *yap* upstream of *egfp*. Secondly, we could exchange the *egfp* to a Turbo-GFP sequence to minimise protein turnover and equalise the protein half-life to YAP. Thirdly, we could use an alternative linker sequence such as 2A peptide instead of a flexible linker, as this approach seems to work for Zebrafish studies (Kim et al. 2011).

4.3.4 Future characterisation of the *Dct*:eGFP-YAP(wt/S87A) transgenic lines and investigation of YAP's autonomy within melanocytes

Because we were not able to distinguish individual transgenics from founder's progeny pool of both lines, *Dct*:eGFP-YAP(wt) and *Dct*:eGFP-YAP(S87A), I decided to grow up all the offspring. Once this F1 generation is older than 3 months, we would need to fin clip and PCR genotype each adult fish to re-find carriers of our transgene. Then we would cross F1 carriers with heterozygous HB32C$^{J50\text{-}20C}$ to obtain the J50-20C *hirame* allele, in case the carrier does not already have one. Once the F2 generation has been established, we would hope to have a sufficient number of adult fish to start and analysing those two lines. Again, first, we would need to re-genotype individual adults to identify carriers, because I assume that we would still not see any eGFP expression. Then, we could attempt to answer the following questions:

1.) Why can we not see detectable levels or eGFP in our transgenics?
2.) Does YAP play a cell-autonomous role in melanocytes and can it rescue the *hirame* melanocyte-patterning defect?

The first question as discussed above, can have multiple possibilities ranging from errors in a transcriptional level up to translational protein missfolding and/or degradation. To check, if our transgene is transcribed, one could perform *in situ* hybridisation with an anti-*gfp* antisense probe, which would bind to the first part of the transgene mRNA. Another way to test transcriptional levels would be via qPCR. mRNA of whole embryos could be isolated, retro-transcribed to cDNA, amplified and compared to non-transgenic embryos. The difference in expression would then indicate if the transgene is active or not. However, the presence of mRNA does not automatically mean protein translation as most mRNAs undergo decay by deadenylation mechanisms or through RNA interference (RNAi) by micro RNAs (miRNAs) or short interfering RNAs (siRNAs) (Valencia-Sanchez et al. 2006; Garneau et al. 2007). Even so, we took care in designing our constructs with a well-validated polyA sequence; we still need to test what happened to our fusion protein on a translational level. One possibility is to perform immunohistochemical GFP amplification in whole-mount embryos, which is unfavourable due to the lack of even low levels of GFP signal (as explained above). Another option could be to extract protein and perform Western-Blotting using and anti-GFP antibody, which might be able to detect even low levels of GFP protein presence not detectable by fluorescence microscopy. We did not consider using an anti-YAP antibody, because none of the available and tested antibodies so far were specific enough in Medaka (D H. Davies observation). As discussed above, we could also attempt to re-design the construct either by swapping the order of our genes or

even exchanging the linker sequence to a possibly bicistronic 2A peptide sequence. Separate protein folding might allow eGFP to fold correctly preventing aggregation or degradation, but it would not provide any evidence about the correct folding of YAP neither its functionality (discussed below).
To answer our second question, if YAP might exhibit a cell-autonomous role in melanocytes, we would observe the melanised melanocyte pattern as well as the melanoblast distribution after *Dct* ISH in j50-20C progeny of transgene carriers. If we would then observe a rescue in *hirame* embryos, it would mean YAP acts cell-autonomous. In case we cannot find a melanocyte rescue it could mean either YAP does not act cell-autonomous, or YAP protein is not present or functional within the melanocyte lineage in our *Dct*:eGFP-YAP(wt/S87A) transgenic lines. To test the latter, we could isolate melanised melanocyte by FACS sorting and qPCR downstream targets of YAP such as *cyclinD* or *itgb2* (Zhao et al. 2007). This would show us if YAP is still active and present in functional levels, therefore confirming the presence in melanocytes. Automatically it would make a strong argument that YAP does not act cell-autonomous *hirame* melanocyte, thus unable to rescue the melanocyte defect. It would also strengthen unpublished data from our collaborator, who showed that YAP acts non-cell autonomous in regard to cuvier's duct development and lens invagination (Porazinski 2013).

5 Chapter: Investigation of neural crest derivatives

5.1 Introduction

The induction of the neural crest involves bone morphogenetic proteins (BMPs) and Wnt signalling within the non-neural ectoderm during gastrulation. Other neural crest induction genes start being expressed during neurulation which include *zic*, *pax3* and *pax7* expressed within the neural plate, msx1/2in the neural fold and non-neural ectoderm, and dlx solely located within the non-neural ectoderm. They together fulfil a function as neural plate border specifiers (Huang & Saint-Jeannet 2004; Donoghue et al. 2008; Sauka-Spengler & Bronner-Fraser 2008). Those border specifier genes prompt the activation of neural crest specifiers such as Foxd3, Slug/Snail, Sox9 and Sox10 during delamination of premigartory neural crest cells (Mayor & Theveneau 2013). Neural crest cells (NCCs) are multipotent stem cells that give rise to neurons, glia, pigment cells and endocrine cells (Le Douarin et al. 2004). In our first results chapter, we have demonstrated that *hirame* displays a unique early melanoblast migration defect especially on the yolk sac, before any anatomical body abnormalities appear and after maternal *yap* transcripts were undetectable. This means that within this time window the defects observed were entirely due to the loss-of-functional YAP protein. This made us wonder if other highly migratory neural crest cell types might feature similar defects in cell movement. Therefore, we aimed to analyse a wide range of NC marker and compare some of them to *hirame* to answer key question of YAP requirement in those cell lineages.

5.2 Results

5.2.1 Investigation of the xanthophore pigment cell lineage in wild type and *hirame* mutants

As mentioned previously in this thesis, one of the affected NC derivatives in *hirame* were pigment cell melanocytes. To remind, pigmentation of Medaka is derived from four different pigment cell markers; brown melanocytes, silverfish iridophores, orange xanthophores and white autofluorescent leucophores; making Medaka an equivalent model for studying pigment cell specification, proliferation, survival and migration (Kelsh et al. 2004).

To address whether *hirame*$^{j50\text{-}20C}$ affects xanthophore and leucophore specification, as well as proliferation and differentiation, we examined the expression pattern of *GTP cyclohydrolase I* (*gch*), known to be the earliest marker within the xanthophore lineage. *GTP cyclohydrolyse* I converts guanosine triphosphate (GTP) to dihydroneopterin triphosphate and later to tetrahydrobiopterin (BH4), a required substrate for pterine pigments in early xantophores (Pelletier et al. 2001).

Additionally BH4 also functions as a cofactor for phenylalanine hydroxylase, converting phenylalanine to tyrosine during melanin synthesis in melanocytes (Ziegler 2003; Pelletier et al. 2001). Furthermore it has been reported that *gch* is transiently expressed in xanthophores and a subset of the population of melanophores in Zebrafish (Parichy & Ransom et al. 2000). However, Nagao et al. (2014) cloned the Medaka *gch* (XM_004085058) fragment and demonstrated that its expression pattern between 24 to 34 somite stage (st. 27-30, 58–74 hpf) does not overlap with the *dopachrome tautomerase* (*Dct*) melanophore pattern. However, it is expressed in all xanthophores and leucophores at all stages during development. Therefore in analysing the *gch* expression pattern, we should be able to examine both xanthophore and leucophore pigment cell distribution in Medaka.

Whole-mount *in situ* hybridisation using a *gch* anti-sense probe was carried out in stage 24 and 28 progeny on a Cab$^{j50\text{-}20C}$ background to visualise spatio-temporal changes in leucophore and xanthophore pigment cell population (Figure 5.1). At stage 24 mainly head leucophores were visible similar to *hirame* and wild type siblings despite morphological differences in general organogenesis. Cell quantifications showed no significant difference in cell numbers at that stage (Figure 5.1 B). As xanthophores become specified and differentiate, we observed a dramatic increase in *gch* positive labelled cells in the head, and dorsal, lateral and ventral stripes of the trunk region within wild type siblings at stage 28, not seen in *hirame*. Due to the pronounced xanthophore pattern, we were not able to distinguish these two cell types at any later stage, therefore cell counts (Figure 5.1 B) represent a combination of leucophore and xanthophore cell numbers within the body. However, the slight increase in *hirame gch*$^{+}$ cells at stage 28 is likely due to proliferation in leucophores, which could mean that *hirame* lacks xanthophores completely.

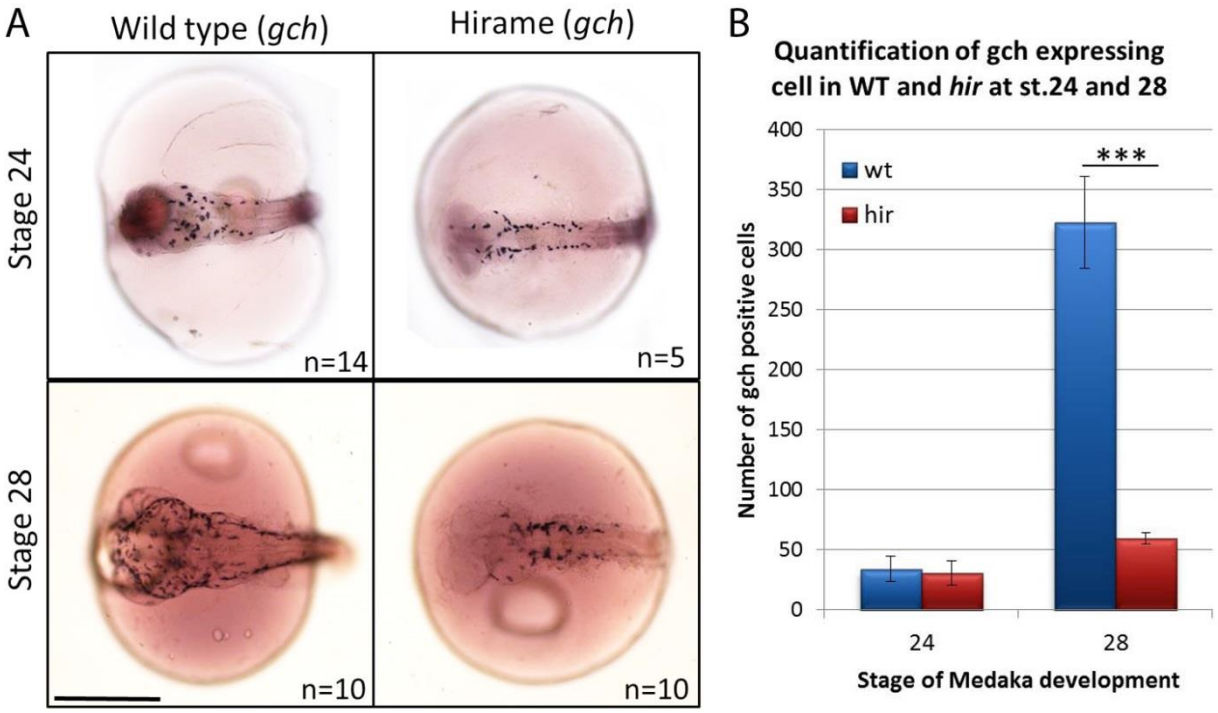

Figure 5.1: *GTP cyclohydrolyse I (gch)* WISH and cell counts in developing Medaka ***hirame* and wild type embryos**

Medaka *hirame* and wild type embryos after *gch* WISH at stage 24 and 28 showing changes in leucophore and xanthophores lineages. **A)** Head leucophores at stage 24 of *hirame* show to be in similar spatio-temporal positions as in wild type siblings (top panel). At stage 28 the number of *gch* positive cells is dramatically increased within the head and trunk region, whereas in *hirame* no visual increase in *gch* cells appeared. **B)** *Gch* cell quantification suggest no significant difference in leucophores within the head region at stage 24, whereas at stage 28 significant increase in *gch+* cell numbers was observed in wild type siblings, but not in *hirame.* The difference in *hirame gch*$^{+}$ cells between those two stages might be solely due to an increase of leucophores indicating an absence in xanthophore specification. All data are means ± SEM. 2-Sample-t-test: *p<0.05, **p<0.01 or ***p<0.001.

5.2.2 Analysis of neuronal marker elavl3/HuC within the head and trunk dorsal root ganglia within wild type and *hirame*

Zebrafish trunk NCCs also give rise to sensory neurons and dorsal root ganglia (DRG) of the peripheral nervous system (PNS) (Le Douarin et al. 2004). Herein their correct specification and migration is essential during PNS development.

To form DRGs they migrate as partially committed neural crest cells along the medial pathway between somites and the neural tube to then coalesce initially as two to five neurons (Raible et al. 1992). This originally small pool of cells differentiates into compact DRG neurons and associated ganglia cells, located between the lateral edge of the spinal cord and each somite pair. DRGs contain

the sensory neurons of the PNS receiving and transmitting sensory information to the dorsal horn of the spinal cord, such as touch, perception of pain, temperature and limb movement (McGraw et al. 2008). In Zebrafish, different from mouse, neurogenin 1 (neurog1) controls the spatial and temporal development of dorsal root ganglia, as knockdown of neurog1 with anti-sense morpholino's led to a complete loss of DRG neurons as well as non-NC neurons of the cranial ganglia (Andermann et al. 2002). In comparison, in mouse neurogenesis the development of DRGs is regulated through the activity of neurogenin 1 and neurogenin 2 followed by Krox20 expressed in boundary cells. In addition, the transcription factor Sox10 is required for initiation of DRGs from the migrating trunk neural crest (Carney et al. 2006). After completion of neurogenesis survival, DRG expansion is regulated by soluble neurotrophins before the end of mammalian embryogenesis (Ma et al. 1999).

DRG's can be labelled by *elavl3*. Elavl3 encodes the ELAV-like neuron-specific RNA binding protein 3, one of several Hu antigens (neuronal-specific RNA-binding proteins) and is recognised by the neuronal anti-HuC antibody, also described as elavl3/HuC. HuC is one of the earliest molecular markers for differentiating neurons. It first appears in the neural plate directly after gastrulation, after which high levels continue to be expressed throughout most regions of the developing nervous system (Kima et al. 1996).

In order to ask whether neuronal patterning and especially DRG numbers are modified in *yap* mutants, we analysed the differential expression of HuC in *hirame* and WT siblings. We carried out whole-mount *in situ* hybridisation in sibling progeny at stage 24 and 28 using digoxygenin-labeled anti-sense probes to Medaka elavl3/HuC (Figure 5.2). The expression pattern of HuC in *hirame* and wild type embryos at both stages was clearly distinguishable. Expression of HuC in the three cranial ganglia (arrow heads) was present in *hirame* embryos at st. 24, but mainly in atypical, ectopic pattern. Even so cranial ganglia are largely derived from neurogenic placodes (epibranchial and dorsolateral) and not from neural crest we wanted to embark on it as it was one of the spatio-temporant differences we could observe. The HuC positive cranial ganglion cell populations were much smaller, and seemed unstructured and dislocated, as parts in the posterior as well as anterior ganglion does not seem to be associated within a close range of the body, which was the case in wild type siblings. This defect seemed partially normalised by stage 28 because posterior ganglia and ganglia arising from rhombomere 4 are in close proximity to the body axis despite the much smaller HuC positive ganglion in the hindbrain region. Rhombomeres 1 to 7 (indicated by white numbers) are labelled in wild type embryos at stage 24 and 28, where we would expect them to be in *hirame.* We were not able to distinguish individual rhombomers because the neuronal zones are ill-defined and small. Furthermore, the hindbrain ventricle opening zone in *hirame* is much narrower compared to

wild type, an effect even more pronounced at stage 28. Note, it also seems that HuC expression is either absent in the (presumably) upper rhombic lip (URL) underneath the cerebellum and the mid-hindbrain-boundary (MHB) (asterisks) at stage 28 or the URL is completely missing in *hirame* compared to wild type. In addition, HuC positive forebrain seems to be dramatically reduced or even absent in *hirame* at both stages.

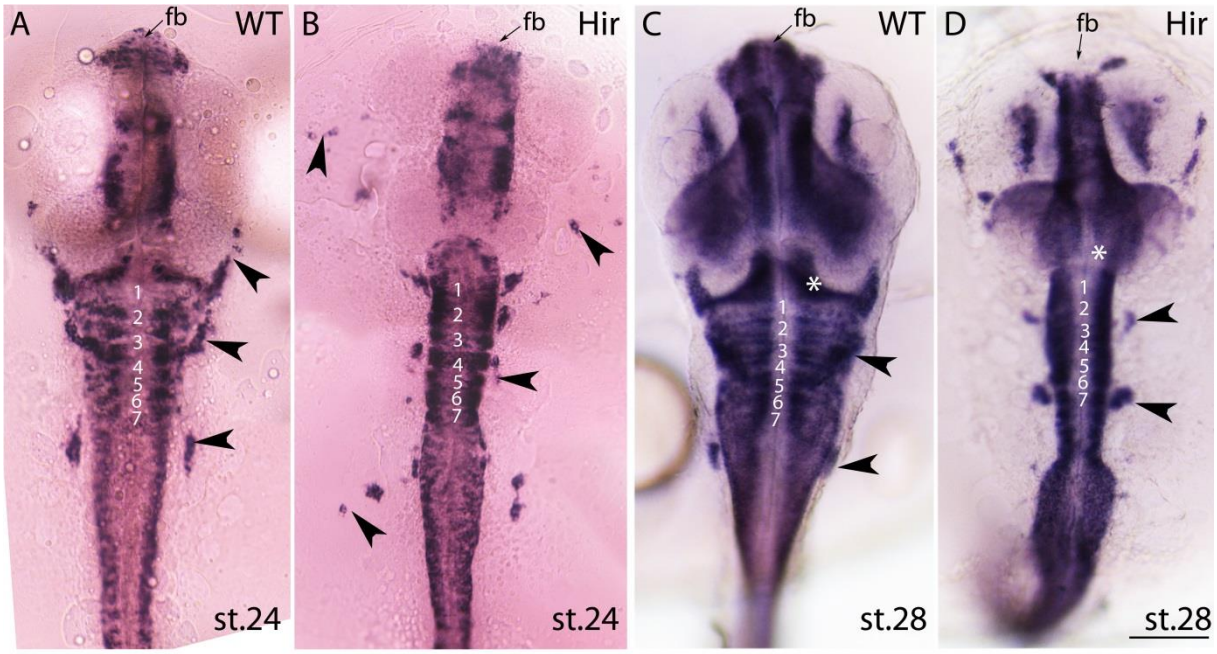

Figure 5.2: elavl3/HuC expression in head and anterior trunk of st. 24 and st. 28 shows differences in *hirame* embryos

Whole-mount *in situ* hybridisation of anti-elav3/HuC in st. 24 and st. 28 wild type and *hirame* embryos. Cranial ganglia (arrow heads) in *hirame* were much smaller in size and observed in ectopic positions (**B**) compared to wild type siblings in which cranial ganglia are closely associated with the body (**A**). This defect seemed partially normalised by stage 28 as some cranial ganglia structures can be observed in expected regions (**D**). The hindbrain ventricle opening is much narrower in *hirame* (more pronounced at st. 28) and presumptive upper rhombic lip (asterisks) is absence as well as rhombomers 1 to 7 are not well distinguishable in *hirame* (**D**) compared to wild type (**C**). Note, forebrain also seems smaller in *hirame* (bot stages). fb = forebrain. Scale bar = 100µm

To investigate if the absence of functional YAP affects the formation dorsal root ganglia from the trunk neural crest, we performed whole-mount *in situ* hybridisation with anti-elavl3/HuC on st. 32 embryos, one of the latest stages in which some *hirame* embryos are still alive. At stage 32 normal embryos have around 30 pairs of dorsal root ganglia (Figure 5.3 A) positioned laterally to the elavl3/HuC expressing neural tube, beginning from the first somite and extending to the tip of the tail (arrows Figure 5.3 B). However, we observed a significant reduction of complete dorsal root ganglia structures in *hirame* with an average number of 9.75 (Figure 5.3 A). DRGs in *hirame* migrate and differentiate next to the first 10 somites (arrows Figure 5.3 B). We could not observe any type of

DRGs beyond somite 11, despite the fact that *hirame* mutants develop the similar numbers of somites compared to its wild type siblings at stage 32 (data not shown). Our observations imply that YAP is required to determine the initiation of DRG pairs therefore might be required for peripheral nervous system development.

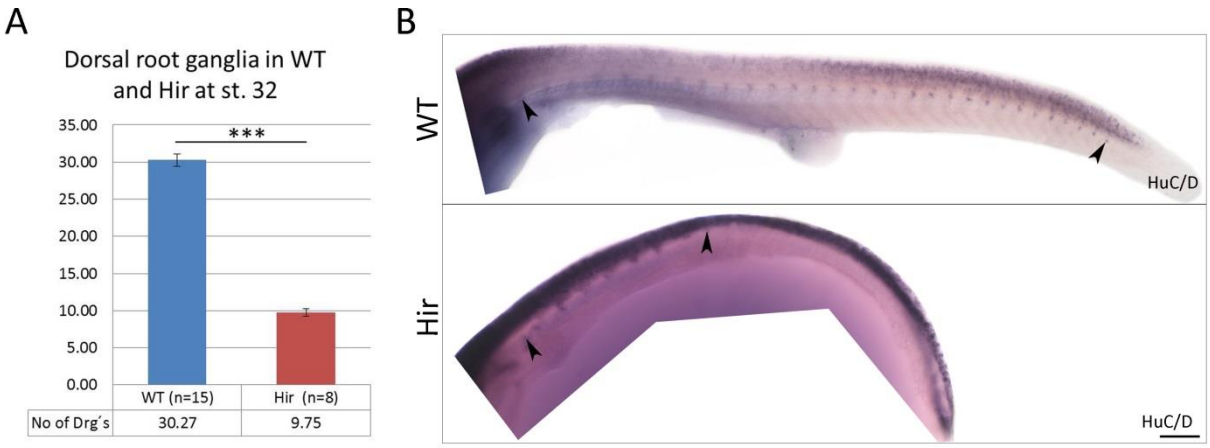

Figure 5.3: Dorsal root ganglia in *hirame* at st.32 are quantitatively reduced

In situ hybridisation to visualise elavl3/HuC expression in dorsal root ganglia (DRG) of late stage *hirame* embryos. **A**) Counts of DRGs in wild type and *hirame* embryos represents a significant decrease in *hirame* mutant siblings. **B**) Elavl3/HuC labels neural tube in both genotypes. DRGs in wild type are present between all, from first to the last somite blocks (arrow heads), in *hirame* however DGRs were only detectable until 10 somits (arrow head). Scale bar = 100µm. All data are means ± SEM. 2-Sample-t-test: *p<0.05, **p<0.01 or ***p<0.001.

5.2.3 *Sox9b* early neural crest marker analysis in *hirame*

The family of Sry -related high-mobility group (HMG) box proteins play important roles in developmental processes, such as CNS neurogenesis, germ layer formation, organ development, and cell type specification (Cui et al. 2011). The family member *Sox9b* is expressed in a subset of neural plate border cells which specify premigratory neural crest cells (Donoghue et al. 2008). Together with RUNX3 and the influence of EGR1, it manipulates BMP-signalling required for NCCs to differentiate into pharyngeal cartilage, therefore influencing cranial cartilage development in Zebrafish (Dalcq et al. 2012). Furthermore *Sox9b* plays an essential role during chondrocyte differentiation in mice (Akiyama et al. 2002), and is next to Sry (sex-determining region on Y chromosome) as of the most important genes during male gonad determination in mammals (Jiang et al. 2013; Clarkson & Harley 2002). Zebrafish carries two orthologues of Sox9 in its genome Sox9a and *Sox9b* both with

overlapping and distinguishable features. Sox9a is expressed in testis, while *sox9b* occurs in the ovaries and the neural crest population (Chiang et al. 2001). Both are expressed in developing craniofacial cartilage, pectoral fin buds and central nervous system (Li et al. 2002).
Before Medaka´s whole genome was sequenced in 2002 by the National Bio Resource Project Medaka Genome Project, only one Sox9 gene was thought to exist (Yokoi et al. 2002). In 2005 Klüver et al. isolated a second Sox9 confirming that both orthologues are derived from the teleost-specific genome duplication (Meyer & Schartl 1999). They described how during embryogenesis, both are expressed within the craniofacial cartilage and pectoral fin buds, but differ considerably in other tissues. Medaka Sox9a is expressed in ceratobranchial arches, mandibular and hyoid arches. *Sox9b* is positive within the early neural crest and otic placode initiation and is generally switched on earlier than Sox9a within the otic placodes. After 2 dpf it is expressed around the eyes, within the forebrain, somites and the mid-hindbrain-boundary (MHB). Around 4 dpf *Sox9b* is also expressed within the tectum, roof and floor plate, within the heart and the anus sphincter.
Our aim was it to investigate the expression pattern of *Sox9b* during embryogenesis of *hirame* mutants whilst focusing on the neural crest lineage. To achieve that I conducted a series of whole-mount *in situ* hybridisation experiments at different stages with a *sox9b* anti-sense riboprobe (a gift by Dr H. Hashimoto).
Our first observations were that at early stage 20 (1d 7.5h) wild type embryos exhibited strong *sox9b* expression within the preplacodal ectoderm that will develop into the otic placode (Figure 5.4 A'). It also showed expression in the neural crest within the hindbrain, i.e. the cranial neural crest which later contributes to the cranial cartilage, as well as more posteriorly, i.e, in trunk neural crest which, eventually develop into pigment cells and the peripheral nervous system (PNS). In contrast, *sox9b* expression in *hirame* mutants showed a mixed cell distribution in which some *sox9b*$^{+}$ cells could be seen in the hindbrain, otic placode and trunk neural crest locations, but at the same tissue, most cells still remained in ectopic yolk sac positions (Figure 5.4 B'). 13 hours later in Medaka embryonic development at stage 24 wild type embryos remained positive *sox9b* expression within the otic placode, within the forebrain, inner optic cup region of the developing eye and the mid-hindbrain boundary (MHB) (Figure 5.4 C'). Surprisingly, we observe the same *sox9b* expression pattern in *hirame* mutant siblings at st. 24 (Figure 5.4 D').

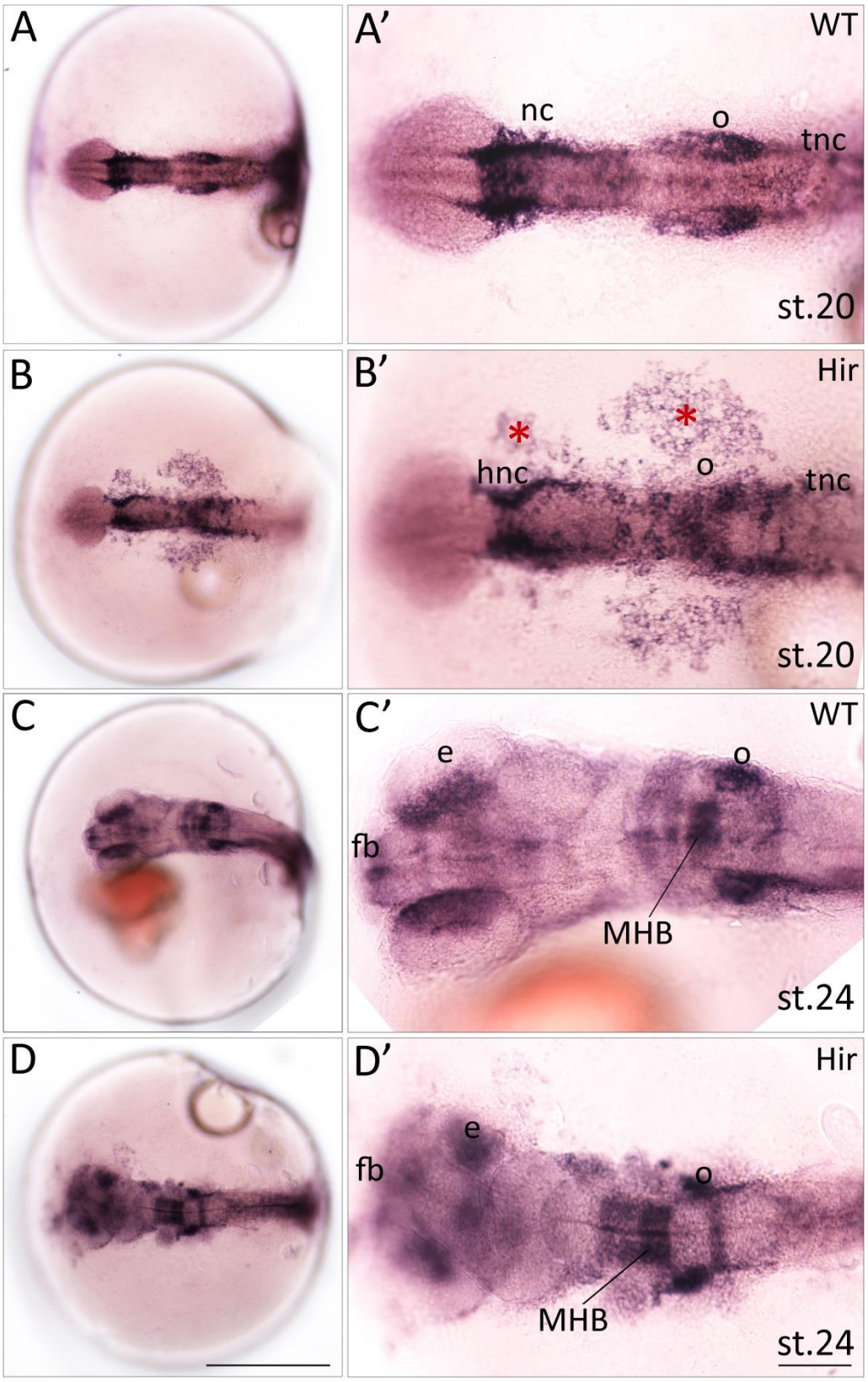

Figure 5.4: *Sox9b* WISH in *hirame* and wild type at st.20 and st.24 reveals differences at early stages

Whole-mount in-situ hybridisation of early neural crest marker Sry-box containing protein 9b (*Sox9b*). Left panels show whole embryo, right panels represent higher magnification. **A-B**) During early embryogenesis at st.20 *sox9b* is expressed within the hindbrain neural crest, the presumptive otic placode population and neural crest within the trunk region (WT A, A' n=39).

In contrast *hirame* demonstrates a mixed pattern in which some *sox9b*+ cells are already within the expected regions and some are located ectopically on the yolk sac region close-by (red asterisks) (n=12). **C-D**) At st.24, 13h later, *sox9b* was strongly expressed around the developing eye, forebrain, mid-hindbrain-boundary (MHB) and otic placodes (n=23), an expression pattern also found in *hirame* (n=6). It seems despite morphological differences the areas of *sox9b* expression is the same as in WT siblings at that stage. Abbreviation: e, eye; fb, forebrain; hnc, neural crest in hindbrain; MHB, mid-hindbrain boundary; o, otic placode; tnc, neural crest in trunk. Scale bar A-D=500µm, A'-D'=100µm.

It is possible that the ectopic *sox9b*$^{+}$ cells in *hirame* at stage 20 were created by a slower conversion process during gastrulation of *hirame* causing them to remain on the embryonic mesenchyme. To address this, I carried out resin sectioning (Figure 5.5). This revealed that the *sox9b* positive cell population seen in *hirame* stage 20 embryos are possibly ectodermal cells that remain on top of the existing mesenchyme, possibly at the end of gastrulation, as compared to wild type siblings in which those cells have already migrated to the presumptive otic placode. Supporting, when we analysed earlier embryonic developmental stages between st.17 and st.19 (Figure 5.6) we could observe a developmental delay in *sox9b*$^{+}$ cell migration during *hirame* embryogenesis. The migration of *sox9b*$^{+}$ cells towards the hindbrain, otic placodal and prospective trunk neural crest cell seemed persistently delayed in *hirame* mutants. It appears that the cell migration was around 5.5 hours delayed, e.g. st.20 *hirame* mutants looked similar to st.17/18 wild type siblings. Genotyping with tetra-ARMS primer PCR confirmed the genotype of individual embryos. These findings from st.17 to st.19 *hirame* embryos coincided with observations we made during gastrulation in which the speed of epiboly closure was behind in *hirame* mutant embryos (Appendix 12), wherein the blastoderm migrated slower towards the vegetal pole.

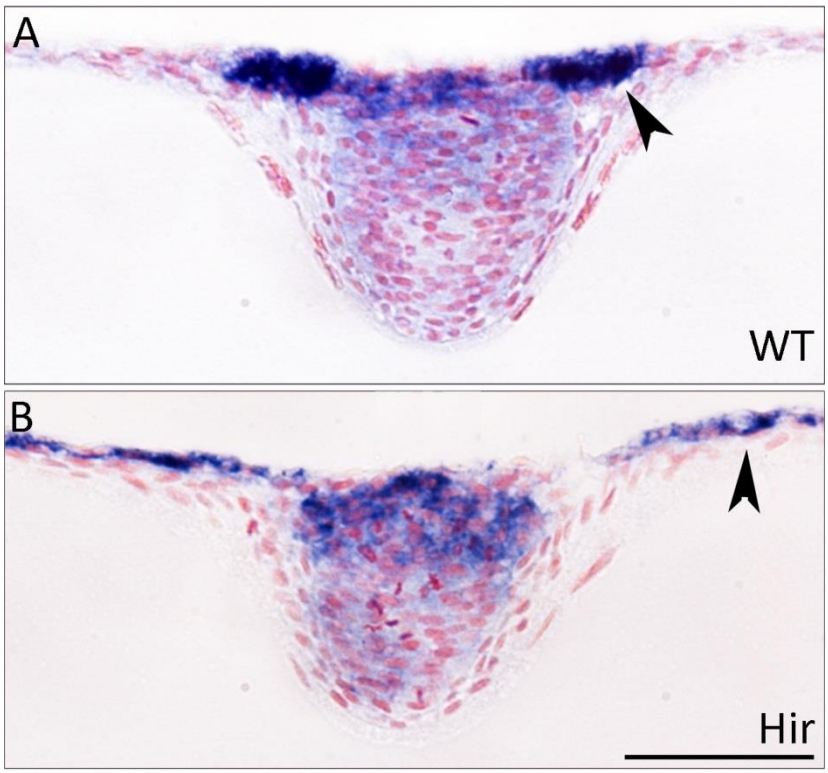

Figure 5.5: Trunk cross sections of st.20 embryos shows *sox9b* labelled cells remain on the yolk sac in *hirame*

Resin sections of stage 20 wild type and *hirame* representing the tissue morphology and *sox9b* staining within the trunk region. **A**) *sox9b*$^{+}$ cells are strongly expressed within the presumptive otic placode and a gradient of *sox9b* expression runs from the dorsal towards the ventral side of the neural tube. **B**) In *hirame* mutants *sox9b*$^{+}$ cells remain above the extending mesoderm on top of the yolk sac and are not yet accumulated within otic placodal region. The gradient of *sox9b* expression within the neural tube is similar although the dorsal part is slightly thicker. Resin sections = 8µm. Scale bar = 500µm

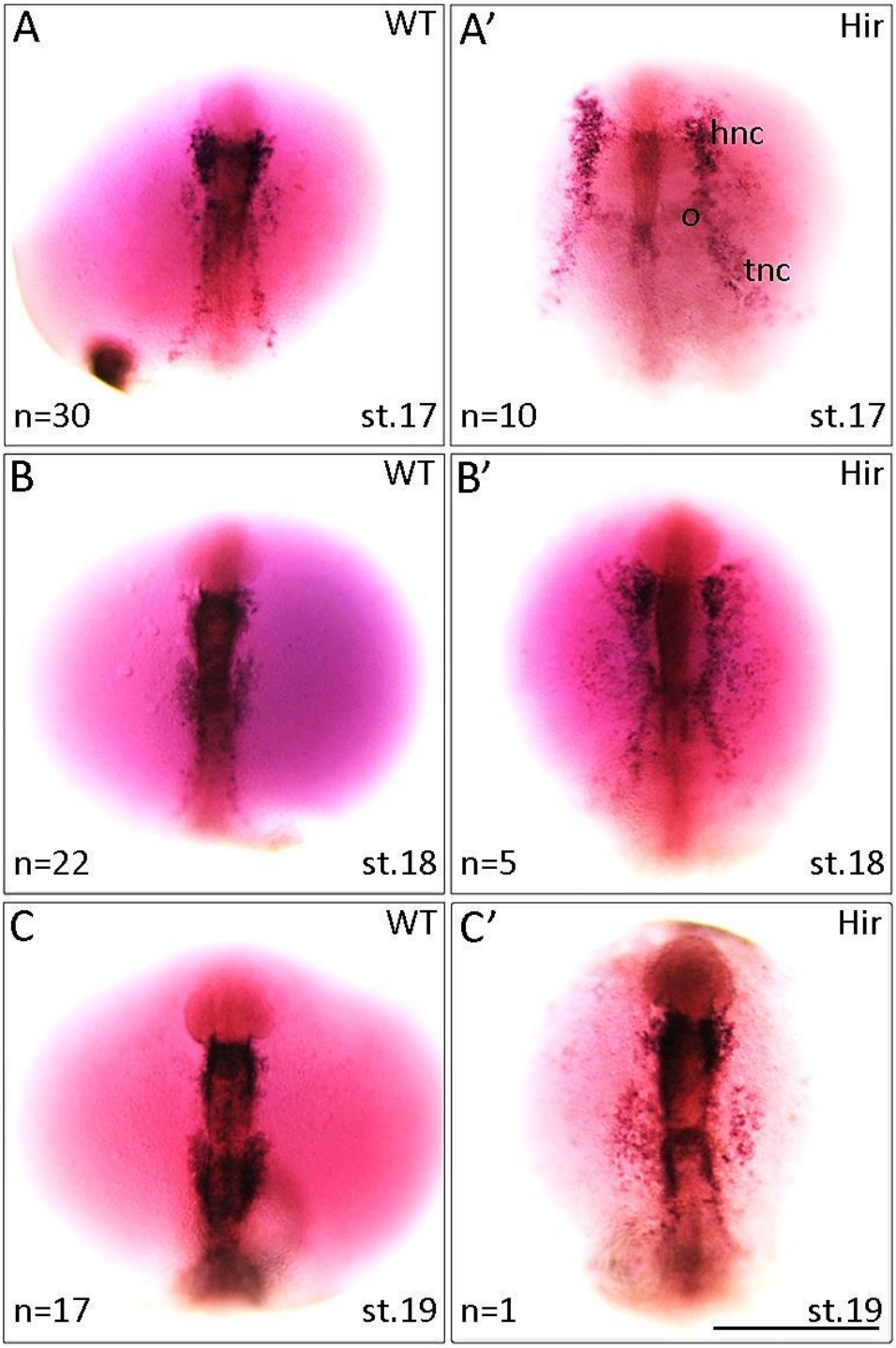

Figure 5.6: *Sox9b* expression during gastrulation between st.17 and st.19 in wild type and *hirame* highlights the convergence defect in *hirame*

Series of images representing cell migration at the end of gastrulation at st.17 (1d 1h) (**A,A'**), st.18 (1d 2h) (**B,B'**) and st.19 (1d 3.5h) (**C,C'**) in wild type and *hirame* embryos. *Sox9b*$^{+}$ cell migration in *hirame* embryos is slower than its wild type sibling. Whereas in wild type sox9m expressing cells within the presumptive cranial neural crest, otic placode and trunk neural crest are located within their specified body region, in *hirame* those cell pools are still remaining on top of the mesenchyme above the yolk sac. All embryos were genotyped with tetra-ARMS primer PCR. Abbreviations: hnc, neural crest within the hindbrain region (cranial neural crest); o, otic placode precursors; tnc, neural crest of the trunk. Scale bar = 500µm.

Next we wanted to investigate if expression of *sox9b* is affected during later stages. We chose to examine 3 dpf embryos and expected to find *sox9b* labelling within somites and dorsal trunk neural crest precursors as described in Zebrafish (Li et al. 2002). Lateral views of whole-mount in-situ hybridisations show that *Sox9b* is expressed in somites within wild type embryos as well as *hirame* mutant siblings (Figure 5.7). The overall expression in somitic mesoderm was relatively week which made a clear description of each somite impossible. We also observed a strong expression within a dorsally-located, caudal cell population in the wild type, which we could not identify clearly in *hirame.* Dorsal views of those embryos provide a clearer sight of this area which presumably labels neural crest precursor cells. As previously mentioned *hirame* embryos are generally very weak and the yolk sac membrane seems to have problems with mechanical tension, making these embryos difficult to work with. This can in some cases lead to an ingrown tail end, at later stages (chapter 1 Figure 1.4). Because we could not observe any neural crest-like dorsal cell population at the tail end of *hirame* mutants, we wondered whether tail curling might have masked the signal and given us a false-positive image in Figure 5.7 *A' and B'*. Therefore we attempted to remove all embryo bodies from the yolk sac after *sox9b* WISH, embedded them in resin and subsequently sectioned them. Sections revealed that within the trunk region (Figure 5.8 A, A') *Sox9b* is expressed within the medial pathway lining the most inner region along the neural tube, notochord and somites. In wild type embryos *sox9b* also marked a region within the dorsal midline, which we could not clearly identify in *hirame* embryos as the whole dorsal side was labelled. Cross sections from the tail end revealed a distinctive layer of strong *sox9b*$^{+}$ cells within wild type (Figure 5.8 B), which we could not clearly distinguish in *hirame* (B'). Meanwhile in *hirame*, the *sox9b* riboprobe labels a broad area within the neural tube, with strongest expression dorsally.

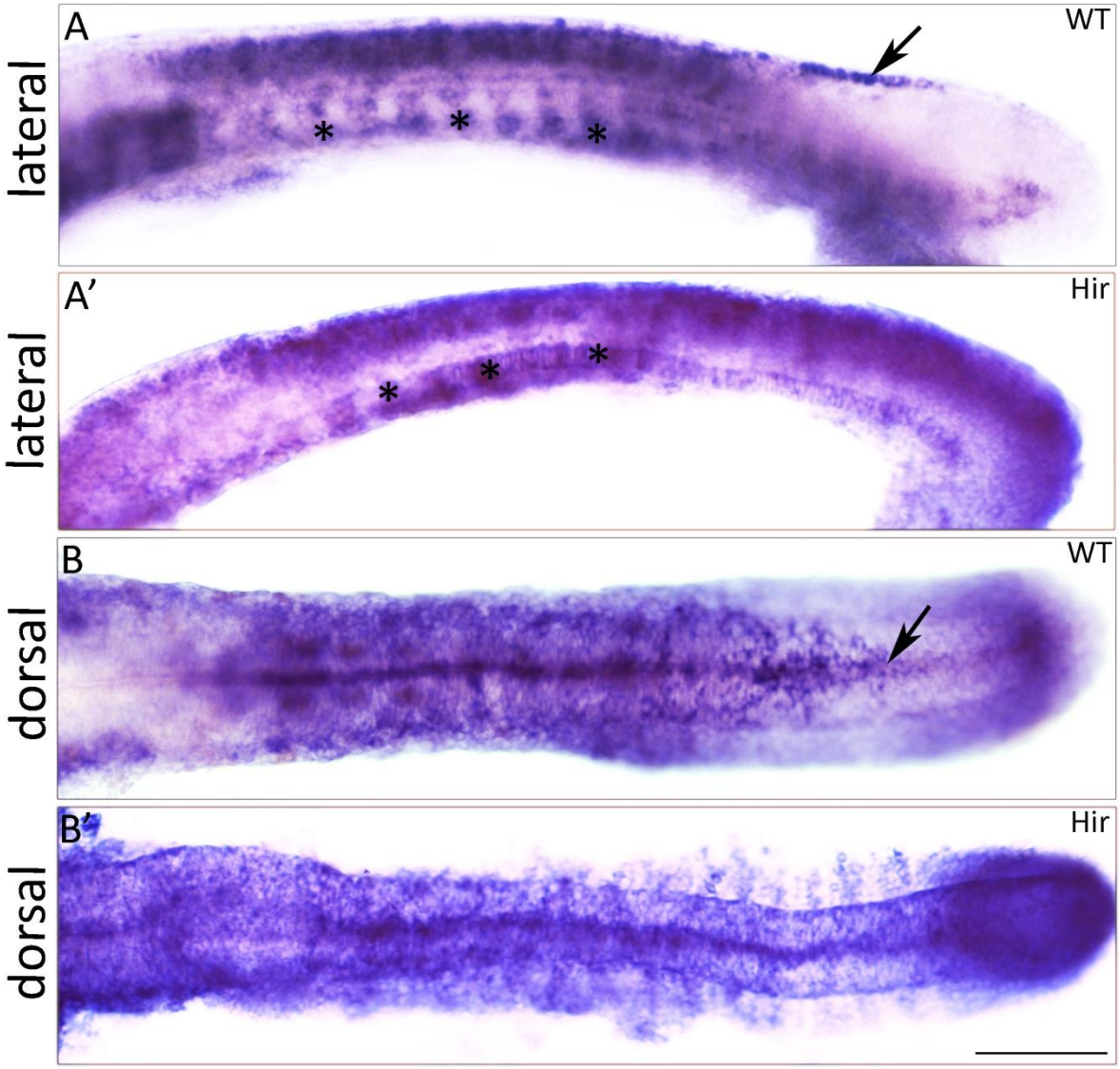

Figure 5.7: *Sox9b* expression within the trunk of 3 dpf old wild type and *hirame* embryos

Lateral and dorsal view of the trunk region in 3dpf embryos after WISH with anti-sense *sox9b.* Lateral view shows weak expression of somites (asterisks) in wild type and *hirame*. Noticeable wild type embryos indicate strong *sox9b* expression within the dorsal stripe especially at the tail end presumably labelling neural crest precursors (**A**, arrows) not observable in *hirame* (**A'**). Dorsal view highlights the extent of *sox9b*$^{+}$ cells at the tail in wild type (**B**) not present in *hirame* (**B'**). Scale bar = 100µm

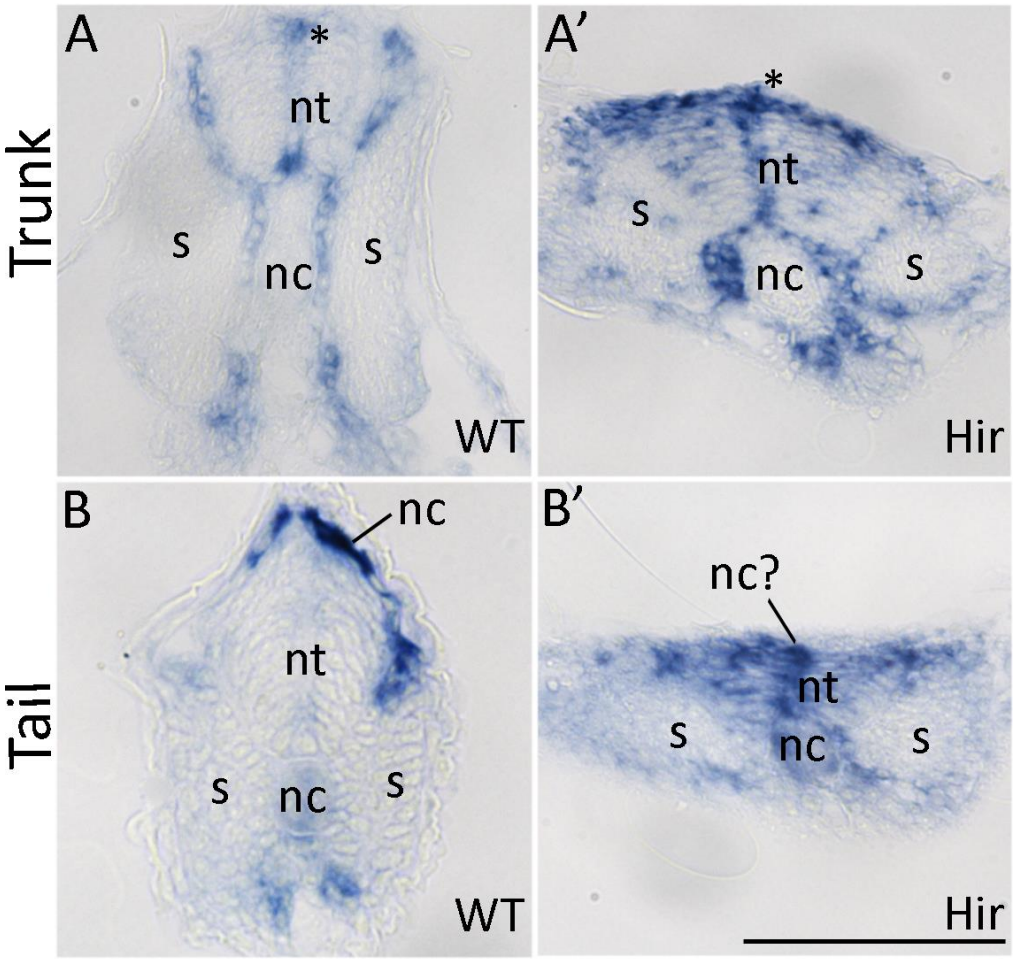

Figure 5.8: Localisation of *sox9b* within the body of 3 dpf wild type and *hirame* embryos

Trunk (top row: **A, A'**) and Tail (bottom row: **B, B'**) resin cross sections of *sox9b* WISH in 3dpf old wild type and *hirame* embryos. Trunk cross sections show *sox9b* was expression within the medial migration path in both embryos; however the dorsal midline was clearly *sox9b*$^{+}$ in wild type (**A**) which was difficult to identify in *hirame* mutants (**A'**). Tail sections highlight the layer of strong *sox9b* expression dorsally of the neural tube (**B**) which could not be found in *hirame* (**B'**). In *hir* mutants *sox9b* marked broad regions within the neural tube rather than a specific location. Sections = 8µm, Scale bar = 50µm

To complement these observations, we obtained the *Sox9b*:gfp transgenic line originally established to analyse morphological reorganisation of the gonads during gonadal development in Medaka fish (Nakamura et al. 2007). The aim was to validate the expression pattern seen with the *sox9b* riboprobe, and monitor in real time the neural crest cell migration during early embryogenesis in wild type and *hirame*. We especially wanted to see if it would be possible to highlight dorsal early neural crest migrating populations within the trunk, as we could not clearly labels those cells in WISH in *hirame*.

Up to now, we were able test this transgenic line in late stage embryos and in wild type only and could confirm the *sox9b* expression pattern within the craniofacial cartilage and forebrain region (Figure 5.9). We could also see expression within the epiphyseal and possibly the basihyoid as

described previously in early st.32 (4 dpf) embryos (Klüver et al. 2005). In addition we were able to see Sox9b expression within the cartilage of the spine vertebrae (initiated from somites), pectorial fins, the anus sphincter and the atrioventricular canal of the developing heart (Figure 5.10) (Klüver et al. 2005), confirming the *sox9b in situ* expression pattern already published. Unfortunately, we were not able to obtain data from earlier stages yet and investigate the possibilities to highlight dorsal trunk *sox9b* cells, which we would have compared to *hirame* mutants in vivo. However, these findings demonstrate the usefulness of this fluorescent transgenic line, which we are likely to use for further studies in earlier developmental stages with the *j50-20C hirame* genetic background.

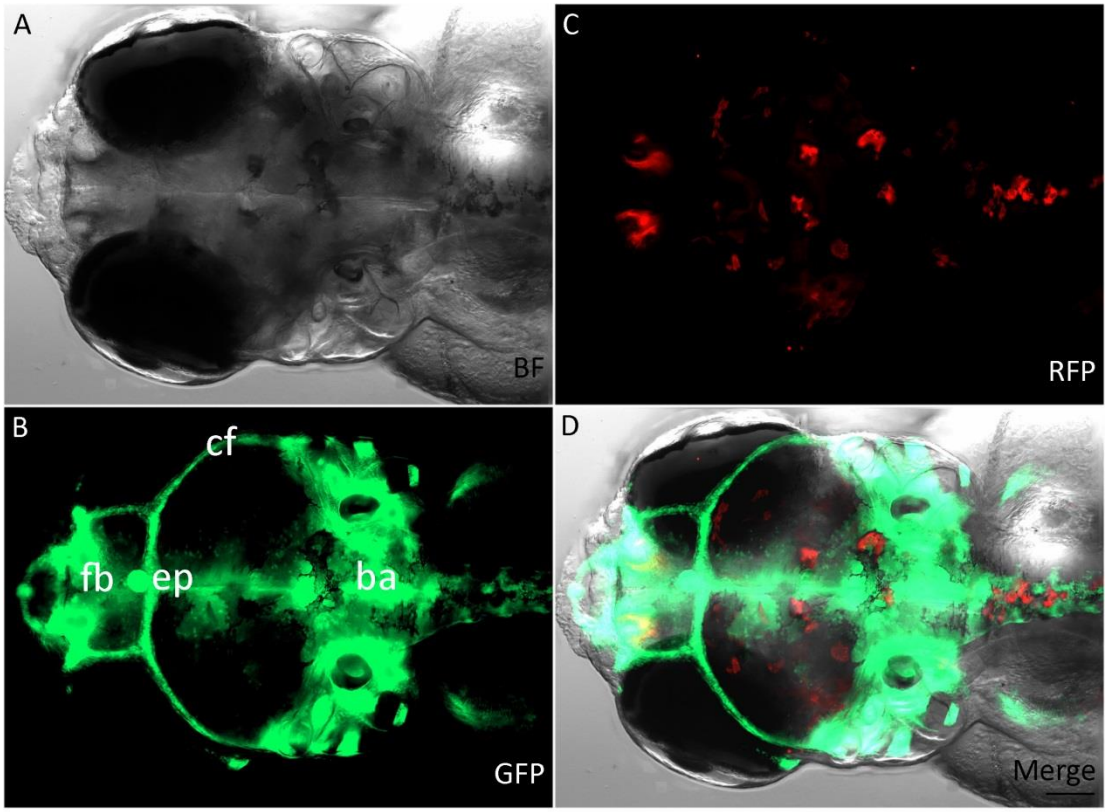

Figure 5.9: *Sox9b*:gfp in 7 dpf wild type embryos highlighting the head region

Transgenic line *sox9b*:gfp shows fluorescence expression within the craniofacial cartilage, forebrain, epiphyseal and possibly the basihyoid at 7dpf. Red channel represents autofluorescence of leucophores and possibly medial rectus. Abbreviations: cf, craniofacial cartilage; fb, forebrain; ep, epiphesis; ba, basihoid. Scale bar = 100µm

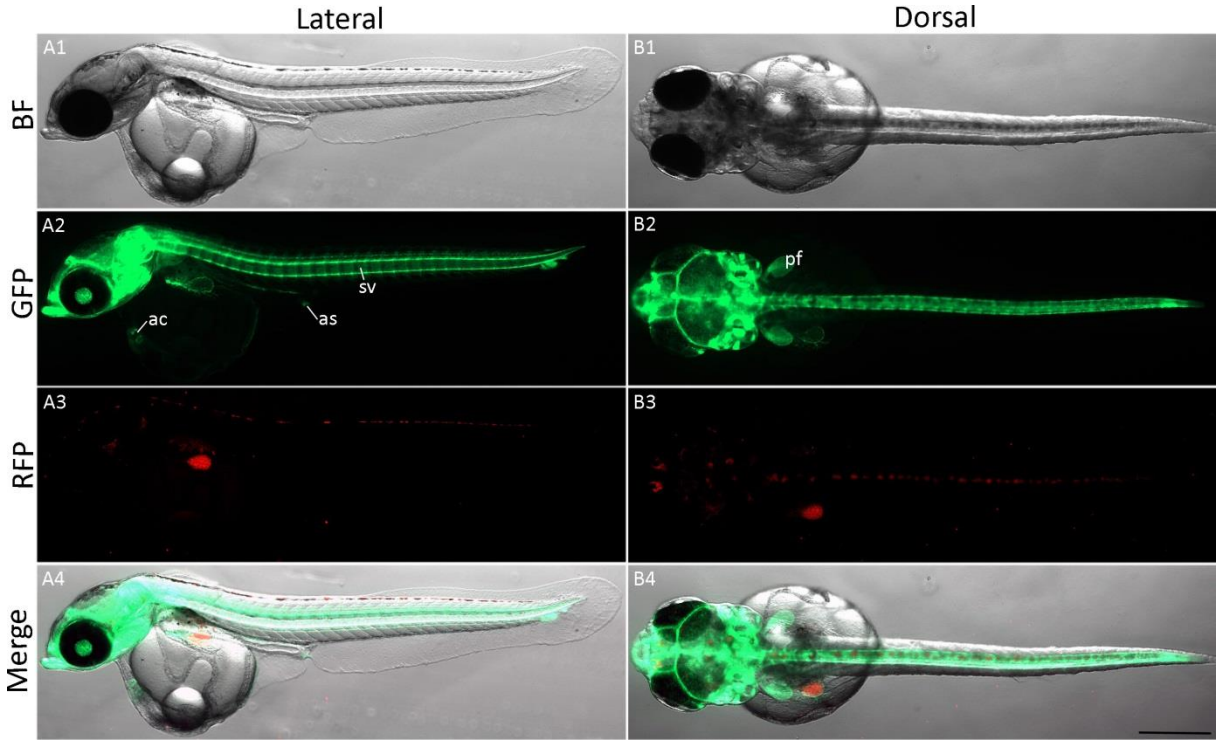

Figure 5.10: *Sox9b*:gfp transgenic wild type at 7dpf whole embryo

Sox9b:gfp transgenic embryos at 7pf labelling the cartilage of spine vertebrae, pectorial fins, the anus sphincter and the atrioventricular canal of the developing heart. Abbreviations: ac, atrioventricular canal; as, anus sphincter; pf, pectorial fin; sv, spine vertebrae. Scale bar = 500µm

5.2.4 Analysing the CNS and PNS marker *mbp* in wild type as potential marker for neural crest derivatives

The major function of Oligodendrocytes in the central nervous system (CNS) and Schwann cells in the peripheral nervous system (PNS) is to provide myelination to axons by repeatedly wrapping their membranes around axons to form densely compacted myelin sheaths. This allows rapid and efficient conduction of action potentials along axons. Schwann cells and Oligodendrocytes also aid nerve development and regeneration, and provide trophic support for neurons, production of the nerve extracellular matrix and the modulation of neuromuscular synaptic activity. Despite similar functions these two cell types differ from each other in several ways. Oligodendrocytes are a type of neuroglia residing within the central nervous system which provides around 1µm myelin wrapping for up to 50 axons, compared to Schwann Cells which myelinate one axon only (Sherman & Brophy 2005). Oligodendrocytes develop from oligodendrocyte progenitor cells (OPCs) which migrate to their final destination where they differentiate and become fully matured. OPCs are located in the subventricular zone of the cerebrum or cerebellum and in the spinal cord, and arise from ventral regions of the neural tube. Extrinsic factors such as platelet derived growth factor (PDGF) or

fibroblast growth factor (FGF) released from neurons or astrocytes have been shown to play a role in oligodendrocyte proliferation (Kettenmann & Verkhratsky 2011). In contrast, Schwann cells can be of myelinating or nonmyelinating type. They are the main glia within the PNS and support neurons such as satellite cells, olfactory ensheathing cells, enteric glia and glia that reside at sensory nerve endings, for instance Pacinian corpuscle. The migration and differentiation of developing Schwann cells from the neural crest is controlled by Sox10 (Carney et al. 2006), whilst the initiation of myelination has been shown to require G protein-coupled receptor (GPCR) Gpr126 (Monk et al. 2011), in addition to the transcription factor Egr2, also known as Krox20 (Svaren & Meijer 2008). Neuronal neuregulin 1 type III specifically directs Schwann cell migration (Perlin et al. 2011). Disruption of myelination can cause a wide range of neuropathies. In the CNS disruption of oligodendrocyte myelination leads to Multiple Sclerosis, Pelizaeus-Merzbacher disease and other forms of leukodystrophies (Kettenmann & Verkhratsky 2011). Defects in Schwann Cells can result in Guillain-Barré syndrome (GBS) and schwannomatosis, and acute inflammatory demyelinating polyradiculopathy. Because the failure in glia development can cause such dramatic neurological diseases, it is vital that we understand the mechanisms involved in functional cell development and subsequent myelination (Reeves & Swenson 2008) .

Because markers for glia in the CNS and PNS are not yet published in Medaka, we aimed to investigate *myogenic basic protein (mbp)* expression in wild type embryos, and then to analyse glia differentiation and myelination in *hirame* mutants later. The myelin basic protein (*mbp*) is the most abundant protein in CNS myelin and is responsible for adhesion of the cytosolic surfaces of multi-layered compact myelin. It has been shown to be a robust marker for differentiated Schwann cells in the peripheral nervous system and oligodendrocytes within the CNS (Jung et al. 2010).

Mbp in situ hybridisation was carried out on 5 dpf, 7 dpf and 9 dpf wild type embryos (Figure 5.11, left panel) with the probe provided by Dr H. Hashimoto. Mainly *Mbp*$^{+}$ oligodendrocytes were clearly labelled within the head in which nerve branching was detectable. Nerves from cranial ganglia (black arrow) seemed thicker and fully matured at 9 dpf and anterior cranial ganglia have migrated towards the anterior optic cup. Individual cell bodies (white arrow heads) and axial processes of oligodendrocytes (white arrows) were most visible at 7 dpf and 9 dpf within the CNS midbrain region. In addition the development and branching of the presumably reticulospinal neurons could be followed from individual cell bodies to a refined network at 9 dpf (asterisks) within the hindbrain. Resin sections (Figure 5.12 A) showing the eye region in which nerves of cranial ganglia (black arrow) are present at 7 dpf. Furthermore, spinal cord oligodendrocytes within the posterior hindbrain strongly expressed mbp from 5 dpf onwards (black arrow head). In addition, Schwann cells were clearly visible at 7dpf within the posterior lateral line (red arrow heads).

Within the trunk region the *mbp*$^{+}$ oligodendrocytes developed within the spinal cord from 5 dpf onwards (Figure 5.11, right panel). Hereby ventral spinal cord oligodendrocytes are higher in numbers than dorsal nerve cells (black arrow heads). Oligodendrocyte cell density increases during development, so that a strong nerve line is visible at 7 dpf. Slight thickening innervating this line especially at 9 dfp might show individual sensory organs (neuromast) (black arrow heads). Fine Schwann cell nerves are visible at 5 and 7 dpf extending ventrally from the spinal cord (red arrow heads) Schwann cells within the posterior lateral line (pLL) were undetectable, because their location was out of focus plane within those images. The oligodendrocyte and Schwann cell distribution is better visualised in resin sections (Figure 5.12 B). Herein, at 7 dpf *mbp* labels ventral and dorsal spinal cord oligodendrocytes (black arrow head) and posterial lateral line (pLL) residing Schwann cells (red arrow head).

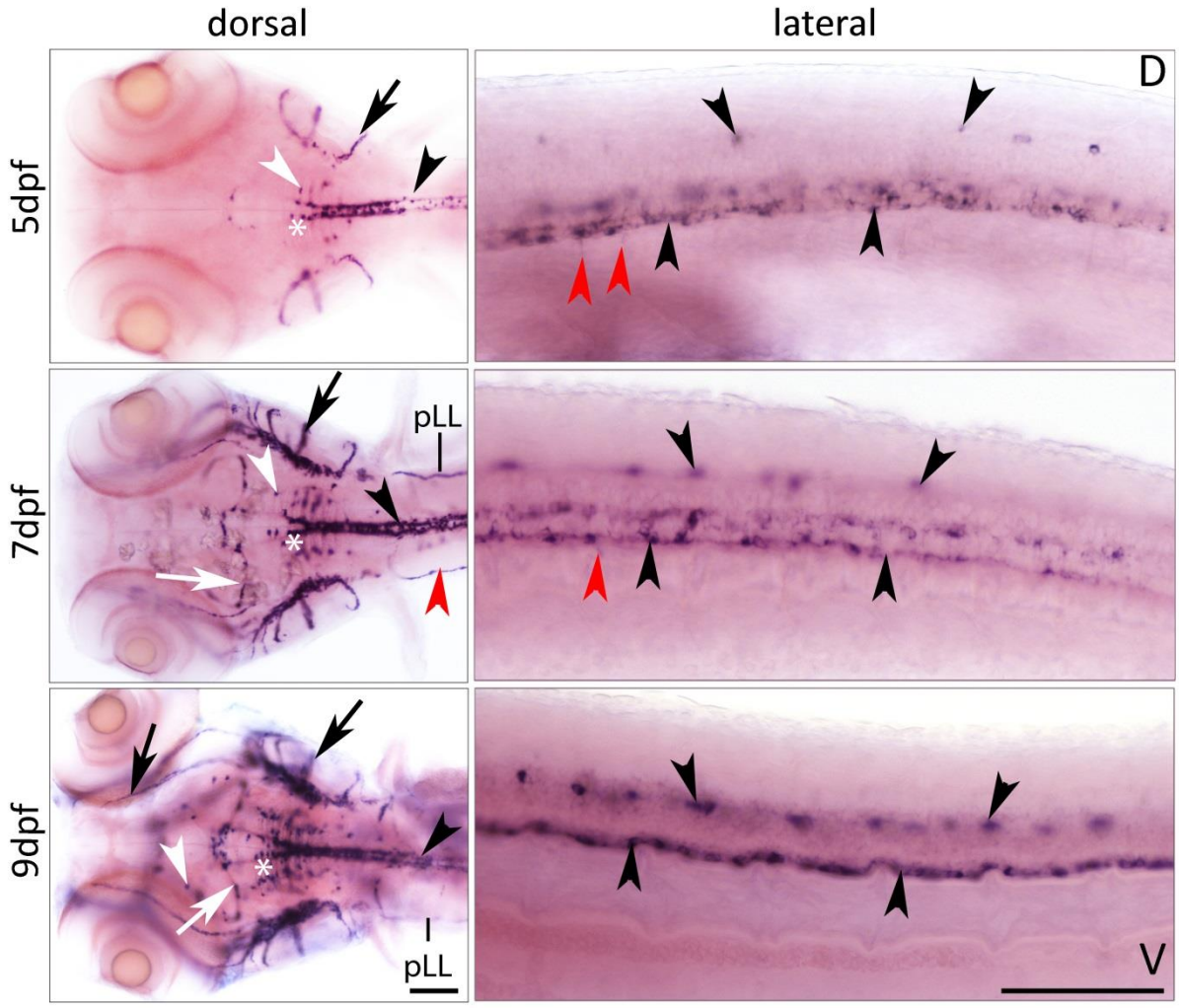

Figure 5.11: *Mbp* expression in oligodendrocytes and Schwann cells of Medaka **embryos at 5, 6 and 9 dpf**

Myogenic basic protein (mbp) WISH within the CNS and PNS of wild type Medaka embryos at 5, 6 and 9 dpf. **Left panel)** shows the central nervous system (CNS) at different stages of embryonic development in which cranial ganglia (black arrow), reticulospinal neurons

(asterisks) and individual cell bodies (white arrow head) and long axial protrusions of individual oligodendrocytes (white arrows) are visible. Note oligodendrocyte branching extents to fully maturation by 9 dpf. Spinal cord residing oligodendrocytes are visible within the posterior hindbrain region (black arrow heads). Posterior lateral line Schwann cells (red arrow head) are detectable especially at 7 dpf (red arrow head). **Right panel)** labels trunk oligodendrocytes within dorsal and ventral spinal cord (black arrow heads). Individual Schwann cell axons are detectable in 5 and 7 dpf embryos extending ventrally from the spinal cord (red arrow heads). Left panels scale bar = 100µm, right panels scale bar = 500µm.

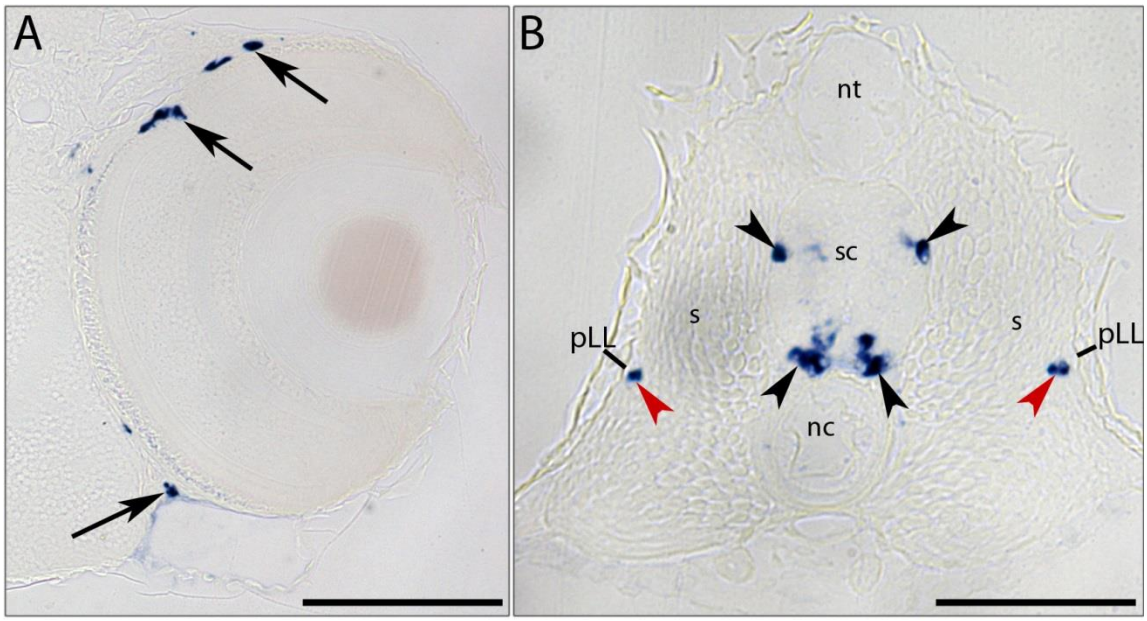

Figure 5.12: Resin sections from 7 dpf wild type embryos after *mbp* WISH

Resin sections from 7 dpf old embryos representing *mbp*$^{+}$ cells within the eye (A) and trunk (B) region. **A)** Oligodendrocytes (black arrow) in the anterior region of the optic cup. **B)** Trunk region showing morphological features such as neural tube (nt), spinal cord (sc), notochord (nc) and somites (s). *Mbp*$^{+}$ oligodendrocytes (black arrow head) situated ventrally and dorsally of the spinal cord, whereas Schwann cells are located within the posterior lateral line region (red arrow heads. Resin sections = 8µm. Scale bar = 50µm

In summary, we have successfully shown that CNS oligodendrocytes and PNS Schwann cells are labelled in Medaka embryos beyond 5 dpf. It would be interesting to analyse *mbp* expression pattern at 4 dpf and earlier and compare it to *hirame* at the same time. This would enable us to study *hirame's* CNS and PNS development in detail for any defects. For instance, we could envisage that a defect in Schwann glia cells might be due to Neuregulin I type III (NrgI), as studies have shown that it regulates directed Schwann cell migration along the posterior lateral line nerve in mice (Perlin et al. 2011). This migration herein was dependent on ErbB receptors. Signals from *nrg1* ligand might therefore be essential to ensure that these glia are present in the correct numbers and positions in the developing nerves. A defect in migrating Schwann cells might connect the Hippo pathway to neural crest guiding signals such as NrgI expression and ErbB receptor.

5.2.5 Enteric nervous system progenitors

Neural crest cells form the preganglionic neurons of the enteric nervous system (ENS) after they migrate into and colonise the entire gut primordium of the gastrointestinal tract (Le Douarin et al. 2004).

The migration distance NC enteric neurons and glia undertake, exceeds that of any other neural crest cell derivatives. Chick and mice studies have shown that ENS derived NCCs initiate mainly from a vagal (hindbrain) region in the head and a subset of neural crest from a sacral trunk region caudal to somite 28 in chick and 24 in mammals (Yntema & Hammond 1955; Douarin & Teillet 1987; Anderson et al. 2013). After colonising the gut, neural crest-derived cells within the gut wall then differentiate into glial cells plus many different types of neurons, and generate the most complex part of the peripheral nervous system (Anderson et al. 2013). Failure of NCCs to populate the entire gut with enteric neurons can lead to congenital diseases such as, Hirschsprung's disease (HSCR) leading to defects in which patients suffer from intestinal obstruction or severe constipation.

The paired-like homeobox 2 protein (Phox2b) is a homeodomain neuronal-type-specific transcription factor expressed in a pattern which suggests their involvement in neural fate determination. Pattyn et al. in 1999 demonstrated the requirement of phox2b for complete differentiation of the enteric nervous system (ENS). His study described enteric neurons in *phox2b* homozygous null mice failed to migrate beyond the anterior gut primordium leading to embryonic lethality between e10 and e13.5 (Pattyn et al. 1999). Because of its involvement in neuronal development, studies have used *phox2b* to label the following structures in Zebrafish: enteric nervous system, epibranchial ganglion, epibranchial placode, facial ganglion, glossopharyngeal ganglion, hindbrain, pharyngeal arch 3-7, statoacoustic (VIII) ganglion, superior cervical ganglion, sympathetic chain ganglion and vagal ganglion (Elworthy et al. 2005; Z-Fin webpage 2014).

To date there are no publications analysing the expression pattern of the paired-like homeobox 2 protein (PHOX2b) in Medaka fish. Here, we attempted the optimisation of an anti-sense *phox2b* riboprobe via WISH (a gift from Dr H. Hashimoto) and a representative set of images of 4 dpf old embryos was analysed using comparison with the existing expression patterns found in Zebrafish. Within the head region (Figure 5.13) we were able to visualise epibranchial arch structures, especially the *phox2b* expressing facial placode or ganglion, glossopharyngeal placode or ganglion and vagal placode or ganglion. Furthermore, a subpopulation of vagal neural crest cells could be visualised, known to contribute to the enteric nervous system (ENS) of the developing gut primordium. In addition we have seen strong *phox2b*-positive cells in regions in the hindbrain not comparable to the *phox2b* pattern in Zebrafish (Pei et al. 2013). This included the presumptive lateral rhombomeric lip, a region closely related to published data describing ventricular hindbrain opening (Wullimann et al.

2011) and presumably *phox2b*$^{+}$ regions which might relate to the anterior and posterior trigeminal motor neuron and facial motor neuron (Ohata et al. 2009). Within the trunk of wild type embryos, neural crest cells completely populated the entire gut primordium up to the anus (Figure 5.14) by 4 dpf. The dorsal aorta also expressed *phox2b* in a comparable fashion to Zebrafish (Elworthy et al. 2005).

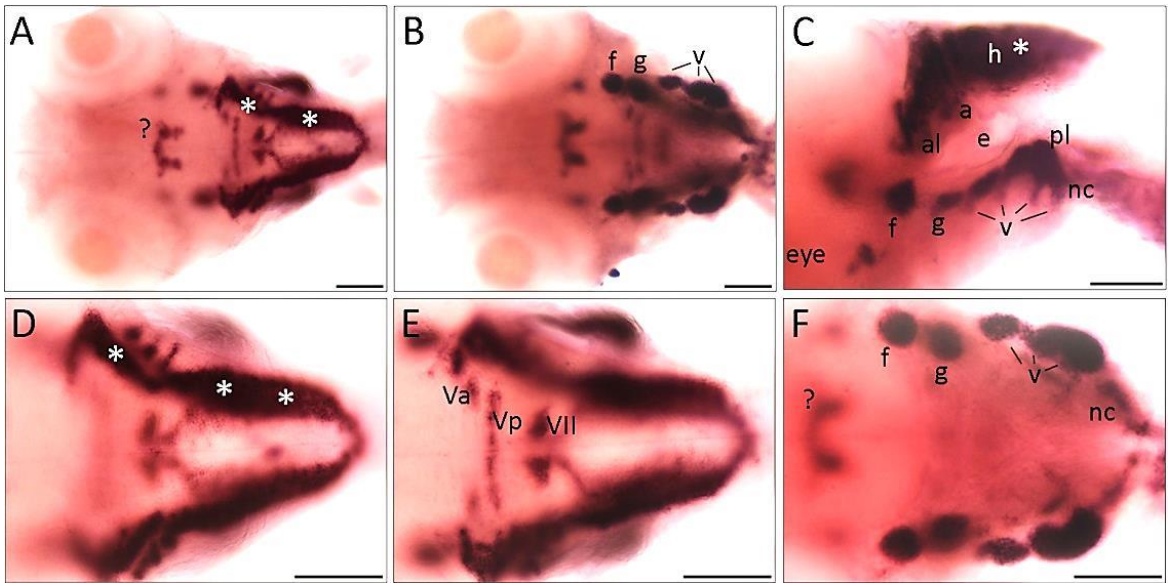

Figure 5.13: *Phox2b* expression in the head of 4 dpf wild type embryos reveals new locations

Images at different vocal planes after *phox2* WISH. **A)** Dorsal focal plane of the head highlighting the presumptive lateral rhombomeric lip of the hindbrain ventricular opening (white asterisks) and an unspecified *phox2b*$^{+}$ region within the midbrain **B)** Ventral focal plane of the head showing epibranchial arches **C)** lateral view labels head ganglion, including facial placode or ganglion (f), glossopharyngeal placode or ganglion (g) and vagal placode or ganglion (v). In addition neural crest derived vagal ganglion contributing to the enteric nervous system (ENS) are seen (nc) **D-F)** higher magnification of B respectively in different focal planes highlighting *phox2b*$^{+}$ cells. **D**, highlighting the ventricular opening (white asterisks) of the hindbrain; **E**, representing presumably the anterior and posterior trigeminal motor neuron (Va and Vp) and facial (VII) motor neuron; **F**, epibranchial arches as described in C. Abbreviations: a, acoustic ganglion; al, anterior lateral line ganglion; e, ear; f, facial placode or ganglion; g, glossopharyngeal placode or ganglion; h, hindbrain; nc, neural crest population; pl, posterior lateral line; v, vagal placode or ganglion. Scale bars = 100µm (at different magnifications)

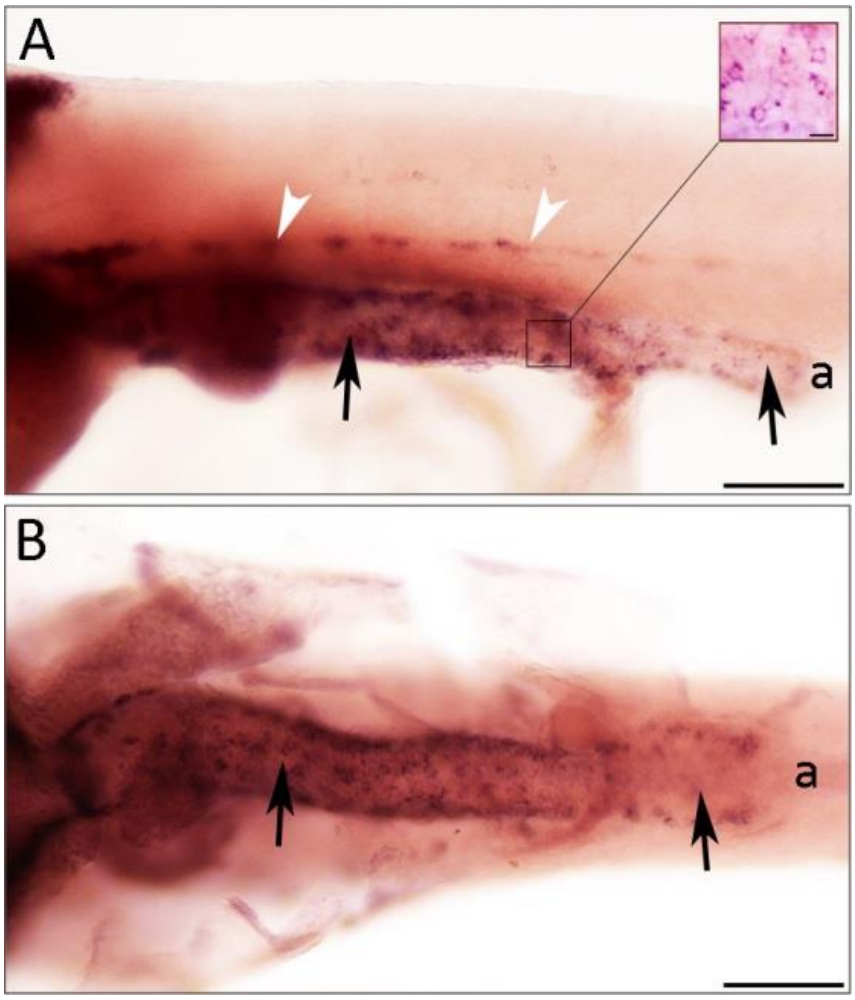

Figure 5.14: Phox2b in enteric neurons and trunk region of 4dpf wild type embryos.

WISH of 4 dpf embryos labelling *phox2b*$^{+}$ cells within the trunk region. **A)** lateral view, enteric neurons (arrows) have fully penetrated the developing gut up to the anus. Inset showing single neurons within the posterior region of the gut. Above the gut *phox2b* also labels the presumptive dorsal aorta (white arrow heads) **B)** Ventral view of the trunk showing enteric neurons (arrows) throughout the entire gut area. Scale bar = 100µm

The expression profile of Medaka phox2b matches the one of Zebrafish, in which enteric neurons in the gut including the ventral aorta (Elworthy et al. 2005). This suggests that despite any dissimilarity, the *phox2b* anti-sense probe labels neural crest enteric gut derivatives in both Zebrafish and Medaka. Based on this, it should therefore be possible to investigate further neural crest migration towards the gut primordium in *hirame* mutants at 4 dpf (st.32) and earlier, which could provide insights into how far the loss of functional YAP affects intestinal NC cell migration.

5.3 Discussion

5.3.1 Reduction of xanthophores in *hirame* mutants

Analysis of a second pigment cell marker *GTP cyclohydrolyse I (gch)* labelling the leucophore and xanthophore pigment cell lineage in Medaka revealed that *gch* positive cell numbers and distribution at stage 24 is similar in *hirame* to wild type sibling embryos. At that stage it is likely we observed only leucophores present within the fore- and hindbrain area as the onset of xanthophore differentiation in Nagao's study was only detected later around 27 somite stage (st.27), meaning that leucophore development at stage 24 in *hirame* is not compromised by the loss of functional YAP protein.
In contrast, as soon as xanthophore lineage specification occurs, we could observe a dramatic increase in *gch* positive cells within the whole body of wild type embryos, not detectable in *hirame* siblings at stage 28. Although at this stage the marker labels both leucophores and xantophores, we speculate that this significant difference in cell numbers most likely reflects an abolishment of the xanthophore lineage only. We could speculate that the defect in xanthopore proliferation might be caused by altered PAX3 levels as *pax3* is one of the earliest known marker for NC in Zebrafish and plays an important role for NCC EMT delamination from the neural tube, and is necessary for subsequent NC lineage specification in Zebrafish (Donoghue et al. 2008).
To test the possibility of a complete xanthophore absence, we need to analyse both cell types separately. First we could image and quantify autofluorescent leucophores within living stage 28 embryos, then substract this number from totals obtained after *gch* WISH, resulting in separation of leucophore and xanthophore populations. Secondly, we could analyse the expression pattern of another xanthophore specific marker like *xanthine dehydrogenase* (*xdh*) known to be lineage specific in Zebrafish (Parichy & Ransom et al. 2000). However Nagao et al. showed in his study that *xdh* also labels leucophores and xanthophores underpinning the fact that both cell types contain pteridines (sepiapterin in xanthophores and drosopterin in leucophores), making *xdh* non-specific marker of xanthophore lineage. Indeed their observations indicate that a xanthophore-specific marker may be very difficult to identify in Medaka. Furthermore, Nagao´s data strengthens our assumption of a lack of xanthophore formation as the *hirame gch* cell counts in stage 28 are comparable to leucophore counts obtained by Nagoa in 5dpf wild type embryos suggesting that we were only quantifying leucophores in stage 28 *hirame* embryos and not xanthophores.
One hypothesis is *hirame* decreased xanthophore proliferation. This idea is based on the assumption that the gch^{+} cell incline in st.28 is due to a slight increase in leucophore numbers. We could speculate that the defect in xanthopore development might be caused by altered PAX3 levels. Pax3 is the earliest known marker for NC in Zebrafish and plays an important role for NCC EMT delamination

from the neural tube, and is necessary for subsequent NC lineage specification in Zebrafish (Donoghue et al. 2008). Mutations in PAX3 cause human congenital pigmentation disorders such as Waardenburg syndrome type I leading to a pigmentary disturbances of the iris, hair, and skin, along with hearing loss (Milunsky 2001). In mice, the pax3 mutant *Splotch* exhibits a reduced melanocyte pigment cell phenotype. However, melanocyte precursors (melanoblasts) develop and migrate normally, suggesting a role for pax3 in the expansion of melanoblasts (reviewed by Tremblay and Gruss, 1994) (Tajbakhsh et al. 1997). In fact another study by Gee et al. in (2011) demonstrated in Xenopus that YAP directly regulates *pax3* via the TEAD DNA-binding domain and is able to expand the $pax3^{+}$ neural plate border zone (pax3+) when overexpressed, indicating a direct relationship. Contributing data comes from recent studies in Zebrafish by Minchin & Hughes (2010). They have shown that knockdown of pax3 led to specific xanthophore and enteric neuron reduction especially in the trunk along with a dramatic increase of melanocytes in later stages after an initial reduction in melanoblast numbers and migration at early stages. The decrease in xanthophores later strongly correlated with an increase in the numbers of melanocytes at later stages. This correlation has not been observed in homozygous *hirame* mutants as melanocyte numbers seem to be reduced and do not recover until embryonic lethality at 4 dpf. The melanophore development and migration failure prior to 48 hpf Minchin & Hughes have observed, could reflect either a cell autonomous requirement for Pax3 in early NC cells, or an environmental effect on NC initiation and migration. In splotch mouse mutants however, it is not clear if the observed melanocyte defect might have recovered as splotch homozygous mice die at E14, but it is shown that heterozygous mice do exhibit melanoblast migration defects, and humans with Wardenburg Syndrome I with dominant *PAX3* loss of function mutation show pigmentation alterations. In fact another study by Gee et al. in (2011) demonstrated in Xenopus that YAP directly regulates *pax3* via the TEAD DNA-binding domain and is able to expand the $pax3^{+}$ neural plate border zone (pax3+) when overexpressed, indicating a direct relationship. Therefore, it might be possible that YAP influences or controls PAX, thus resulting in early melanoblast migration defects. Because *hirame* is embryonic lethal, we cannot know if this defect would recover later or not. Our data however firmly suggests that loss of YAP in *hirame* before 4 dpf ablates xanthophore development and reduces later melanocyte numbers dramatically as previously shown.

5.3.2 Abnormalities of elavl3/HuC expression within the head and developmental defects within DRG's in *hirame* mutants

Aspects of Zebrafish sensory neurogenesis are controlled by a single neurogenin 1 (neurog1) gene compared to two neurog1 and neurog2 in mammals and birds. In Zebrafish, neurogenin1 is expressed in all neurogenic placodes including trigeminal, lateral line, epibranchial placodes and otic vesicle, which will later form the acoustic ganglion and in neural crest precursors for DRGs. In mouse studies, even so the expression of ngn1 was transient, and knockdown of ngn1 blocks differentiation of all Zebrafish cranial ganglia as well as trunk dorsal root ganglia (Ma et al. 1999; Andermann et al. 2002). The early neuronal marker HuC antibody recognises Hu antigens encoded by elavl3. It marks neuronal precursors and the differentiated peripheral nervous system, and has been used to analyse neuronal structures in the *hirame* mutant at different stages of embryonic development.

Our findings in section 5.2.2 indicate that loss of YAP leads to misplaced cranial ganglia in stage 24 *hirame* embryos, which seem partially recovered by stage 28, in which posterior cranial ganglia and ganglia arising in the region of rhombomere 4 are positioned more closely to the body axis. However, the size and overall structure is still dissimilar from its wild type siblings. We also observed that the hindbrain ventricular zone opening is much narrower in *hirame* mutants in which rhombomeric structures 1 to 7 were hardly distinguishable due to smaller neuronal boundaries. The hindbrain also seems to lack expression of elavl3/HuC within the presumptive upper rhombic lip underneath the cerebellum and the mid-hindbrain-boundary (MHB). Determining whether this structure is completely missing or just lacking neuronal expression requires further investigation. Two possibilities present themselves for this: firstly to section st.32 embryos and analyse morphological differences, and secondly label the individual hindbrain regions. The hindbrain ventricle opening could be labelled with ZIC family member 1 and 4 (*zic1* and *zic4*) (Elsen et al. 2008), upper rhombic lip and dorsal neural progenitors could be specifically labelled with *atonal homolog 1a-c* (*atoh1*) and the underlying ventricular zone with *pancreas specific transcription factor 1a (ptf1a)* (Kani et al. 2010). This would more reliably determine which tissue structures are partly or fully present, or absent. Another observation was the absence of complete forebrain structures throughout both stages in *hirame*, which might be analysed through morphological structure examinations as well.

Furthermore we observed a significant reduction in the number of dorsal root ganglia within the trunk region in *hirame* mutants. Our somite counts at stage 32 revealed that *hirame* develops similar quantities of somite pairs to wild type embryos, which excludes the possibility of general developmental retardation. This suggests that the defects seen within the DRGs are likely to reflect a real role for YAP in DRG neural development. We hypothesise that the level of neurogenic factors such as ngn1 driving DRG specification and migration could be affected. Analysing the expression

levels of ngn1 with in-situ hybridisation could be taken into consideration. We have recently obtained and tested the ngn1 anti-sense probe for Medaka (gift from Dr H. Hashimoto), however the purity and specificity of the signal remains to be optimised fully (Appendix 13). Even after optimisation, such as altering permeabilisation time or probe length, the background levels were still high and neurogenic signal remained weak, making the Medaka ngn1 a difficult probe to use reliably. Another possibility would be to quantify expression levels in separate trunk sections of st. 32 *hirame* embryos, as we would assume a drop in neurogenin levels. The same experimental approach could be taken when analysing Sox10 levels in *hirame* mutants to investigate whether defects in neural crest derivatives investigated so far could be due to altered levels of the early NC marker.

5.3.3 *Sox9b* expression analysis within wild type and *hirame*

In 2005 Klüver et al. identified the second *sox9* orthologue in Medaka through sequence analysis and linkage mapping as well as expression pattern. Our aim was to investigate the *sox9b* expression in *hirame* mutants at different stages of development to establish any links between the loss of YAP and the expression of early neural crest marker *sox9b*. In general the expression pattern we have observed with the *sox9b* anti-sense probe made by Dr H. Hashimoto matched the published data from Klüver et al. which means we have successfully labelled the same orthologue of *sox9*.
Our *in situ* hybridisation at early stage 20 (1 day 7.5 hpf) showed strong expression within the craniofacial neural crest in the hindbrain region, otic placode precursors and trunk neural crest along the lateral body axis. Our finding affirm the *sox9b* expression pattern found in early zebrafish development (Li et al. 2002) in which the neural crest and otic placode lineage was marked. In wild type this expression pattern was very distinct. However, in *hirame* siblings we observed additional *sox9b*$^{+}$ cells still situated on top of the yolk sac. Because the ectopic cell expression in *hirame* was diminished in later stage 24 embryos, we conducted cross sections in the region of the preplacodal ectoderm and analysed *in situ* hybridisation at earlier stages of embryonic development. Whole-mount *in situ* hybridisation confirmed that between st.17 and st.19 *hirame* embryos exhibited a 5.5h delay in migration of *sox9b*$^{+}$ prospective neuroectoderm towards the midline, and ectodermal *sox9*$^{+}$ cells in *hirame* remained on top of the mesenchyme. We speculated that the migration delay is likely due to a slower convergence during gastrulation. A real-time imaging series confirmed that in *hirame* embryos the migration of the enveloping shield of the blastoderm seem to be delayed, resulting in slower *sox9b* expression in cells towards the embryonic shield.
However, the migration delay of *sox9b*$^{+}$ cells within the blastoderm seen in *hirame* mutants is possibly a secondary effect of the delay in epiboly closure itself caused by a migration delay in underlying cell layers. It is likely that deep cells (mesodermal and endodermal) migrate slower, which

consequently delays epiblast (ectoderm) migration. This would indicate that the *sox9b*$^{+}$ ectodermal neural crest and placodal precursors are migrating slower on top of the hypoblast, an arrangement we have seen in our resin sections (Figure 5.5).

Studies of *sox9b* at later stages in Medaka and Zebrafish have shown a *sox9*- expressing neural crest population within the trunk region (Klüver et al. 2005; Li et al. 2002; Chiang et al. 2001). Our findings using *in situ* hybridisation for *sox9b* at 3 dpf confirmed these data. Additionally we were able to observe *sox9b* expression within somites and neural crest cell populations at the dorsal midline region. Noticeably, at the tail end *sox9b* is strongly labelled in wild type embryos (Figure 5.8), a signal which seemed to be weaker towards the anterior trunk region. As well as this, in *hirame* we could not clearly identify a distinctive *sox9b*$^{+}$ region above the neural tube, unlike its wild type siblings. In Zebrafish, Li et al. argue that this region in the caudal-most proximal part of the dorsal midline is where *sox9b* cells mark the formation of the median fin. However, my speculation is that this marks premigratory trunk neural crest cells emerging from the dorsal part of the neural tube, a similar pattern observed in the neural crest marker foxd3 (Kelsh & Dutton et al. 2000). Supporting this, studies in Xenopus have shown that *sox9b* and *foxd3* are downstream targets of transcription factors of PAX3 and ZIC1, both essential to specify the NC fate in the amphibian ectoderm (Hong & Saint-Jeannet 2007; Sato et al. 2005; Bae et al. 2014).

Liu et al. have shown in 2013 that *Sox9b* is not only important for NC fat specification, but also for NC delamination in its phosphorylated state, which is induced by morphogenetic protein (BMP) and canonical Wnt signalling. This could indicate that the *sox9b*$^{+}$ cells in the proximal posterior region of the trunk close to the tail end are present during events of NCC delamination. As we could not see any of these regions more upstream anteriorly, it could mean that *sox9b* is only transiently switched on during epithelia-mesenchymal transition events and downregulated after NCCs have left premigratory positions, as low expression in the anterior wild type trunk sections confirmed. Our observed sox9b+ pattern within the dorsal trunk neural crest region at the tail end was supported by Zebrafish records (Li et al. 2002). We concluded, that the *sox9b*:gfp transgenic line established by Nakamura et al. in 2008 would provide a valuable tool for analysing neural crest processes *in vivo* in real-time. Our examination of 7 dpf embryos revealed GFP expression within the craniofacial cartilage, pectoral fin buds, the heart and the anus sphincter, confirming previously published *sox9b* expression patterns in Medaka (Klüver et al. 2005). Future experiments could include the cross of *sox9b*:gfp transgenics with Cab$^{j50\text{-}20C}$ or HB32C$^{j50\text{-}20C}$ to analyse the neural crest delamination process in vivo as we were not able to produce conclusive results of this event in *hirame* with *in situ* hybridisation followed by resin sectioning.

In this chapter we analysed various neural crest markers to draw conclusion about the role of YAP during neural crest development. Our previous melanocyte studies revealed two major findings: 1.)

Hirame exhibits an early yolk sac specific melanoblast migration defect and 2.) *Hirame* displays a drastic melanocyte reduction in later stages of development. Our aim was to complement our findings with further NC cell type defects. During early stages, the only abnormality we could find was a slower cell convergence during epiboly resulting in delayed *sox9b*$^{+}$ cells arriving to their destination sites. Other than that, all other NC defects were observed beyond st.28 (~ 3dpf). Herein, the lack of functional YAP results in a possibly complete lack of xanthophore lineage and dorsal root ganglia formation is compromised. Therefore, defects observed here cannot simply be explained by cell migration deficiencies. Late stage defects by be a result of missing YAP protein, but it might also be a secondary effect due to changed body morphology of *hirame* mutants. For instance, the shape of somite structures might influence the DRG development in some aspects. In addition, novel marker including the *myogenic basic protein 1 (mbp)* and *paired-like homeobox 2 protein (phox2b)* have been validated in wild type embryos and could be tested in future in *hirame* mutants.

6 Chapter: Conclusions and Future implications

6.1 Background

During a random mutagenesis screen carried out in 2004, Furutani-Seiki et al. discovered a unique Medaka mutant named *hirame*. This embryonic lethal mutant carries a point mutation within the first WW domain in the Yes-associated protein exchanging leucine to a stop amino acid codon in the 164th position in allele j54-20C (L164X). In teleosts maternal *yap* transcripts are ubiquitous until mid-blastula-transition. After that zygotic *yap* is enriched in tissues such as notochord, brain, eyes, branchial arches and pectoral fin (Jiang et al. 2009). *Hirame* mutants exhibit defects in convergent cell movements resulting in reduced dorso-ventral thickening. Later in development *hirame* mutants remain flat bodied including a flattening of the CNS, and develop liver abnormalities due to a failure in endodermal convergence and rod formation. Furthermore, the mutants also present mislocated tissues such as heart and the lens (Furutani-Seiki et al. 2004; Watanabe et al. 2004; Kitagawa et al. 2004). YAP is a transcriptional co-activator downstream of the Hippo Signalling Pathway which promotes cell survival, proliferation and maintenance of the 3-dimensional tissue structure (Jiang et al. 2009a; Sudol et al. 1995; Lian et al. 2010; Huang et al. 2005). Disturbance of the Hippo pathway downstream effector YAP has been described in great detail. Impressive studies demonstrate the oncogenic potential of YAP in liver enlargement (Camargo et al. 2007) and hepatocellular carcinoma (Dong et al. 2007) as well as epidermal stem cell proliferation and tissue expansion (Schlegelmilch et al. 2011). In addition overexpression in mammalian in vitro cultures revealed features of oncogenic transformation such as anchorage-independent growth, epithelial-mesenchymal transition and accelerated cell migration (Overholtzer et al. 2006; Fu et al. 2014) suggesting that overexpression of YAP in these tumours alters cell physiology causing increased primary melanoma tumour growth and metastasis formation (Lamar et al. 2012; Nallet-Staub et al. 2014). In regards to the neural crest, YAP seems to regulate the proliferation of neural progenitors within the dorsal neural tube and controls Pax3 expression (Milewski et al. 2004; Gee et al. 2011).

Our initial microscopic observations of 3 dpf (st.28) *hirame* embryos hinted towards a reduction of neural crest melanocyte numbers on the yolk sac (RN Kelsh personal communication).

However, those very limited studies of YAP function in neural crest left many questions unanswered, so that we felt that we have been given a unique opportunity with the *hirame* mutant to analyse the effects of *yap* on neural crest development.

6.2 YAP regulates melanoblast migration during early embryogenesis

Our initial microscopic observations of 3 dpf (st.28) *hirame* embryos hinted towards a reduction of neural crest melanocyte numbers on the yolk sac (RN Kelsh personal communication). We began by examining this phenotype in some detail. We have shown using *dopachrome tautomerase (Dct) in situ* studies that the first detectable melanoblast alteration in *hirame* occurs as early as st.20 (1d 7.5h). Up to stage 21 total melanoblast numbers are unaffected, however their distribution is altered and cells seem to rest and accumulate alongside the embryonic body axis rather than migrating proportionally onto the yolk sac. This is the earliest neural crest defect after maternal yap transcripts were undetectable and before the *hirame* body collapses (st.22) (Porazinski 2013), indicated that this melanoblast defect is likely directly due to the lack of functional YAP and not because the three-dimensional body structure has been compromised. Beyond st.21, the number of melanocytes stabilises or gradually decreases in *hirame* mutants, compared to wild type in which those numbers increase dramatically. To date, we are not sure if a lack of proliferation or apoptosis causes the reduction of melanocytes observed in *hirame*. To test the possibility of low cell survival, a terminal transferase dUTP nick end labelling (TUNEL) assay could be performed in parallel to *Dct in situ* whole-mount hybridisation. This approach would reveal if melanoblast survival is limited in *hirame* embryos. Another hypothesis is that melanoblast proliferation in *hirame* is reduced. Cell proliferation can be tested with 5-bromo-2´-deoxyuridine (BrdU) and possibly could be connected with *Dct* whole-mount *in situ* hybridisation. The idea is to treat embryos with BrdU, which incorporates into newly synthesized DNA during cell proliferation. After BrdU treatment over a 24h period, embryos could then be fixed and *Dct in situ* hybridisation will be carried out. Anti-BrdU antibody staining will follow to obtain double staining and determine proliferation within the melanoblasts cell population. *Hirame* mutants provide a currently unique model in which to assess the role of Hippo signalling in melanoblast migration during early embryonic stages. This may be of particular relevance to address key aspects of cancer migration as well. Both, NC and cancer cells are known to migrate alone or as collective groups (Woods et al. 2014; Wong et al. 2014). In addition, active and highly migratory neural crest cells exhibit features during development similar to cancer cell progression, starting from epithelial-mesenchymal transition to active migration into distant sites of the body which requires the need to adapt to numerous tissue environment (Uong & Zon 2010). Because of those similarities, it has been suggested that some tumours might recapitulate parts of NC development in a dysregulated manner (Duband, 2010; Kerosuo and Bronner-Fraser, 2012; Lim and Thiery, 2012; Theveneau and Mayor, 2012; Thiery et al., 2009).

6.3 Future potential of the novel Medaka *Dct*:eGFP transgenic lines

To broaden our analysis of the melanocyte defect observed in *hirame*, we aimed to utilise a promoter under which we could one hand label melanoblasts and track their *in vivo* progression and on the other hand express target genes in future studies. We do know of another Medaka fish line expressing GFP in melanocytes under the control of Medaka tyrosinase promoter (Martinez-Morales et al. 2009). However, the expression pattern in this line has not been published in detail. In addition, we were not able to obtain the *tyr* anti-sense probe for comparison studies to *Dct.*

We characterised and validated a Medaka *Dct* promoter fragment recapitulating endogenous expression in melanocytes, which we utilised to establish *Dct*:eGFP transgenic lines. Germline transmission was achieved in 8 lines revealed melanocyte-specific eGFP expression up to larvae stage, although 2 of these lines melanocyte expression was mosaic, likely due to clonogenic silencing mechanisms. None, of the lines showed ectopic cell expression making our construct remarkably reliable for transgenesis studies. Although not achieved in this work due to time constraints, a natural next step would be to use these *Dct*:eGFP transgenic lines to analyse the *in vivo* melanocyte patterning defect in *hirame* mutants in real-time during embryonic development by time-lapse microscopy. This would nicely complement the proliferation and TUNEL experiments suggested above, as well as providing direct evidence of the proposed melanoblast migration defect.

During polarised cell migration, molecular events at the leading edge of the cell are coordinated with those at the trailing edge, an organisation which is well characterised, especially in regards to the actin cytoskeleton and adhesion molecules (Ridley et al. 2003). Actin assembly at the leading edge of the cell is associated with the filopodia formation required for directed migration, whereas at the back molecules connecting to actin get disassembled and retract from the surface the cell migrates on (Le Clainche & Carlier 2008). The formation of filopodia is a result of the cell acting to external stimuli. This leads to an asymmetric redistribution of cell-surface receptors, internal cytoskeleton arrangement and establishment of a leading protruding edge (Ridley et al. 2003). If the internal polarity network is inhibited, the cell cannot perform directed cell migration, resulting in decreased migration speed and increased filopodia number. With our new *Dct*:eGFP transgenic lines we now have a platform with which to track individual melanoblast cells *in vivo* in *hirame* and wild type embryos as early as st. 20 to determine the polarity of individual melanoblasts during yolk sac cell migration. Widespread cytoplasmic eGFP would label the entire cell, highlighting cell protrusions and the position of the nuclei. Consequently, they should permit assessment of the amounts and direction of protrusions, allowing us to establish whether in *hirame* mutants melanoblasts undergo

directed migration, or if polarity is lost. The Medaka *Dct*:eGFP transgenic lines would also provide a valuable tool for pigment cell researchers studying other Medaka pigment cell mutants (Kelsh et al. 2004). For example, it could be a used to determine at what stage and region neural crest cells become committed to the melanocyte lineage in Medaka embryos, as this has not been done to our knowledge. In addition, the promoter now provides a well-characterised tool for transgenesis purposes and could be combined with pigment cell mutants to answer questions about their genetic influence on the melanocyte lineage. The Dct:eGFP line could also be utilised to isolate cells for instance with FACS sorting. Once the pigment cell population is isolated it can then be individually analysed for instance for its transcriptional finger print or proteomics.

6.4 Yolk sac membrane cells undergo apoptosis

We unexpectedly observed fragmented nuclei within the yolk sac membrane in *hirame* embryos, which we hypothesised could contribute to why melanoblasts do not migrate onto the yolk sac. Transmission electron microscopy revealed that karyorrhexis is accompanied by apoptotic bodies separated by a membrane, one of the characteristics of programmed cell death compared to necrosis (Corcoran et al. 1994).

We hypothesised that, if YAP action in melanoblast migration is non-cell autonomous to the melanoblast, *yap* mRNA injection into the yolk sac would rescue the melanoblast migration defect through restoration of environmental factors in the yolk sac membrane. The principle of this experiment is insofar attractive, because it might propose another way of introduce mRNA or other substances into the embryonic tissue. Sadly, this experimental method yielded no success, either due to biological uncertainties with the experimental approach, or because YAP functions cell-autonomously within melanoblasts. So far, we are not sure, if yap mRNA was taken up by the syncytial layer and translated into functional protein to exhibit any non-cell autonomous function. One approach to help resolve this issue would be to extract cells of the yolk sac layers and then perform quantitative PCR for YAP downstream target genes to evaluate if functional YAP protein was present.

In addition, *yap* mRNA injection into the cytoplasm of one-cell stage embryos restored the melanoblast migration defect an astonishing frequency. The rescue was aided by the fact that in addition to the blastoderm, injected solutions distribute widely within the membranous layers surrounding the yolk cell as well, in which yolk sac melanoblasts migrate. Our additional data confirms that solutions do not mix between the yolk sac cytoplasm and the blastoderm, because cytoplasmic streaming does not occur in Medaka. One of the possibilities discussed is that functional

YAP protein restores the extracellular matrix components that provide cues for migrating melanocytes (Duband & Thiery 1987; Sternberg & Kimber 1986; Trainor 2013). To test that, we could perform immunohistochemical analyses for ECM components to assess their polymerisation status.

6.5 Drawbacks and potential of a *Dct*:eGFP-YAP transgenic line

One of our interests was to investigate if overexpression of YAP within the melanocyte lineage driven by the Medaka *Dct* promoter could rescue the melanocyte patterning defect in a cell-autonomous fashion. We successfully established an overexpression cassette in which an *egfp* reporter gene is linked to either a wild type or a mutated activated form of YAP (S87A). Unfortunately, we came across some major setbacks when we established those overexpression lines. We did not observe evenly distributing and lasting eGFP expression within cells. EGFP-YAP fusion protein seemed to aggregate and photobleach within some cells, whereas the majority of melanoblasts remained unlabelled. In general, most transgenic embryos exhibited this phenotype and further investigations need to be carried out to explain this phenomenon. Our favoured explanation is that the error might be due to protein misfolding or toxic fusion protein levels.

The important question is whether we obtained any functional YAP fusion protein within the melanocyte lineage. This could be assessed by qPCR for altered expression of YAP downstream target genes. The opportunities given by a successful transgenic line, even if we are not able to see eGFP, would be immense. It would first answer the question whether YAP can act cell-autonomously for melanocyte migration and possibly could influence their numbers as well. It might also have the potential to alter the melanocyte physiology and might generate melanocytes of a precancerous state. This would be a feature to look out for as overexpression of YAP has been reported to have oncogenic potential and transform epithelial cells as well as accelerate metastatic melanoma growth (Overholtzer et al. 2006; Nallet-Staub et al. 2014). In that case, our transgenic line could turn into a another teleost melanoma model to already existing well know ones available to date (Patton et al. 2005; Michailidou et al. 2009; Anelli et al. 2009; Feng et al. 2010; Schartl et al. 2010).

One general setback on which we have not embarked before, was that we do not have a refined YAP anti-sense *in situ* probes, which would clearly label the spatio-temporal expression of *yap* either in normal melanocytes or within the melanocyte pattern of our *Dct*:eGFP-YAP transgenic lines. ISH analyses in Zebrafish have demonstrated that *yap* is nearly ubiquitous without distinctive melanocyte pattern (Jiang et al. 2009b). This could mean that either YAP is not present within melanocytes or the transcription level is below the detection threshold. Alternatively, we could consider an antibody

detection method. However, so far we could not manage to find an optimal antibody without background noise, as Western Blotting using Medaka cell extractions included non-specific antibody binding (Dr H. Davies personal communication; data not shown),

The potentials of this transgenic line lay towards drug screening models and models to study cancer initiation and progression *in vivo*. If it could be shown that these lines in some way promoted melanoma formation, we could face a potential drug screening system in which we could test YAP specific targeting in a live *in vivo* melanoma model. Some of the drugs, we might be able to use are to limit oncogenic YAP activity are: Verteporfin, Latrunculin A/B/C, Blebbistatin, ML7, Botulinum and Y27632. Verteporfin (brand name *Visudyne)* inhibits the YAP–TEAD interaction and subsequently transcriptional activity mammalian *in vitro* culture studies. It also reversed the liver expansion and development of hepatocellular carcinoma caused by YAP overexpression or *Nf2* deletion in mouse livers (Liu-Chittenden et al. 2012) (Wada et al. 2011). YAP is regulated by the amount of F-actin stress fibers, the mechanical tension through extracellular force and the cell geometry (Dupont et al. 2011). The disruption of F-actin stress fibers or actin polymerisation with F-actin targeting Latrunculin A/B/C indirectly inhibited YAP nuclear localisation as well as YAP/TEAD activity in numerous *in vitro* cell lines, as (Dupont et al. 2011; Wada et al. 2011). Some other less well studied drugs which might indirectly inhibit YAP`s nuclear presence are Blebbistatin which targets through the non-muscle myosin tested in various cell lines (Johnson & Halder 2014; Dupont et al. 2011). The same applies to ML7 actin through MLCK, Botulinum toxin C3 through RHO and Y27632 (Dupont et al. 2011) having an impact on YAP activity by effecting with RHO kinases (Johnson & Halder 2014).

6.6 YAP regulates the development of late stage xanthophores and dorsal root ganglia

We demonstrated that the number of late deriving melanocytes was compromised. Similar results were obtained in xanthophores, the second pigment cell type, using the marker GTP *cyclohydrolyse* I (*gch*). *Gch* is the enzyme converting guanosine triphosphate (GTP) to dihydroneopterin triphosphate and later to tetrahydrobiopterin (BH4), a required substrate for pterine pigments in early xantophores. Compared to Zebrafish *gch* does not label early melanocytes (Parichy & Ransom et al. 2000), but has been reported to include leucophores (Nagao et al. 2014). We observed that the early population of leucophores within the ventral head and the anterior trunk is not affected in *hirame* embryos before xanthophore differentiation occurs. In contrast, the xanthophore numbers are

dramatically reduced or even completely lacking in *hirame* beyond 3 dpf. A complete loss of xanthophore differentiation would have major implications of the requirement of YAP for xanthophore commitment and would identify YAP as a potential specifier of this lineage. To establish the complete loss of xanthophore differentiation, we would need to find a way to distinguish leucophores and xanthophores. Studies suggest that xanthophores can be visualised via UV (Nagao et al. 2014), whereas leucophores exhibit strong autofluorescence when excited within the wavelength of green to red light (equivalent to 488-564nm). This might be one way to separate those two cell types. Within the trunk region, we observed a reduced number of peripheral dorsal root ganglia in late stage embryos. Just like the melanocyte phenotype, this defect may result directly from a lack of YAP, rather than simply a result of developmental retardation since somite counts are normal in stage-matched embryos. Despite the fact that somite pairs were deformed, the actual numbers were very similar to wild type embryos.

6.7 YAP regulates migration of *sox9b* positive cells during gastrulation

We have shown that the Medaka *sox9b* isoform we obtained matched the early expression profile in wild type embryos described in published records (Klüver et al. 2005). At st. 20 wild type siblings exhibited strong cranial and trunk neural crest labelling as well as otic placodal precursor. It also highlighted that in *hirame* those ectodermal cell populations showed a pattern consistent with slower convergent-extension movements. At later stages, *sox9b* marks premigratory trunk neural crest in wild type embryos, which we were not able to visualise in *hirame*, possibly to the collapsed body morphology and weak *sox9b* expression.

6.8 Expression pattern of novel Medaka neural crest markers *mbp* and *phox2b*

We also attempted an initial analysis of novel Medaka neural crest markers *myelin basic protein (mbp)* and the *paired-like homeobox 2 protein (phox2b*). When we examined the spatio-temporal expression pattern of *mpb*, we could observe striking similarities to those in Zebrafish. It clearly labelled the branchial arches within the lateral region of the head. It also revealed some anatomical structures we have not been able to find in the Zebrafish literature. We observed individual cell

bodies and axonal branching, which might be reticulospinal neurons within the hindbrain region. Within the trunk region, characteristic *mbp*$^{+}$ Schwann cells were clearly labelled as well as individual oligodendrocytes. Because Schwann cells have already fully migrated along the posterior lateral line towards the tail end and oligodendrocytes within the spinal cord are formed by 5 dpf, we hypothesise that it might be possibly to assess the *mbp* expression pattern in *hirame* embryos to assess whether there may be an effect on the peripheral nervous system in this mutant.
The phox2b expression pattern turned out to label structures comparable to those seen in Zebrafish as well as ones. It labelled clearly facial placodes or ganglion, glossopharyngeal placode or ganglion and vagal placode or ganglion, as well as vagal neural crest cells known to contribute to the enteric nervous system (ENS) of the developing gut primordium. All of those structures can be found in Zebrafish as well (Elworthy et al. 2005; phox2b on Z-fin database). We also observed *phox2b* expression in new locations, not described in Zebrafish before. This included the presumptive rhombomeric lip (Wullimann et al. 2011) and a population of trigeminal and facial motor neurons. Within the trunk we observed close similarities to the phox2b expression pattern seen in Zebrafish, in which the enteric neurons and ganglia are labelled as well as the ventral aorta.
The difference we have found especially within the head region might be due to evolutionary convergence between Zebrafish and Medaka placing them 115-200M apart from each other (Furutani-Seiki & Wittbrodt 2004) . Zebrafish has two duplicates of *phox2* genes, *phox2a* and *phox2b* (ensemble). Medaka seems to have different duplicates or isoforms of *phox2b* transcripts, however only one *phox2b* has been annotated (ensemble). Our hypothesis is that the distant placement of Medaka and Zebrafish in evolution might have provided enough time for Medaka to develop gene duplications within the *phox2b* gene. In that case either fragments of duplicates might have been transferred or other gene fragments might have been inserted into the *phox2b* gene location. In the latter, a gene fragment required for rhombomeric lip development might have been inserted, explaining the additional expression pattern.
Overall, those two newly described neural crest markers provide another great tool for the Medaka community to study the cellular development of the central and peripheral nervous system, including neural crest derived glia.

6.9 Impact of this work

The novel findings and potentials within this work can be summarised as follows:

1. YAP regulates melanoblast migration during early stages of development and is responsible for the increase of melanocyte population beyond 1 day and 10 hours after

fertilisation. Therefore, the migration defects can be seen as a specific effect caused by lack of functional YAP protein as phenotypicall defects are not present before 1d10h. This means, cellular mechanisms involved in cell migration can be studied excusively *in vivo* in real-time during this time window.

2. YAP is required for the cell survival of yolk sac cells. This observation to our knowledge is novel and suggests that YAP is required for the extra-embryonic tissue in Medaka. Therefore, analysis of this particular type of tissue, including the syncytial layers during early gastrulation would give an interesting insight into the involvement of the Hippo pathway during gastrulation. In that regard, the delayed epiboly closure during gastrulation, we have observed, would provide additional results strengthening this proposed experimental direction.

3. YAP controls the differentiation of xanthophores as well as dorsal root ganglia. The specific hinderniss of complete xanthophore development in *hirame* is very interesting insofar any other pigment cell lineage has not been compromised in its initiation. This could hint towards the requirement of YAP in the xanthophore cell specification process originating from a pigment cell precursor. Therfore, one hypothesis could be that the loss of xanthophores could compromise for the low decrease of melanocyte numbers beyong 3dpf.

4. *Dct*:eGFP transgenic lines have been established expressing eGFP in a melanocyte specific expression as early as 1 day and 7.5 hours after fertilisation. The establishment of this transgenic line is providing a valuable tool for the wider Medaka research community. It contributes to future research output, as we are now able to investigate and monitor pigment cell development in a living Medaka fish.

5. Novel Medaka neural crest markers elavl3/HuC, mbp, phox2b and have been characterised via *in situ* hybridisation. The establishment of those probes and their thorough evaluation provides indeed another very useful tool for the wider research community wanting to utilise easy-handable neural crest markers. The availability of those markers would safe valuable time and expenses for future studies. In addition, it makes Medaka an equal model organism to work with compared to the widely-used Zebrafish, as in this field more markers are available and distributed within the community.

APPENDICES

Appendix 1: Zebrafish embryo pigmentation pattern

Dark coloured melanin-rich melanophores develop three distinct body stripes and an additional fourth stripe on the ventral side of the body. D, dorsal stripe; L, lateral stripe; V, ventral stripe and YS, yolk sac stripe. In addition, silver iridophores are present in dorsal, ventral and within the yolk sac stripe and xanthophores appear yellowish mainly in the dorsal stripe. Image taken from (Kelsh 2004).

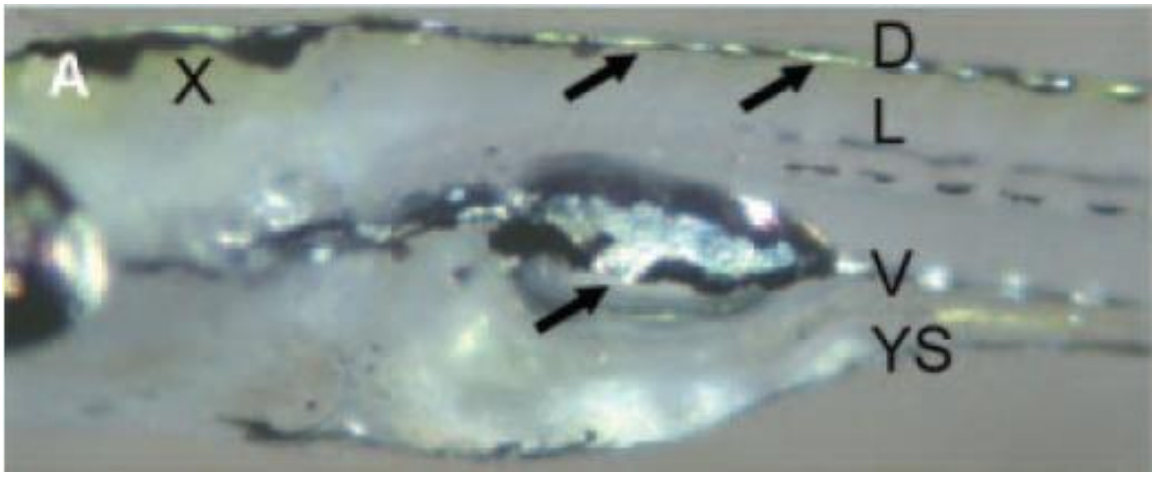

Appendix 2: Methods

In-house mini-prep DNA purification

Inoculate bacteria and grow overnight at 37°C, 225rpm

↓centrifuge at 15000 rpm, 1min

Precipitation:

↓ 100µl Sol I → vortex

↓ 200µl Sol II → invert 3-4 times

↓ 150µl Sol III → invert 3-4 times

↓ 100µl Phenoly/Chlorophorm → vortex

↓ centrifuge 15000 rpm, 3min → transfer upper layer into new tube

↓ 500µl isopropanol → vortex

↓ centrifuge at 1500rpm, 10-20min → remove supernantant

↓ was with 70% Ethanol

↓ add 20µl TE or water including 1µl RNAseA

Sol I = 50mM Glucose, 25mM TrisHCl pH 8, 10mM EDTA (autoclave)

Sol II = 0.3M NaOH, 1% SDS

Sol III = 60ml of 5M KOAc, 11.5ml acetic acid, 28.5ml ddH_2O

Preparation of resin samples

Day 1: Agarose block preparation

- Wash embryos in PBS to remove residues of glycerol
- Prepare 1.5% agarose in dH_2O
- Place embryo on clean 10cm petri dish
- Cover the embryo with a few drops of warm, but not hot agarose
- Orientate embryos quickly with forceps so that area of interest faces up and embryo is centered
- Cut out agarose blocks after solidification in the width of the mould later used
- Place blocks in acetone overnight at RT, wrap in foil

Day 2: Hardener I

- Take 0.06g of Hardener I and fill up to 10ml with cold curin resin, dissolve completely
- Exchange prepared Hardener with acetone
- Leave overnight at RT, wrap in foil

Day 3: Hardener II and embedding

- Premix 0.06g Hardener I in 10ml of cold curin resin, dissolve completely
- Take 3ml of premix and add 100µl of Hardener II (with cutted pipette tip)
  Now work fast! – once the Hardener II mix turns brown it should not be used anymore
- Place agarose block with embryo in premix (rinsing) and place it subsequently up-side-down into the well of the mould and adjust orientation with forceps
- Add Hardener II mix to the mould to cover the agarose block completely
- Seal the resin with film (if it swims on solution, take off a bit of Hardener II solution to make it air-tight)
- Place mould gently into 4°C fridge overnight

Day 4: Clean blocks – ready for use

- Remove film from mould
- Remove blocks from mould and clean with tissue
  Note: blocks should be solid and transparent; if brown and jelly-like, the resin was exposed to oxygen during polymerisation (remove more Hardener II before placing film on top)

Neutral Red counter staining

Resin sections are dried on Superfrost Plus slides (Menzel, Germany) overnight at RT

Rehydrate:	100% Ethanol	rinse
	100% Ethanol	5 min
	90% Ethanol	1-2 min
	70% Ethanol	1-2 min
	50% Ethanol	1-2 min
	dH_2O	30 min

- Stain with 1% Neutral Red (Sigma Aldrich, Cat# N7005, in dH_2O) for 3 min

Dehydrate:	dH2O	rinse
	50% Ethanol	rinse
	70% Ethanol	rinse
	90% Ethanol	rinse
	100% Ethanol	5 min

- Dry on air or heater at 37°C
- Was with Xylene to remove oil pen (if applied on slides)
- Dry on air
- Mount in DePex

Transmission electron microscopy sample preparation

Pre-fix:	4% PFA in phosphate buffer, incubate overnight at 4°C, then embed, fix again
Fixation:	2.5% Glutaraldehyde + 2% PFA + 0.05% $CaCl_2$ in 0.1M Sodium Cacodylate Buffer pH 7, incubate overnight at 4°C
Rinse 1:	0.1M Sodium Cacodylate buffer pH 7.4
Postfixation:	1% Osmium tetroxide + 1.5% Potassium Ferricyanide in distilled water, leave for 1h at RT
Rinse 2:	Distilled water 4x over 15min
Stain:	1% aqueous Uranyl Acetate, incubate for 1h in the dark
Dehydration:	in acetone:
	50% - 15 min at 4°C
	70% - 20 min with 2 changes at 0-4°C
	80% - 20 min with 2 changes at 0-4°C

90% - 15 min aith 2 changes at 0-4°C

95% - 15 min with 2 changes at RT

100% dry – 30 min with 2 changes at RT

Infiltration: 1:1 Acetone 100% dry: LV Epoxy Resin for 1 hour

100% Resin – overnight

100% Resin – 1 hour

Embedding: Embedding in LV Premix Epoxy Resin for

Polymerisation:for 24 hours at 60°C

Preparation of Competent Cells

Streak DH5-alpha stock in LB plate (no antibiotics)

- Culture at 37°C overnight
- Pick single colony and seed into SOB medium
- Culture at 18°C for 19-60 hours
  (DH5a 17:30 on Sunday – 11:30 on Wednesday = OD 0.67 (66 h)
  (Stbl3 19:00 on Sunday – 14: 00 on Tuesday = =D 0.54 (43 h)
- Check OD600 (until 0.4 – 0.8)
- Place culture on ice for 10 min
- Centrifuge at 3000 rpm for 15 min at 4°C
- Discard supernatant
- Suspend bacteria in 67ml of chilled TB gently
- Centrifuge at 3000 rpm for 15 min at 4°C
- Discard supernatant
- Suspend bacteria in 16ml of chilled TB gently (TB can be reduced to make appropriate density)
- Add 1.2ml DMSO (= final 7%) and leave on ice for 10 min
- Bring tools and suspension to cold room
- Prepare liquid nitrogen
- Dispense 50µl of suspension into 1.5ml tubes and put into liquid nitrogen immediately
- Store at -80°C

Appendix 3: Comparison of resin section adherence on a selection of Menzel slides

During Neutral Red staining procedure resin section are likely to come off. Therefore, a comparison of resin sections was made on Polysine, Superfrost Plus, Superfrost Ultra Plus and Superfrost Excell slides. Pictures (above) and table (below) represent the outcome in which Superfrost Plus indicates strongest adherence potential of resin slides during staining procedure and therefore best results

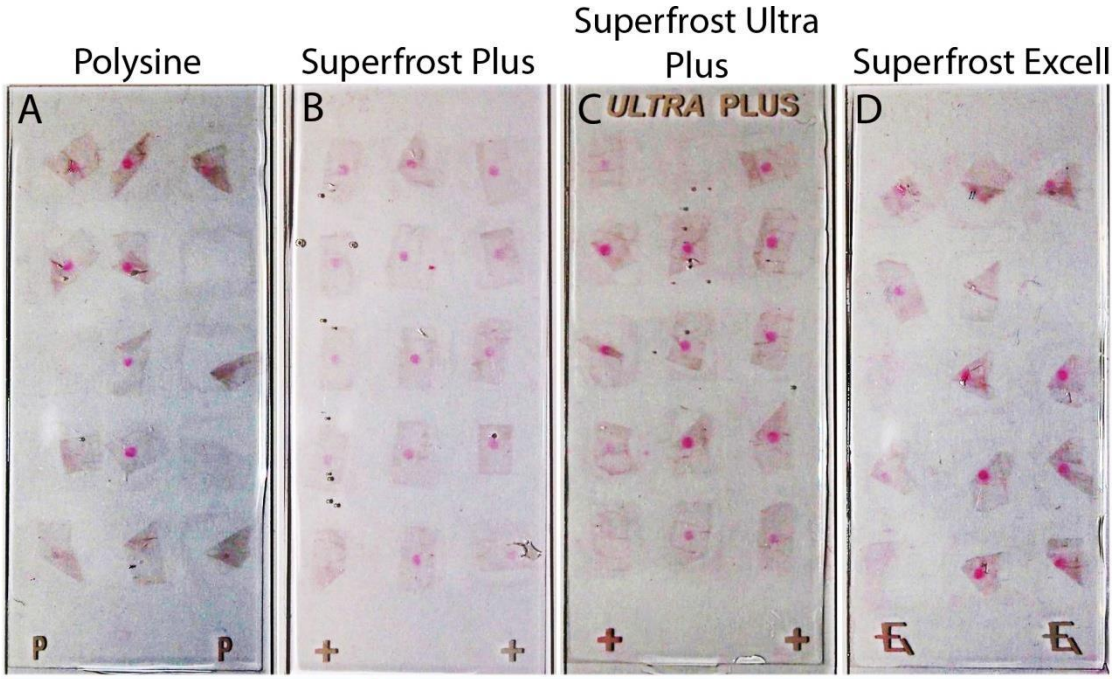

	Total sections number before stain	Total section number after stain
Polysine	30	19 (folded)
Superfrost Ultra	30	30 (flat)
Superfrost Ultra Plus	30	29 (folded)
Superfrost Excell	30	24

Appendix 4: Staging of Zebrafish embryos before free-feeding stage

Images according to developmental stages during Zebrafish embryonic development according to Kimmel et al. (1995) when embryos are bred at 28°C. Note hatching period in Zebrafish is around 48 hpf and free feeding is after 72 hpf.

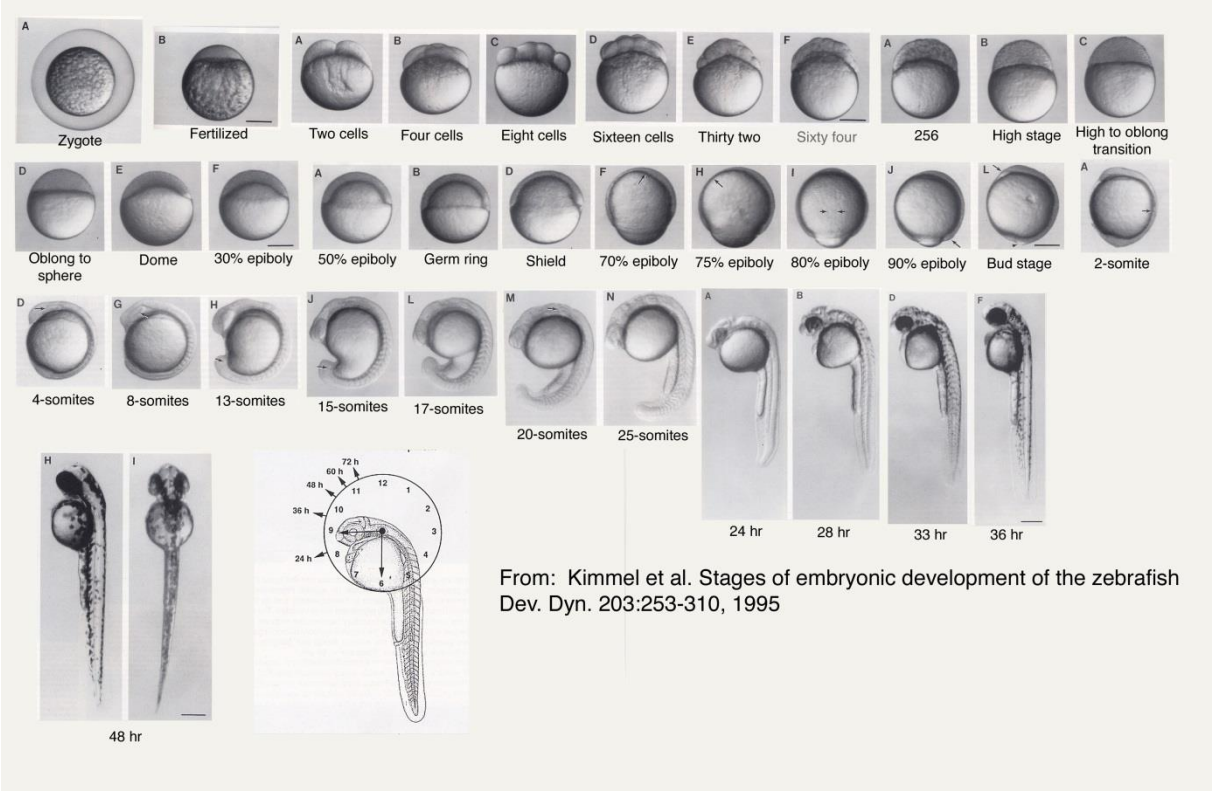

Appendix 5: Stages of Medaka development

Drawings according to developmental timing during Medaka embryogenesis. Staging is according to Iwamatsu (2004) when bred at 26°C. Note, hatching takes place at 9 dpf after which the larvae is able to swim and feed independently.

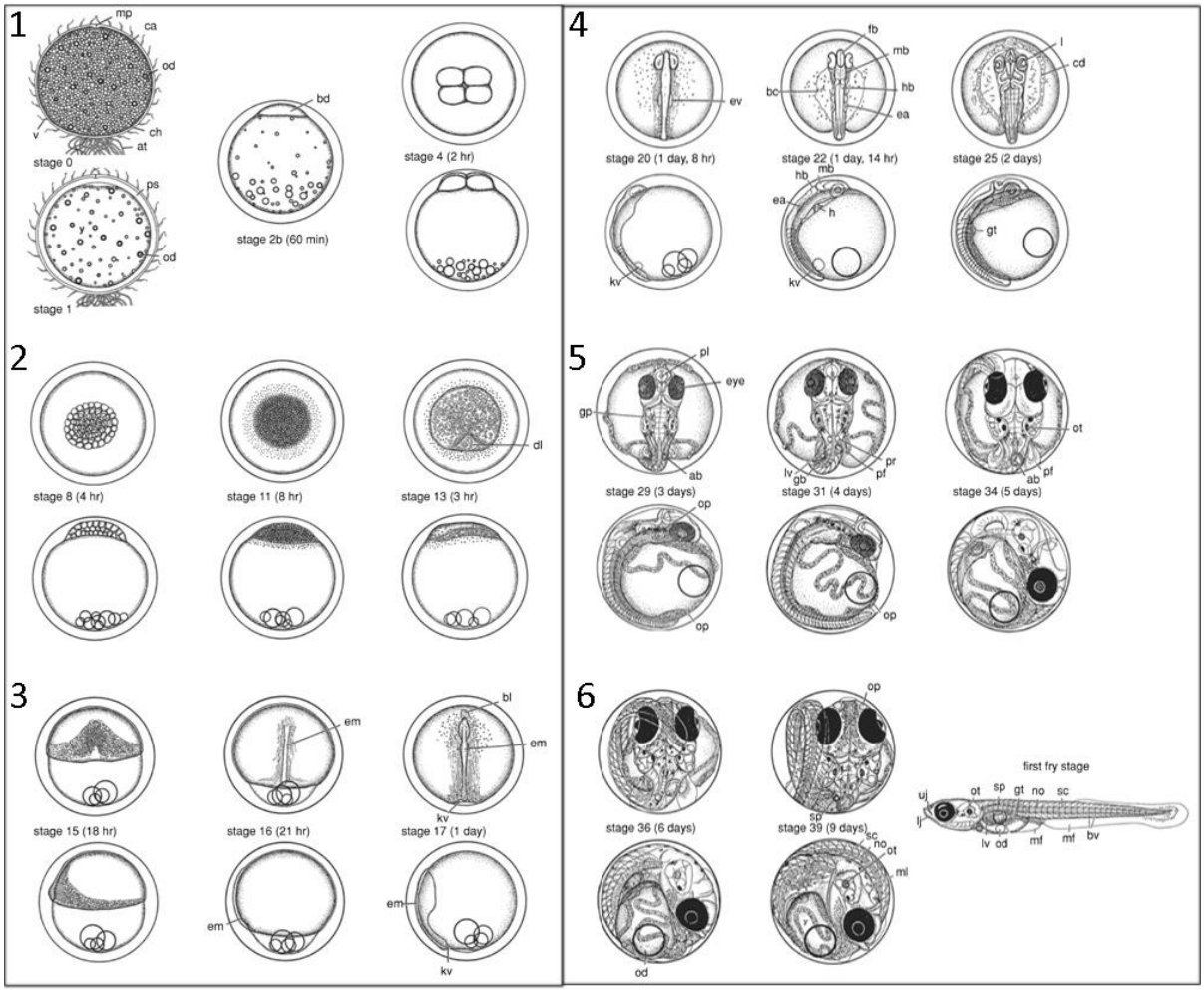

Appendix 6: Temperature shift graph for Medaka developmental

To manipulate the timing required to reach a certain developmental stage during Medaka development, a temperature shift in a viable range can be carried out. Lower temperatures slow down development and higher temperatures accelerate embryogenesis taking less time to obtain a certain stage. Left y-axis displays days and hours it takes to reach a certain stage of development (right y-axis axis) depending on the temperature (x-axis) in which embryos were incubated. Graph obtained from Dr M. Furutani-Seiki (Yamamoto 1975).

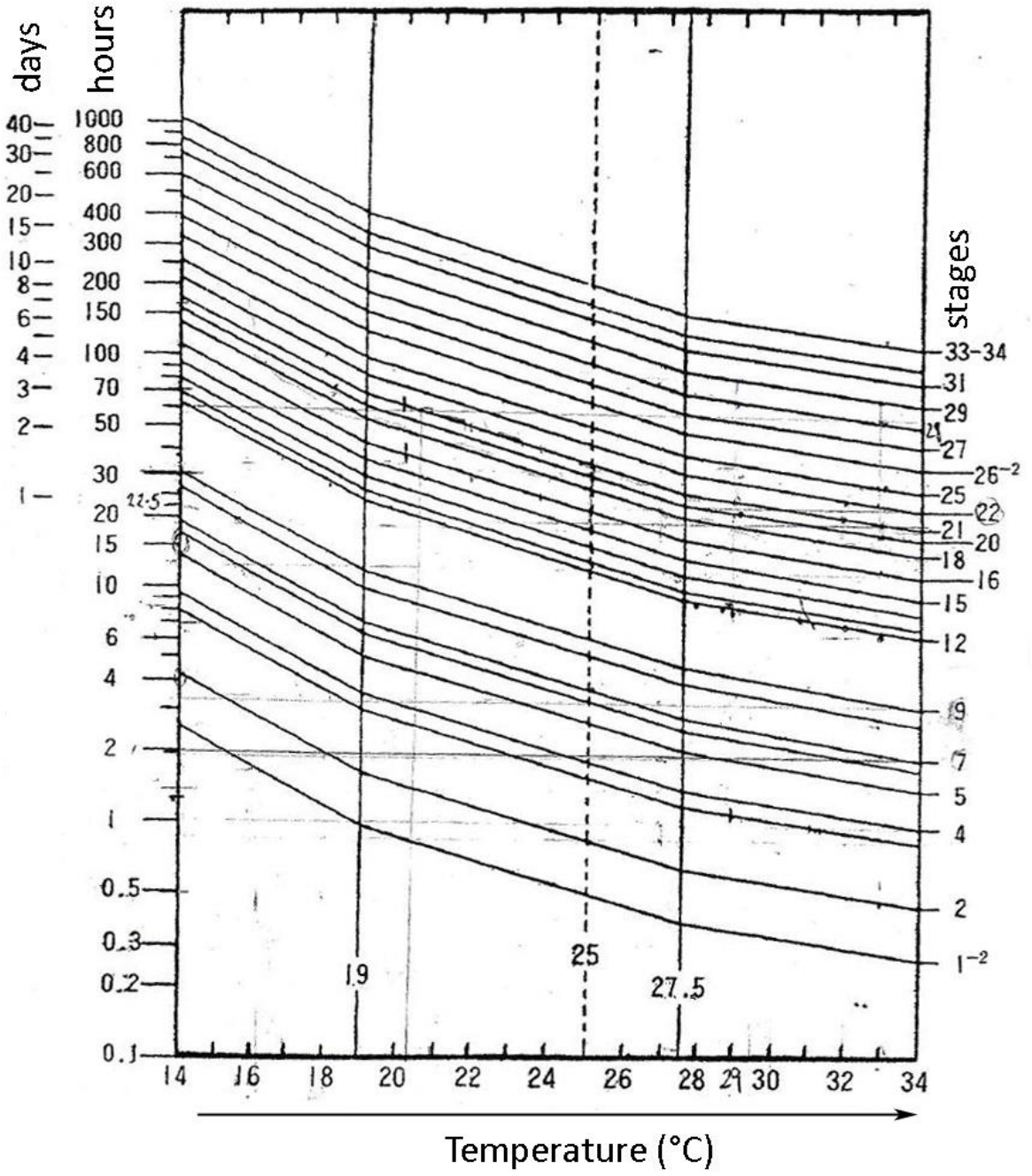

ref: Yamamoto 1975

Appendix 7: Hydrolysis times for probe fractioning (at 60°C)

Both tables indicate the incubation time (column within) at 60°C required to fraction a certain starting probe length (outer left column) to a final nucleotide fragment length (top row) (Parichy 2011).

Page 1: Hydrolysis times

Starting nt \ Final nt	200	250	300	350	400	450	500	550	600
200									
250	9.1								
300	15.2	6.1							
350	19.5	10.4	4.3						
400	22.7	13.6	7.6	3.2					
450	25.3	16.2	10.1	5.8	2.5				
500	27.3	18.2	12.1	7.8	4.5	2.0			
550	28.9	19.8	13.8	9.4	6.2	3.7	1.7		
600	30.3	21.2	15.2	10.8	7.6	5.1	3.0	1.4	
650	31.5	22.4	16.3	12.0	8.7	6.2	4.2	2.5	1.2
700	32.5	23.4	17.3	13.0	9.7	7.2	5.2	3.5	2.2
750	33.3	24.2	18.2	13.9	10.6	8.1	6.1	4.4	3.0
800	34.1	25.0	18.9	14.6	11.4	8.8	6.8	5.2	3.8
850	34.8	25.7	19.6	15.3	12.0	9.5	7.5	5.8	4.5
900	35.4	26.3	20.2	15.9	12.6	10.1	8.1	6.4	5.1
950	35.9	26.8	20.7	16.4	13.2	10.6	8.6	7.0	5.6
1000	36.4	27.3	21.2	16.9	13.6	11.1	9.1	7.4	6.1
1050	36.8	27.7	21.6	17.3	14.1	11.5	9.5	7.9	6.5
1100	37.2	28.1	22.0	17.7	14.5	11.9	9.9	8.3	6.9
1150	37.5	28.5	22.4	18.1	14.8	12.3	10.3	8.6	7.2
1200	37.9	28.8	22.7	18.4	15.2	12.6	10.6	9.0	7.6
1250	38.2	29.1	23.0	18.7	15.5	12.9	10.9	9.3	7.9
1300	38.5	29.4	23.3	19.0	15.7	13.2	11.2	9.5	8.2
1350	38.7	29.6	23.6	19.2	16.0	13.5	11.4	9.8	8.4
1400	39.0	29.9	23.8	19.5	16.2	13.7	11.7	10.0	8.7
1450	39.2	30.1	24.0	19.7	16.5	13.9	11.9	10.3	8.9
1500	39.4	30.3	24.2	19.9	16.7	14.1	12.1	10.5	9.1
1550	39.6	30.5	24.4	20.1	16.9	14.3	12.3	10.7	9.3
1600	39.8	30.7	24.6	20.3	17.0	14.5	12.5	10.8	9.5
1650	39.9	30.9	24.8	20.5	17.2	14.7	12.7	11.0	9.6
1700	40.1	31.0	25.0	20.6	17.4	14.9	12.8	11.2	9.8
1750	40.3	31.2	25.1	20.8	17.5	15.0	13.0	11.3	10.0
1800	40.4	31.3	25.3	20.9	17.7	15.2	13.1	11.5	10.1
1850	40.5	31.4	25.4	21.1	17.8	15.3	13.3	11.6	10.2
1900	40.7	31.6	25.5	21.2	17.9	15.4	13.4	11.7	10.4
1950	40.8	31.7	25.6	21.3	18.1	15.5	13.5	11.9	10.5
2000	40.9	31.8	25.8	21.4	18.2	15.7	13.6	12.0	10.6
2050	41.0	31.9	25.9	21.5	18.3	15.8	13.7	12.1	10.7
2100	41.1	32.0	26.0	21.6	18.4	15.9	13.9	12.2	10.8
2150	41.2	32.1	26.1	21.7	18.5	16.0	14.0	12.3	10.9
2200	41.3	32.2	26.2	21.8	18.6	16.1	14.0	12.4	11.0
2250	41.4	32.3	26.3	21.9	18.7	16.2	14.1	12.5	11.1
2300	41.5	32.4	26.4	22.0	18.8	16.2	14.2	12.6	11.2
2350	41.6	32.5	26.4	22.1	18.9	16.3	14.3	12.7	11.3
2400	41.7	32.6	26.5	22.2	18.9	16.4	14.4	12.7	11.4

Page 2: Hydrolysis times

Starting nt	Final nt 200	250	300	350	400	450	500	550	600
2450	41.7	32.7	26.6	22.3	19.0	16.5	14.5	12.8	11.4
2500	41.8	32.7	26.7	22.3	19.1	16.6	14.5	12.9	11.5
2550	41.9	32.8	26.7	22.4	19.2	16.6	14.6	13.0	11.6
2600	42.0	32.9	26.8	22.5	19.2	16.7	14.7	13.0	11.7
2650	42.0	32.9	26.9	22.5	19.3	16.8	14.8	13.1	11.7
2700	42.1	33.0	26.9	22.6	19.4	16.8	14.8	13.2	11.8
2750	42.1	33.1	27.0	22.7	19.4	16.9	14.9	13.2	11.8
2800	42.2	33.1	27.1	22.7	19.5	17.0	14.9	13.3	11.9
2850	42.3	33.2	27.1	22.8	19.5	17.0	15.0	13.3	12.0
2900	42.3	33.2	27.2	22.8	19.6	17.1	15.0	13.4	12.0
2950	42.4	33.3	27.2	22.9	19.6	17.1	15.1	13.4	12.1
3000	42.4	33.3	27.3	22.9	19.7	17.2	15.2	13.5	12.1
3050	42.5	33.4	27.3	23.0	19.7	17.2	15.2	13.5	12.2
3100	42.5	33.4	27.4	23.0	19.8	17.3	15.2	13.6	12.2
3150	42.6	33.5	27.4	23.1	19.8	17.3	15.3	13.6	12.3
3200	42.6	33.5	27.5	23.1	19.9	17.4	15.3	13.7	12.3
3250	42.7	33.6	27.5	23.2	19.9	17.4	15.4	13.7	12.4
3300	42.7	33.6	27.5	23.2	20.0	17.4	15.4	13.8	12.4
3350	42.7	33.6	27.6	23.3	20.0	17.5	15.5	13.8	12.4
3400	42.8	33.7	27.6	23.3	20.1	17.5	15.5	13.9	12.5
3450	42.8	33.7	27.7	23.3	20.1	17.6	15.5	13.9	12.5
3500	42.9	33.8	27.7	23.4	20.1	17.6	15.6	13.9	12.6
3550	42.9	33.8	27.7	23.4	20.2	17.6	15.6	14.0	12.6
3600	42.9	33.8	27.8	23.4	20.2	17.7	15.7	14.0	12.6
3650	43.0	33.9	27.8	23.5	20.2	17.7	15.7	14.0	12.7
3700	43.0	33.9	27.8	23.5	20.3	17.7	15.7	14.1	12.7
3750	43.0	33.9	27.9	23.5	20.3	17.8	15.8	14.1	12.7
3800	43.1	34.0	27.9	23.6	20.3	17.8	15.8	14.1	12.8
3850	43.1	34.0	27.9	23.6	20.4	17.8	15.8	14.2	12.8
3900	43.1	34.0	28.0	23.6	20.4	17.9	15.9	14.2	12.8
3950	43.2	34.1	28.0	23.7	20.4	17.9	15.9	14.2	12.9
4000	43.2	34.1	28.0	23.7	20.5	17.9	15.9	14.3	12.9
4050	43.2	34.1	28.1	23.7	20.5	18.0	15.9	14.3	12.9
4100	43.2	34.1	28.1	23.8	20.5	18.0	16.0	14.3	12.9
4150	43.3	34.2	28.1	23.8	20.5	18.0	16.0	14.3	13.0
4200	43.3	34.2	28.1	23.8	20.6	18.0	16.0	14.4	13.0
4250	43.3	34.2	28.2	23.8	20.6	18.1	16.0	14.4	13.0
4300	43.3	34.2	28.2	23.9	20.6	18.1	16.1	14.4	13.0
4350	43.4	34.3	28.2	23.9	20.6	18.1	16.1	14.4	13.1
4400	43.4	34.3	28.2	23.9	20.7	18.1	16.1	14.5	13.1
4450	43.4	34.3	28.3	23.9	20.7	18.2	16.1	14.5	13.1
4500	43.4	34.3	28.3	24.0	20.7	18.2	16.2	14.5	13.1
4550	43.5	34.4	28.3	24.0	20.7	18.2	16.2	14.5	13.2
4600	43.5	34.4	28.3	24.0	20.8	18.2	16.2	14.6	13.2
4650	43.5	34.4	28.3	24.0	20.8	18.2	16.2	14.6	13.2
4700	43.5	34.4	28.4	24.0	20.8	18.3	16.2	14.6	13.2
4750	43.5	34.4	28.4	24.1	20.8	18.3	16.3	14.6	13.2
4800	43.6	34.5	28.4	24.1	20.8	18.3	16.3	14.6	13.3
4850	43.6	34.5	28.4	24.1	20.9	18.3	16.3	14.7	13.3
4900	43.6	34.5	28.4	24.1	20.9	18.3	16.3	14.7	13.3
4950	43.6	34.5	28.5	24.1	20.9	18.4	16.3	14.7	13.3
5000	43.6	34.5	28.5	24.2	20.9	18.4	16.4	14.7	13.3

Appendix 8: *Dct* at st.20 - st.32 in wild type and *hirame* mutants

WISH with *Dct* in wild type and *hirame* embryos indicating location of individual melanoblasts and differentiated melanocytes between stage 20 to stage 32. Anterior head is left, posterior tail end is right. Wild type embryos in two left columns, *hirame* mutants in two right columns. Dorsal and lateral views are alternating. n= number of individuals, scale bar = 500µm.

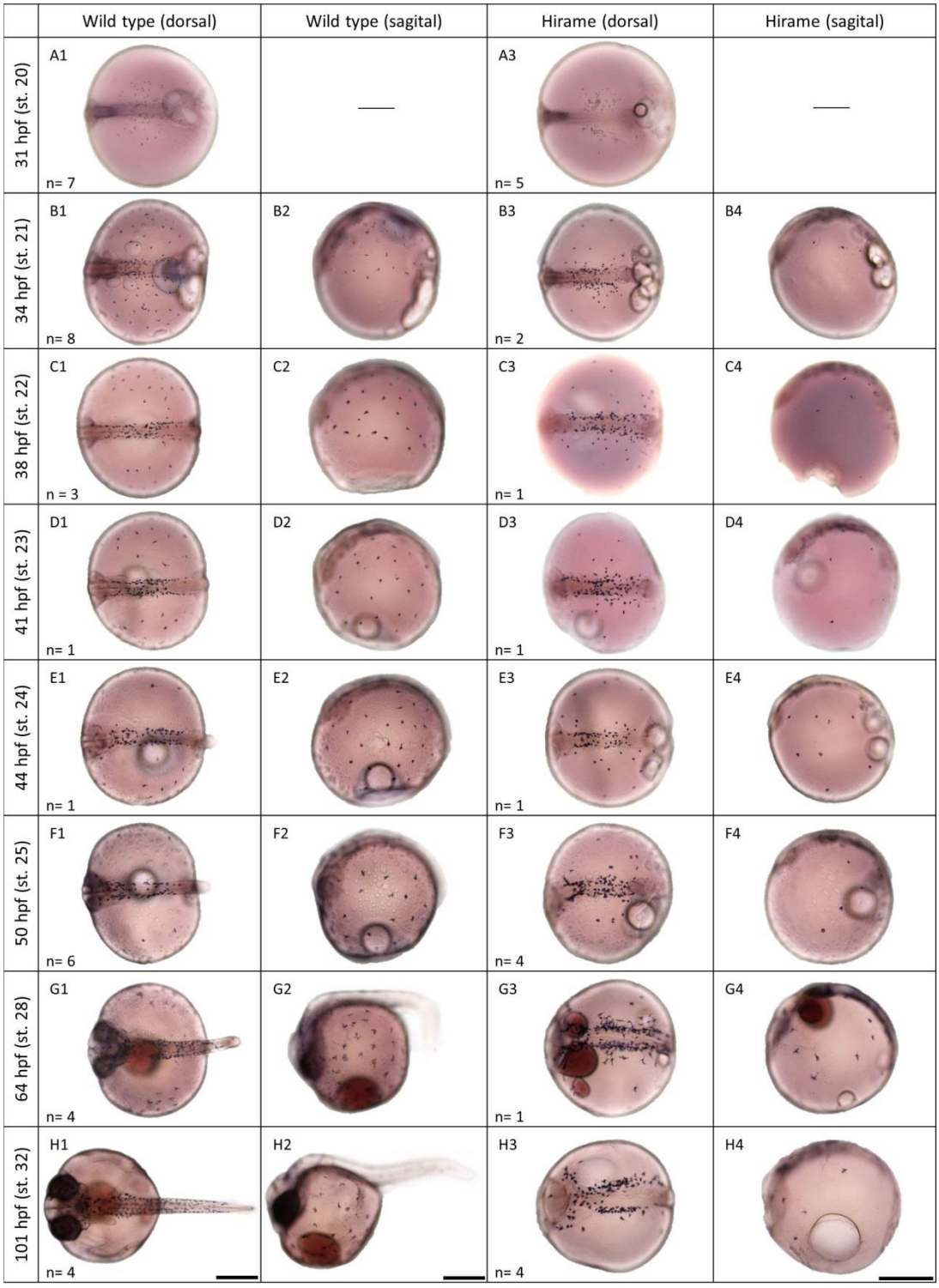

Appendix 9: Renamed individual Tg(*Dct*:eGFP) lines

Trangenic lines originated from individual *Dct*:eGFP founders have been renamed into line 1 to 8 for simplification. Second column shows the number ond gender of the F0 generation as reported in the database.

Tg(*Dct*:eGFP) strain renamed	Tg(*Dct*:eGFP) line originated from individually founders as named in database records	Number of transgenic F1 progeny grown up
line 1	line 1	33
line 2	line 2	5
line 3	line 3	17
line 4	line 4	3
line 5	line 5	2
line 6	line 53	32
line 7	line 58	27
line 8	feline 5	28

Appendix 10: TEM on Medaka yolk sac membrane

Transmission electron microscopy (TEM) reveals a three layered membrane arrangement surrounding the yolk cell in st. 21 wild type (A) and *hirame* (B) embryos. A: Layers 1-3, in which 1 is the yolk syncytial layer, 2 is a middle epidermal layer and 3 is the most outer enveloping layer. B: Nuclei (asterics) could be located within the lower and middle layer as well as the top layer (not shown). Scale = 1µm

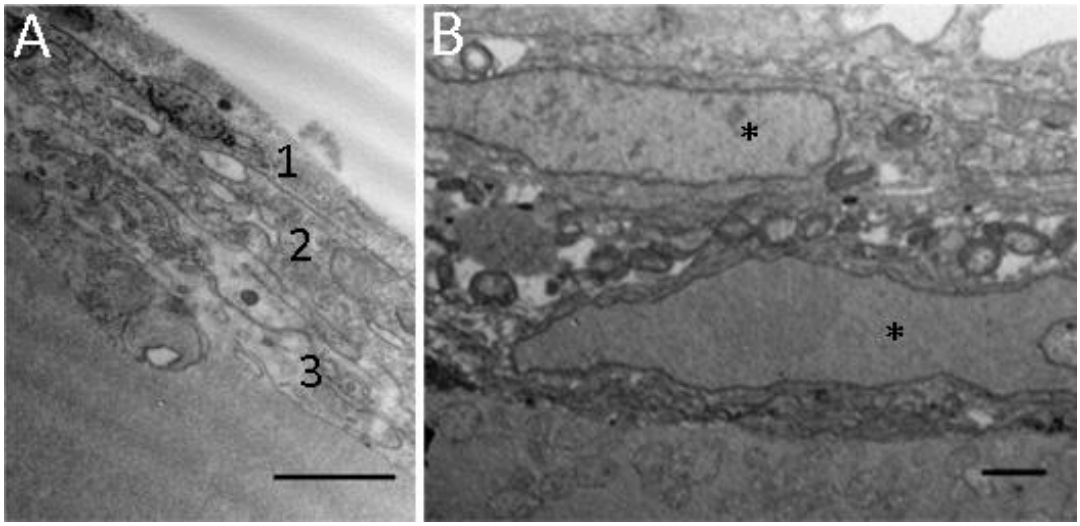

Appendix 11: TEM of yolk sac membrane structures in wild type and *hirame* st.21 embryos

Common structures within both, wild type and *hirame* embryos. A, A': tight juntions (black error) connecting outwards protruding cells within the enveloping layer, additional desmosome (A', white error) visible. B,B': Inclusions (arrow) within the yolk sac cell connected to the yolk syncytial layer. In *hirame* those reservoirs held various sized particles in it (B'). C, C': Lipid droplets (arrow head) located within close proximity to the yolk syncytial layer. Scale bar = 1µm.

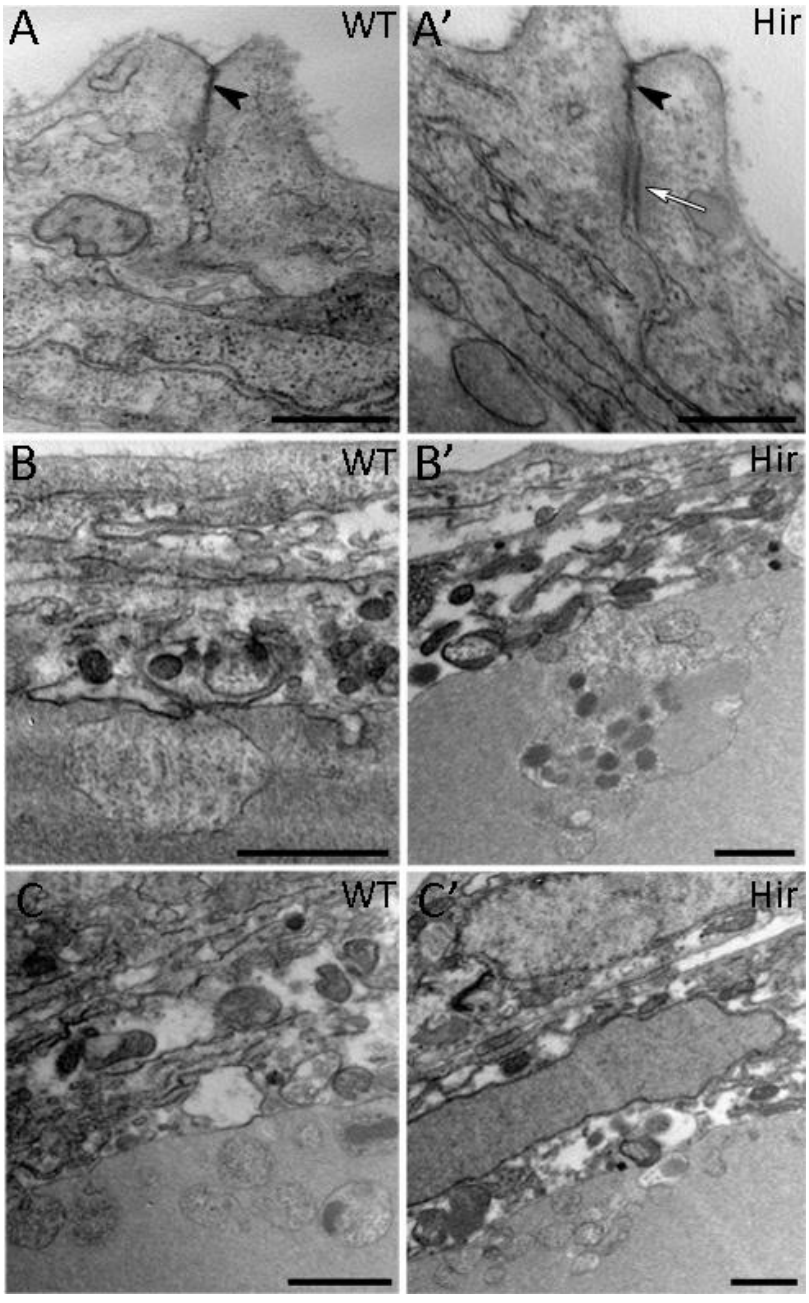

Appendix 12: Epiboly closure during wild type and *hirame* gastrulation

Live imaging of developing embryos to observe the difference of wild type (top row, n=4) and *hirame* (bottom row, n=3) embryos. The epiderm covers ¾ of the yolk sphere in wild type and the embryonic shield in visible. Blastoderm during epiboly closure migrates slower in *hirame* mutants towards the vegetal pole compared to wild type siblings (dotted lines). The blastopore (bp) at st.17 remains wider in *hirame* exposing the yolk syncytial layer (YSL). The difference between genetics was identified after letting them develop until 1.5 dpf. Scale bar = 500µm

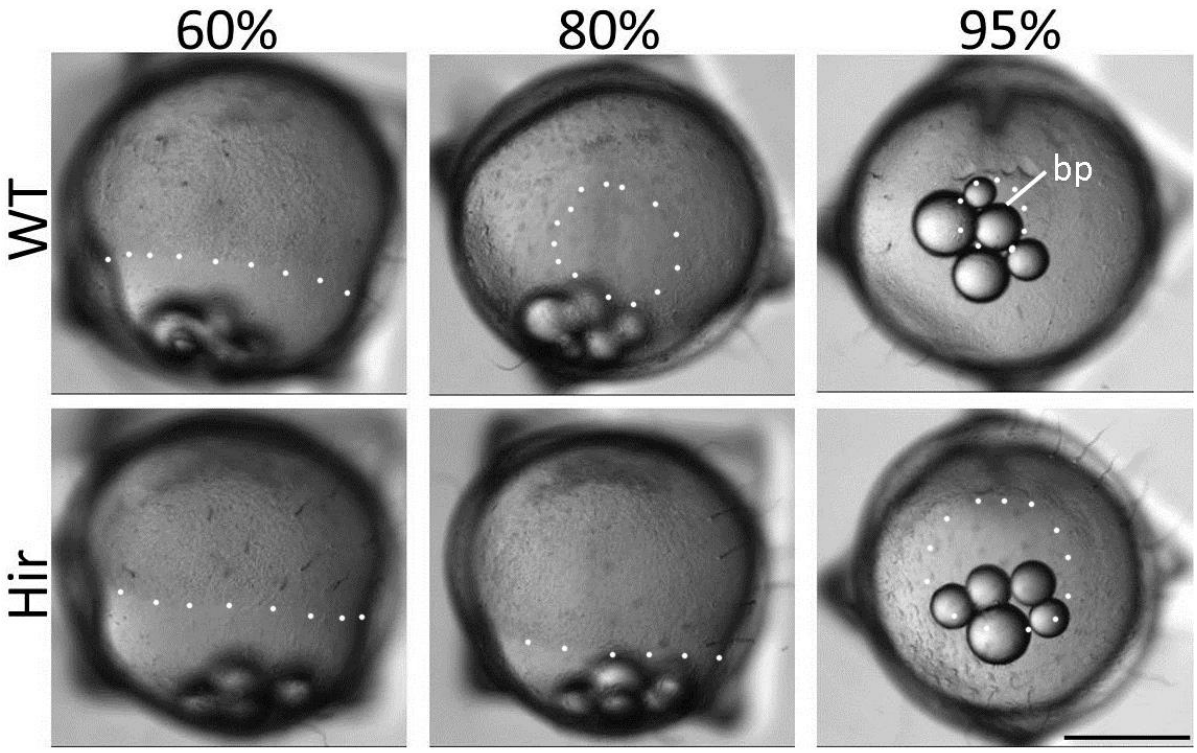

Appendix 13: Neurogenin 1 expression detected via whole-mount *in situ* hybrisidation in 3 dpf embryos

WISH of neurogenin 1 (ngn1) to label developing neurons of 3 dpf Medaka embryos. Indicated regions include the spinal cord and initiation of neuronal differentiation in medial-lateral clusters.

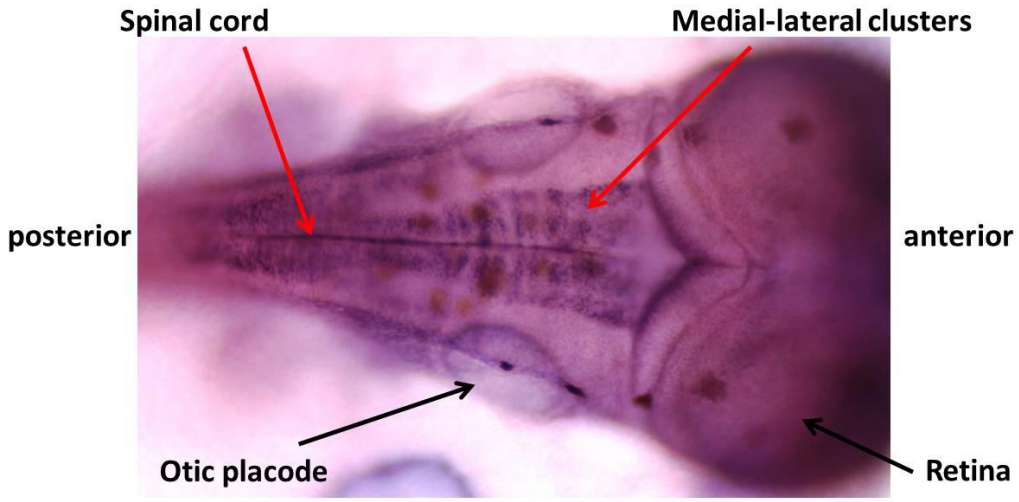

References

Adams, R., Diella, F., Hennig, S., Helmbacher, F., Deutsch, U., & Klein, R. (2001). The cytoplasmic domain of the ligand ephrinB2 is required for vascular morphogenesis but not cranial neural crest migration. *Cell*, *104*(1), 57–69.

Addgene. (2014). Plasmid Cloning by PCR. [Online] [Accessed 18.07.2014]. Available from: http://www.addgene.org/plasmid_protocols/PCR_cloning/

Akiyama, H., Chaboissier, M.-C., Martin, J. F., Schedl, A., & de Crombrugghe, B. (2002). The transcription factor Sox9 has essential roles in successive steps of the chondrocyte differentiation pathway and is required for expression of Sox5 and Sox6. *Genes & Development*, *16*(21), 2813–28.

Alberts, B., Johnson, A., & Lewis, J. (2002). Programmed Cell Death (Apoptosis). In *Molecular Biology of the Cell* (4th ed.). New York: Garland Science.

Albino, A., Nanus, D., Mentle, I., Cordon-Cardo, C., McNutt, N., Bressler, J., & Andreeff, M. (1989). Analysis of ras oncogenes in malignant melanoma and precursor lesions: correlation of point mutations with differentiation phenotype. *Oncogene*, *4*(11), 1363–1374.

Alfandari, D., Cousin, H., Gaultier, A., Hoffstrom, B. G., & DeSimone, D. W. (2003). Integrin α5β1 supports the migration of Xenopus cranial neural crest on fibronectin. *Developmental Biology*, *260*(2), 449–464.

Amrani, A. El, Barakate, A., Askari, B. M., Li, X., Roberts, A. G., Ryan, M. D., & Halpin, C. (2004). Coordinate Expression and Independent Subcellular Targeting of Multiple Proteins from a Single Transgene 1, *135*(May), 16–24.

Andermann, P., Ungos, J., & Raible, D. W. (2002). Neurogenin1 Defines Zebrafish Cranial Sensory Ganglia Precursors. *Developmental Biology*, *251*(1), 45–58.

Anderson, R. B., Newgreen, D. F., & Young, H. (2013). Neural Crest and the Development of the Enteric Nervous System. [Online] [Accessed 06.09.2014] Available from: http://www.ncbi.nlm.nih.gov/books/NBK6273/

Anelli, V., Santoriello, C., Distel, M., Köster, R. W., Ciccarelli, F. D., & Mione, M. (2009). Global repression of cancer gene expression in a zebrafish model of melanoma is linked to epigenetic regulation. *Zebrafish*, *6*(4), 417–24.

Arpino, J. a J., Rizkallah, P. J., & Jones, D. D. (2012). Crystal structure of enhanced green fluorescent protein to 1.35 Å resolution reveals alternative conformations for Glu222. *PloS One*, *7*(10), e47132.

Bae, C.-J., Park, B.-Y., Lee, Y.-H., Tobias, J. W., Hong, C.-S., & Saint-Jeannet, J.-P. (2014). Identification of Pax3 and Zic1 targets in the developing neural crest. *Developmental Biology*, *386*(2), 473–83.

Barrow, K. M., Perez-Campo, F. M., & Ward, C. M. (2006). Use of the Cytomegalovirus Promoter for Transient and Stable Transgene Expression in Mouse Embryonic Stem Cells. *Methods in Molecular Biology*, *329*, 283–294.

Basu, S., Totty, N. F., Irwin, M. S., Sudol, M., & Downward, J. (2003). Akt phosphorylates the Yes-associated protein, YAP, to induce interaction with 14-3-3 and attenuation of p73-mediated apoptosis. *Molecular Cell*, *11*(1), 11–23.

Belmadani, A., Jung, H., Ren, D., & Miller, R. J. (2009). The chemokine SDF-1/CXCL12 regulates the migration of melanocyte progenitors in mouse hair follicles. *Differentiation; Research in Biological Diversity*, *77*(4), 395–411.

Belmadani, A., Tran, P. B., Ren, D., Assimacopoulos, S., Grove, E. a, & Miller, R. J. (2005). The chemokine stromal cell-derived factor-1 regulates the migration of sensory neuron progenitors. *The Journal of Neuroscience*, *25*(16), 3995–4003.

Bondurand, N., Dastot-Le Moal, F., Stanchina, L., Collot, N., Baral, V., Marlin, S., … Pingault, V. (2007). Deletions at the SOX10 gene locus cause Waardenburg syndrome types 2 and 4. *American Journal of Human Genetics*, *81*(6), 1169–85.

Böttcher, R. T., & Niehrs, C. (2005). Fibroblast Growth Factor Signaling during Early Vertebrate Development. *Endocrine Reviews*, *26*(1), 63–77.

Braasch, I., Schartl, M., & Volff, J.-N. (2007). Evolution of pigment synthesis pathways by gene and genome duplication in fish. *BMC Evolutionary Biology*, *7*, 74.

Calero-Nieto, F. J., Bert, A. G., & Cockerill, P. N. (2010). Transcription-dependent silencing of inducible convergent transgenes in transgenic mice. *Epigenetics & Chromatin*, *3*(1), 3.

Camargo, F. D., Gokhale, S., Johnnidis, J. B., Fu, D., Bell, G. W., Jaenisch, R., & Brummelkamp, T. R. (2007). YAP1 increases organ size and expands undifferentiated progenitor cells. *Current Biology*, *17*(23), 2054–60.

Cao, X., Pfaff, S. L., & Gage, F. H. (2008). YAP regulates neural progenitor cell number via the TEA domain transcription factor, 3320–3334.

Carmany-Rampey, A., & Moens, C. B. (2006). Modern mosaic analysis in the zebrafish. *Methods (San Diego, Calif.)*, *39*(3), 228–38.

Carney, T. J., Dutton, K. a, Greenhill, E., Delfino-Machín, M., Dufourcq, P., Blader, P., & Kelsh, R. N. (2006). A direct role for Sox10 in specification of neural crest-derived sensory neurons. *Development (Cambridge, England)*, *133*(23), 4619–30.

Carvalho, L., & Heisenberg, C.-P. (2010). The yolk syncytial layer in early zebrafish development. *Trends in Cell Biology*, *20*(10), 586–92.

Casini, P., Nardi, I., & Ori, M. (2012). Hyaluronan is required for cranial neural crest cells migration and craniofacial development. *Developmental Dynamics*, *241*(2), 294–302.

Cells, G. (1998). Zebrafish organizer development and germ-layer formation require nodal-related signals. *Letters to Nature*, *395*(September), 181–185.

Chiang, E. F., Pai, C. I., Wyatt, M., Yan, Y. L., Postlethwait, J., & Chung, B. (2001). Two sox9 genes on duplicated zebrafish chromosomes: expression of similar transcription activators in distinct sites. *Developmental Biology*, *231*(1), 149–63.

Clark, J. W., Elder, D., Guerry, D., Epstein, M., Greene, M., & Horn, M. Van. (1984). A study of tumor progression: the precursor lesions of superficial spreading and nodular melanoma. *Human Pathology*, *15*(12), 1147–1165.

Clarkson, M. J., & Harley, V. R. (2002). Sex with two SOX on: SRY and SOX9 in testis development. *Trends in Endocrinology and Metabolism: TEM*, *13*(3), 106–11.

Clontech Takara Bio Company. (2014). Bicistronic IRES Vectors. [Online] [Accessed 20.08.2014] Available from: http://www.clontech.com/GB/Products/Fluorescent_Proteins_and_Reporters/Coexpression/IRES_Bicistronic?sitex=10030:22372:US

Conway, S. J., Henderson, D. J., & Copp, a J. (1997). Pax3 is required for cardiac neural crest migration in the mouse: evidence from the splotch (Sp2H) mutant. *Development*, *124*(2), 505–514.

Corcoran, G. B., Fix, L., Jones, D. P., Moslen, M. T., Nicotera, P., Oberhammer, F. a, & Buttyan, R. (1994). Apoptosis: molecular control point in toxicity. *Toxicology and Applied Pharmacology*. 1195.

Corish, P., & Tyler-Smith, C. (1999). Attenuation of green fluorescent protein half-life in mammalian cells. *Protein Engineering*, *12*(12), 1035–40.

Cousin, H., Abbruzzese, G., Kerdavid, E., Gaultier, A., & Alfandari, D. (2011). Translocation of the cytoplasmic domain of ADAM13 to the nucleus is essential for Calpain8-a expression and cranial neural crest cell migration. *Developmental Cell*, *20*(2), 256–263.

Cousin, H., Abbruzzese, G., McCusker, C., & Alfandari, D. (2012). ADAM13 function is required in the 3 dimensional context of the embryo during cranial neural crest cell migration in Xenopus laevis. *Developmental Biology*, *368*(2), 335–344.

Cui, J., Shen, X., Zhao, H., & Nagahama, Y. (2011). Genome-wide analysis of Sox genes in Medaka (Oryzias latipes) and their expression pattern in embryonic development. *Cytogenetic and Genome Research*, *134*(4), 283–94.

Curran, K., Lister, J. A., Kunkel, G. R., Prendergast, A., David, M., & Raible, D. W. (2011). Interplay between Foxd3 and Mitf regulates cell fate plasticity in the zebrafish neural crest. *Developmental Biology*, *344*(1), 107–118.

Dahl, C., & Guldberg, P. (2007). The genome and epigenome of malignant melanoma. *APMIS : Acta Pathologica, Microbiologica, et Immunologica Scandinavica*, *115*(10), 1161–76.

Dalcq, J., Pasque, V., Ghaye, A., Larbuisson, A., Motte, P., Martial, J. a, & Muller, M. (2012). RUNX3, EGR1 and SOX9B form a regulatory cascade required to modulate BMP-signaling during cranial cartilage development in zebrafish. *PloS One*, *7*(11), e50140.

Davies, H., Bignell, G. R., Cox, C., Stephens, P., Edkins, S., Clegg, S., … Futreal, P. A. (2002). Mutations of the BRAF gene in human cancer. *Nature*, *417*(6892), 949–54.

Davy, A., Aubin, J., & Soriano, P. (2004). Ephrin-B1 forward and reverse signaling are required during mouse development. *Genes & Development*, *18*(5), 572–583.

Day, C. D. (2000). Transgene integration into the same chromosome location can produce alleles that express at a predictable level, or alleles that are differentially silenced. *Genes & Development*, *14*(22), 2869–2880.

De Bellard, M. E., Rao, Y., & Bronner-Fraser, M. (2003). Dual function of Slit2 in repulsion and enhanced migration of trunk, but not vagal, neural crest cells. *The Journal of Cell Biology*, *162*(2), 269–279.

De Cristofaro, T., Di Palma, T., Ferraro, A., Corrado, A., Lucci, V., Franco, R., … Zannini, M. (2011). TAZ/WWTR1 is overexpressed in papillary thyroid carcinoma. *European Journal of Cancer*, *47*(6), 926–33.

Delacôte, F., Perez, C., Guyot, V., Duhamel, M., Rochon, C., Ollivier, N., … Duchateau, P. (2013). High frequency targeted mutagenesis using engineered endonucleases and DNA-end processing enzymes. *PloS One*, *8*(1), e53217.

Densham, R. M., O'Neill, E., Munro, J., König, I., Anderson, K., Kolch, W., & Olson, M. F. (2009). MST kinases monitor actin cytoskeletal integrity and signal via c-Jun N-terminal kinase stress-activated kinase to regulate p21Waf1/Cip1 stability. *Molecular and Cellular Biology*, *29*(24), 6380–90.

Detrich, H., Westerfield, M., & Zon, L. (1998). *The Zebrafish: Biology* (1st ed., Vol. 58, p. 392). Academic Press.

Dimitrijevic, N., Winkler, C., Wellbrock, C., Gómez, a, Duschl, J., Altschmied, J., & Schartl, M. (1998). Activation of the Xmrk proto-oncogene of Xiphophorus by overexpression and mutational alterations. *Oncogene*, *16*(13), 1681–90.

Dong, J., Feldmann, G., Huang, J., Wu, S., Zhang, N., A, S., … Maitra, A. (2005). Supplemental Data Elucidation of a Universal Size-Control Mechanism in Drosophila and Mammals. *System*, *130*.

Dong, J., Feldmann, G., Huang, J., Wu, S., Zhang, N., Comerford, S. a, … Pan, D. (2007). Elucidation of a universal size-control mechanism in Drosophila and mammals. *Cell*, *130*(6), 1120–33.

Donnelly, M. L., Luke, G., Mehrotra, a, Li, X., Hughes, L. E., Gani, D., & Ryan, M. D. (2001). Analysis of the aphthovirus 2A/2B polyprotein "cleavage" mechanism indicates not a proteolytic reaction, but a novel translational effect: a putative ribosomal "skip". *The Journal of General Virology*, *82*(Pt 5), 1013–25.

Donoghue, P. C. J., Graham, A., & Kelsh, R. N. (2008). The origin and evolution of the neural crest. *BioEssays : News and Reviews in Molecular, Cellular and Developmental Biology*, *30*(6), 530–41.

Douarin, N. Le, & Teillet, M. (1987). The migration of neural crest cells to the wall of the digestive tract in avian embryos. *Journal of Embryological Experimental Morphology*, *30*, 31–48.

Downs, K. M., & Davies, T. (1993). Staging of gastrulating mouse embryos by morphological landmarks in the dissecting microscope. *Development*, *118*(4), 1255–66.

Driever, W., Solnica-Krezel, L., Schier, a F., Neuhauss, S. C., Malicki, J., Stemple, D. L., … Boggs, C. (1996). A genetic screen for mutations affecting embryogenesis in zebrafish. *Development*, *123*, 37–46.

Driever, W., Stemple, D., Schier, a, & Solnica-Krezel, L. (1994). Zebrafish: genetic tools for studying vertebrate development. *Trends in Genetics : TIG*, *10*(5), 152–9.

Duband, J. L., & Thiery, J. P. (1987). Distribution of laminin and collagens during avian neural crest development. *Development*, *101*(3), 461–78.

Dupont, S., Morsut, L., Aragona, M., Enzo, E., Giulitti, S., Cordenonsi, M., … Piccolo, S. (2011). Role of YAP/TAZ in mechanotransduction. *Nature*, *474*(7350), 179–83.

Dutt, S., Kléber, M., Matasci, M., Sommer, L., & Zimmermann, D. R. (2006). Versican V0 and V1 guide migratory neural crest cells. *The Journal of Biological Chemistry*, *281*(17), 12123–31.

Dutton, K. a, Pauliny, A., Lopes, S. S., Elworthy, S., Carney, T. J., Rauch, J., … Kelsh, R. N. (2001). Zebrafish colourless encodes sox10 and specifies non-ectomesenchymal neural crest fates. *Development*, *128*(21), 4113–4125.

Dyer, M. a. (2004). Mouse models of childhood cancer of the nervous system. *Journal of Clinical Pathology*, *57*(6), 561–576.

Edery, P., Attié, T., Amiel, J., Pelet, A., Eng, C., Hofstra, R., … Lyonnet, S. (1996). Mutation of the endothelin-3 gene in the Waardenburg-Hirschsprung disease (Shah-Waardenburg syndrome). *Nat Genet*, *12*(4), 442–444.

Elsen, G. E., Choi, L. Y., Millen, K. J., Grinblat, Y., & Prince, V. E. (2008). Zic1 and Zic4 regulate zebrafish roof plate specification and hindbrain ventricle morphogenesis. *Developmental Biology*, *314*(2), 376–92.

Elworthy, S. (2003). Transcriptional regulation of mitfa accounts for the sox10 requirement in zebrafish melanophore development. *Development*, *130*(12), 2809–2818.

Elworthy, S., Pinto, J. P., Pettifer, A., Cancela, M. L., & Kelsh, R. N. (2005). Phox2b function in the enteric nervous system is conserved in zebrafish and is sox10-dependent. *Mechanisms of Development*, *122*(5), 659–69.

Emgrid Pty, Ltd. (2013). Kulzer Technovit® 8100. [Online] [Accessed 01.09.2014] Available from: http://www.emgrid.com.au/kulzer-technovit-8100.html

Endo, Y., Osumi, N., & Wakamatsu, Y. (2002). Bimodal functions of Notch-mediated signaling are involved in neural crest formation during avian ectoderm development. *Development*, *129*(4), 863–73.

Erter, C. E., Solnica-Krezel, L., & Wright, C. V. (1998). Zebrafish nodal-related 2 encodes an early mesendodermal inducer signaling from the extraembryonic yolk syncytial layer. *Developmental Biology*, *204*(2), 361–72.

Evrogen. (2014). Green fluorescent protein TurboGFP. [Online] [Accessed 05.09.2014] Available from: http://www.evrogen.com/products/TurboGFP/TurboGFP_Detailed_description.shtml

Fan, T.-J., Han, L.-H., Cong, R.-S., & Liang, J. (2005). Caspase Family Proteases and Apoptosis. *Acta Biochimica et Biophysica Sinica*, *37*(11), 719–727.

Feiner, L., Webber, a L., Brown, C. B., Lu, M. M., Jia, L., Feinstein, P., … Raper, J. a. (2001). Targeted disruption of semaphorin 3C leads to persistent truncus arteriosus and aortic arch interruption. *Development*, *128*(16), 3061–70.

Feng, Y., Santoriello, C., Mione, M., Hurlstone, A., & Martin, P. (2010). Live Imaging of Innate Immune Cell Sensing of Transformed Cells in Zebrafish Larvae: Parallels between Tumor Initiation and Wound Inflammation. *PLoS Biology*, *8*(12), e1000562.

Fu, D., Lv, X., Hua, G., He, C., Dong, J., M, L. S., … Wang, C. (2014). YAP regulates cell proliferation, migration, and steroidogenesis in adult granulosa cell tumors. *Endocr Relat Cancer*, *21*(2), 297–310.

Fujita, M., Isogai, S., & Kudo, A. (2006). Vascular anatomy of the developing medaka, Oryzias latipes: a complementary fish model for cardiovascular research on vertebrates. *Developmental Dynamics*, *235*(3), 734–46.

Fukamachi, S., Kinoshita, M., Tsujimura, T., Shimada, A., Oda, S., Shima, A., … Mitani, H. (2008). Rescue from oculocutaneous albinism type 4 using medaka slc45a2 cDNA driven by its own promoter. *Genetics*, *178*(2), 761–9.

Furutani-Seiki, M., Sasado, T., Morinaga, C., Suwa, H., Niwa, K., Yoda, H., … Kondoh, H. (2004). A systematic genome-wide screen for mutations affecting organogenesis in Medaka, Oryzias latipes. *Mechanisms of Development*, *121*(7-8), 647–58.

Furutani-Seiki, M., & Wittbrodt, J. (2004). Medaka and zebrafish, an evolutionary twin study. *Mechanisms of Development*, *121*(7-8), 629–37.

Gaiano, N., Allende, M., Amsterdam, A., Kawakami, K., & Hopkins, N. (1996). Highly efficient germ-line transmission of proviral insertions in zebrafish. *Proceedings of the National Academy of Sciences of the United States of America*, *93*(15), 7777–7782.

Gammill, L. S., & Bronner-Fraser, M. (2003). Neural crest specification: migrating into genomics. *Nature Reviews. Neuroscience*, *4*(10), 795–805.

Gammill, L. S., Gonzalez, C., & Bronner-Fraser, M. (2007). Neuropilin 2/semaphorin 3F signaling is essential for cranial neural crest migration and trigeminal ganglion condensation. *Developmental Neurobiology*, *67*(1), 47–56.

Gammill, L. S., Gonzalez, C., Gu, C., & Bronner-Fraser, M. (2006). Guidance of trunk neural crest migration requires neuropilin 2/semaphorin 3F signaling. *Development*, *133*(1), 99–106.

García-Castro, M. I., Marcelle, C., & Bronner-Fraser, M. (2002). Ectodermal Wnt Function as a Neural Crest Inducer. *Science*, *297*(5582), 848–851.

Gardner, H., Kreidberg, J., Koteliansky, V., & Jaenisch, R. (1996). Deletion of integrin alpha 1 by homologous recombination permits normal murine development but gives rise to a specific deficit in cell adhesion. *Developmental Biology*, *175*(2), 301–13.

Garneau, N. L., Wilusz, J., & Wilusz, C. J. (2007). The highways and byways of mRNA decay. *Nature Reviews. Molecular Cell Biology*, *8*(2), 113–126.

Gee, S. T., Milgram, S. L., Kramer, K. L., Conlon, F. L., & Moody, S. a. (2011). Yes-associated protein 65 (YAP) expands neural progenitors and regulates Pax3 expression in the neural plate border zone. *PloS One*, *6*(6), e20309.

Gilbert, S. F., & Singer, S. (2006). *Developmental Biology*. (C. Wigg, Ed.) (8th Editio., p. 785). Massachusetts, USA: Sinauer Associates, Inc.

Gilmour, D. T., Jessen, J. R., & Lin, S. (2002). Manipulating gene expression in the zebrafish. In N.-V. C. & R. Dahm (Eds.), *Zebrafish: a practical approach* (pp. 121–143). Oxford: Oxford University Press.

Gines, T. B., John, K. A., Dragoo, T., & Davidson, M. W. (2014). Enhanced Green Fluorescent Protein (EGFP) Chromophore Formation. [Online] [Accessed 21.07.2014] Available from: http://zeiss-campus.magnet.fsu.edu/tutorials/fluor

Gogas, H. J., Kirkwood, J. M., & Sondak, V. K. (2007). Chemotherapy for metastatic melanoma: time for a change? *Cancer*, *109*(3), 455–64.

Greenhill, E. R. (2008). *Genetic Regulation of Neural Crest Cell Differentiation*. PhD thesis. University of Bath.

Greenhill, E. R., & Kelsh, R. N. (2008). A pigment evolution Kitlg. *Pigment Cell & Melanoma Research*, *21*(2), 113–4.

Griffith, C., Wiley, M., & Sanders, E. (1992). The vertebrate tail bud: three germ layers from one tissue. *Anat Embryol (Berl).*, *185*(2), 101–113.

Gruber, F., Kastelan, M., Brajac, I., Saftić, M., Peharda, V., Cabrijan, L., … Simonić, E. (2008). Molecular and genetic mechanisms in melanoma. *Collegium Antropologicum*, *32 Suppl 2*, 147–52.

Haffter, P., Granato, M., Brand, M., Mullins, M. C., Hammerschmidt, M., Kane, D. a, … Nüsslein-Volhard, C. (1996). The identification of genes with unique and essential functions in the development of the zebrafish, Danio rerio. *Development*, *123*, 1–36.

Halder, G., & Johnson, R. L. (2011). Hippo signaling: growth control and beyond. *Development (Cambridge, England)*, *138*(1), 9–22.

Hama, T. (1975). Medaka (KILLFISH): Biology and Strains. In T. Yamamoto (Ed.), *Medaka (KILLFISH)* (pp. 138–153). Tokyo: Keigaku Publishing Company.

Hamaratoglu, F., Willecke, M., Kango-Singh, M., Nolo, R., Hyun, E., Tao, C., … Halder, G. (2006). The tumour-suppressor genes NF2/Merlin and Expanded act through Hippo signalling to regulate cell proliferation and apoptosis. *Nature Cell Biology*, *8*(1), 27–36.

Hamilton, G., Yee, K. S., Scrace, S., & O'Neill, E. (2009). ATM regulates a RASSF1A-dependent DNA damage response. *Current Biology : CB*, *19*(23), 2020–5.

Hao, Y., Chun, A., Cheung, K., Rashidi, B., & Yang, X. (2008). Tumor suppressor LATS1 is a negative regulator of oncogene YAP. *The Journal of Biological Chemistry*, *283*(9), 5496–509.

Harris, M. L., Hall, R., & Erickson, C. a. (2008). Directing pathfinding along the dorsolateral path - the role of EDNRB2 and EphB2 in overcoming inhibition. *Development*, *135*(24), 4113–22.

Hartl, F., & Hayer-Hartl, M. (2002). Molecular Chaperones in the Cytosol: from Nascent Chain to Folded Protein. *Science*, *295*(5561), 1852–1858.

Hasegawa, S., Maruyama, K., Takenaka, H., Furukawa, T., & Saga, T. (2009). A medaka model of cancer allowing direct observation of transplanted tumor cells in vivo at a cellular-level resolution. *Proceedings of the National Academy of Sciences of the United States of America*, *106*(33), 13832–7.

Hemesath, T. J., Price, E. R., Takemoto, C., Badalian, T., & Fisher, D. E. (1998). MAP kinase links the transcription factor Microphthalmia to c-Kit signalling in melanocytes. *Nature*, *391*(6664), 298–301.

Henderson, D. J., Ybot-gonzalez, P., & Copp, A. J. (1997). Over-expression of the chondroitin sulphate proteoglycan versican is associated with defective neural crest migration in the Pax3 mutant mouse (splotch). *Mechanisms of Development*, *69*, 39–51.

Herbarth, B., Pingault, V., Bondurand, N., Kuhlbrodt, K., Hermans-Borgmeyer, I., Puliti, a, … Wegner, M. (1998). Mutation of the Sry-related Sox10 gene in Dominant megacolon, a mouse model for human Hirschsprung disease. *Proceedings of the National Academy of Sciences of the United States of America*, *95*(9), 5161–5.

Ho, R., & Kane, D. (1990). Cell-autonomous action of zebrafish spt-1 mutation in specific mesodermal precursors. *Nature*, *348*(6303), 728–730.

Hodgkinson, C. a, Moore, K. J., Nakayama, a, Steingrímsson, E., Copeland, N. G., Jenkins, N. a, & Arnheiter, H. (1993). Mutations at the mouse microphthalmia locus are associated with defects in a gene encoding a novel basic-helix-loop-helix-zipper protein. *Cell*, *74*(2), 395–404.

Holmdahl, D. (1932). Die zweifache Bildungsweise des zentralen Nervensystems bei den Wirbeltieren. Eine formgeschinchtliche und materialgeschichtliche Analyse. *Wilhelm Roux' Arch Entwicklungsmech Org*, *129*, 206 – 254.

Holst, J., Szymczak-Workman, A. L., Vignali, K. M., Burton, A. R., Workman, C. J., & Vignali, D. a a. (2006). Generation of T-cell receptor retrogenic mice. *Nature Protocols*, *1*(1), 406–17.

Hong, C., & Saint-Jeannet, J.-P. (2007). The Activity of Pax3 and Zic1 Regulates Three Distinct Cell Fates at the Neural Plate Border. *Molecular Biology of the Cell*, *18*(June), 2192–2202.

Howe, K., Clark, M. D., Torroja, C. F., Torrance, J., Berthelot, C., Muffato, M., … Stemple, D. L. (2013). The zebrafish reference genome sequence and its relationship to the human genome. *Nature*, *496*(7446), 498–503.

Huang, J., Wu, S., Barrera, J., Matthews, K., & Pan, D. (2005). The Hippo signaling pathway coordinately regulates cell proliferation and apoptosis by inactivating Yorkie, the Drosophila Homolog of YAP. *Cell*, *122*(3), 421–34.

Huang, X., & Saint-Jeannet, J.-P. (2004). Induction of the neural crest and the opportunities of life on the edge. *Developmental Biology*, *275*(1), 1–11.

Huck-Hui, N., & Bird, A. (1999). DNA methylation and chromatin modification. *Current Opinion in Genetics & Development*, *9*(2), 158–163.

Hyodo-Taguchi, Y. (1996). Inbred strains of the medaka, Oryzias latipes. *Fish Biol. J.*, *8*(Medaka), 11–14.

Inoue, T., Chisaka, O., Matsunami, H., & Takeichi, M. (1997). Cadherin-6 expression transiently delineates specific rhombomeres, other neural tube subdivisions, and neural crest subpopulations in mouse embryos. *Developmental Biology*, *183*(2), 183–194.

Ishikawa, Y. (2000). Medakafish as a model system for vertebrate developmental genetics. *Bioessays*, *22*(5), 487–495.

Ito, T., Umehara, T., Sasaki, K., Nakamura, Y., Nishino, N., Terada, T., … Yoshida, M. (2011). Real-time imaging of histone H4K12-specific acetylation determines the modes of action of histone deacetylase and bromodomain inhibitors. *Chemistry & Biology*, *18*(4), 495–507.

Iwai, T., Inoue, S., Kotani, T., & Yamashita, M. (2009). Production of transgenic medaka fish carrying fluorescent nuclei and chromosomes. *Zoological Sciences*, *26*(1), 9–16.

Iwamatsu, T. (2004). Stages of normal development in the medaka Oryzias latipes. *Mechanisms of Development*, *121*(7-8), 605–18.

Jang, S. K., Kräusslich, H. G., Nicklin, M. J., Duke, G. M., Palmenberg, a C., & Wimmer, E. (1988). A segment of the 5' nontranslated region of encephalomyocarditis virus RNA directs internal entry of ribosomes during in vitro translation. *Journal of Virology*, *62*(8), 2636–43.

Jesus Carvalho, L. C. de. (2007). *The role of yolk syncytial layer and blastoderm movements during gastrulation in zebrafish*. PhD Thesis. Technische Universität Dresden.

Jia, L., Cheng, L., & Raper, J. (2005). Slit/Robo signaling is necessary to confine early neural crest cells to the ventral migratory pathway in the trunk. *Developmental Biology*, *282*(2), 411–21.

Jiang, Q., Liu, D., Gong, Y., Wang, Y., Sun, S., Gui, Y., & Song, H. (2009). Yap Is Required for the Development of Brain, Eyes, and Neural Crest in Zebrafish. *Biochemical and Biophysical Research Communications*, *384*(1), 114–9.

Jiang, T., Hou, C.-C., She, Z.-Y., & Yang, W.-X. (2013). The SOX gene family: function and regulation in testis determination and male fertility maintenance. *Molecular Biology Reports*, *40*(3), 2187–94.

Jiang, Z., Li, X., Hu, J., Zhou, W., Jiang, Y., Li, G., & Lu, D. (2006). Promoter hypermethylation-mediated down-regulation of LATS1 and LATS2 in human astrocytoma. *Neuroscience Research*, *56*(4), 450–458.

Jiao, Z., Zhang, Z. G., Hornyak, T. J., Hozeska, A., Zhang, R. L., Wang, Y., … Chopp, M. (2006). Dopachrome tautomerase (Dct) regulates neural progenitor cell proliferation. *Developmental Biology*, *296*(2), 396–408.

Johnson, R., & Halder, G. (2014). The two faces of Hippo: targeting the Hippo pathway for regenerative medicine and cancer treatment. *Nature Reviews. Drug Discovery*, *13*(1), 63–79.

Jung, S.-H., Kim, S., Chung, A.-Y., Kim, H.-T., So, J.-H., Ryu, J., … Kim, C.-H. (2010). Visualization of myelination in GFP-transgenic zebrafish. *Developmental Dynamics*, *239*(2), 592–7.

Kaji, K., Norrby, K., Paca, A., Mileikovsky, M., Mohseni, P., & Woltjen, K. (2009). Virus-free induction of pluripotency and subsequent excision of reprogramming factors. *Nature*, *458*, 771–775.

Kanai, F., Marignani, P. a, Sarbassova, D., Yagi, R., Hall, R. a, Donowitz, M., … Yaffe, M. B. (2000). TAZ: a novel transcriptional co-activator regulated by interactions with 14-3-3 and PDZ domain proteins. *The EMBO Journal*, *19*(24), 6778–91.

Kani, S., Bae, Y.-K., Shimizu, T., Tanabe, K., Satou, C., Parsons, M. J., … Hibi, M. (2010). Proneural gene-linked neurogenesis in zebrafish cerebellum. *Developmental Biology*, *343*(1-2), 1–17.

Kapur, R. P., Sweetser, D. a, Doggett, B., Siebert, J. R., & Palmiter, R. D. (1995). Intercellular signals downstream of endothelin receptor-B mediate colonization of the large intestine by enteric neuroblasts. *Development*, *121*(11), 3787–95.

Kashef, J., Köhler, A., Kuriyama, S., Alfandari, D., Mayor, R., & Wedlich, D. (2009). Cadherin-11 regulates protrusive activity in Xenopus cranial neural crest cells upstream of Trio and the small GTPases. *Genes & Development*, *23*(12), 1393–1398.

Kawakami, K. (2007). Tol2: a versatile gene transfer vector in vertebrates. *Genome Biology*, *8* (Suppl 1), 1–10.

Kelsh, R. N., Brand, M., Jiang, Y. J., Heisenberg, C. P., Lin, S., Haffter, P., … Nüsslein-Volhard, C. (1996). Zebrafish pigmentation mutations and the processes of neural crest development. *Development*, *123*, 369–89.

Kelsh, R. N., Dutton, K., Medlin, J., & Eisen, J. S. (2000). Expression of zebrafish fkd6 in neural crest-derived glia, *93*, 1998–2001.

Kelsh, R. N., & Eisen, J. S. (2000). The zebrafish colourless gene regulates development of non-ectomesenchymal neural crest derivatives. *Development*, *127*(3), 515–25.

Kelsh, R. N., Schmid, B., & Eisen, J. S. (2000). Genetic analysis of melanophore development in zebrafish embryos. *Developmental Biology*, *225*(2), 277–93.

Kelsh, R. N., Inoue, C., Momoi, A., Kondoh, H., Furutani-Seiki, M., Ozato, K., & Wakamatsu, Y. (2004). The Tomita collection of medaka pigmentation mutants as a resource for understanding neural crest cell development. *Mechanisms of Development*, *121*(7-8), 841–59.

Kelsh, R. N. (2004). Genetics and Evolution of Pigment Patterns in Fish. *Pigment Cell Research*, *17*(1), 326–336.

Kelsh, R. N., Harris, M. L., Colanesi, S., & Erickson, C. a. (2009). Stripes and belly-spots -- a review of pigment cell morphogenesis in vertebrates. *Seminars in Cell & Developmental Biology*, *20*(1), 90–104.

Kettenmann, H., & Verkhratsky, A. (2011). Neuroglia - Living Nerve Glue. *Fortschritte Der Neurologie Und Psychiatrie*, *79*, 588–597.

Khokhlatchev, A., Rabizadeh, S., Xavier, R., Nedwidek, M., Chen, T., Zhang, X., … Avruch, J. (2002). Identification of a novel Ras-regulated proapoptotic pathway. *Current Biology : CB*, *12*(4), 253–65.

Kikkawa, Y., Miura, I., Takahama, S., Wakana, S., Yamazaki, Y., Moriwaki, K., … Yonekawa, H. (2001). Microsatellite database for MSM/Ms and JF1/Ms, molossinus-derived inbred strains. *Mammalian Genome*, *12*(9), 750–2.

Kil, S., & Bronner-Fraser, M. (1996). Expression of the avian alpha 7-integrin in developing nervous system and myotome. *Int J Dev Neurosci*, *14*(3), 181–190.

Killian, E. C. O., Birkholz, D. A., & Artinger, K. B. (2009). A role for chemokine signaling in neural crest cell migration and craniofacial development. *Developmental Biology*, *333*(1), 161–172.

Kim, J. E., Finlay, G. J., & Baguley, B. C. (2013). The role of the hippo pathway in melanocytes and melanoma. *Frontiers in Oncology*, *3*(May), 123.

Kim, J. H., Lee, S.-R., Li, L.-H., Park, H.-J., Park, J.-H., Lee, K. Y., … Choi, S.-Y. (2011). High cleavage efficiency of a 2A peptide derived from porcine teschovirus-1 in human cell lines, zebrafish and mice. *PloS One*, *6*(4), e18556.

Kima, C.-H., Ueshimaa, E., Muraokaa, O., Tanakaa, H., Yeob, S.-Y., Huhb, T.-L., & Miki, N. (1996). Zebrafish elav/HuC homologue as a very early neuronal marker. *Neuroscience Letters*, *2*(2), 109–112.

Kimmel, C. B., Ballard, W. W., Kimmel, S. R., Ullmann, B., & Schilling, T. F. (1995). Stages of embryonic development of the zebrafish. *Developmental Dynamics*, *203*(3), 253–310.

Kinoshita, M., Murata, K. ., Naruse, K., & Tanaka, M. (2009). Medaka: Biology, Management, and Experimental Protocols. *Wiley-Blackwell*, Ames, Iowa.

Kitagawa, D., Watanabe, T., Saito, K., Asaka, S., Sasado, T., Morinaga, C., … Furutani-Seiki, M. (2004). Genetic dissection of the formation of the forebrain in Medaka, Oryzias latipes. *Mechanisms of Development*, *121*(7-8), 673–85.

Klüver, N., Kondo, M., Herpin, A., Mitani, H., & Schartl, M. (2005). Divergent expression patterns of Sox9 duplicates in teleosts indicate a lineage specific subfunctionalization. *Development Genes and Evolution*, *215*(6), 297–305.

Koide, T., Moriwaki, K., Uchida, K., Mita, A., Sagai, T., & Yonekawa, H. (1998). A new inbred strain JF1 established from Japanese fancy mouse carrying the classic piebald allele. *Mammalian Genoome*, *19*, 15–19.

Körner, A. M., & Pawelek, J. (1980). Dopachrome conversion: a possible control point in melanin biosynthesis. *The Journal of Investigative Dermatology*. 192-195.

Kozak, M. (2005). A second look at cellular mRNA sequences said to function as internal ribosome entry sites. *Nucleic Acids Research*, *33*(20), 6593–602.

Krull, C. (1998). Inhibitory interactions in the patterning of trunk neural crest migration. *Ann N Y Acad Sci*, *23*(857), 13–22.

Krull, C. E., Lansford, R., Gale, N. W., Collazo, a, Marcelle, C., Yancopoulos, G. D., … Bronner-Fraser, M. (1997). Interactions of Eph-related receptors and ligands confer rostrocaudal pattern to trunk neural crest migration. *Current Biology*, *7*(8), 571–80.

Kubota, Y., & Ito, K. (2000). Chemotactic migration of mesencephalic neural crest cells in the mouse. *Developmental Dynamics*, *217*(2), 170–9.

Kumar, R., Angelini, S., Snellman, E., & Hemminki, K. (2004). BRAF mutations are common somatic events in melanocytic nevi. *The Journal of Investigative Dermatology*, *122*(2), 342–8.

Kuo, B. R., & Erickson, C. a. (2010). Regional differences in neural crest morphogenesis. *Cell Adhesion & Migration*, *4*(4), 567–585.

LaBonne, C., & Bronner-Fraser, M. (1998). Neural crest induction in Xenopus: evidence for a two-signal model. *Development*, *125*(13), 2403–14.

Lai, Z.-C., Wei, X., Shimizu, T., Ramos, E., Rohrbaugh, M., Nikolaidis, N., … Li, Y. (2005). Control of cell proliferation and apoptosis by mob as tumor suppressor, mats. *Cell*, *120*(5), 675–85.

Lamar, J. M., Stern, P., Liu, H., Schindler, J. W., Jiang, Z.-G., & Hynes, R. O. (2012). The Hippo pathway target, YAP, promotes metastasis through its TEAD-interaction domain. *Proceedings of the National Academy of Sciences of the United States of America*, *109*(37), E2441–50.

Lamatsch, D., Steinlein, C., Schmid, M., & Schartl, M. (2000). Noninvasive determination of genome size and ploidy level in fishes by flow cytometry: detection of triploid Poecilia formosa. *Cytometry*, *39*(2), 91–95.

Landolt, R. M., Vaughan, L., Winterhalter, K. H., & Zimmermann, D. R. (1995). Versican is selectively expressed in embryonic tissues that act as barriers to neural crest cell migration and axon outgrowth, 2303–2312.

Langenau, D. M., Feng, H., Berghmans, S., Kanki, J. P., Kutok, J. L., & Look, a T. (2005). Cre/lox-regulated transgenic zebrafish model with conditional myc-induced T cell acute lymphoblastic leukemia. *Proceedings of the National Academy of Sciences of the United States of America*, *102*(17), 6068–73.

Le Clainche, C., & Carlier, M.-F. (2008). Regulation of actin assembly associated with protrusion and adhesion in cell migration. *Physiological Reviews*, *88*(2), 489–513.

Le Douarin, N., & Kalcheim, C. (1999). *The Neural Crest* (2nd ed.). Cambridge: Cambridge Univ. Press.

Le Douarin, N. M., Creuzet, S., Couly, G., & Dupin, E. (2004). Neural crest cell plasticity and its limits. *Development (Cambridge, England)*, *131*(19), 4637–50.

Lennon, S., Martin, S., & Cotter, T. (1991). Dose-dependent induction of apoptosis in human tumour cell lines by widely diverging stimuli. *Cell Prolif. 1991*, *24*(2), 203–214.

Levy, D., Adamovich, Y., Reuven, N., & Shaul, Y. (2008). Yap1 phosphorylation by c-Abl is a critical step in selective activation of proapoptotic genes in response to DNA damage. *Molecular Cell*, *29*(3), 350–61.

Lewis, J. L., Bonner, J., Modrell, M., Ragland, J. W., Moon, R. T., Dorsky, R. I., & Raible, D. W. (2004). Reiterated Wnt signaling during zebrafish neural crest development. *Development (Cambridge, England)*, *131*(6), 1299–308.

Li, M., Zhao, C., Wang, Y., Zhao, Z., & Meng, A. (2002). Zebrafish sox9b is an early neural crest marker. *Development Genes and Evolution*, *212*(4), 203–6.

Lian, I., Kim, J., Okazawa, H., Zhao, J., Zhao, B., Yu, J., … Guan, K. L. (2010). The role of YAP transcription coactivator in regulating stem cell self-renewal and differentiation. *Genes & Development*, *24*(11), 1106–1118.

Lister, J., Robertson, C. P., Lepage, T., Johnson, S. L., & Raible, D. W. (1999). Nacre Encodes a Zebrafish Microphthalmia-Related Protein That Regulates Neural-Crest-Derived Pigment Cell Fate. *Development*, *126*(17), 3757–67.

Liu, J. A. J., Wu, M., Yan, C. H., Chau, B. K. H., So, H., Ng, A., … Cheung, M. (2013). Phosphorylation of Sox9 is required for neural crest delamination and is regulated downstream of BMP and canonical Wnt signaling, *PNAS, 2(110),* 2882-2887.

Liu-Chittenden, Y., Huang, B., Shim, J. S., Chen, Q., Lee, S.-J., Anders, R. a, … Pan, D. (2012). Genetic and pharmacological disruption of the TEAD-YAP complex suppresses the oncogenic activity of YAP. *Genes & Development*, *26*(12), 1300–5.

Loosli, F., Köster, R. W., Carl, M., Kühnlein, R., Henrich, T., Mücke, M., … Wittbrodt, J. (2000). A genetic screen for mutations affecting embryonic development in medaka fish (Oryzias latipes). *Mechanisms of Development*, *97*(1-2), 133–9.

Lopes, S. S., Yang, X., Müller, J., Carney, T. J., McAdow, A. R., Rauch, G.-J., … Kelsh, R. N. (2008). Leukocyte tyrosine kinase functions in pigment cell development. *PLoS Genetics*, *4*(3), e1000026.

Lorenzetto, E., Brenca, M., Boeri, M., Verri, C., Piccinin, E., Gasparini, P., … Modena, P. (2014). YAP1 acts as oncogenic target of 11q22 amplification in multiple cancer subtypes. *Oncotarget*, *5*(9), 2608–2621.

Lowery, L. A., & Sive, H. (2004). Strategies of vertebrate neurulation and a re-evaluation of teleost neural tube formation. *Mechanisms of Development*, *121*(10), 1189–97.

Lynn Lamoreux, M., Kelsh, R. N., Wakamatsu, Y., & Ozato, K. (2005). Pigment pattern formation in the medaka embryo. *Pigment Cell Research, 18*(2), 64–73.

Ma, L., Tamarina, N., Wang, Y., Kuznetsov, A., Patel, N., Kending, C., … Philipson, L. H. (2000). Baculovirus-Mediated Gene Transfer Into Pancreatic Islet Cells. *Diabetes*, *49*(12).

Ma, Q., Fode, C., Guillemot, F., & Anderson, D. J. (1999). Neurogenin1 and neurogenin2 control two distinct waves of neurogenesis in developing dorsal root ganglia, 1717–1728.

Mackenzie, M. a, Jordan, S. a, Budd, P. S., & Jackson, I. J. (1997). Activation of the receptor tyrosine kinase Kit is required for the proliferation of melanoblasts in the mouse embryo. *Developmental Biology*, *192*(1), 99–107.

Maden, M. (2002). Retinoid signalling in the development of the central nervous system. *Nature Reviews. Neuroscience*, *3*(11), 843–53.

Marchant, L., Linker, C., Ruiz, P., Guerrero, N., & Mayor, R. (1998). The inductive properties of mesoderm suggest that the neural crest cells are specified by a BMP gradient. *Developmental Biology*, *198*(2), 319–29.

Marie, H., Pratt, S. J., Betson, M., Epple, H., Kittler, J. T., Meek, L., … Braga, V. M. M. (2003). The LIM protein Ajuba is recruited to cadherin-dependent cell junctions through an association with alpha-catenin. *The Journal of Biological Chemistry*, *278*(2), 1220–1228.

Martinez-Morales, J. R., Rembold, M., Greger, K., Simpson, J. C., Brown, K. E., Quiring, R., … Wittbrodt, J. (2009). Ojoplano-Mediated Basal Constriction Is Essential for Optic Cup Morphogenesis. *Development*, *136*(13), 2165–75.

Matakatsu, H., & Blair, S. S. (2004). Interactions between Fat and Dachsous and the regulation of planar cell polarity in the Drosophila wing. *Development*, *131*(15), 3785–3794.

Matzke, a J., & Matzke, M. a. (1998). Position effects and epigenetic silencing of plant transgenes. *Current Opinion in Plant Biology*, *1*(2), 142–8.

Mayanil, C. S., George, D., Freilich, L., Miljan, E. J., Mania-Farnell, B., McLone, D. G., & Bremer, E. G. (2001). Microarray analysis detects novel Pax3 downstream target genes. *The Journal of Biological Chemistry*, *276*(52), 49299–49309.

Mayor, R., Guerrero, N., & Martínez, C. (1997). Role of FGF and noggin in neural crest induction. *Developmental Biology*, *189*(1), 1–12.

Mayor, R., & Theveneau, E. (2013). The neural crest. *Development*, *140*(11), 2247–51.

McGraw, H. F., Nechiporuk, A., & Raible, D. W. (2008). Zebrafish dorsal root ganglia neural precursor cells adopt a glial fate in the absence of neurogenin1. *The Journal of Neuroscience*, *28*(47), 12558–69.

McKeown, S. J., Wallace, A. S., & Anderson, R. B. (2013). Expression and function of cell adhesion molecules during neural crest migration. *Developmental Biology*, *373*(2), 244–57.

McLennan, R., Dyson, L., Prather, K. W., Morrison, J. a, Baker, R. E., Maini, P. K., & Kulesa, P. M. (2012). Multiscale mechanisms of cell migration during development: theory and experiment. *Development*, *139*(16), 2935–2944.

McLennan, R., & Kulesa, P. M. (2007). In vivo analysis reveals a critical role for neuropilin-1 in cranial neural crest cell migration in chick. *Developmental Biology*, *301*(1), 227–239.

McLennan, R., Teddy, J., Kasemeier-Kulesa, J., Romine, M., & Kulesa, P. (2010). Vascular endothelial growth factor (VEGF) regulates cranial neural crest migration in vivo. *Developmental Biology*, *339*(1), 114–125.

Meierjohann, S., & Schartl, M. (2006). From Mendelian to molecular genetics: the Xiphophorus melanoma model. *Trends in Genetics : TIG*, *22*(12), 654–661.

Mella-Alvarado, V., Gautier, A., Le Gac, F., & Lareyre, J. (2013). Tissue and cell-specific transcriptional activity of the human cytomegalovirus immediate early gene promoter (UL123) in zebrafish. *Gene Expr Patterns*, *13*(3-4), 91–103.

Meyer, A., & Schartl, M. (1999). Gene and genome duplications in vertebrates: the one-to-four (-to-eight in fish) rule and the evolu- tion of novel gene functions. *Curr Opin Cell Biol.*, *11*(6), 699–704.

Michailidou, C., Jones, M., Walker, P., Kamarashev, J., Kelly, A., & Hurlstone, A. F. L. (2009). Dissecting the roles of Raf- and PI3K-signalling pathways in melanoma formation and progression in a zebrafish model. *Disease Models & Mechanisms*, *2*(7-8), 399–411.

Milewski, R. C., Chi, N. C., Li, J., Brown, C., Lu, M. M., & Epstein, J. a. (2004). Identification of minimal enhancer elements sufficient for Pax3 expression in neural crest and implication of Tead2 as a regulator of Pax3. *Development*, *131*(4), 829–937.

Miller, A. ., & Mihm, M. (2006). Mechanisms of Disease - Melanoma. *The New England Journal of Medicine*, 51–65.

Milunsky, J. M. (2001). Waardenburg Syndrome Type I. [Online] [Accessed 08.09.2014] Available from: http://www.ncbi.nlm.nih.gov/books/NBK1531/

Minchin, J. E. N., & Hughes, S. M. (2010). Sequential actions of Pax3 and Pax7 drive xanthophore development in zebrafish neural crest, *317*(2), 508–522.

Mione, M. C., & Trede, N. S. (2010). The zebrafish as a model for cancer. *Disease Models & Mechanisms*, *3*(9-10), 517–23.

Miyayama, Y., & Fujimoto, T. (1977). Fine morphological study of neural tube formation in the teleost, Oryzias latipes. *Okajimas Folia Anat Jpn*, *54*(2-3), 97–120.

Mo, J.-S., Park, H. W., & Guan, K.-L. (2014). The Hippo signaling pathway in stem cell biology and cancer. *EMBO Reports*, *15*(6), 642–56.

Moase, C. E., & Trasler, D. G. (1992). Splotch locus mouse mutants: models for neural tube defects and Waardenburg syndrome type I in humans. *Journal of Medical Genetics*, *29*(3), 145–51.

Monk, K. R., Oshima, K., Jörs, S., Heller, S., & Talbot, W. S. (2011). Gpr126 is essential for peripheral nerve development and myelination in mammals, *2680*, 2673–2680.

Monsonego-Ornan, E., Kosonovsky, J., Bar, A., Roth, L., Fraggi-Rankis, V., Simsa, S., … Sela-Donenfeld, D. (2012). Matrix metalloproteinase 9/gelatinase B is required for neural crest cell migration. *Developmental Biology*, *364*(2), 162–77.

Monsoro-Burq, A.-H., Fletcher, B. R., & Harland, R. M. (2003). Neural crest induction by paraxial mesoderm in Xenopus embryos requires FGF signals. *Development*, *130*(14), 3111–3124.

Montero, J.-A., Carvalho, L., Wilsch-Bräuninger, M., Kilian, B., Mustafa, C., & Heisenberg, C.-P. (2005). Shield formation at the onset of zebrafish gastrulation. *Development*, *132*(6), 1187–98.

Nagao, Y., Suzuki, T., Shimizu, A., Kimura, T., Seki, R., Adachi, T., … Hashimoto, H. (2014). Sox5 functions as a fate switch in medaka pigment cell development. *PLoS Genetics*, *10*(4), e1004246.

Nakagawa, S., & Takeichi, M. (1995). Neural crest cell-cell adhesion controlled by sequential and subpopulation-specific expression of novel cadherins. *Development*, *121*(5), 1321–1332.

Nakamura, S., Aoki, Y., Saito, D., Kuroki, Y., Fujiyama, A., Naruse, K., & Tanaka, M. (2008). Sox9b / sox9a2-EGFP Transgenic Medaka Reveals the Morphological Reorganization of the Gonads and a Common Precursor of Both the Female and Male Supporting Cells, *476*(May 2007), 472–476.

Nakamura, S., Yumiko, A., Saito, D., Kuroki, Y., Fujiyama, A., And, K. N., & Tanaka, M. (2007). Sox9b/sox9a2-EGFP transgenic medaka reveals the morphological reorganization of the gonads and a common precursor of both the female and male supporting cells. *Molecular Reproduction and Development*, *75*(3), 472–476.

Nallet-Staub, F., Marsaud, V., Li, L., Gilbert, C., Dodier, S., Bataille, V., … Mauviel, A. (2014). Pro-invasive activity of the Hippo pathway effectors YAP and TAZ in cutaneous melanoma. *The Journal of Investigative Dermatology*, *134*(1), 123–32.

Nano, & Drop Technologies, I. (2007). 260/280 and 260/230 ratios. [Online] [Accessed 31.08.2014] Available from: http://www.bio.davidson.edu/projects/gcat/protocols/NanoDrop_tip.pdf

Neill, E. O. ', Rushworth, L., Baccarini, M., & Kolch, W. (2004). Role of the Kinase MST2 in Suppression of Apoptosis by the Proto-Oncogene Product Raf-1. *Science*, *306*(5705), 2267–2270.

Nelms, B., & Labosky, P. (2010a). Fox Genes. [Online] In *Transcriptional Control of Neural Crest Development.* Chapter 5, Morgan & Claypool Life Sciences.

Nelms, B., & Labosky, P. (2010b). Pax Genes. [Online] In *Transcriptional Control of Neural Crest Development*. Chapter 9.1, Morgan & Claypool Life Sciences.

Niehrs, C. (2004). Regionally specific induction by the Spemann-Mangold organizer. *Nature Reviews. Genetics*, *5*(6), 425–34.

Nobukuni, Y., Watanabe, a, Takeda, K., Skarka, H., & Tachibana, M. (1996). Analyses of loss-of-function mutations of the MITF gene suggest that haploinsufficiency is a cause of Waardenburg syndrome type 2A. *American Journal of Human Genetics*, *59*(1), 76–83.

Nüsslein-Volhard, C. (2012). The zebrafish issue of Development. *Development*, *139*(22), 4099–103.

Odenthal, J., & Nüsslein-Volhard, C. (1998). fork head domain genes in zebrafish. *Development Genes and Evolution*, *208*(5), 245–258.

Ohata, S., Kinoshita, S., Aoki, R., Tanaka, H., Wada, H., Tsuruoka-Kinoshita, S., … Okamoto, H. (2009). Neuroepithelial cells require fucosylated glycans to guide the migration of vagus motor neuron progenitors in the developing zebrafish hindbrain. *Development*, *136*(10), 1653–63.

Oka, T., Mazack, V., & Sudol, M. (2008). Mst2 and Lats kinases regulate apoptotic function of Yes kinase-associated protein (YAP). *The Journal of Biological Chemistry*, *283*(41), 27534–46.

Oliphant, L., & Hudon, J. (1993). Pteridines as reflecting pigments and components of reflecting organelles in vertebrates. *Pigment Cell Research*, *6*(4 Pt 1)), 205–208.

Oren, M., & Aylon, Y. (2013). *The Hippo Signaling Pathway and Cancer* (pp. 75–77).

Ori, M., Nardini, M., Casini, P., Perris, R., & Nardi, I. (2006). XHas2 activity is required during somitogenesis and precursor cell migration in Xenopus development. *Development*, *133*(4), 631–640.

Ota, M., & Sasaki, H. (2008). Mammalian Tead proteins regulate cell proliferation and contact inhibition as transcriptional mediators of Hippo signaling. *Development*, *135*(24), 4059–69.

Overholtzer, M., Zhang, J., Smolen, G. a, Muir, B., Li, W., Sgroi, D. C., … Haber, D. a. (2006). Transforming properties of YAP, a candidate oncogene on the chromosome 11q22 amplicon. *Proceedings of the National Academy of Sciences of the United States of America*, *103*(33), 12405–10.

Palmer, E., & Freeman, T. (2004). Investigation into the use of C- and N-terminal GFP fusion proteins for subcellular localization studies using reverse transfection microarrays. *Comparative and Functional Genomics*, *5*(4), 342–53.

Pan, D. (2010a). The hippo signaling pathway in development and cancer. *Developmental Cell*, *19*(4), 491–505.

Papan, C., & Campos-Ortega, J. A. (1994). On the formation of the neural keel and neural tube in the zebrafishDanio (Brachydanio) rerio. *Developmental Biology*, *203*(4), 178–186.

Paramasivam, M., Sarkeshik, A., Yates, J. R., Fernandes, M. J. G., & McCollum, D. (2011). Angiomotin family proteins are novel activators of the LATS2 kinase tumor suppressor. *Molecular Biology of the Cell*, *22*(19), 3725–33.

Parichy, D. M. (2011). *mRNA IN SITU HYBRIDIZATION FOR LARVAL FISH* (pp. 1–18). [Online] [Accessed 02.07.2014] Available from: http://faculty.washington.edu/dparichy/Protocols_files/ISH120823.pdf

Parichy, D. M., Mellgren, E. M., Rawls, J. F., Lopes, S. S., Kelsh, R. N., & Johnson, S. L. (2000). Mutational analysis of endothelin receptor b1 (rose) during neural crest and pigment pattern development in the zebrafish Danio rerio. *Developmental Biology*, *227*(2), 294–306.

Parichy, D. M., Ransom, D. G., Paw, B., Zon, L. I., & Johnson, S. L. (2000). An orthologue of the kit-related gene fms is required for development of neural crest-derived xanthophores and a subpopulation of adult melanocytes in the zebrafish, Danio rerio. *Development*, *127*(14), 3031–44.

Parichy, D. M., Rawls, J. F., Pratt, S. J., Whitfield, T. T., & Johnson, S. L. (1999). Zebrafish sparse corresponds to an orthologue of c-kit and is required for the morphogenesis of a subpopulation of melanocytes, but is not essential for hematopoiesis or primordial germ cell development. *Development*, *126*(15), 3425–36.

Parinov, S., Kondrichin, I., Korzh, V., & Emelyanov, A. (2004). Tol2 transposon-mediated enhancer trap to identify developmentally regulated zebrafish genes in vivo. *Developmental Dynamics : An Official Publication of the American Association of Anatomists*, *231*(2), 449–59.

Patton, E. E., Widlund, H. R., Kutok, J. L., Kopani, K. R., Amatruda, J. F., Murphey, R. D., … Zon, L. I. (2005). BRAF mutations are sufficient to promote nevi formation and cooperate with p53 in the genesis of melanoma. *Current Biology*, *15*(3), 249–54.

Pattyn, A., Morin, X., Cremer, H., Goridis, C., & Brunet, J.-F. (1999). The homeobox gene Phox2b is essential for the development of autonomic neural crest derivatives. *Nature*, *399*, 366–370.

Pei, D., Luther, W., Wang, W., Paw, B. H., Stewart, R. a, & George, R. E. (2013). Distinct neuroblastoma-associated alterations of PHOX2B impair sympathetic neuronal differentiation in zebrafish models. *PLoS Genetics*, *9*(6), e1003533.

Pelletier, I., Bally-Cuif, L., & Ziegler, I. (2001). Cloning and developmental expression of zebrafish GTP cyclohydrolase I. *Mechanisms of Development*, *109*(1), 99–103.

Pelletier, J., & Sonenberg, N. (1988). Internal initiation of translation of eukaryotic mRNA directed by a sequence derived from poliovirus RNA. *Nature*, *334*, 320 – 325.

Perissinotto, D., Iacopetti, P., Bellina, I., Doliana, R., Colombatti, a, Pettway, Z., … Perris, R. (2000). Avian neural crest cell migration is diversely regulated by the two major hyaluronan-binding proteoglycans PG-M/versican and aggrecan. *Development*, *127*(13), 2823–42.

Perlin, J. R., Lush, M. E., Stephens, W. Z., Piotrowski, T., & Talbot, W. S. (2011). Neuronal Neuregulin 1 type III directs Schwann cell migration. *Development*, *138*(21), 4639–48.

Perris, R., & Perissinotto, D. (2000). Role of the extracellular matrix during neural crest cell migration. *Mechanisms of Development*, *95*(1-2), 3–21.

Piccioli, P., Serra, M., Gismondi, V., Pedemonte, S., Loiacono, F., Lastraioli, S., … Notaro, R. (2006). Multiplex Tetra-Primer Amplification Refractory Mutation System PCR to Detect 6 Common Germline Mutations of the MUTYH Gene Associated with Polyposis and Colorectal Cancer. *Clinical Chemistry*, *52*(4), 739–743.

Pierce, B. A. (2012). Programmed Cell Death Is an Integral Part of Development. In *Genetics: A conceptual approach* (4th ed., pp. 633–643f). New York: W.H. Freeman an Company.

Piston, D. W., Patterson, G. H., Lippincott-Schwartz, J., & Davidson, N. S. C. M. W. (2013). Introduction to Fluorescent Proteins. [Online] [Accessed 24.09.2014] Available from: http://www.microscopyu.com/articles/livecellimaging/fpintro.html

Porazinski, S. (2013). *YAP-regulation of dynamic cell behaviour underlying organogenesis*. PhD thesis. University of Bath.

Porazinski, S. R., Wang, H., & Furutani-Seiki, M. (2010). Microinjection of medaka embryos for use as a model genetic organism. *Journal of Visualized Experiments : JoVE*, (46), 2–5.

Price, E. R., Ding, H.-F., Badalian, T., Bhattacharya, S., Takemoto, C., Yao, T.-P., … Fisher, D. E. (1998). Lineage-specific Signaling in Melanocytes: c-Kit STIMULATION RECRUITS p300/CBP TO MICROPHTHALMIA. *Journal of Biological Chemistry*, *273*(29), 17983–17986.

Qin, J. Y., Zhang, L., Clift, K. L., Hulur, I., Xiang, A. P., Ren, B.-Z., & Lahn, B. T. (2010). Systematic comparison of constitutive promoters and the doxycycline-inducible promoter. *PloS One*, *5*(5), e10611.

Raible, D. W., & Eisen, J. S. (1994). Restriction of neural crest cell fate in the trunk of the embryonic zebrafish. *Development*, *120*(3), 495–503.

Raible, D. W., Wood, a, Hodsdon, W., Henion, P. D., Weston, J. a, & Eisen, J. S. (1992). Segregation and early dispersal of neural crest cells in the embryonic zebrafish. *Developmental Dynamics : An Official Publication of the American Association of Anatomists*, *195*(1), 29–42.

Rawls, A., & Olson, E. N. (1997). MyoD meets its Marker. *Cell*, *89*, 5–8.

Rebagliati, M. R., Toyama, R., Haffter, P., & Dawid, I. B. (1998). Cyclops Encodes a Nodal-Related Factor Involved in Midline Signaling. *Proceedings of the National Academy of Sciences of the United States of America*, *95*(17), 9932–7.

Reeves, A. G., & Swenson, R. S. (2008). Demyelinating diseases of the nervous system. In J. Cohen, C. Fadul, L. Jenkyn, & T. Ward (Eds.), *Disorders of the Nervous System.* Chapter 3. [Online]. Dartmouth Medical School. [Accessed 23.08.2014] Available from: http://www.dartmouth.edu/~dons/part_3/chapter_23.html

Richter, A. M., Pfeifer, G. P., & Dammann, R. H. (2009). The RASSF proteins in cancer; from epigenetic silencing to functional characterization. *Biochimica et Biophysica Acta*, *1796*(2), 114–128.

Ridley, A. J., Schwartz, M. a, Burridge, K., Firtel, R. a, Ginsberg, M. H., Borisy, G., … Horwitz, A. R. (2003). Cell migration: integrating signals from front to back. *Science*, *302*(5651), 1704–1709.

Ryan, M. D., King, a M., & Thomas, G. P. (1991). Cleavage of foot-and-mouth disease virus polyprotein is mediated by residues located within a 19 amino acid sequence. *The Journal of General Virology*, *72(11)*, 2727–32.

SAMBROOK, J., FRITSCH, E. D., & MANIATIS, T. (1989). Molecular Cloning: A Laboratory Manual. In *Cold Spring Harbor: Cold Spring Harbor Laboratory Press* (2nd ed.), 49–55.

Sampath, K., & Sudipto, R. (2010). Live Imaging in Zebrafish: Insights Into Development and Disease. *World Scientific.* 1–151.

Santiago, A., & Erickson, C. a. (2002). Ephrin-B ligands play a dual role in the control of neural crest cell migration. *Development (Cambridge, England)*, *129*(15), 3621–32.

Santoriello, C., Gennaro, E., Anelli, V., Distel, M., Kelly, A., Köster, R. W., … Mione, M. (2010). Kita driven expression of oncogenic HRAS leads to early onset and highly penetrant melanoma in zebrafish. *PloS One, 5(12)*, e15170.

Sasselli, V., Pachnis, V., & Burns, A. J. (2012). The enteric nervous system. *Developmental Biology*, *366*(1), 64–73.

Sato, T., Sasai, N., & Sasai, Y. (2005). Neural crest determination by co-activation of Pax3 and Zic1 genes in Xenopus ectoderm. *Development*, *132*(10), 2355–63.

Saucedo, L. J., & Edgar, B. a. (2007). Filling out the Hippo pathway. *Nature Reviews. Molecular Cell Biology*, *8*(8), 613–21.

Sauka-Spengler, T., & Bronner-Fraser, M. (2008). A gene regulatory network orchestrates neural crest formation. *Nature Reviews. Molecular Cell Biology*, *9*(7), 557–68.

Schartl, M., Wilde, B., Laisney, J. a G. C., Taniguchi, Y., Takeda, S., & Meierjohann, S. (2010). A mutated EGFR is sufficient to induce malignant melanoma with genetic background-dependent histopathologies. *The Journal of Investigative Dermatology*, *130*(1), 249–58.

Schlegelmilch, K., Mohseni, M., Kirak, O., Pruszak, J., Rodriguez, J. R., Zhou, D., … Camargo, F. D. (2011). Yap1 acts downstream of α-catenin to control epidermal proliferation. *Cell*, *144*(5), 782–95.

Schwarz, Q., Maden, C. H., Davidson, K., & Ruhrberg, C. (2009). Neuropilin-mediated neural crest cell guidance is essential to organise sensory neurons into segmented dorsal root ganglia. *Development*, *136*(11), 1785–9.

Schwarz, Q., Maden, C. H., Vieira, J. M., & Ruhrberg, C. (2009). Neuropilin 1 signaling guides neural crest cells to coordinate pathway choice with cell specification. *Proceedings of the National Academy of Sciences of the United States of America*, *106*(15), 6164–9.

Seidel, C., Schagdarsurengin, U., Blümke, K., Würl, P., Pfeifer, G. P., Hauptmann, S., … Dammann, R. (2007). Frequent hypermethylation of MST1 and MST2 in soft tissue sarcoma. *Molecular Carcinogenesis*, *46*(10), 865–871.

Serbedzija, G. N., & McMahon, a P. (1997). Analysis of neural crest cell migration in Splotch mice using a neural crest-specific LacZ reporter. *Developmental Biology*, *185*(2), 139–47.

Sherman, D., & Brophy, P. (2005). Mechanisms of axon ensheathment and myelin growth. *Nature Reviews Neuroscience*, *6*, 683–690.

Sigma Aldrich (2014). CMV Vectors for High Level Mammalian Expression. [Online] [Accessed 28.07.2014] Available from: http://www.sigmaaldrich.com/life-science/molecular-biology/cloning-and-expression/vector-systems/transient-expression.html

Singh, P., Carraher, C., & Schwarzbauer, J. E. (2010). Assembly of fibronectin extracellular matrix. *Annual Review of Cell and Developmental Biology*, *26*, 397–419.

Slominski, A., & Paus, R. (1993). Melanogenesis is coupled to murine anagen: toward new concepts for the role of melanocytes and the regulation of melanogenesis in hair growth. *J Invest Dermatol*, *101*(1), 90S–97S.

Soroldoni, D., Hogan, B. M., & Oates, A. C. (2009). Simple and Efficient Transgenesis with Meganuclease Constructs in Zebrafish. *Methods in Molecular Biology*, *546*, 117–130.

Steel, K. P., Davidson, D. R., & Jackson, I. J. (1992). TRP-2/DT, a new early melanoblast marker, shows that steel growth factor (c-kit ligand) is a survival factor. *Development*, *115*(4), 1111–9.

Steinhardt, A. A., Gayyed, M. F., Klein, A. P., Dong, J., Maitra, A., Pan, D., … Anders, R. A. (2008). Expression of Yes-associated Protein, YAP, in Common Solid Tumors. *Science*, *39*(11), 1582–1589.

Sternberg, J., & Kimber, S. J. (1986). Distribution of fibronectin, laminin and entactin in the environment of migrating neural crest cells in early mouse embryos. *Journal of Embryology and Experimental Morphology*, *91*, 267–82.

Strano, S., Munarriz, E., Rossi, M., Castagnoli, L., Shaul, Y., Sacchi, a, … Blandino, G. (2001). Physical interaction with Yes-associated protein enhances p73 transcriptional activity. *The Journal of Biological Chemistry*, *276*(18), 15164–73.

Streisinger, G., Walker, C., Dower, N., Knauber, D., & Singer, F. (1981). Production of clones of homozygous diploid zebra fish (Brachydanio rerio). *Nature*, *291*, 293–296.

Stuart, G. W., McMurray, J. V, & Westerfield, M. (1988). Replication, integration and stable germ-line transmission of foreign sequences injected into early zebrafish embryos. *Development*, *103*(2), 403–412.

Sudol, M., Bork, P., Einbond, a, Kastury, K., Druck, T., Negrini, M., … Lehman, D. (1995). Characterization of the mammalian YAP (Yes-associated protein) gene and its role in defining a novel protein module, the WW domain. *The Journal of Biological Chemistry*, *270(16)*, 14733-41.

Svaren, J., & Meijer, D. (2008). The molecular machinery of myelin gene transcription in Schwann cells. *Glia*, *56*(14), 1541–51.

Tachibana, M., Kobayashi, Y., & Matsushima, Y. (2003). Mouse Models for Four Types of Waardenburg Syndrome. *Pigment Cell Research*, *16*(5), 448–454.

Tajbakhsh, S., Rocancourt, D., Cossu, G., & Buckingham, M. (1997). Redefining the genetic hierarchies controlling skeletal myogenesis: Pax-3 and Myf-5 act upstream of MyoD. *Cell*, *89*(1), 127–38.

Takahashi, K., & Yamanaka, S. (2006). Induction of pluripotent stem cells from mouse embryonic and adult fibroblast cultures by defined factors. *Cell*, *126*(4), 663–76.

Takahashi, Y., Miyoshi, Y., Takahata, C., Irahara, N., & Taguchi, T. (2005). Down-Regulation of LATS1 and LATS2 mRNA Expression by Promoter Hypermethylation and Its Association with Biologically Aggressive Phenotype in Human Breast Cancers Down-Regulation of LATS1 and LATS2 mRNA Expression by Promoter Hypermethylation and Its Asso. *Clinical Cancer Research*, *11*, 1380–1385.

Tamm, C., Böwer, N., & Annerén, C. (2011). Regulation of mouse embryonic stem cell self-renewal by a Yes-YAP-TEAD2 signaling pathway downstream of LIF. *Journal of Cell Science*, *124*(Pt 7), 1136–44.

Taniguchi, Y., Takeda, S., Furutani-Seiki, M., Kamei, Y., Todo, T., Sasado, T., … Cuppen, E. (2006). Generation of medaka gene knockout models by target-selected mutagenesis. *Genome Biology*, *7*(12), R116.

Tapon, N., Harvey, K. F., Bell, D. W., Wahrer, D. C. R., Schiripo, T. a, Haber, D. a, & Hariharan, I. K. (2002). salvador Promotes both cell cycle exit and apoptosis in Drosophila and is mutated in human cancer cell lines. *Cell*, *110*(4), 467–78.

Tassabehji, M., Newton, V., & Read, A. (1994). Waardenburg syndrome type 2 caused by mutations in the human microphthalmia (MITF) gene. *Nat Genet*, *8*(3), 251–255.

Thakur, M. Das, Feng, Y., Jagannathan, R., Seppa, M. J., James, B., Longmore, G. D., & Mo, L. (2010). Ajuba LIM proteins are negative regulators of the Hippo signaling pathway. *Current Biology*, *20*(7), 657–662.

Thermes, V., Grabher, C., Ristoratore, F., Bourrat, F., Choulika, A., Wittbrodt, J., & Joly, J.-S. (2002). I-SceI meganuclease mediates highly efficient transgenesis in fish. *Mechanisms of Development*, *118*(1-2), 91–8.

Theveneau, E., Marchant, L., Kuriyama, S., Gull, M., Moepps, B., Parsons, M., & Mayor, R. (2010). Collective chemotaxis requires contact-dependent cell polarity. *Developmental Cell*, *19*(1), 39–53.

Theveneau, E., & Mayor, R. (2012). Neural crest delamination and migration: from epithelium-to-mesenchyme transition to collective cell migration. *Developmental Biology*, *366*(1), 34–54.

Thummel, R., Burket, C. T., & Hyde, D. R. (2006). Two different transgenes to study gene silencing and re-expression during zebrafish caudal fin and retinal regeneration. *TheScientificWorldJournal*, *6 Suppl 1*, 65–81.

Trainor, P. (2013). Neural Crest Cells: Evolution, Development and Disease, *Academic Press, 1st Ed, Abstract,* 488

Tremblay, P., Dietrich, S., Mericskay, M., Schubert, F. R., Li, Z., & Paulin, D. (1998). A crucial role for Pax3 in the development of the hypaxial musculature and the long-range migration of muscle precursors. *Developmental Biology*, *203*(1), 49–61.

Trinh, R., Gurbaxani, B., Morrison, S. L., & Seyfzadeh, M. (2004). Optimization of codon pair use within the (GGGGS)3 linker sequence results in enhanced protein expression. *Molecular Immunology*, *40*(10), 717–712.

Udan, R. S., Kango-Singh, M., Nolo, R., Tao, C., & Halder, G. (2003). Hippo promotes proliferation arrest and apoptosis in the Salvador/Warts pathway. *Nature Cell Biology*, *5*(10), 914–20.

Uong, A., & Zon, L. I. (2010). Melanocytes in development and cancer. *Journal of Cellular Physiology*. 38-41

Valencia-Sanchez, M. A., Liu, J., Hannon, G. J., & Parker, R. (2006). Control of translation and mRNA degradation by miRNAs and siRNAs. *Genes & Development*, *20*(5), 515–524.

Van Hateren, N. J., Das, R. M., Hautbergue, G. M., Borycki, A.-G., Placzek, M., & Wilson, S. a. (2011). FatJ acts via the Hippo mediator Yap1 to restrict the size of neural progenitor cell pools. *Development*, *138*(10), 1893–902.

Van Otterloo, E., Li, W., Bonde, G., Day, K. M., Hsu, M.-Y., & Cornell, R. a. (2010). Differentiation of zebrafish melanophores depends on transcription factors AP2 alpha and AP2 epsilon. *PLoS Genetics*, *6*(9), e1001122.

Vassilev, A., Kaneko, K. J., Shu, H., Zhao, Y., & Depamphilis, M. L. (2001). TEAD / TEF transcription factors utilize the activation domain of YAP65 , a Src / Yes-associated protein localized in the cytoplasm. *Genes & Development, 15*, 1229–1241.

Voorhoeve, P. M., le Sage, C., Schrier, M., Gillis, A. J. M., Stoop, H., Nagel, R., … Agami, R. (2006). A genetic screen implicates miRNA-372 and miRNA-373 as oncogenes in testicular germ cell tumors. *Cell*, *124*(6), 1169–81.

Wada, K.-I., Itoga, K., Okano, T., Yonemura, S., & Sasaki, H. (2011). Hippo pathway regulation by cell morphology and stress fibers. *Development*, *138*(18), 3907–3914.

Watanabe, T., Asaka, S., Kitagawa, D., Saito, K., Kurashige, R., Sasado, T., … Furutani-Seiki, M. (2004). Mutations affecting liver development and function in Medaka, Oryzias latipes, screened by multiple criteria. *Mechanisms of Development*, *121*(7-8), 791–802.

Willecke, M., Hamaratoglu, F., Kango-Singh, M., Udan, R., Chen, C.-L., Tao, C., … Halder, G. (2006). The fat cadherin acts through the hippo tumor-suppressor pathway to regulate tissue size. *Current Biology : CB*, *16*(21), 2090–100.

Wittbrodt, J., Adam, D., Malitschek, B., Maueler, W., Raulf, F., Telling, A., … Schartl, M. (1989). Novel putative receptor tyrosine kinase encoded by the melanoma-inducing Tu locus in Xiphophorus. *Nature*, *341*(6241), 415–421.

Wittbrodt, J., Shima, A., & Schartl, M. (2002). Medaka--a model organism from the far East. *Nature Reviews. Genetics*, *3*(1), 53–64.

Wong, I. Y., Javaid, S., Wong, E. a, Perk, S., Haber, D. a, Toner, M., & Irimia, D. (2014). Collective and individual migration following the epithelial-mesenchymal transition. *Nature Materials*.[Online] [Accessed 25.08.2014]

Woods, M. L., Carmona-Fontaine, C., Barnes, C. P., Couzin, I. D., Mayor, R., & Page, K. M. (2014). Directional collective cell migration emerges as a property of cell interactions. *PloS One*, *9*(9), e104969.

Wu, S., Huang, J., Dong, J., & Pan, D. (2003). hippo encodes a Ste-20 family protein kinase that restricts cell proliferation and promotes apoptosis in conjunction with salvador and warts. *Cell*, *114*(4), 445–456.

Wullimann, M. F., Mueller, T., Distel, M., Babaryka, A., Grothe, B., & Köster, R. W. (2011). The long adventurous journey of rhombic lip cells in jawed vertebrates: a comparative developmental analysis. *Frontiers in Neuroanatomy*, *5*(4), 27.

Xia, Y., Chang, T., Wang, Y., Liu, Y., Li, W., Li, M., & Fan, H.-Y. (2014). YAP promotes ovarian cancer cell tumorigenesis and is indicative of a poor prognosis for ovarian cancer patients. *PloS One*, *9*(3), e91770.

Xiao, L., Chen, Y., Ji, M., & Dong, J. (2011). KIBRA regulates Hippo signaling activity via interactions with large tumor suppressor kinases. *The Journal of Biological Chemistry*, *286*(10), 7788–96.

Xu, Y., Stamenkovic, I., & Yu, Q. (2010). CD44 attenuates activation of the hippo signaling pathway and is a prime therapeutic target for glioblastoma. *Cancer Research*, *70*(6), 2455–2464.

Yang, X., Scheffler, B. E., & Weston, L. a. (2006). Recent developments in primer design for DNA polymorphism and mRNA profiling in higher plants. *Plant Methods*, *2*(1), 4.

Ye, S., Dhillon, S., Ke, X., Collins, a R., & Day, I. N. (2001). An efficient procedure for genotyping single nucleotide polymorphisms. *Nucleic Acids Research*, *29*(17), E88–8.

Yi, C., Troutman, S., Fera, D., Stemmer-rachamimov, A., Avila, L., Christian, N., … Kissil, J. L. (2011). A tight junction-associated Merlin-angiomotin complex mediates Merlin's regulation of mitogenic signaling and tumor suppressive functions. *Cancer Cell*, *19*(4), 527–540.

Yntema, C., & Hammond, W. (1955). Experiments on the origin and development of the sacral autonomic nerves in the chick embryo. *Journal of Experimental Zoology*, *129*(2), 375–413.

Yokoi, H., Kobayashi, T., Tanaka, M., Nagahama, Y., Wakamatsu, Y., Takeda, H., … Ozato, K. (2002). Sox9 in a teleost fish, medaka (Oryzias latipes): evidence for diversified function of Sox9 in gonad differentiation. *Mol Reprod Dev.*, *63*(1), 5–16.

Young, H. M., Hearn, C. J., Farlie, P. G., Canty, a J., Thomas, P. Q., & Newgreen, D. F. (2001). GDNF is a chemoattractant for enteric neural cells. *Developmental Biology*, *229*(2), 503–16.

Z-Fin (2014). Phox2bb ZFIN ID: ZDB-GENE-050407-3. [Online] [Accessed 06.09.2014] Availabel from: http://zfin.org/action/marker/view/ZDB-GENE-050407-3

Zhang, G., Gurtu, V., & Kain, S. R. (1996). An Enhanced Green Fluorescent Protein Allows Sensitive Detection of Gene Transfer in Mammalian Cells. *Biochemical and Biophysical Research Communications*, *227*(3), 707–711.

Zhang, J., Ji, J., Yu, M., Overholtzer, M., Smolen, G. A., Wang, R., … Haber, D. A. (2010). YAP-dependent induction of amphiregulin identifies a non-cell-autonomous component of the Hippo pathway. *Cell*, *11*(12), 1–16.

Zhao, B., Li, L., Lei, Q., & Guan, K.-L. (2010). The Hippo-YAP pathway in organ size control and tumorigenesis: an updated version. *Genes & Development*, *24*(9), 862–74.

Zhao, B., Li, L., Lu, Q., Wang, L. H., Liu, C.-Y., Lei, Q., & Guan, K.-L. (2011). Angiomotin is a novel Hippo pathway component that inhibits YAP oncoprotein. *Genes & Development*, *25*(1), 51–63.

Zhao, B., Wei, X., Li, W., Udan, R. S., Yang, Q., Kim, J., … Guan, K. (2007). Inactivation of YAP oncoprotein by the Hippo pathway is involved in cell contact inhibition and tissue growth control. *Genes & Development*, 2747–2761.

Ziegler, I. (2003). The pteridine pathway in zebrafish: regulation and specification during the determination of neural crest cell-fate. *Pigment Cell Research / Sponsored by the European Society for Pigment Cell Research and the International Pigment Cell Society*, *16*(3), 172–82.

Zlotogora, J., Lerer, I., Bar-David, S., Ergaz, Z., & Abeliovich, D. (1995). Homozygosity for Waardenburg syndrome. *Am J Hum Genet*, *56*(5), 1173–1178.